2016-03-01

Development, Evaluation, and Validation of a High-Resolution Directivity Measurement System for Played Musical Instruments

K Joshua Bodon
Brigham Young University - Provo

2016-03-01

Development, Evaluation, and Validation of a High-Resolution Directivity Measurement System for Played Musical Instruments

K Joshua Bodon
Brigham Young University - Provo

Development, Evaluation, and Validation of a High-Resolution Directivity Measurement System for Played Musical Instruments

K. Joshua Bodon

A thesis submitted to the faculty of
Brigham Young University
in partial fulfillment of the requirements for the degree of

Master of Science

Timothy W. Leishman, Chair
Brian D. Jeffs
Tracianne B. Neilsen
William J. Strong

Department of Physics and Astronomy

Brigham Young University

March 2016

ABSTRACT

Development, Evaluation, and Validation of a High-Resolution
Directivity Measurement System for
Played Musical Instruments

K. Joshua Bodon
Department of Physics and Astronomy, BYU
Master of Science

A high-resolution directivity measurement system at Brigham Young University has been renovated and upgraded. Acoustical treatments have been installed on the microphone array, professional-grade audio hardware and cabling have been utilized, and user-friendly MATLAB processing and plotting codes have been developed. The directivities of 16 played musical instruments and several loudspeakers have been measured by the system, processed, and plotted. Using loudspeakers as simulated musicians, a comprehensive analysis was completed to validate the system and understand its error bounds. A comparison and evaluation of repeated-capture to single-capture spherical systems was made to demonstrate the high level of detail provided by the 5^o resolution system. Analysis was undertaken to determine how nonanechoic effects in anechoic chambers influence results. An overview of directivity measurement systems from the literature is provided as well as a dedicated discussion of the directivity measurement system at Brigham Young University.

Keywords: musical instrument, acoustic directivity, directivity measurement system, anechoic chamber

ACKNOWLEDGMENTS

The contents of this volume contain more than just words and plots about directivity. It contains late nights, skipped meals, worry, fear, love, tears, and joy. This is the culmination of more than two years of work, which I could not have accomplished had I been on my own. I would like to thank all those who helped bring about this document.

First and foremost, I must thank my wife Maranda and children Eleanor and Gabriel for being so supportive and giving up so much time with their husband and daddy. The surprise treats in my lunches and notes in my notebooks always kept me going. This thesis truly belongs to you also.

I thank my parents who have comforted me and have always encouraged me to be the best I can be, and for providing me with so much support while in school. I also thank my Father in heaven for His love and the gospel, which provided me with purpose and clarity in difficult times.

I thank Dr. Timothy Leishman and the rest of my committee for guiding me along this journey with their considerable knowledge.

A special thank you to the Institute for Scientific Research in Music for funding this thesis work and to Mark Philbrick for allowing the use of one of his photos taken of the directivity system.

I also thank all of the undergraduates who have come and gone during the course of these few years. For the work you did and for keeping me sane during countless hours spent in the anechoic chamber—Jeshua, Daniel, Michael, Michael, Claire and anyone else who fought the chamber with me—you guys are the best.

Contents

List of Figures

List of Tables

Nomenclature

Coordinate system

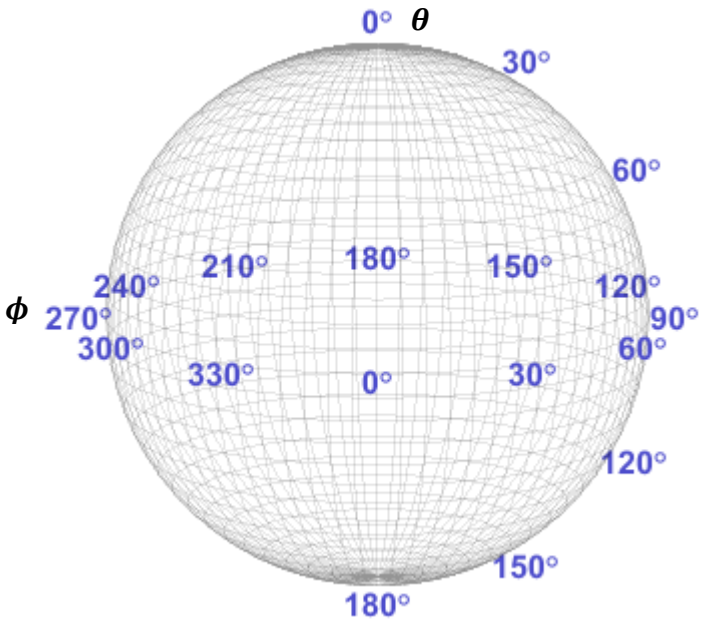

$\hat{a}_{l,i}(f,T)$	Complex frequency domain amplitude of the l^{th} reference signal
$\hat{b}_{mn,i}(f,T)$	Complex frequency domain amplitude of the m^{th} polar angle index and n^{th} azimuthal angle index measurement signal
D_{H_1}	Normalized acoustic directivity of a loudspeaker at the $(m,n)^{th}$spatial index
L	Normalized directivity level with an adjusted +40 dB offset
$L_{L_{m,n}}(f)$	Normalized directivity level of a loudspeaker at the $(m,n)^{th}$ spatial index
$L_{M_{m,n}}(f)$	Normalized directivity level of a simulated musician at the $(m,n)^{th}$ spatial index
$L_{R_{m,n}}$	Normalized directivity level of the repeated-capture system at the $(m,n)^{th}$ spatial index
$L_{S_{m,n}}$	Normalized directivity level of the single-capture system at the $(m,n)^{th}$ spatial index
DMS	Directivity measurement system
$E_l(f)$	Response of electronics in the system of the l^{th} reference signal

$E_m(f)$	Response of electronics in the system of the m^{th} polar angle index
$E_{\mathrm{rms}}(f)$	Area-weighted root mean square error of levels
$G_{aaln}(f)$	Single sided auto-spectrum of the l^{th} reference signal at the nth azimuthal index
$G_{ablmn}(f)$	Single sided cross-spectrum of the $(m,n)^{th}$ spatial index location using the l^{th} reference signal
$G_{bbmn}(f)$	Single sided auto-spectrum of the measurement signal at the $(m,n)^{th}$ spatial index location
$H_{1lmn}(f)$	Frequency response of the $(m,n)^{th}$ spatial index location utilizing an input signal from the l^{th} reference microphone
$\lvert H_{1l}(f)\rvert_{\max}$	Frequency dependent maximum value of the magnitude of the frequency response using the l^{th} reference signal
$H_{\mathrm{CAL}_{lm}}$	Relative calibration frequency response for the m^{th} polar index using the l^{th} reference channel
$H_{\mathrm{Cal,I}_{lm}}$	Frequency response for the m^{th} polar index using the l^{th} reference channel for the primary arrangement of microphones using a switching technique
$H_{\mathrm{Cal,II}_{lm}}$	Frequency response for the m^{th} polar index using the l^{th} reference channel for the secondary arrangement of microphones using a switching technique
$H_{\mathrm{Cor}_{lm}}$	Frequency response after the calibration has been applied for the m^{th} polar index using the l^{th} reference channel
m_σ	The number of standard deviations
$M_l(f)$	Response of the l^{th} reference microphone and microphone preamplifier
$M_m(f)$	Response of the m^{th} polar index microphone and microphone preamplifier
n_d	The number of total blocks
$\hat{p}(f)$	Frequency domain acoustic pressure
$\hat{p}_l(f)$	Frequency domain acoustic pressure measured at the l^{th} reference microphone
$\hat{p}_m(f)$	Frequency domain acoustic pressure measured at the m^{th} index polar angle
r	Measurement radius
RMS	Root mean square
$S_{m,n}$	Surface area represented by the $(m,n)^{th}$ spatial index location microphone on a sphere
S/N	Signal-to-noise ratio

T	Record length
θ	Polar angle
ϕ	Azimuthal angle
$\gamma^2_{ablmn}(f)$	Frequency dependent coherence of the $(m,n)^{th}$ spatial index using the l^{th} reference channel
$\sigma(f)$	Frequency dependent standard deviation
$\sigma_{\mathrm{dB}_{\mathrm{diff}}}(f)$	Frequency dependent maximum deviation in dB of the maximum to minimum value
$\mu(f)$	Frequency dependent mean of the magnitude of the frequency response
*	Complex conjugate of preceding term

Chapter 1

Introduction

Many systems have been implemented to study the directivity of acoustic sources, like the human voice, musical instruments, and loudspeakers. While standards exist for measuring loudspeakers [1], none have been established for measuring musical instruments. Without a commonly accepted measurement standard, anyone developing a directivity measurement system (DMS) for musical instruments must do so based on individual and unique research goals and constraints.

1.1 Questions for Consideration

There are four basic questions that should be answered in the design of such a system: First, which coordinate system will be used for the measurements? Second, will the measurements be made all at once or obtained as a series of measurements (as repeated captures)? Third, what are the desired spectral and spatial resolutions for the system? Fourth, what quality is required for the audio recordings? Each decision affects the ability to choose in the other areas. The following sections address each question in greater detail.

1.1.1 Which Coordinate System will be used for the Measurements?

At the outset of measuring directivities, it is important to determine the coordinate system that will be used. Three common systems have been used by various groups: Cartesian, polar, and spherical. Wang [2], and Comesana et al. [3], used a Cartesian coordinate system. Wang measured the directivity of an artificially excited violin and preformed nearfield acoustical holography (NAH) to understand the radiation near the violin surface. Comesana et al. also used a series of six planar measurement grids in conjunction with NAH to map pressure data to the surface of a sphere [3].

Jürgen Meyers' work is both notable and extensive, but his methods for gathering directivity data remain largely undocumented. It is known that several of his measurements were taken with a polar coordinate system, as the results were depicted with polar plots [4]. The most commonly used system in the last 20 years has been the spherical coordinate system, typically with a single fixed radius. Groups such as Pätynen et al. [5], Pollow et al. [6], Carrillo et al. [7], and Eyring [8], have all utilized a spherical system to obtain directivity measurements. The presentations of results from these studies vary widely, but most commonly appear in the forms of cross-sectional polar plots or three-dimensional balloon plots.

Choosing a coordinate system often limits the flexibility of how the data can be collected. It has become common in recent years to obtain directivity information by sampling spherically around the musician. This allows the data to be utilized in common architectural acoustics simulation packages and provides a more complete understanding of radiation patterns. Cartesian or polar measurement coordinate systems for microphone array placements require repeated captures to achieve a spherical directivity. This has been accomplished both by repeatedly rotating

the source with fixed measurement locations or using a fixed source orientation while repeatedly moving microphones or microphone arrays around the source [2]. A spherical array system is not so limiting in that it allows for either simultaneous recordings over a sphere or rotationally repeated recordings [5], [8], [9].

1.1.2 Will the Measurements Be Taken in Stages with Repeated Captures or as a Single Capture?

Repeated-capture measurement systems involve repeated measurements, typically using arrays of microphones to reduce overall measurement time. In this type of system, either a single microphone, a microphone array, or the source is rotatable with respect to the rest of the system. Several measurements are completed in different orientations to form a sphere of data. In theory, this method has no limit placed on maximum spatial resolution. Carrillo et al. [7] and Eyring [8] utilized the technique with 1,260 and 2,522 unique measurement locations over a sphere, respectively. However, using this type of system with live sources of sound potentially introduces repeatability errors into directivity results.

Single-capture measurement systems typically use large spherical arrays of microphones to assess acoustic pressures around a source in a single multichannel measurement. This method has the benefit of eliminating repetition error. However, it can severely reduce the possible spatial resolution of the directivity measurement. Financial and other logistical constraints have limited groups to 64 or fewer microphones [10].

1.1.3 What are the Desired Spectral and Spatial Resolutions for the System?

Unlike loudspeaker measurements, no standard exists for musical instrument directivity regarding the number of data locations required over a sphere. Having a fine spatial resolution is normally desirable, as sparse arrays can skew results (see Ch. 4), but it does come with multiple disadvantages. As indicated earlier, due to physical, acoustical, and financial limitations, the use of hundreds or thousands of microphones over a sphere in a single-capture system is not practical. Having a fine spatial resolution requires a repeated-capture system. This equates to a more complex system and longer recording times for each directivity measurement.

For example, Eyring required 72 repeated captures to complete a sphere of data [8], instead of only one required by a single-capture system. The recording time is magnified when recording live sources. A musician may not have sufficient stamina to repeat many takes at each angle or capture without intermissions. Additionally, repeating a note exactly becomes improbable. Variations in pitch, amplitude, and position of the musician and instrument are likely to change with every repetition, rendering it difficult to process directivity without special methods.

1.1.4 What Level of Quality is Required for the Audio Recordings?

Because many groups have intended to use the audio recordings for more than the calculation of directivity in their work, the quality of these recordings must be considered. The recordings can have applications for auralizations and creation of virtual orchestras [11], while other applications, such as MIDI virtual instrument sound files, are not beyond the imagination. Various sampling frequencies from 8 kHz to 65.53 kHz and bit depths from 16 to 24 have been used to fulfill the needs of the projects.

If high-quality audio is required, high sampling rate and bit depth are important factors. To record in CD quality or better requires at least a 44.1 kHz sampling rate and 16 bits. As these two factors increase, file sizes also grow, as do the demands on hardware to convert and record the acoustic signals. Low noise and distortion in the hardware is crucial. As a result, recording quality must be carefully considered, as it can affect the budget, storage constraints, and equipment used in the measurement system.

1.2 A Suggested Resolution

Unfortunately, these same questions that allow for so much flexibility in measuring musical instrument directivity also hinder the progression of the field of study in some ways. Having no standard for measuring or presenting musical instrument directivity makes comparing data between different parties challenging. Additional details about past work in this area, along with their references, are given in App. A and are summarized in Tables 1.1 and 1.2.

One possible solution may be to introduce a standard similar to those of loudspeaker directivity measurements. Based on the requirements of the AES56-2008 type A standard for loudspeakers, musical instrument directivities should also be held to a 5^{o} uninterpolated angular resolution, which realistically requires a repeated-capture system [1]. This has the added benefit of matching Common Loudspeaker Format (CLF) type 1 requirements [12], which are commonly used in simulation and auralization packages [13], [14].

While difficulties with this type of system can be substantial, it is not impossible to either correct them or take preventative measures to reduce their impacts on results. For example, the use of a frequency response function (FRF) with a reference microphone input, rather than an auto-

spectrum, allows amplitude deviations to be readily corrected [8]. The use of tuners and appropriate averaging reduces errors due to small frequency deviations. A simple laser positioning system may be employed to prevent some positional errors. Finally, advanced processing algorithms that detect pitch shift might be utilized to correct pitch variation of musicians.

By utilizing such tools, it is possible to develop a high-resolution DMS, which provides rich detail in musical instrument directivity, while also being practical to implement. This will allow further studies to sequentially improve while, at the same time, providing a basis for comparison of results.

1.3 Motivations

Current architectural acoustic software modeling packages, such as EASE [15], Odeon [13], and CATT-Acoustic [14] incorporate source directivities for room modeling and auralizations. While EASE utilizes the Generic Loudspeaker Library (GLL) format [16] with a variable angular resolution from 1^o to 90^o, Odeon and Catt Acoustic utilize the CLF [12]. This requires a 5^o angular resolution for type 2, matching Type A requirements prescribed by the AES56-2008 standard [1]. Only the work by Eyring [8] provides such a dense measurement grid for musical instruments without interpolation.

Aside from such applications in architectural acoustics, high-resolution directivities could lead to improvements in music. Musical instrument manufacturers could analyze directivity patterns of current instruments in conjunction with other methods to improve radiation of future models. Conductors of musical ensembles could better understand location-based differences in sound to modify placements of musicians to spatially improve overall sound quality.

Table 1.1. A summary of the system type, directivity geometry, the total number of microphones used to measure directivity, and the number of unique data locations used by each group outlined in App. A. Cells with no input are unknown based on literature searches. Piezo is short for piezoelectric transducer.

Group	System Type	Directivity Geometry	Number of Mics.	Measurement Locations	Measurement Environment
Hughes	Repeated Capture	Spherical	19	2,522	Anechoic
Leishman et al.	Repeated Capture	Spherical	19	2,522	Anechoic
Marshal and Meyer	-	Planar	-	49	Anechoic
Kob and Jers	Repeated Capture	Partial sphere	2	-	Hemi-anechoic
Bazzoli et al.	Repeated Capture	Partial sphere	5	73	Anechoic
Halkosaari et al.	Repeated Capture	Planar	11	-	Anechoic
Katz and d'Allessandro	Repeated Capture	Partial sphere	24	334	Anechoic
Chu and Warnock	Repeated Capture	Partial sphere	16	324	Anechoic
Jürgen Meyer	Repeated Capture	Planar	1	-	Anechoic
Štěpánek and Otčenašek	Repeated Capture	Cylinder	16	96	Anechoic
Wang	Repeated Capture	Planar	1	142	Unknown
Vos et al.	Repeated Capture	Spherical	1 Piezo	1,154	Anechoic
Carrillo et al.	Repeated Capture	Spherical	21	1,260	Anechoic
Pollow et al.	Single Capture	Spherical	32	32	Anechoic
Comesana et al.	Repeated Capture	Spherical	2	-	Anechoic
Jaques et al.	Single Capture	Planar	8	40	Anechoic
Gautier and Dauchez	Repeated Capture	Planar	1 Intensity Probe	141	Hemi-anechoic
Le Carrou et al.	Single and Repeated Capture	Partial sphere	32/35	32/579	Hemi-anechoic
Pätynen et al.	Single Capture	Spherical	22	22	Anechoic
Hole, Nachbar et al.	Single Capture	Spherical	64	64	Nonanechoic
Otondo and Rindel	Single Capture	Planar	13	13	Anechoic
Grothe and Kob	Repeated Capture	Planar	2	Continuous	Anechoic
Eyring	Repeated Capture	Spherical	37	2,522	Anechoic

Table 1.2. A summary of the plot type, what type of microphone calibration was used, source, how each source was excited, and the directivity bin sizes for each group outlined in App. A. Cells with no input are unknown based on literature searches. Here OB stands for octave bands.

Group	Plot Type	Calibration	Source Type	Excitation Method	Freq. Resolution
Hughes	N/A	Substitution	Loudspeaker	Digital Signal	-
Leishman et al.	Balloon	Single Frequency	Loudspeaker	Digital Signal	12.5 Hz
Marshal / Meyer	Polar	-	Voice	Human Voice	1/1 OB
Kob and Jers	Balloon	Relative	Voice	Human Voice	1/3 OB
Bazzoli et al.	Polar	-	Voice	Human Voice	1/1 OB
Halkosaari et al.	FR	-	Voice	Artificial Voice	1/3 OB
Katz and d'Allessandro	Polar	Equal Excitation	Voice	Human Voice	1/3 OB
Chu and Warnock	Polar	-	Voice	Human Voice	1/3 OB
Jürgen Meyer	Prob. diagram	-	Instrument	Shaker	1/3 OB
Štěpánek and Otčenašek	Descriptive polar	-	Instrument	Live Musician	Note
Wang	Polar	-	Instrument	Artificial Bowing	1/3 OB
Vos et al.	Balloon	N/A	Instrument	Loudspeaker	6 Hz
Carrillo et al.	Polar	Yes	Instrument	Non-stationary Musician	0.67 Hz
Pollow et al.	Balloon	Yes	Instrument	Live Musician	-
Comesana et al.	Balloon	-	Instrument	Live Musician	1/3 OB
Jaques et al.	Polar	-	Instrument	Live Musician	1/1 OB
Gautier and Dauchez	Vector Plot	-	Instrument	Shaker	-
Le Carrou et al.	Polar	-	Instrument	Shaker	>1/3 OB
Pätynen et al.	Polar / Cartesian	Substitution	Instrument	Live Musician	1/3 OB
Hole, Nachbar et al.	Balloon	Single Frequency	Instrument	Live Musician	-
Otondo and Rindel	Polar	-	Instrument	Live Musician	1/1 OB
Grothe and Kob	Polar	-	Instrument	Artificial Blowing	1/3 OB
Eyring	Balloon	Relative	Instrument	Live Musician	10 Hz

Audio recordings could be improved through the use of microphone placements that have been optimized by directivity data. Beyond this, information about microphone placements could be built into post-production audio packages, allowing sound engineers to virtually move microphones without having to bring artists back into a studio and rerecord excerpts with new microphone placements. This would save considerable time and money, and expand the creative abilities of the engineers. The multidirectional recordings associated with directivity measurements could also be used to improve virtual instrument and digital instrument sampling qualities, while increasing accuracies to those of true recordings at any location.

Although musical instrument directivity research has involved more than 40 years of active research, researchers do not fully understand the comparative effects and values of one measurement system type over another. Several questions merit investigation. For example, what details are seen in high-resolution musical instrument directivity measurements that are not seen in lower-resolution measurements? What is the relative value of a repeated-capture system with high spatial resolution and associated musician-induced errors, verses a single-capture system with lower resolution but fewer musician induced errors? Furthermore, can errors due to musician inconstancies be clearly defined? In addition to introducing refinements to the BYU DMS, this thesis addresses these questions and outlines their ramifications for musical instrument directivity measurements. An understanding of these details will help shape future research of musical instrument directivities and their use in industry, and provide the groundwork for standardized measurement methods.

1.4 The Current Research

Building on Eyring's preliminary work, the author has taken steps to answer the questions posed in Sec. 1.3. These include (1) updating the BYU DMS to quantify and reduce errors induced by the apparatus and musicians, (2) measuring the directivities of 16 wind and string instruments, (3) evaluating the relative values of a high-resolution repeated-capture system over a lower-resolution single-capture system, and (4) providing preliminary analysis of nonanechoic effects measured by the DMS in an anechoic chamber. This thesis recounts the steps taken to improve, validate, and compare the current DMS, and provides results for the directivity measurements of 16 musical instruments.

Although much has been accomplished in the current work, there are inevitable limitations that have not been addressed. For example, directivity measurements were made for only one representative of each instrument and each of these were played by a single musician. To obtain more generalized directivity patterns for each instrument, multiple representatives would need to be measured, with each being played by multiple musicians. While there are multiple ways to calculate directivities, those presented here are reported for individual harmonics rather than note-based or even instrument-based average directivities. Over defined spectral bands, it may be possible to achieve averaged directivities for instruments, but this would require additional considerations. An additional limitation includes the fact that only one spatial resolution was used for a single-capture DMS for comparison to the BYU repeated-capture DMS. Furthermore, while the impact of nonanechoic behaviors of anechoic chambers was brought to light by the latter, the effects were not corrected.

1.5 Plan of Development

The following chapters provide many additional details about the work. Chapter 2 provides an overview of the updated BYU DMS and gives details on steps taken to incorporate high-quality measurements and efficiency into a single system. Validation of the DMS is outlined in Ch. 3, including quantifiable error bounds expected from a live musician with a repeated-capture system. Chapter 4 provides a direct comparison of measured results from a single-capture system versus those of the BYU DMS. Chapter 5 includes preliminary information of the discovery and explanation of nonanechoic directivity-related effects occurring in the anechoic chamber at BYU. In Ch. 6, several example directivity results are provided for each of the 16 musical instruments measured in the study, including a violin, viola, cello, double bass, trumpet, trombone, French horn, euphonium, tuba, baritone saxophone, tenor saxophone, flute, oboe, bassoon, clarinet, and bass clarinet. Conclusions are then drawn in Ch. 7, which includes a summary of the findings of the entire study.

Two appendices are also included as supplemental material to the reader. Appendix A summarizes a literature search undertaken to ensure that the updated DMS implemented the best features of previous systems while also introducing advantages. Details of a phantom-to-integrated circuit piezoelectric (ICP) power converter design are included as Appendix B. Further results and a complete user handbook of the DMS written by the author may be accessed as supplemental material to the electronic version of this thesis [17].

References

[1] AES56-2008 AES standard on acoustics – Sound source modeling – Loudspeaker polar radiation measurements (Audio Eng. Soc. Inc., New York, 2008).

[2] L. W. Wang, "Radiation Mechanisms from Bowed Violins," Ph. D. dissertation, Pennsylvania State University, State College, PA (1999), available online at < http://search.proquest.com/docview/304486063> (Last viewed December 7, 2015).

[3] F. Comesana, T. Takeuchi, S. M. Morales, and K. Holland, "Measuring musical instruments directivity patterns with scanning techniques," in *ICSV19, Vilnius, Lithuania*, (2012).

[4] J. Meyer, *Acoustics and the Performance of Music: Manual for Acousticians, Audio Engineers, Musicians, Architects and Musical Instrument Makers*, 5th ed. (Springer, Berlin, 2009).

[5] J. Pätynen, V. Pulkki, and T. Lokki, "Anechoic recording system for symphony orchestra," Acta Acustica united with Acustica, **94**, 856-865 (2008).

[6] M. Pollow, G. Behler, and B. Masiero, "Measuring directivities of natural sound sources with a spherical microphone array," *Proc. 1st Ambisonics Symposium*, Graz, 1-6 (2009) [available online at < http://ambisonics.iem.at/symposium2009/proceedings/ambisym09-pollowmasiero-musicalinstrumentdirectivity.pdf/@@download/file/AmbiSym09_PollowMasiero_MusicalInstrumentDirectivity.pdf> (Last viewed December 7, 2015).

[7] A. Pérez Carrillo, J. Bonada, J. Pätynen, and V. Välimäki, "Method for measuring violin sound radiation based on bowed glissandi and its application to sound synthesis," J. Acoust. Soc. Am. **130**, 1020-1029 (2011).

[8] N. J. Eyring, "Development and Validation of an Automated Directivity Acquisition System Used in the Acquisition, Processing, and Presentation of the Acoustic Far-Field Directivity of Musical Instruments in an Anechoic Space," M.S. thesis, Brigham Young University, Provo, UT (2013), available online through Brigham Young University Electronic Theses & Dissertations at <http://etd.lib.byu.edu> (Last viewed December 7, 2015).

[9] F. Bozzoli, A. Farina, and M. Viktorovitch, "Balloons of directivity of real and artificial mouth used in determining speech transmission index," *Audio Eng. Soc. Convention* 118, Convention Paper 6492 (2005).

[10] F. Hohl, “Kugelmikrofonarray zur Abstrahlungsvermessung von Musikinstrumenten” (“Spherical microphone array for radiation survey of musical instruments”), Master’s thesis, University of Music and Performing Arts, Graz, Austria (2009) [available at <http://old.iem.at/projekte/acoustics/musik/kugel/hohl.pdf > (last viewed December 7, 2015)].

[11] J. Pätynen, V. Pulkki, and T. Lokki, “Anechoic recording system for symphony orchestra,” Acta Acust. United Acust. **94**, 856-865 (2008).

[12] Common Loudspeaker Format, <http://www.clfgroup.org/> (Last viewed December 7, 2015).

[13] Odeon Room Acoustics Software, <http://www.odeon.dk> (Last viewed December 7, 2015).

[14] CATT-Acoustic, <http://www.catt.se/> (Last viewed December 7, 2015).

[15] EASE software, <http://ease.afmg.eu> (Last viewed December 7, 2015).

[16] GLL Loudspeaker File Format, <http://ease.afmg.eu/index.php/gll-loudspeaker-format.html> (Last viewed December 7, 2015).

[17] K. J. Bodon, “Masters Thesis Supplemental Materials,” Brigham Young University (2016) [available at <http://scholarsarchive.byu.edu/cgi/viewcontent.cgi?filename=276&article=6652&context=etd&type=additional>]

Chapter 2

Directivity Measurement System

The DMS developed for this work was an extension and improvement of repeated-capture systems used previously at BYU [1], [2]. Special care was taken in the design of both the hardware and directivity calculation algorithms to overcome the challenges faced when using a repeated-capture measurement system in conjunction with a live musician.

The DMS is shown in Fig. 2.1 with a seated trombonist. The measurements were completed in an anechoic chamber with working dimensions of 8.61 m × 5.66 m × 5.74 m and a cutoff frequency of approximately 80 Hz. It has a suspended cable floor that reduces scattering while keeping the typical working level near the center of the chamber. A semicircular array with 37 microphones at a 1.83 m radius was used in conjunction with a source on a rotating turntable to take most directivity measurements reported in this thesis. The following sections describe the setup and basic procedures taken to record the directivities of loudspeakers and live musical

instruments. Additional details about the system are given in the following sections and in the user's manual [3], written by the author.

2.1 Turntable

The repeated-capture method requires rotation of either a microphone array or the source. For logistical reasons, the sources for this system were rotated. Four acoustically treated stanchions were placed near the center of the chamber, which rise from the floor to create anchoring points for the turntable. The custom turntable [2] had four legs, each of which attached to a separate stanchion, enabling the turntable to be located roughly in the center of the chamber (see Fig. 2.2). The turntable was controlled from a separate room and driven by an onboard worm-gear and stepper motor. A set of four threaded rods, variable in height, mounted onto a rotating platform on the turntable were used to adjust the height of the seated musician or loudspeaker via various mounting systems.

2.2 Arc Array

The support system for the microphone array was a semicircular arc oriented vertically and supported from the structural chamber ceiling (see Fig. 2.1). The arc itself consisted of a 2.54 cm tubular aluminum rod, bent into a C shape, with a radius of 2.13 m. Holes were drilled in the arc, in the radial direction, with a 5^{o} spacing. Threaded rods with microphone holders attached to their ends were secured in each hole. The rod length is such that when the microphones are placed in their mounts, the measurement radius was reduced to 1.83 m. A combination of G.R.A.S. 40AE 1.25 cm microphones and Larson Davis 2551 1.25 cm microphones were used with Larson Davis PRM 426 microphone preamplifiers.

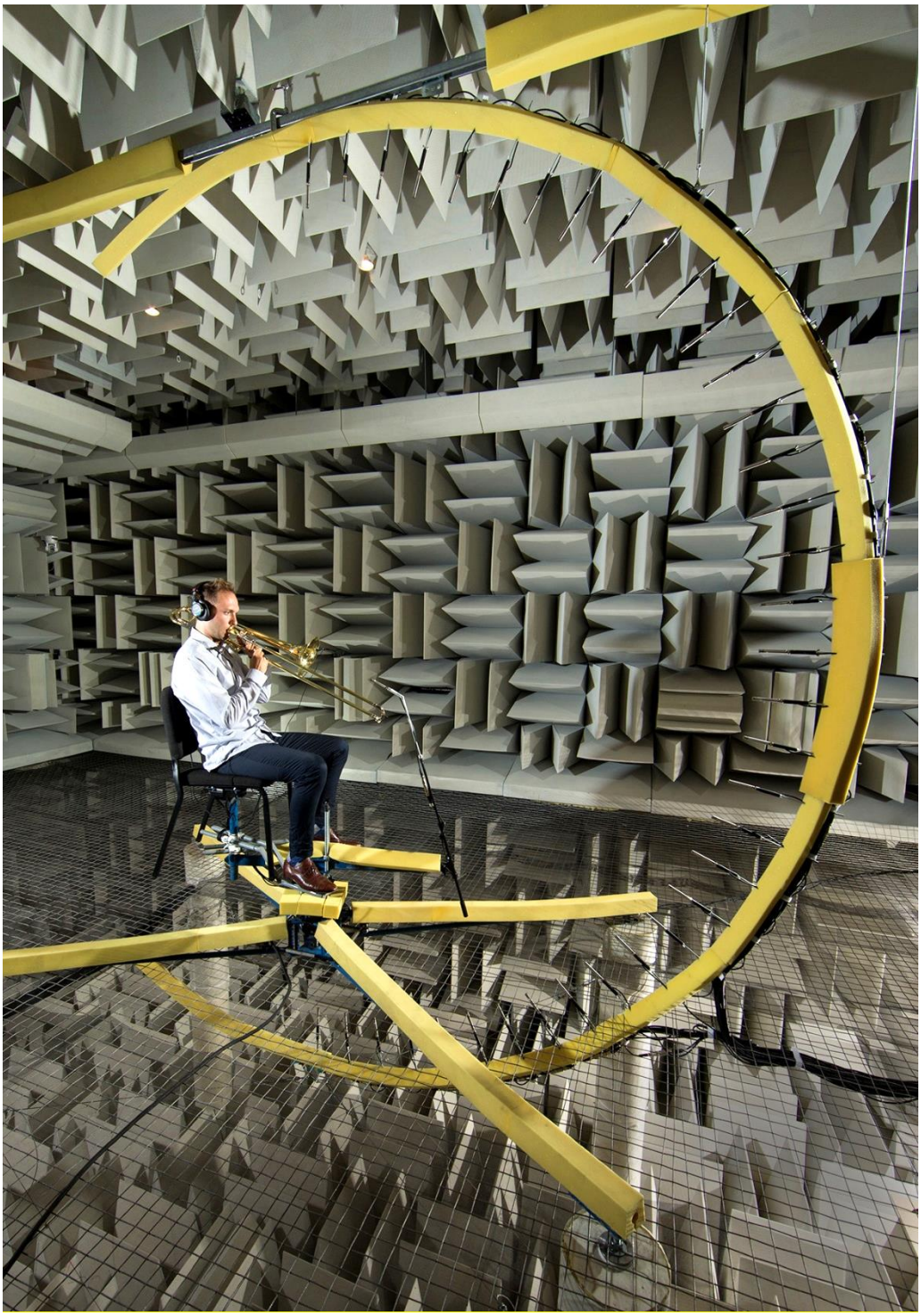

Figure 2.1. Musical instrument DMS.

Figure 2.2. Turntable and musician chair setup for the repeated-capture musical instrument DMS.

2.3 Musician Setup

In order to properly record the musical instruments, their acoustic centers had to be placed near the center of the measurement array. As this location was not defined concretely for any instrument, and would shift as different notes were played, a best estimate of the geometric center was used instead. When the musician arrived, the particulars of the instrument were noted and adjustments were made to position the instrument at the center of the measurement arc. This was accomplished using a series of intersecting lasers to locate the center of the arc and translating the chair so the instrument's geometric center met this point.

To reduce variation in performance, a tuner was placed in front of the musician with the initial stipulation that no note could vary more than ±20 cents from perfect pitch as tuned relative

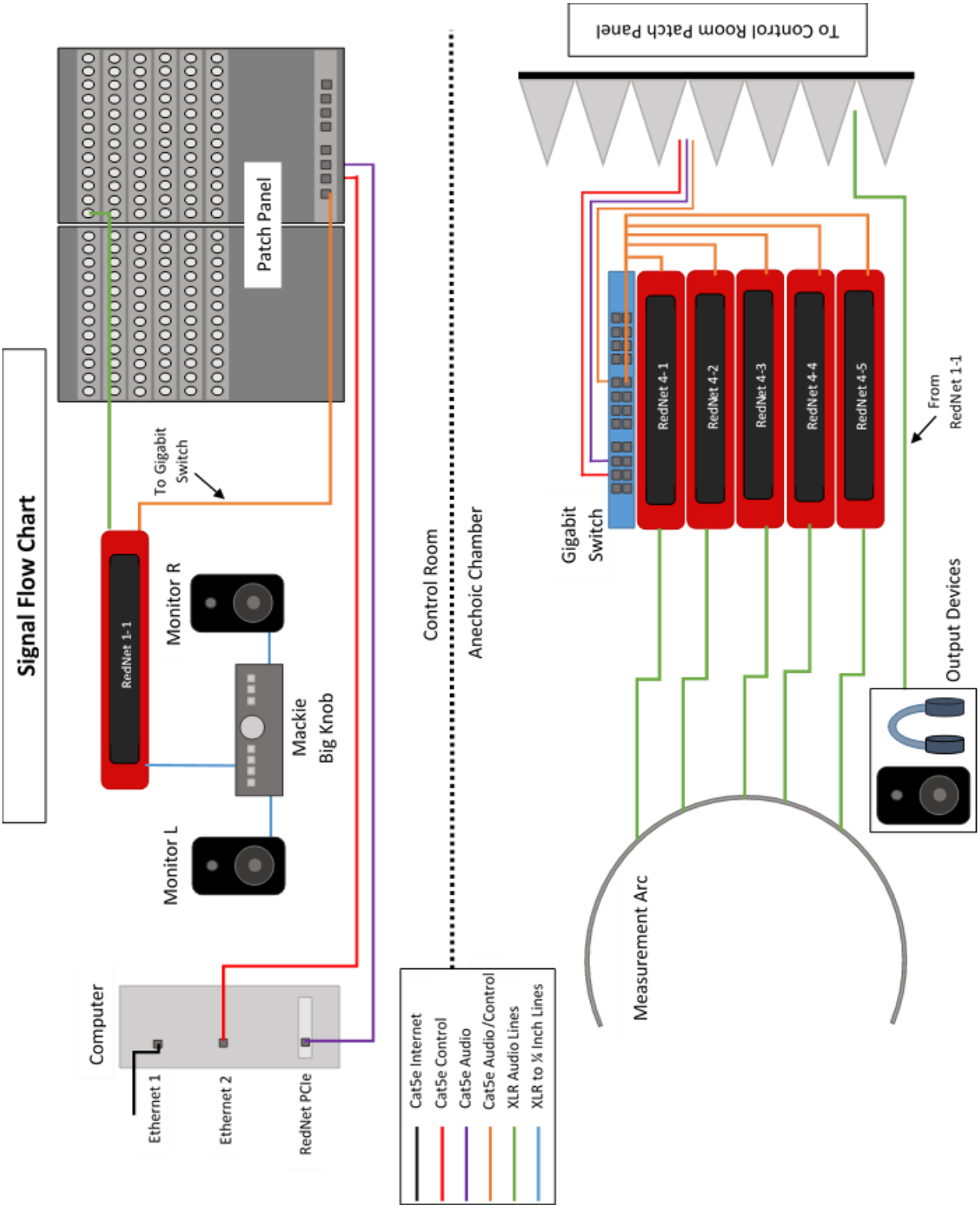

Figure 2.3. System diagram of the DMS.

to A4 = 440 Hz. The tolerance was later altered to ±10 cents for several of the instruments, as it was found that the musicians were capable of consistently playing to this tolerance. Pitch was simultaneously monitored by the musician and the recording engineer of the session. This provided a quantifiable maximum drift of every pitch. All notes were played using standard fingering without vibrato or tremolo at mezzo forte, as defined by the musician.

The musicians were instructed to sit as if they were playing in an orchestra, while remaining as still as possible. A small laser was mounted to their instruments and a 2.5 cm square target was attached to the turntable near the tuner. The musicians were instructed to play with the laser always on the target. As a result, the musician's movements were limited, on average, to ±1.25 cm translationally and ±1.1^{o} in both polar and azimuthal angles. Initial orientation of each musician was toward the 90^{o} polar-angle microphone on the array.

2.4 Cabling and Other Hardware

The signal path from the microphones to the recording computer contained several elements. First, a short 45.7 cm BNC cable was used to connect the microphone preamplifiers to custom-built BNC to XLR adapters. These adapters served the dual purpose of both cable conversion and conversion of phantom power (+48 ±4 V and up to 10 mA) [4] supplied by the digital audio interfaces to the 20 V to 32 V and 2 mA to 4 mA ICP power [5] required by the microphone preamplifiers. A full description of this converter and the quality test results are addressed in App. B.

From these adapters, XLR cables of various lengths were run down the back of the arc, under the suspended cable floor of the chamber, and into five Focusrite RedNet 4 digital audio

interfaces. These functioned as both preamplifiers and analog-to-digital converters. Each RedNet 4 contained 8 XLR input channels and a single ethernet as an output, and provided up to 63 dB of gain in single dB increments per channel. Ethernet outputs were run through a NetGear GS716Tv3 switch and into a computer located in the adjoining control room via a RedNet PCIe card. The signals from each capture were then recorded simultaneously using the REAPER audio software package with each signal saved as an individual *.wav file. Three additional microphones with similar signal paths were attached to the turntable to provide reference signals from the rotating reference frame.

A RedNet 1 unit was located in the control room to provide output channels to the JBL LSR305 control room monitors and a headphone mix to the musician. The latter included a click track, a real time signal of the musician from one of the recording microphones, and a talk-back feature as a way to communicate with the musician from the control room. The output signals were all routed through a Mackie Big Knob controller interface. Additional details and diagrams of the system are given in the DMS handbook [3] and in Fig. 2.3.

2.5 Recording Musicians

Once the chamber setup was completed, test scales were performed at several azimuthal angles to set appropriate gain levels on the RedNet 4 units. All microphone channels for the measurement arc were set to the same gain level and were not altered after the initial setting for the duration of the recording session. The gain settings for the reference microphones were adjusted independently. The levels broadcast to the musician's headset were also adjusted at the request of the musician. Closed-back over-ear SONY MDR-7506 headphones were used to avoid

leakage from the headset to the microphones. The signal was panned to only one ear or the other if the musician desired to use only one earphone.

The musicians then recorded chromatic scales of quarter notes with intervening quarter-note rests at 60 beats per minute. Notes over the entire standard working range of the instruments were recorded, with the musicians pausing for a minimum of one beat between notes. Measurements were taken at a 48 kHz sampling frequency and a depth of 24 bits. At the discretion of either the musician or the recording engineer, notes were repeated for accuracy, clarity, and tonal characteristics before the recordings were accepted. Upon completion of the scale, the turntable was rotated by 5^{o} and the measurements were repeated. This process continued until a complete revolution occurred.

Recording sessions averaged approximately six hours in length and included several short breaks for the musician to rest. To ensure consistent conditions in the chamber over the course of each session, temperature, barometric pressure, and humidity were recorded multiple times over the course of the recordings. A complete procedure is outlined in the DMS user's manual [3].

2.6 Processing

Using a repeated-capture system to measure loudspeakers is relatively simple, as they reproduce and repeat a user-defined input signal. If a loudspeaker is linear and time invariant, its output should not vary and a simple auto-spectrum could in principle be used to calculate directivity, simply by comparing amplitudes from various measurement locations. Musical instruments do not have the luxury of such exactly repeatable signals, so a different method must be used to calculate directivity. Based on the work of Leishman et al. [1], an FRF may be used to

calculate directivity. Since an input signal of a musical instrument played by a live musician is not available, signals from reference microphones placed near the instrument, which remain fixed in the rotating reference frame, may be used as a substitute.

In order to process the large amounts of data collected in the measurements, several MATLAB scripts were developed. They captured the best take of each note at each recording angle (see DMS user's manual Sec. 2.5 [3]) and isolated only the steady-state portion. The result was approximately 0.85 s of usable data at each angle, for every note played. The single-sided cross-spectrum and auto-spectrum of the reference signal were respectively calculated using

$$G_{ablmn}(f) \approx \frac{2}{n_d T} \sum_{i}^{n_d} \hat{a}_{l,i}^{*}(f,T)\hat{b}_{mn,i}(f,T) \tag{2.1}$$

and

$$G_{aal}(f) \approx \frac{2}{n_d T} \sum_{i}^{n_d} \hat{a}_{l,i}^{*}(f,T)\hat{a}_{l,i}(f,T)\,, \tag{2.2}$$

with n_d time records of length T and a 50% overlap. A flat top window was applied to blocks containing 4,800 samples to reduce harmonic amplitude assessment errors. This block size resulted in a 10 Hz frequency resolution. Complex frequency-domain amplitudes $\hat{a}_{l,i}(f)$ of the l^{th} reference signal and $\hat{b}_{mn,i}(f)$ of the $(m,n)^{\text{th}}$ spatial index output measurement signal were used for the i^{th} block in their formulations. Here, m and n represent multipliers of 5° in the polar and azimuthal directions, respectively, where $m = 0, 1, 2 \ldots 37$ and $n = 0, 1, 2, \ldots 72$. The asterisk (*) denotes the complex conjugate of the preceding term. These spectra were subsequently divided to form the time-averaged FRF:

$$H_{1lmn}(f) = \frac{G_{ablmn}(f)}{G_{aaln}(f)}. \tag{2.3}$$

A normalized directivity function was then calculated using

$$D_{H_1}(r, \theta_m, \phi_n, f) = \frac{|H_{1lmn}(f)|}{|H_{1l}(f)|_{\max}}, \tag{2.4}$$

where $|H_{1l}(f)|_{max}$ is the spatial maximum value for each frequency bin. (Complex directivity values are also possible [6], [7]). The normalized directivity function was then placed on a logarithmic scale with a 40 dB offset

$$L(r, \theta_m, \phi_n, f) = 40 + 20\, log_{10}\left(D_{H_1}\right), \tag{2.5}$$

which was used to create balloon plots where the maximum value is represented as 0 dB. Directivity levels from Eq. (2.5) that were less than -40 dB were artificially set to -40 dB for plotting purposes only.

Calculating directivity in this manner also easily permits the calculation of coherence:

$$\gamma^2_{ablmn}(f) = \frac{|G_{ablmn}(f)|^2}{G_{aal}(f) G_{bbmn}(f)}, \tag{2.6}$$

where

$$G_{bbmn}(f) \approx \frac{2}{n_d T} \sum_{i}^{n_d} \hat{b}^*_{mn,i}(f, T) \hat{b}_{mn,i}(f, T). \tag{2.7}$$

This describes the linear cause and effect between the input and output signals of the system and can help quantify the quality of the directivity at each angle and frequency. By using multiple reference microphones, one can then determine which directivity pattern is most reliable and even

create a composite directivity using a combination of results from different reference-microphone signals.

As individual tones from musical instruments contain sparse rather than continuous broadband data, the directivity of only the fundamental frequency and several harmonics were processed for each note. The directivity and coherence functions were represented as balloon plots at each frequency. Three orthogonal polar plots in the median, frontal, and transverse planes were also plotted for each frequency.

When played notes varied slightly in pitch with each rotational increment, local spectral peaks also tended to vary by several frequency bins from one rotation to another. Spectral data were therefore analyzed with an adaptive local peak-finding algorithm for every incremental rotation. This ensured that the correct bin was selected at each angle to represent the fundamental frequency and harmonic directivity of each note.

This was accomplished by analyzing the auto-spectral content of each note from the reference microphones. The algorithm calculated the number of frequency bins that fall within a ±20 cent deviation from perfect pitch for each harmonic of every note. Tuning was relative to A4 = 440 Hz. Using the bin number associated with perfect pitch for each harmonic as the central bin, a search was performed both above and below the given frequency within the bins associated with ±20 cents. Within these limits, the bin containing the maximum auto-spectral value was recorded. This bin number was then used in calculating the directivity. The process was repeated for every incremental rotation of the musician for each harmonic of every note. Spherical directivity was then calculated after stitching all rotational calculations together from similar notes and harmonics.

2.7 Calibration

A total of 40 microphones were utilized in the DMS and it was vital that they were calibrated to achieve accurate results. Absolute calibration was not completed on every microphone, because a fine frequency resolution calibration would take many hours to complete. Only a single microphone was calibrated in this manner and all other microphones were relatively calibrated to it. Relative calibrations were performed with the microphones remaining in the system in order to include all elements of their signal chains. Three different methods were utilized in calibration: the equal excitation method, the switching method, and the substitution method.

2.7.1 Equal Excitation

The equal excitation method [8] utilizes a source, typically in a small cavity or plane-wave tube, where two microphones are inserted near one another. The assumption is made that the microphones experience equal pressure values over frequency and a calibration function can be calculated as

$$H_{\mathrm{CAL}_{lm}}(f) = \frac{\hat{p}(f)\, M_m(f)\, E_m(f)}{\hat{p}(f) M_l(f)\, E_l(f)}\,, \tag{2.8}$$

where the variable $\hat{p}(f)$ denotes the presumably uniform complex acoustic pressure at the microphone locations, while $M(f)$ and $E(f)$ represent the microphone and electronic FRFs in the signal chain, respectively. The index m represents the microphone to be calibrated and index l represents the reference microphone. This calibration can then be applied to the measured frequency response to eliminate hardware effects:

$$H_{\mathrm{Cor}_{lm}} = \frac{H_{1_{lm}}}{H_{\mathrm{CAL}_{lm}}} = \frac{\frac{\hat{p}_m(f)\, M_m(f)\, E_m(f)}{\hat{p}_l(f) M_l(f)\, E_l(f)}}{H_{\mathrm{CAL}}} = \frac{\hat{p}_m}{\hat{p}_l}. \tag{2.9}$$

In practice, a G.R.A.S. 51AB sound intensity calibrator was utilized for this method, which had a usable bandwidth of 60 Hz to 6.3 kHz, over which the equal pressure assumption remained valid.

2.7.2 Switching

The switching method does not depend on equal pressure at both microphone positions [9], so there is no theoretical upper-frequency limit imposed by the apparatus. The method consists of measuring pressure fields with the microphone to be calibrated and a reference microphone in separate locations. Their positions are then switched and measurements are repeated. Assuming a linear time-invariant system, a calibration frequency response may be achieved as follows:

$$H_{\mathrm{Cal,I}_{lm}} = \frac{\hat{p}_m(f)\, M_m(f)\, E_m(f)}{\hat{p}_l(f) M_l(f)\, E_l(f)}, \tag{2.10}$$

$$H_{\mathrm{Cal,II}_{lm}} = \frac{\hat{p}_l(f)\, M_m(f)\, E_m(f)}{\hat{p}_m(f) M_l(f)\, E_l(f)}, \tag{2.11}$$

$$H_{\mathrm{CAL}_{lm}} = (H_{\mathrm{Cal,I}_{lm}}\, H_{\mathrm{Cal,II}_{lm}})^{1/2}. \tag{2.12}$$

The result of Eq. (2.12) may then be substituted into Eq. (2.9) to yield a calibrated frequency response function. The G.R.A.S. 51AB was again used for the switching technique by switching the microphone locations and repeating the measurement a second time. This provided

a calibration function valid to higher frequencies and a basis for comparison of calibration functions at lower frequencies.

2.7.3 Substitution

The final method employed for the DMS was the substitution technique [10]. It is similar to the switching method, but rather than taking measurements in two locations and switching the microphone positions, measurements were taken one at a time at the same location. Since calibration measurements were taken in an anechoic chamber, equal pressure was assumed for a linear time-invariant system for exact position substitution. Equations (2.8) and (2.9) are again used to compute a calibrated frequency response.

2.7.4 Calibration Results

The calibration methods were tested with five different excitations signals: white noise, pseudo random noise, a 1 s linear swept sine, a 1 s logarithmic swept sine, and a 2 s logarithmic swept sine. Consistent results were achieved using all methods and signal types. However, noise signals and the substitution method proved to be the most challenging for achieving accurate results. All calibrations applied to the data presented in this thesis utilized a 1 s linear swept sine signal in conjunction with the switching technique from Sec. (2.7.2).

In order to validate that the calculated calibrations on each microphone were accurate, a known, consistent signal was provided to each microphone individually. A 1 kHz G.R.A.S. 42AB calibrator was used for this purpose. Auto-spectral amplitudes of the received signals were calculated using this signal and the calibration functions were applied as a correction factor. Optimal results would show a consistent amplitude across all microphones in the array after

calibrations are applied. Amplitude results using the G.R.A.S. 42AB are plotted in Fig. 2.4 at 1 kHz after several calibrations were applied. It can be seen that there is a $\pm$ 0.2 dB variation across all 37 microphones at this frequency regardless of the calibration used.

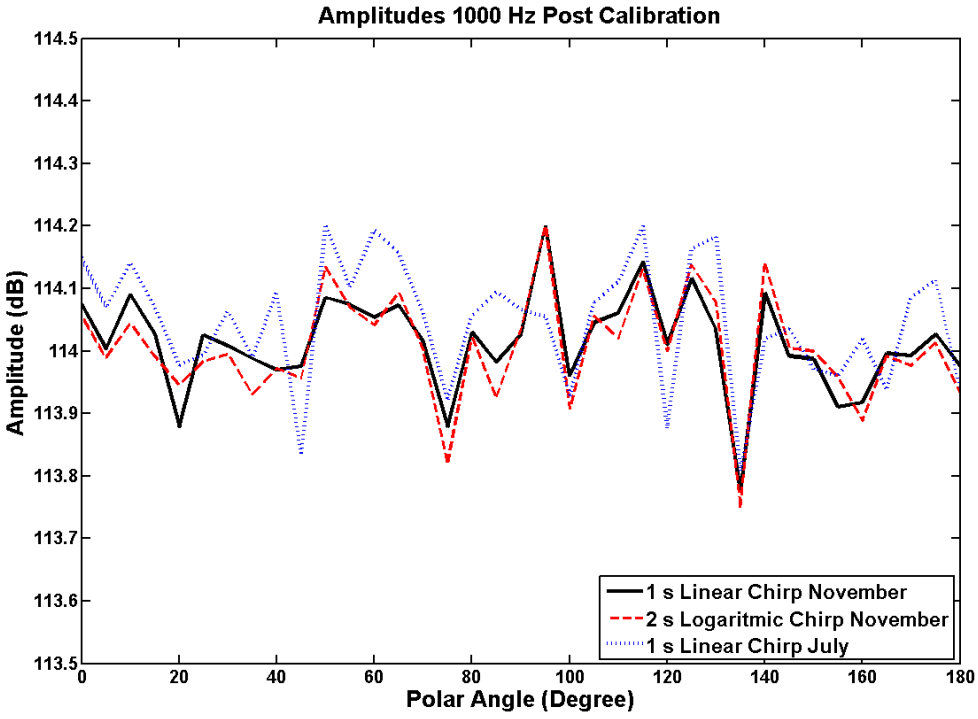

Figure 2.4. Calibrated pressure levels at 1 kHz for each microphone on the directivity measurement array when a G.R.A.S. 42AB sound calibrator signal was applied to each microphone. Microphones were located every 5°. The colors represent different calibrations that were applied, demonstrating stability and consistency in the different calibration instances.

References

[1] T. W. Leishman, S. Rollins, and H. Smith, "An experimental evaluation of regular polyhedron loudspeakers as omnidirectional sources of sound," J. Acoust. Soc. Am. **120**, 1411-1422 (2006).

[2] N. J. Eyring, "Development and Validation of an Automated Directivity Acquisition System Used in the Acquisition, Processing, and Presentation of the Acoustic Far-Field Directivity of Musical Instruments in an Anechoic Space," M.S. thesis, Brigham Young University, Provo, UT (2013), available online through Brigham Young University Electronic Theses & Dissertations at <http://etd.lib.byu.edu> (Last viewed December 7, 2015).

[3] K. J. Bodon, "Masters Thesis Supplemental Materials," Brigham Young University (2016) [available at <http://scholarsarchive.byu.edu/etd/5653/>]

[4] IEC 61938:2013: Multimedia systems – Guide to the recommended characteristics of analogue interfaces to achieve interoperability. (International Electrotechnical Commission, Geneva, Switzerland).

[5] Larson Davis, "ICP Microphone Preamplifier Model PRM426" available online at <http://www.grom.com.br/downloads/larson_davis/Microfones/Pre_amp/ICP_Microphone_Preamplifier_PRM426.pdf> (Last viewed January 8, 2016).

[6] C. Hughes, "How Accurate is Your Directivity Data?" (2005) [available online at <http://www.excelsior-audio.com/Publications/NWAA_Labs_WhitePaper.pdf> (last viewed December 7, 2015)].

[7] M. Pollow, G. K. Behler, and F. Schultz, "Musical instrument recording for building a directivity database," in Fortschritte der Akustik **36**. Deutsche Jahrestagung für Akustik, Berlin, Germany (2010).

[8] G. S. K. Wong, and T. F. W. Embleton, "Three-port two-microphone cavity for acoustical calibrations," J. Acoust. Soc. Am. **71**, 1276-1277 (1982).

[9] J. Y. Chung, and D. A. Blaser, "Transfer function method of measuring in-duct properties. I. Theory," J. Acoust. Soc. Am. **68**, 907-913 (1980).

[10] L. E. Kinsler, A. R. Frey, A. B Coppens, and J. V. Sanders, *Fundamentals of Acoustics*, 4th ed. (John Wiley & Sons, New York, 2000).

Chapter 3

Validating a Repeated-Capture System for Musical Instrument Directivity

As mentioned earlier, musical instrument directivity systems can typically be placed into one of two categories: single-capture systems and repeated-capture systems. Single-capture systems lead to quick and efficient data acquisition, but the directivity detail is hindered by the relatively low spatial resolution [1], [2]. Single-capture measurements can lead to misleading and inaccurate directivity results (see Ch. 4). In contrast, repeated-capture systems often require extended recording periods but provide feature rich and highly detailed directivity data.

While high spatial resolution from repeated-capture systems provide great detail in directivity plots, it comes at the cost of longer recording sessions and inaccuracies resulting from repetition variations of live musicians. Measurement duration is a relatively minor inconvenience when compared to inconsistent measurement conditions, which call into question the validity of the entire approach. A validation of the stationarity of repeated-capture systems is thus necessary

for the continued use of such high-resolution systems. If specific methods can be trusted to provide accurate results, directivity-related research can take a significant leap forward.

Several tests were conducted on the BYU DMS using loudspeakers as simulated musicians to determine possible sources of error. Because the loudspeaker is a controlled output, the amplitude pitch and positions can be varied intentionally to simulate several nonideal characteristics of a live musician. The following sections outline the methods used to simulate playing variances and provide details of the resulting errors through directivity plots and other calculations. The techniques are only applied to the BYU system to validate its methodology. Other systems should also be validated using these techniques, but the work is beyond the scope of this thesis.

3.1 Methods

In order to trust and quantify the accuracy of the DMS results, a three-step method was instituted. The first was to measure loudspeakers, which are highly repeatable sources, using common broadband techniques. The second was to reproduce a prerecorded chromatic scale via the loudspeaker and compare the results of a processed note (utilizing a reference microphone as the input signal to the FRF) to those of the standard directivity measurement. Finally, a series of intentional random variations were introduced in the loudspeaker driving signal with each capture and to the loudspeaker's position in the rotating reference frame to simulate possible musician playing variances and test the limits of the system. The following sections provide additional details.

3.1.1 Loudspeaker Measurements

Standard loudspeaker measurements were taken of a Tannoy System 800. A series of five 1 s linear chirps were played through the loudspeaker at each azimuthal angle. The chirps were band limited from 20 Hz to 21.5 kHz. Several other signal types were tested for comparison, including logarithmic chirps, 2 s linear chirps, pseudo-random noise, and 19 s of white noise. The differences in the resulting directivity patterns were negligible, so the 1 s linear chirp was chosen because of its shorter recording period and self-windowing characteristics. Directivity was calculated using the power amplifier input signal as the reference for the various frequency response functions, as documented by Eyring [3]. The entire chirp was used in a single time record block, resulting in a 1 Hz frequency bin width. Five other loudspeakers were tested including: a Mackie HR824, a JBL LSR305, a single 2.5 cm driver in a 20 cm spherical baffle, a 20 cm dodecahedron loudspeaker, and a 30.5 cm horn with a 12.7 cm Electrovoice driver (the horn had parallel tapering angles of 30^{o} and 45^{o} over a 25.4 cm flange). The additional loudspeaker results are available in the supplemental material [4].

3.1.2 Simulated Musician Measurements

A Tannoy System 800 loudspeaker was used to simulate a live musician by first changing its input signal from a noise or chirp to previously recorded chromatic scales played by a real musician in an anechoic chamber. In principle, the directivity results of harmonic frequencies of the chromatic scales should be identical to those of the conventionally measured loudspeaker at the same frequencies. This allows for a measurable figure of merit for the system's accuracy by calculating the area-weighted root mean square (RMS) error it produces when compared to the

standard loudspeaker directivity method. The area weighting ensures that each microphone position contributes equitably to the calculation [5].

In order to mimic the lack of electrical reference signal when recording musical instruments, three additional microphones were used to provide reference signals for the FRFs. These microphones rotated with and therefore remained stationary within the reference frame of the loudspeaker. Using three distinct reference microphones placed randomly around the loudspeaker increased the chances of at least one of them having a continuously good signal-to-noise ratio over the entire spectrum—regardless of a possible complex radiation pattern from the source.

Subsequently several controlled tests were then performed to investigate error due to musician inconsistencies by intentionally altering the amplitude, pitch, and position of the loudspeaker. All variations were first introduced independently to analyze the effects of each in isolation. They were then combined to determine the maximum overall error that might be anticipated for a live musician using the DMS.

Amplitude errors were simulated by adjusting gain levels of the loudspeaker driving signal by a random value between ± 12 dB at each rotational orientation. Pitch variation was simulated by randomly shifting the entire scale between ±20 cents from the original recording at each orientation. This was done using the simple pitch-shifting plug-in ReaPitch standard in the REAPER audio software package used for data recording.

During live musician recordings with the DMS, a small laser was attached to the instrument with a requirement that the musician ensure the beam hit a 2.5 cm square target at all times while playing. The radial positioning of the target would be altered for each musician, but on average,

the musician was held to a 2.5 cm maximum translational variation and a 1.5^{o} angular variation in both the azimuthal and polar angles. These conditions were simulated by physically moving the loudspeaker during the simulated musician tests by random values within these same tolerances with each rotational increment.

3.2 Results

3.2.1 Loudspeaker

A Tannoy System 800 loudspeaker was measured due to its dual-concentric driver design, having both the woofer and tweeter collocated along the same axis. It did not have physical driver separation in the baffle plane to cause directivity interference patterns in the crossover region. Instead, it generally produced a single lobe that narrowed with frequency around the loudspeaker axis. The directivity measurement of the Tannoy served as the standard to which simulated musician measurements were compared. Directivity balloons at several key frequencies are also included in Figs. 3.1 and 3.2. More directivity images and animations for the Tannoy and other loudspeakers can be viewed in the supplemental material [4].

The directivities in these figures are represented as balloon plots, where amplitude is represented by both color and radius of the balloon. The main axis of the Tannoy was aligned with the 0^{o} azimuthal and 90^{o} polar angles. All values have been normalized to the maximum amplitude location over the sphere at each frequency, with an arbitrary 0 dB to -40 dB radial scale. Values below -40 dB down from the maximum are visualized as -40 dB for plotting purposes. Loudspeaker directivity balloons shown in this chapter utilize a 10 Hz bandwidth for comparison to simulated musician directivities. As a result of the narrow bandwidth, latitudinal banding was

visible for some directivity balloons (see Fig.3.2) that were not attributable to the loudspeaker radiation pattern. Upon further investigation it was found that these bands varied with frequency but are not due to microphone calibration errors. Rather, it was a result of free-field deviations in the anechoic chamber and the fixed arc array microphone positions. Qualification standards utilizing 1/3rd octave band measurements for allowable spatial variations [6] do not fully quantify spatial variations for narrow-band data. Further details on this matter are provided in Ch. 5.

For all balloon plots of both the simulated musician and the standard loudspeaker measurements, the axis of the loudspeaker is oriented toward the 0^{o} azimuthal marker in the figures. The simulated musician signal used to generate all figures in this section was the recording of an F4 played by a trumpet. The result in Fig. 3.3 shows the second harmonic of this note as measured by the DMS. This and other notes were played for a single second to simulate a live musician and mimic an actual measurement. To use only the steady-state portion of the note, the processed time was reduced to 0.85 s, meaning a 1 Hz resolution was not practical. Therefore, both the simulated musician and standard loudspeaker measurements presented here utilized a 10 Hz resolution.

After the initial comparison was completed, various attributes of the trumpet signal were altered independently of one another. Amplitude variations were randomly introduced in single decibel increments within ± 12dB from the standard operating level with every rotation. Random pitch variation was then introduced by digitally altering the trumpet recording each time the turntable was moved 5^{o} by up to ± 20 cents.

Most professional musicians have the ability, with the aid of a tuner, to play notes well within ±20 cents repeatedly. This requirement was initially placed on musicians to control pitch

variation as the musician was rotated. However, after recording several instruments, it was found that this tolerance was considerably larger than needed, as musicians could typically remain within ±10 cents with relative ease. This new tolerance was introduced for the final eight instruments recorded in the study. However, to simulate worst-case scenarios, the pitches of simulated musicians were randomly adjusted within the ±20 cent tolerance with every rotational increment.

Three positional variations were also introduced independently of each other to analyze the effects of each type of movement. They included a source translation in the transverse plane, as well as an azimuthal and polar rotation in the rotating reference frame to the previously stated tolerances. These were followed by a combination test wherein both rotational and translational variations were utilized concurrently.

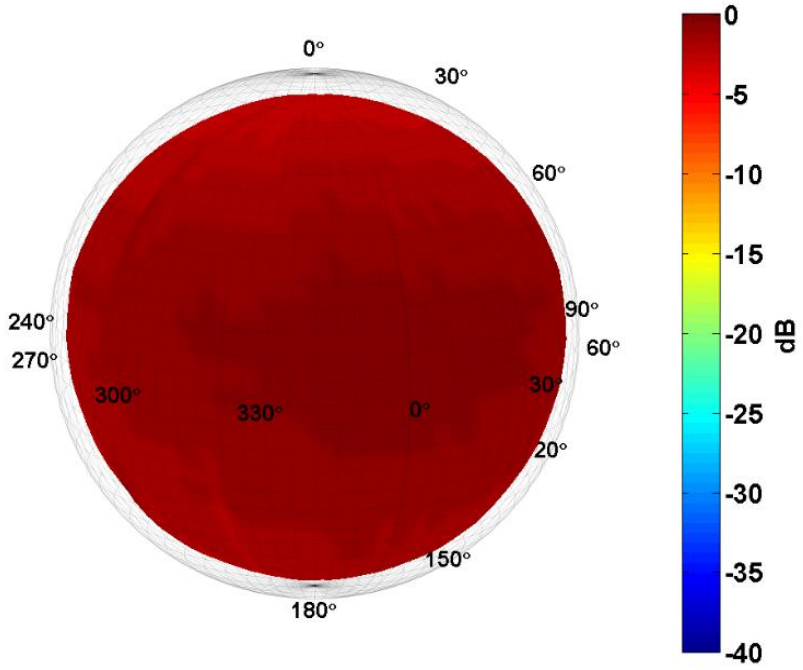

Figure 3.1. Directivity balloon of the Tannoy System 800 loudspeaker at 100 Hz.

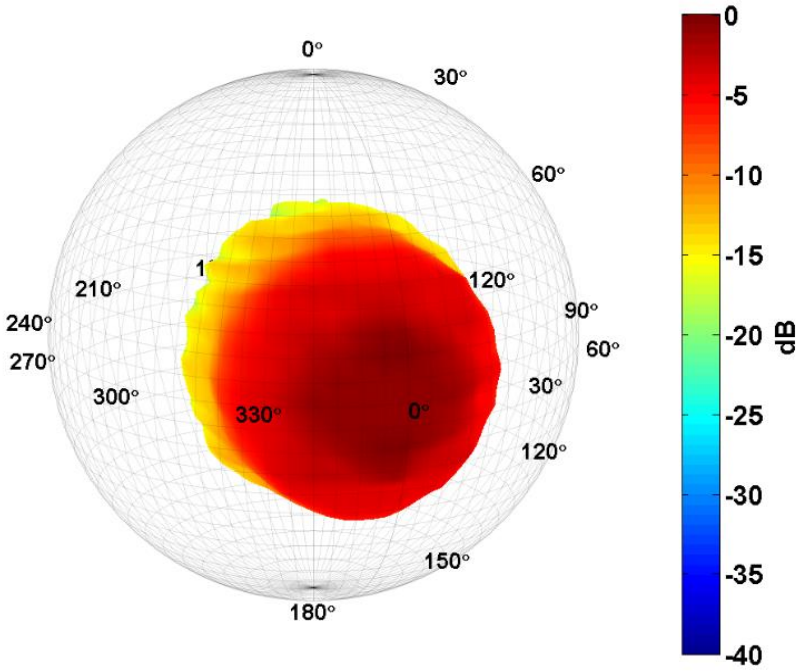

Figure 3.2. Directivity balloon of the Tannoy System 800 loudspeaker at 8 kHz.

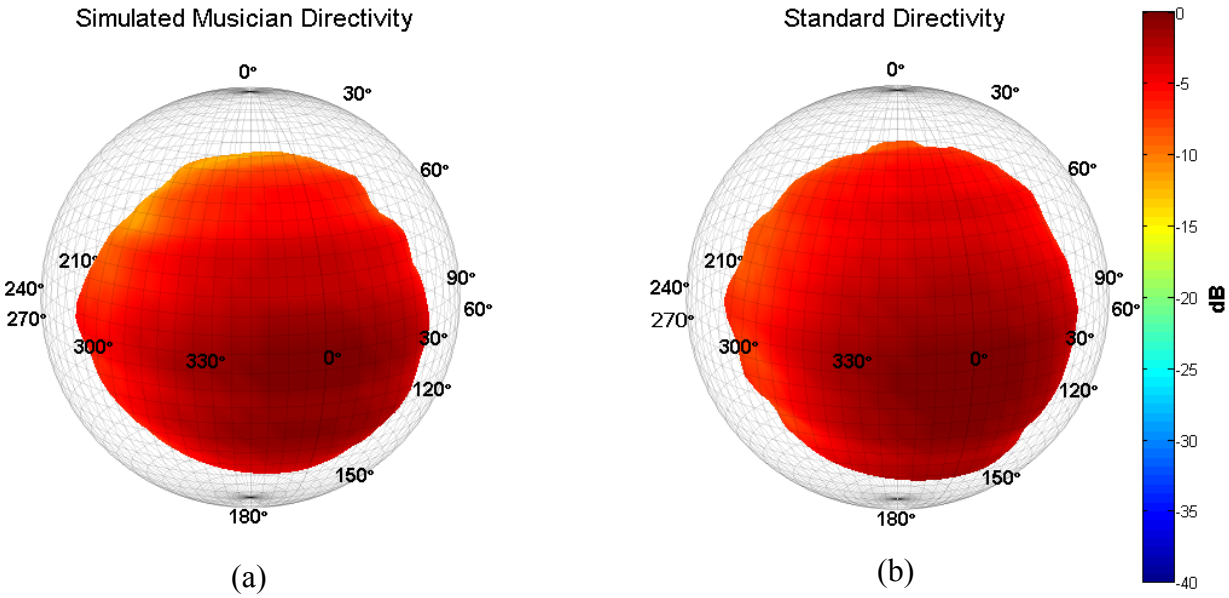

Figure 3.3. (a) Directivity at 700 Hz of a simulated musician with no signal alterations, played through a Tannoy 800 Series loudspeaker using a trumpet recording of an F4. (b) Standard swept sine directivity measurement of a Tannoy 800 Series loudspeaker at 700 Hz.

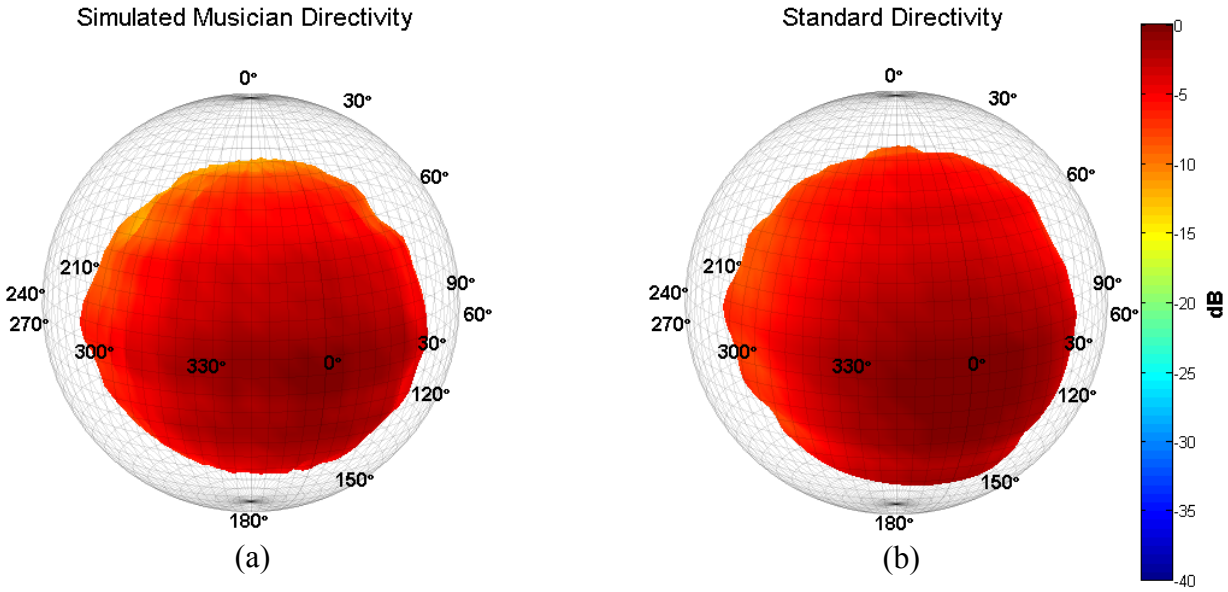

Figure 3.4. (a) Directivity at 700 Hz of a simulated musician with amplitude, pitch, and all position alterations. (b) Standard swept sine directivity measurement of a Tannoy 800 Series loudspeaker at 700 Hz.

A final simulated musician experiment combined amplitude, pitch, and all position variations. A single-frequency result is shown in Fig. 3.4. This introduced a probable worst-case scenario wherein every possible inconsistency from a musician occurred at every incremental rotation. In reality, the variation simulated through this measurement was expected to be far greater than that produced by actual musical instrument recordings.

3.3 Analysis

Visual representations of directivities in the forms of balloon plots are often difficult to compare concretely to one another. Interpretations of amplitude values leave significant room for speculation and are therefore not sufficient for validating the system as a viable method of measuring musical instrument directivity. Therefore, an area-weighed RMS error of levels $[E_{rms}(f)]$ was calculated at each harmonic frequency as a more quantitative metric of consistency.

The arithmetic error between two directivity level measurements was calculated as

$$E_{\mathrm{rms}}(f) = \sqrt{\frac{\sum_{m=1}^{M}\sum_{n=1}^{N} S_{m,n}\left[L_{M_{m,n}}(f) - L_{L_{m,n}}(f)\right]^2}{\sum_{m=1}^{M}\sum_{n=1}^{N} S_{m,n}}}\,, \tag{3.1}$$

where $L_{M_{m,n}}$ represents the level of the simulated musician measurement and $L_{L_{m,n}}$ represents the level of the standard loudspeaker measurement. Here, the subscript indices m, n represent the index values for polar and azimuthal angles respectively. They are calculated according to Eq. (2.5) with sampling areas

$$\begin{aligned} S_{m.n} &= \int_{\phi_n+\frac{\Delta\phi}{2}}^{\phi_n+\frac{\Delta\phi}{2}} \int_{0}^{\Delta\theta/2} r^2 \sin(\theta)\, d\theta d\phi \\ &= 2r^2\Delta\phi \sin^2\left(\frac{\Delta\theta}{4}\right) = \frac{4\pi r^2}{N}\sin^2\left(\frac{\Delta\theta}{4}\right),\ m = 0\,,36 \end{aligned} \tag{3.2}$$

and

$$\begin{aligned} S_{m.n} &= \int_{\phi_n+\frac{\Delta\phi}{2}}^{\phi_n+\frac{\Delta\phi}{2}} \int_{\theta_m-\Delta\theta/2}^{\theta_m+\Delta\theta/2} r^2\, sin(\theta)\, d\theta d\phi \\ &= 2r^2\Delta\phi\, sin(\theta_m)\, sin\left(\frac{\Delta\theta}{2}\right),\ 1 \le m \le\ 35. \end{aligned} \tag{3.3}$$

where, in this study, $\Delta\theta = \Delta\phi = 5^o$. These are the same areas as those used by Leishman et al. [5] to calculate area-weighted standard deviations of directivity balloons.

The error results of the simulated musician studies are shown in Table 3.1 and consist of the lowest errors produced in each cell using any of the three reference microphones. The RMS

Table 3.1. Area-weighted RMS error of levels from a simulated musician. Errors are shown for the first five harmonic frequencies from a prerecorded trumpet playing an F4. They are tabulated for each variation. The position condition includes shifts from the translation, azimuthal angle, and polar angle categories combined. The all shifts condition includes amplitude, pitch, and position categories alterations.

	Frequency				
Variation Condition	350 Hz	700 Hz	1050 Hz	1400 Hz	1750 Hz
No Variation (reference microphones)	0.0	0.7	0.2	0.6	0.8
Amplitude	0.2	0.5	0.2	0.5	1.2
Pitch (within ±20 cents)	0.2	0.7	1.0	0.6	0.4
Translation	0.2	0.2	0.3	0.4	0.2
Azimuthal angle	0.3	0.8	1.0	1.0	0.7
Polar angle	0.2	1.3	0.2	1.2	0.7
Position	0.7	0.5	1.3	1.2	1.3
All Shifts	0.3	1.3	1.0	0.6	1.1

errors produced using the DMS due to the amplitude, pitch, and position variations were reasonably low. All were less than 1.3 dB and many fell under 1.0 dB. This is significant, as these RMS values, obtained for 10 Hz bin widths, are within allowable errors used to qualify anechoic chambers due to spatial deviations in 1/3rd octave bands. As seen in the first row of the table, the simulated musician with no variations had the low error values at each frequency. These errors were associated with utilizing reference microphones to provide the input signal. In some cases, variations to simulated musician measurements resulted in slightly lower error values that were typically within several tenths of a decibel. Some isolated variations or multiple simultaneous variations may have produced compensatory effects that lessened the reference microphone errors on those of another individual variation test on its own. As variations in amplitude, pitch, and position of the simulated musician were greater than those that would typically occur for an actual

musician, this study placed bounds on the maximum expected deviations due to musician inconsistencies that were within standard anechoic chamber tolerances [6].

Although the standard loudspeaker and simulated musician measurements were both taken with the same microphone array, the former used the signal driving the loudspeaker rather than the output signal of a reference microphone as the input signal for the FRF. Reference microphones used in simulated musician measurements rotate with the source, resulting in a different pressure measurement location with each incremental rotation. This effect was not present in the standard loudspeaker measurement because the reference signal was simply the digital signal provided to the loudspeaker prior to D/A conversion and amplification. Reference microphones for simulated musician measurements were relatively calibrated, but no correction was made for differences due to spatial variations in the chamber. This is one cause of errors introduced in the simulated musician measurements.

Another feature that is common to many of the simulations is the appearance of minor longitudinal banding in the directivity data. The bands are more visually pronounced near the poles and smoother near the equator. They result from either changes in pitch or position of the loudspeaker within the rotating reference frame. Initially, it was assumed to be an error in the directivity calculation algorithm, but when a simulated musician signal remains unaltered during rotations, the banding is not present (see Fig. 3.3). Further investigation revealed that the magnitude of the bands increased as the allowed position and/or pitch variation increased.

With regard to pitch variation, suspicion also focused on the peak-finding algorithm, which determined the spectral bin in the directivity data for calculations. Initially, a single bin was chosen for the entire sphere, for each harmonic of every note. Based on allowed pitch variations, the

algorithm searched within fixed bounds of the true fundamental and assumed harmonic frequencies (with A4 = 440 Hz tuning) to select the bin with the maximum autospectrum value. Numerous variations were tried including (1) using the maximum coherence to locate the frequency bin, (2) summing several bins over which the energy was spread, and (3) choosing bins for every rotation increment, independent of the others. Additionally, four separate windowing functions were tested (Hanning, Hamming, flat top, and Blackman), as well as various bin widths from 2.9 Hz to 100 Hz. All algorithm variations were implemented both separately and in combination with one another, but did not provide significant benefits in longitudinal band reduction.

Near-field effects at the reference microphone positions were also suspicious since they were not present at the arc microphones and could have contributed to these bands. However, tests were run using both a far-field microphone signal and the digital excitation signal as references. These tests resulted in the same longitudinal bands, thus casting doubt on the relationship of a reference microphone position to the arc microphones as the culprit causing the effect. Further work is needed to completely isolate the sources of these errors.

References

[1] M. Pollow, "Measuring directivities of musical instruments for auralization," Fortschritte der Anustin: Tagungsband **35**, 1471-1473 (2009).

[2] F. Hohl, "Kugelmikrofonarray zur Abstrahlungsvermessung von Musikinstrumenten" ("Spherical microphone array for radiation survey of musical instruments"), Master's thesis, University of Music and Performing Arts, Graz, Austria (2009) [available at <http://old.iem.at/projekte/acoustics/musik/kugel/hohl.pdf > (last viewed December 7, 2015)].

[3] N. J. Eyring, "Development and Validation of an Automated Directivity Acquisition System Used in the Acquisition, Processing, and Presentation of the Acoustic Far-Field Directivity of Musical Instruments in an Anechoic Space," M.S. thesis, Brigham Young University, Provo, UT (2013), available online through Brigham Young University Electronic Theses & Dissertations at <http://etd.lib.byu.edu> (Last viewed December 7, 2015).

[4] K. J. Bodon, "Masters Thesis Supplemental Materials," Brigham Young University (2016) [available at <http://scholarsarchive.byu.edu/etd/5653/>]

[5] T. W. Leishman, S. Rollins, and H. Smith, "An experimental evaluation of regular polyhedron loudspeakers as omnidirectional sources of sound," J. Acoust. Soc. Am. **120**, 1411-1422 (2006).

[6] ISO 3745:2012: Acoustics—Determination of sound power levels of noise sources using sound pressure—Precision methods for anechoic and hemi-anechoic rooms (International Organization for Standardization, Geneva, Switzerland).

Chapter 4

Repeated-Capture vs. Single-Capture Systems

A DMS may be placed into one of two general measurement categories: single-capture or repeated-capture systems. Single-capture systems typically incorporate microphone arrays surrounding an acoustic source and capture directivity with a single multichannel measurement [1], [2], [3]. Repeated-capture systems contain one or more microphones that either remain stationary while the source is rotated or rotate while the source remains stationary. Measurements are taken for several different orientations then combined to create a complete directivity pattern.

As outlined in Ch. 1, the decision of which system to use is complex and is often determined by the type of source to be measured. Loudspeakers are easily manipulated and produce repeatable signals, so there is little reason to complete a directivity measurement using a single-capture system at low resolution when a higher resolution can be achieved. The Audio Engineering Society standard AES56-2008 requires that type A loudspeaker directivity be taken at 5^{o} resolution over a sphere for directivity measurements [4]. This results in 2,522 unique

microphone locations. To build a single-capture measurement system with this many microphones is impractical, so repeated-capture systems are universally used.

In contrast to loudspeakers, when musical instruments are the sources and played by musicians, they prove difficult to measure with repeated-capture systems. Even the most accomplished musicians will vary slightly in pitch, amplitude, and physical position with every repetition, and eventually tire. Since no standard exists to dictate the resolution for musical instrument directivity measurements, single-capture systems have been used to avoid musician error. The number of microphones in single-capture systems has ranged from 22 to 64. They are typically arranged in a spherical array having nearly equal spacing over the sphere [1], [3].

Some groups have attempted to measure musical instruments at higher resolution using multiple-capture systems, but attempt to reduce musician errors as much as is possible during recording and processing [5], [6]. The systems vary in resolution, with only Eyring producing measurements at the loudspeaker standard resolution of 5^{o} [5]. With such diversity in DMSs, it becomes very challenging for musical instrument directivity research to progress with consistency. It is difficult to compare quantitative results from one group with that of another without a considerable amount of estimation.

Because each system has drawbacks, it is difficult to know if there is a superior method of measuring the directivity of musical instruments. Is it more important to have directivities free of musician error or to have high spatial resolution to observe fine details? A comparison is made in this chapter of the two methodologies by using both a 32-point single-capture system and the developed 2,522-point repeated-capture system.

4.1 Methods

Two separate systems were constructed in a qualified anechoic chamber at BYU with a low-frequency anechoic cutoff frequency of approximately 80 Hz. Both systems utilized Focusrite RedNet analog-to-digital converters and the REAPER digital audio workstation software. Measurements were taken at a 48 kHz sampling frequency and a 24 bit depth. Microphones were relatively calibrated over frequency, and measurements were made using a Mackie HR824 loudspeaker, a 20 cm dodecahedron loudspeaker, a bass clarinet, and a trumpet. Both musical instruments were played by the same musicians for both measurement systems.

The first measurement system tested was the repeated-capture system described earlier, consisting of a semicircular vertical array of 37 microphones spaced 5^{o} apart [see Fig. 4.1 (a)]. The source was placed on a rotating pedestal turntable and measurements were taken at 5^{o} azimuthal increments. Directivity was calculated using FRFs. Loudspeaker measurements utilized the input signal as the reference. The musical instrument measurements involved three reference microphones to generate reference signals [5], [7].

The repeated-capture system was subsequently disassembled and a single-capture spherical array of 32 microphones was erected in its place. This number of microphones was chosen simply because it was the largest array possible given the number of available microphones that could also be conveniently arranged into a spherical pattern. The microphones were suspended from the ceiling and cable floor using fishing line in a pentakis dodecahedron shape [8], with a 1.83 m radius. The angular locations of each microphone are shown in Table 4.1. Directivity for loudspeakers and musicians were calculated using the same methods as the repeated-capture system. For consistency between the two systems, the turntable was left in the chamber and the

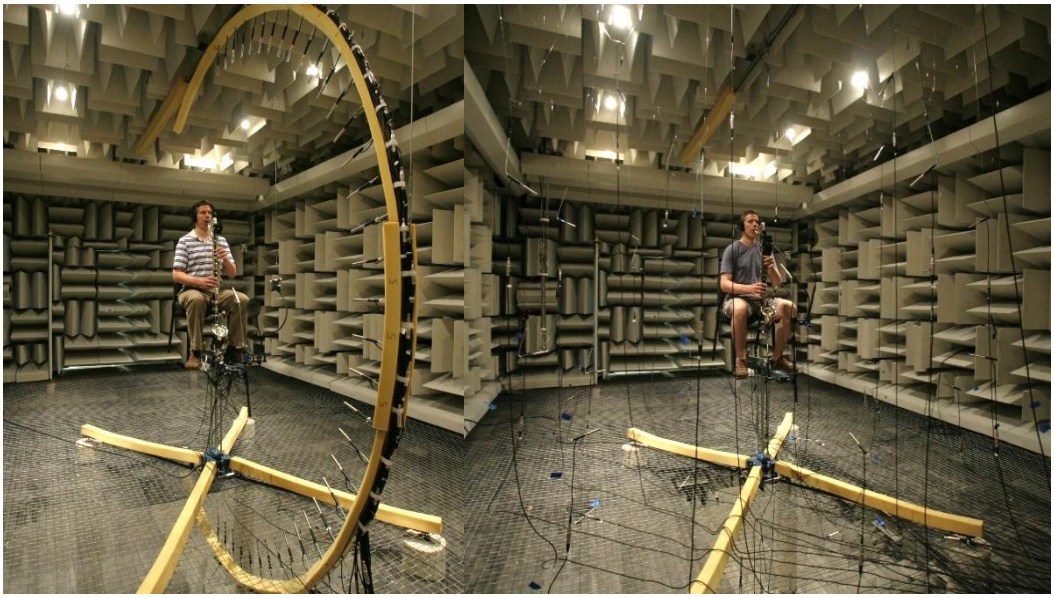

(a) (b)

Figure 4.1. (a) Repeated-capture DMS. (b) Single-capture DMS.

Table 4.1. Spherical coordinates for each of the 32 microphones in the single-capture directivity system. Each microphone was placed at a radius of 1.83 m.

Microphone Placement Angles

θ	ϕ	θ	ϕ	θ	ϕ
0.0	90.0	79.2	330.0	100.8	270.0
41.8	90.0	70.5	292.2	109.5	232.2
37.4	30.0	70.5	247.8	109.5	187.8
41.8	330.0	79.2	210.0	138.2	150.0
37.4	270.0	70.5	172.2	142.6	90.0
41.8	210.0	100.8	150.0	138.2	30.0
37.4	150.0	109.5	112.2	142.6	330.0
70.5	127.8	109.5	67.8	138.2	270.0
79.2	90.0	100.8	30.0	142.6	210.0
70.5	52.2	109.5	352.2	180.0	270.0
70.5	7.8	109.5	307.8		

center of the array remained constant for both measurement systems (see Fig. 4.1). Sources were placed in the same orientation relative to the room for both systems. When producing balloon plots for both systems a standard linear interpolation was used to fill in the gaps between microphones.

4.2 Results

The resulting balloon plots for the loudspeakers are shown in Figs. 4.2 through 4.5. Musical instrument plots are shown in Figs 4.6 through 4.10. If a loudspeaker had a definable main axis, it was aligned to $\theta = 90^o, \phi = 0^o$. Musical instruments were aligned with the musician facing $\phi = 0^o$ and the geometric center of the assumed radiating portion of the instrument centered in the array. Each plot displays two opposite views of the same directivity pattern for each system. Directivity balloons have a 10 Hz bin width.

4.2.1 Mackie HR824

Measurements were first taken for a Mackie HR824 loudspeaker. This is a two-way system containing a woofer under a tweeter with a crossover region near 1.6 kHz. Results for 1 kHz and 1.6 kHz are shown in Figs. 4.2 and 4.3, respectively.

4.2.2 Dodecahedron Loudspeaker

Another set of measurements was taken using a dodecahedron loudspeaker with a 20 cm diameter. While it had a loudspeaker driver on each of its 12 faces, it had no crossover frequency and all drivers radiated in phase. This type of loudspeaker is nominally omnidirectional, up to a certain cutoff frequency [7]. The loudspeaker tested had a cutoff frequency near 2 kHz. Its

directivity results from each system are shown in Figs. 4.4 and 4.5 for 125 Hz and 4 kHz, respectively.

4.2.3 Bass Clarinet

As stark as the comparisons are for loudspeaker measurements, these systems were designed with musical instruments, not loudspeakers, in mind as the source of sound. Musical instruments were accordingly evaluated with both systems to determine the value of utilizing a high-resolution system for instrument directivities. Results for several frequencies are presented here of a bass clarinet and a trumpet (see Figs. 4.6 through 4.10). In both cases the identical instrument and musician were used. Careful consideration was also taken to ensure that the musician's chair and peripherals were exactly the same in both instances.

Figures 4.6 and 4.7 show the fundamental and 5^{th} harmonic of a bass clarinet playing a D3. The fundamental frequency is low and the nearly omnidirectional patterns look very similar between the two systems as expected. However, as frequency increases, the directivity patterns become more complex and differences are clearly visible between the results of the two system types.

4.2.4 Trumpet

Figures 4.8 through 4.10 show the directivity patterns for three frequencies (440 Hz, 990 Hz and 2,470 Hz) played by a trumpet. At the fundamental frequency of an A4, distinct differences are already noticeable, especially behind the instrument. As frequency increases, the high-resolution system becomes choppier, while the 32–point measurement remains smooth.

However, the smooth balloon is a product of the considerable interpolation required to produce a full balloon from 32 data points and is expected to have a smoother pattern.

4.3 Analysis and Discussions

With a single-capture spherical array, the recording times, file sizes, and computational costs are significantly reduced because only a single multichannel measurement is required. Table 4.2 provides a comparison of the average number of hours and file sizes required by each system per instrument. Recording times reflect only the period where the musician was playing, as identical setup time was required for both systems to position the musician and instrument appropriately. Single-capture systems provide a clear advantage in all categories.

A single frequency-dependent value is useful to more generally quantify the differences between the directivity results of the two systems. For loudspeakers, the area-weighted RMS error between the two DMSs was calculated as follows:

$$E_{\mathrm{rms}}(f) = \sqrt{\frac{\sum_{m=1}^{M}\sum_{n=1}^{N} S_{m,n}\left[L_{S_{m,n}} - L_{R_{m,n}}\right]^2}{\sum_{m=1}^{M}\sum_{n=1}^{N} S_{m,n}}}\,, \tag{4.1}$$

where $L_{S_{m,n}}$ represents the level of the single-capture system and $L_{R_{m,n}}$ represents that of the repeated-capture system. All other variables are described in Sec. 3.3.

4.3.1 Loudspeakers

The RMS errors are plotted over frequency for the Mackie HR824 and the dodecahedron in Fig. 4.11. Instrument data were not calculated using this metric due to the sparseness of spectral data and because there is not a consensus on what should be used as the standard for error

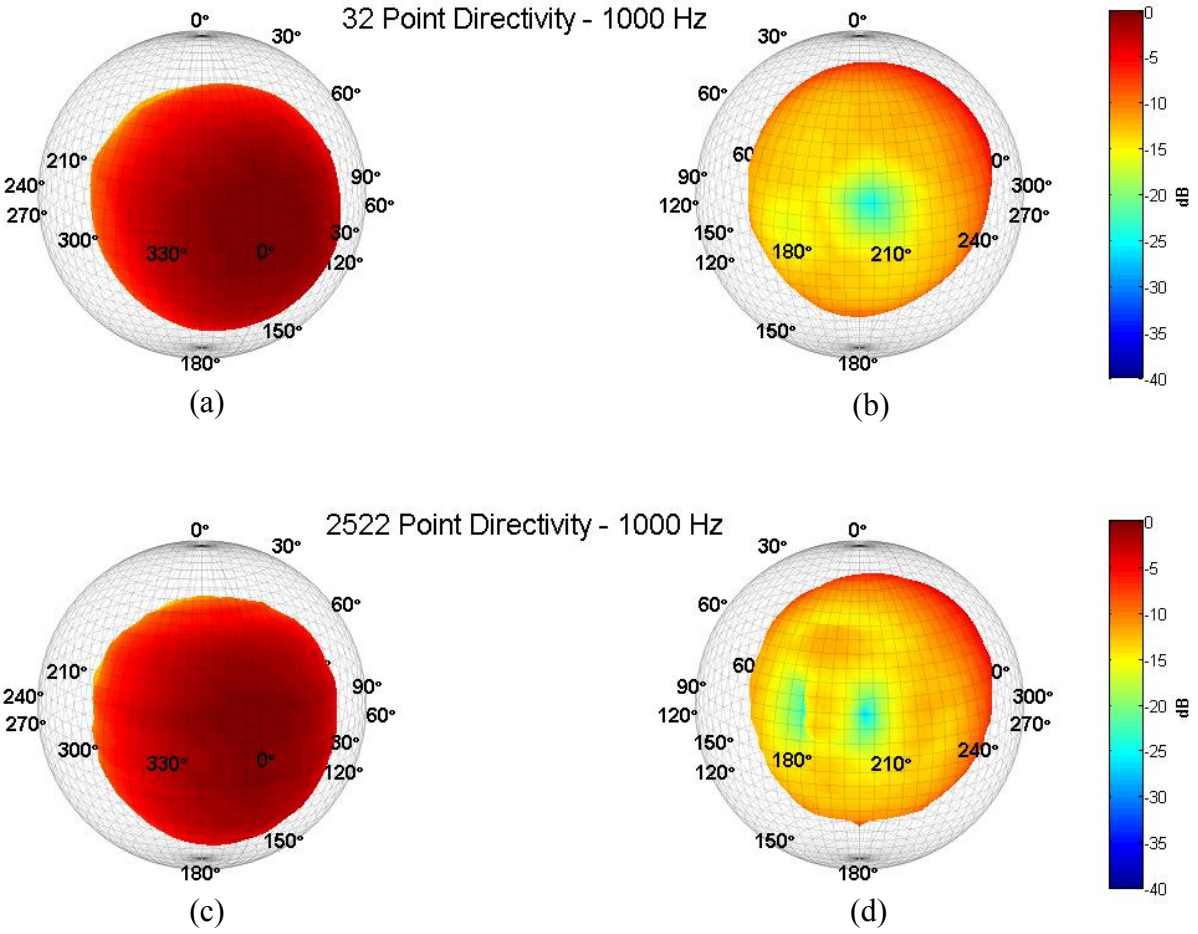

Figure 4.2. Directivity of a Mackie HR824 at 1 kHz. (a) Front hemisphere of the directivity balloon using the single-capture system. (b) Back hemisphere of the balloon using the single-capture system. (c) Front hemisphere of the directivity balloon using the repeated-capture system. (d) Back hemisphere of the balloon using the repeated-capture system.

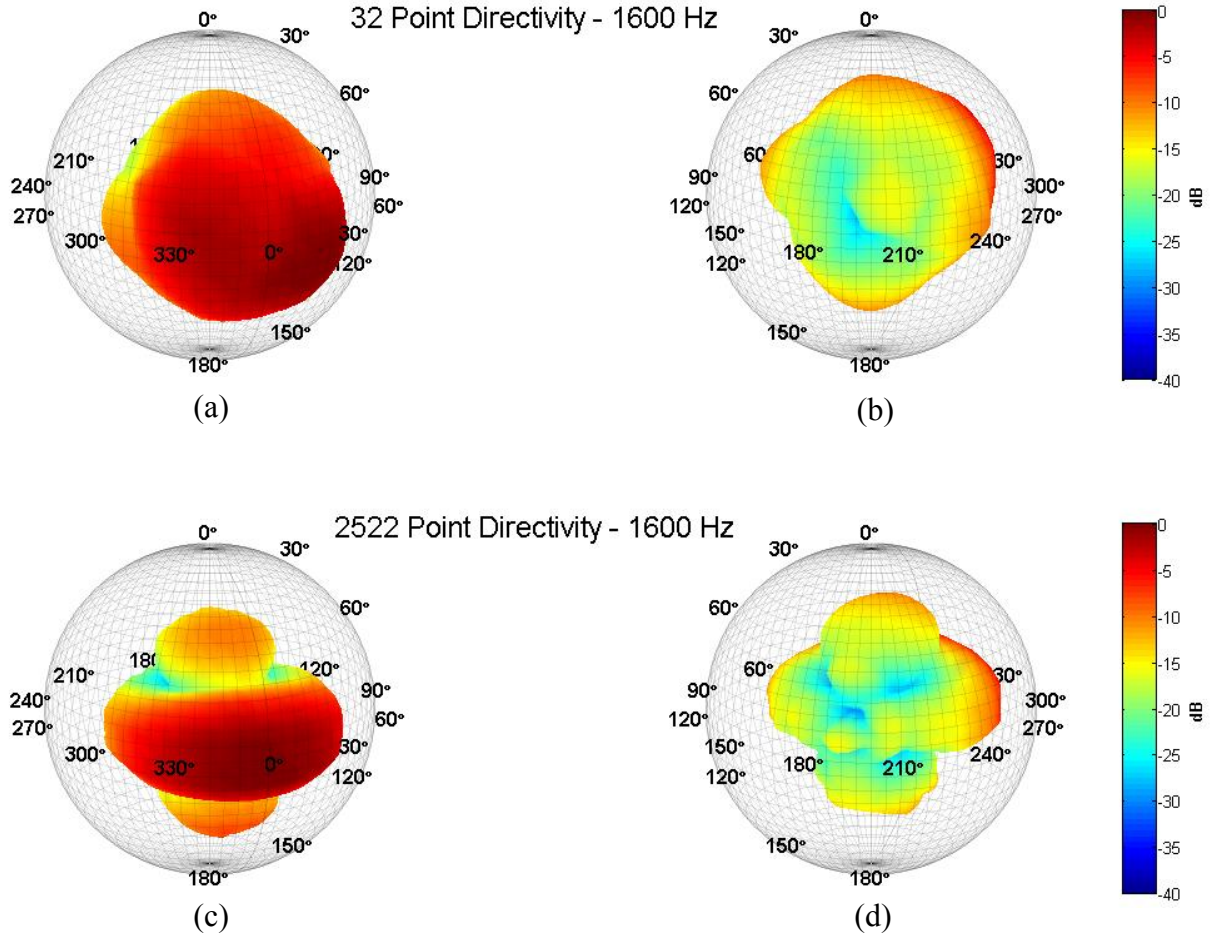

Figure 4.3. Directivity of a Mackie HR824 at 1.6 kHz. Plots (a) through (d) are arranged as described in Fig. 4.2.

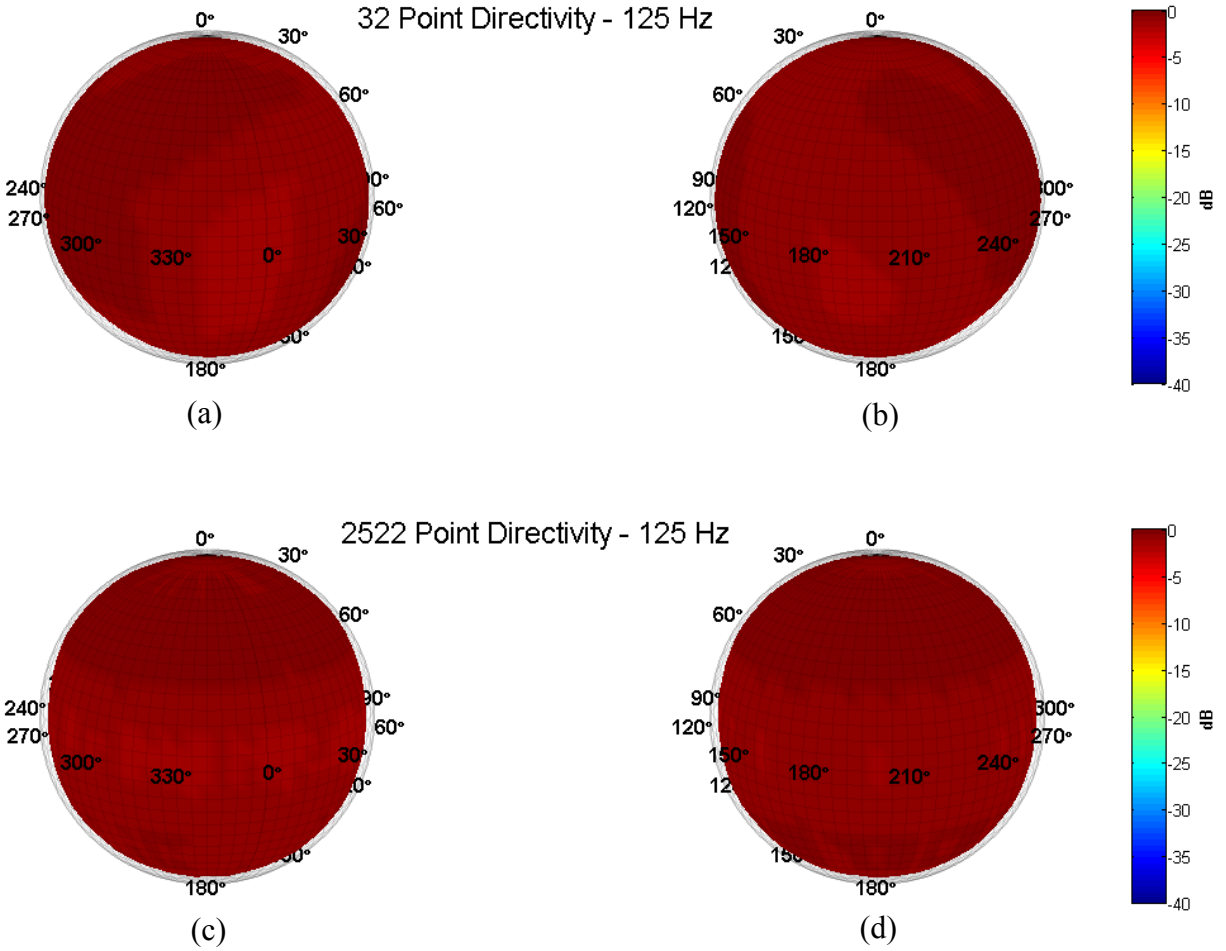

Figure 4.4. Directivity of a 20 cm dodecahedron loudspeaker at 125 Hz. Plots (a) through (d) are arranged as described in Fig. 4.2.

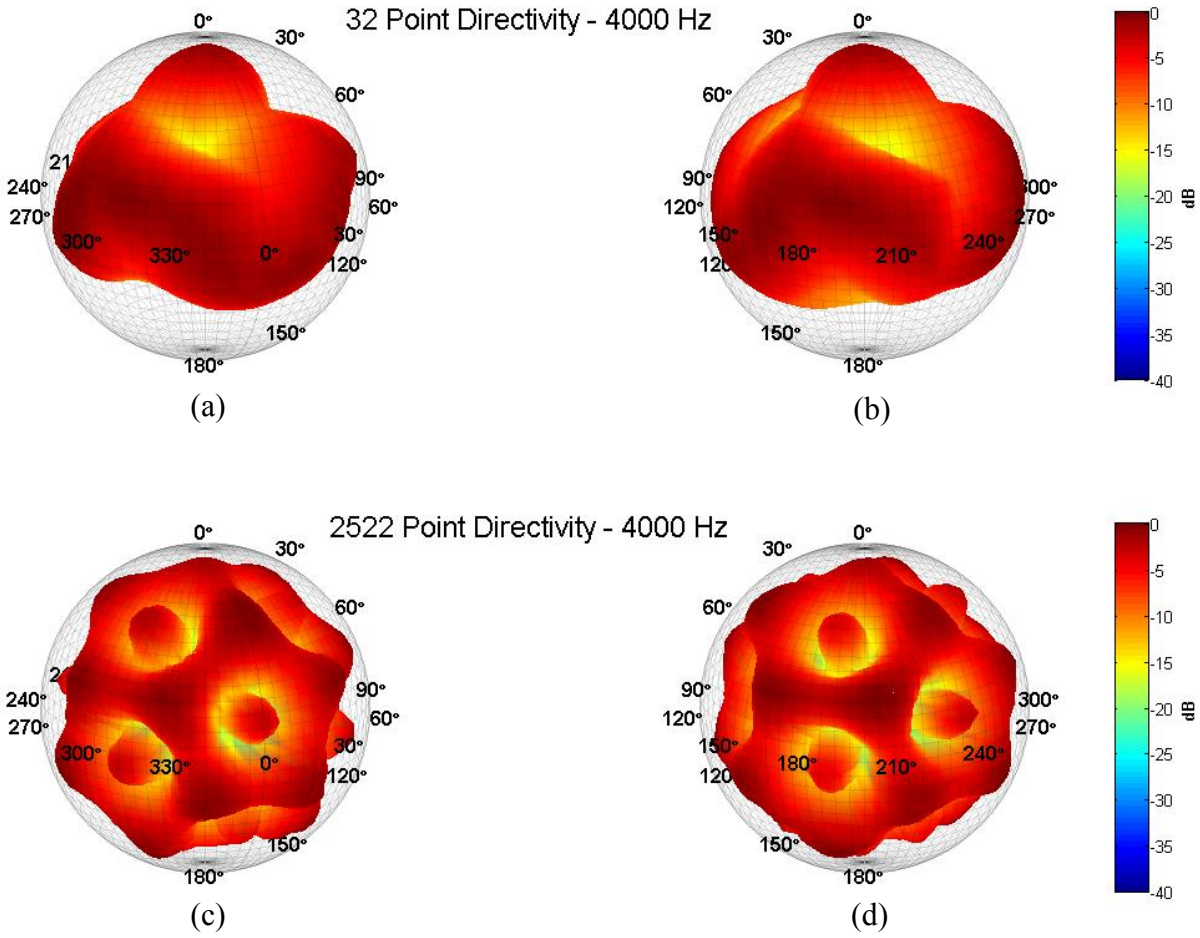

Figure 4.5. Directivity of a 20 cm dodecahedron loudspeaker at 4 kHz. Plots (a) through (d) are arranged as described in Fig. 4.2.

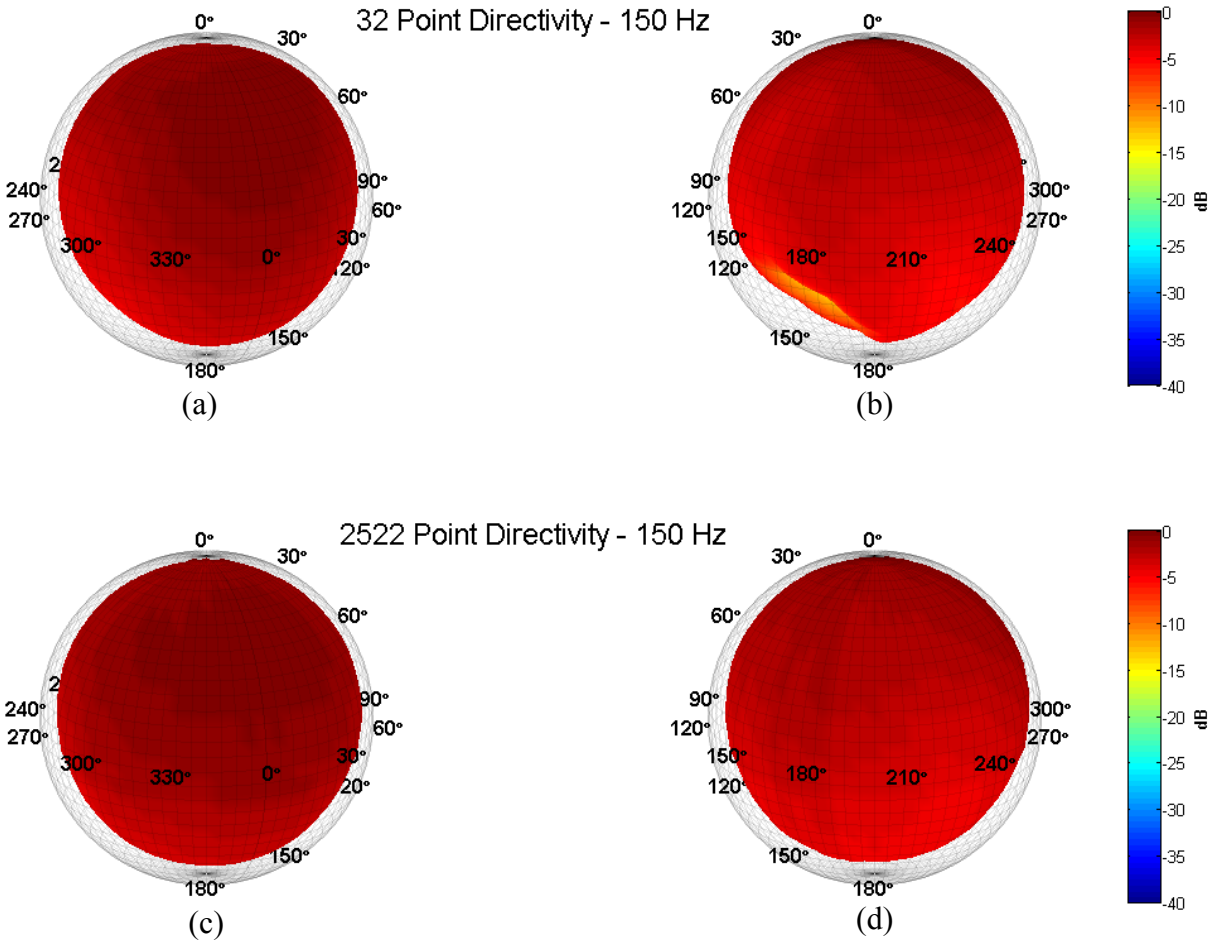

Figure 4.6. Directivity of a Bass Clarinet at 150 Hz. Plots (a) through (d) are arranged as described in Fig. 4.2.

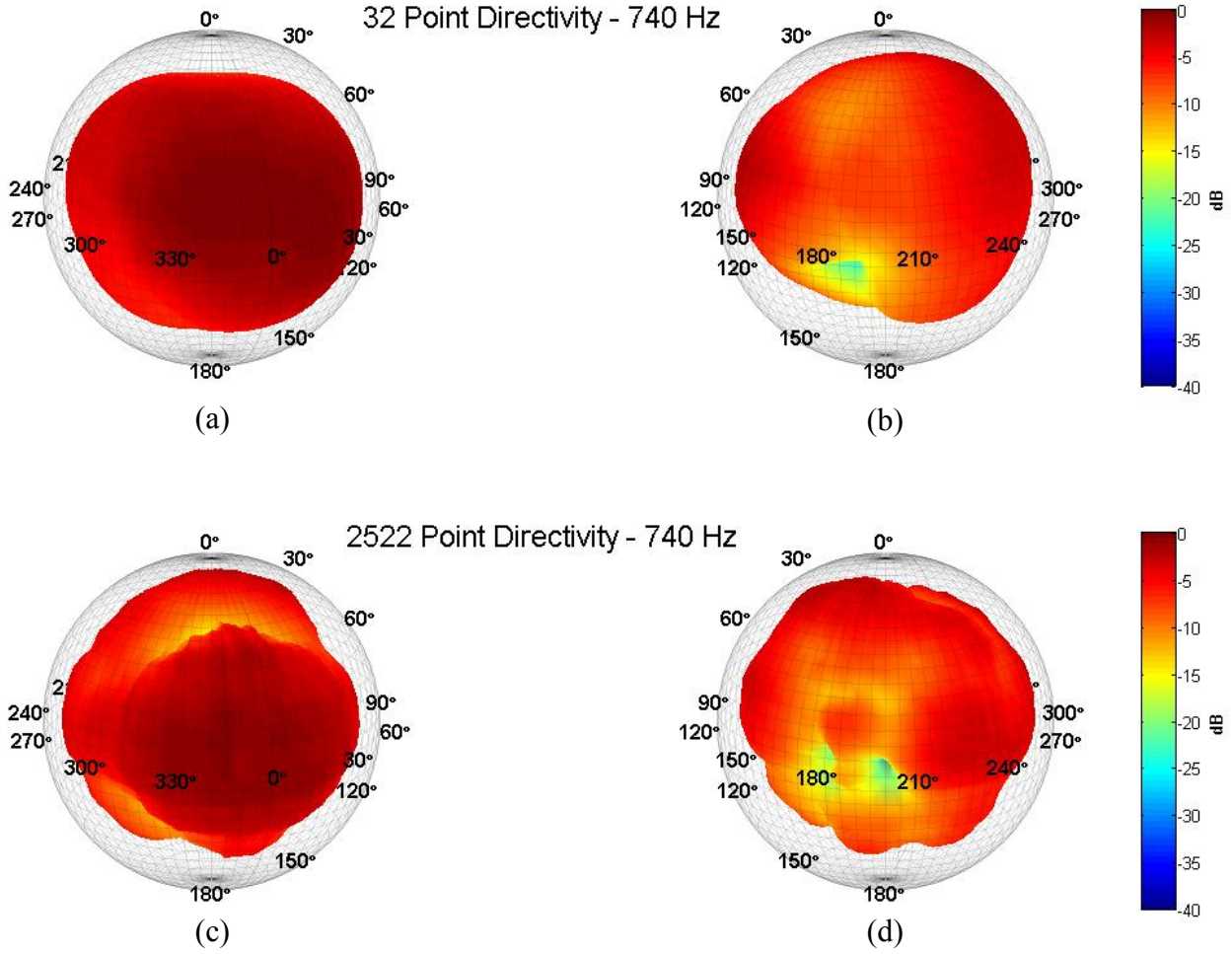

Figure 4.7. Directivity of a Bass Clarinet at 740 Hz. Plots (a) through (d) are arranged as described in Fig. 4.2.

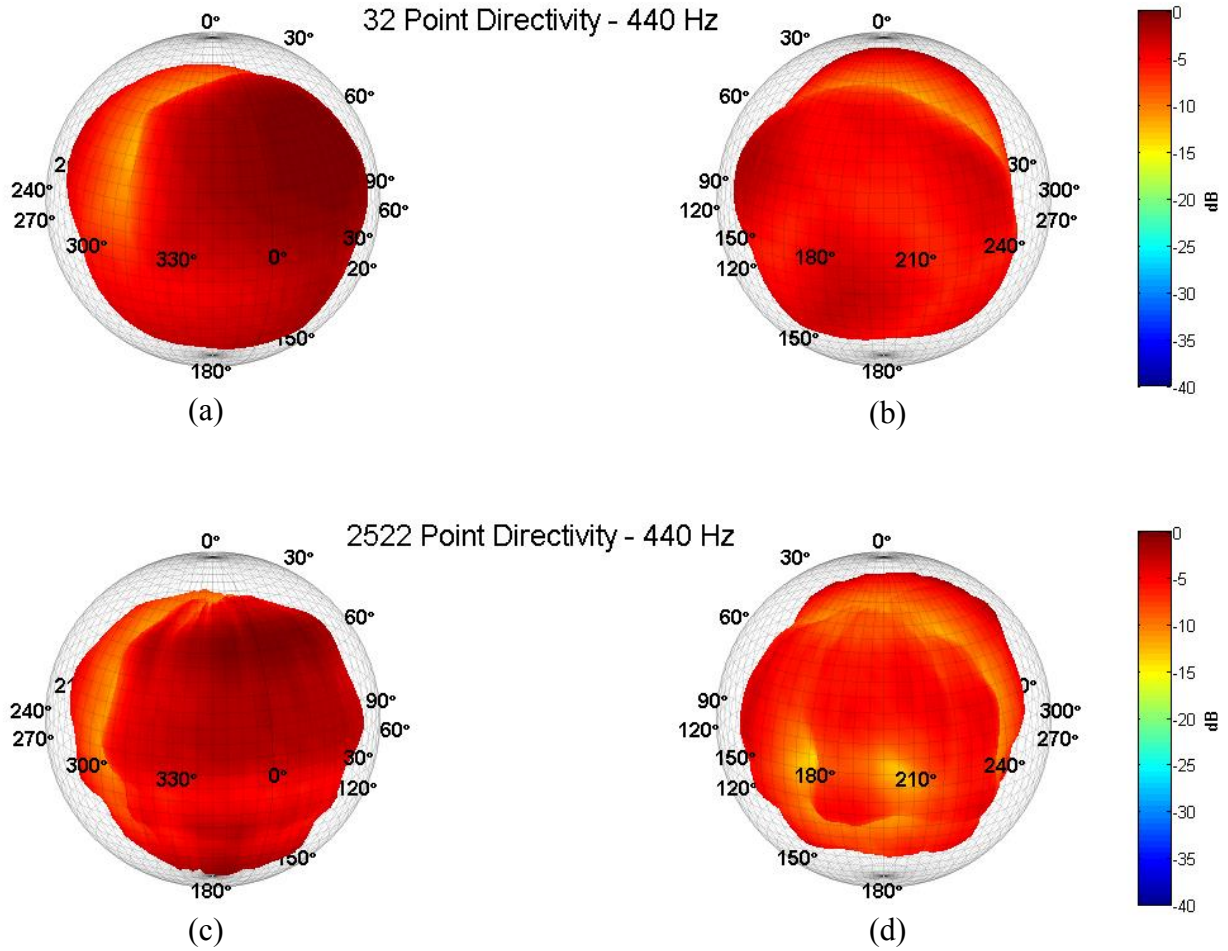

Figure 4.8. Directivity of a Trumpet at 440 Hz. Plots (a) through (d) are arranged as described in Fig. 4.2.

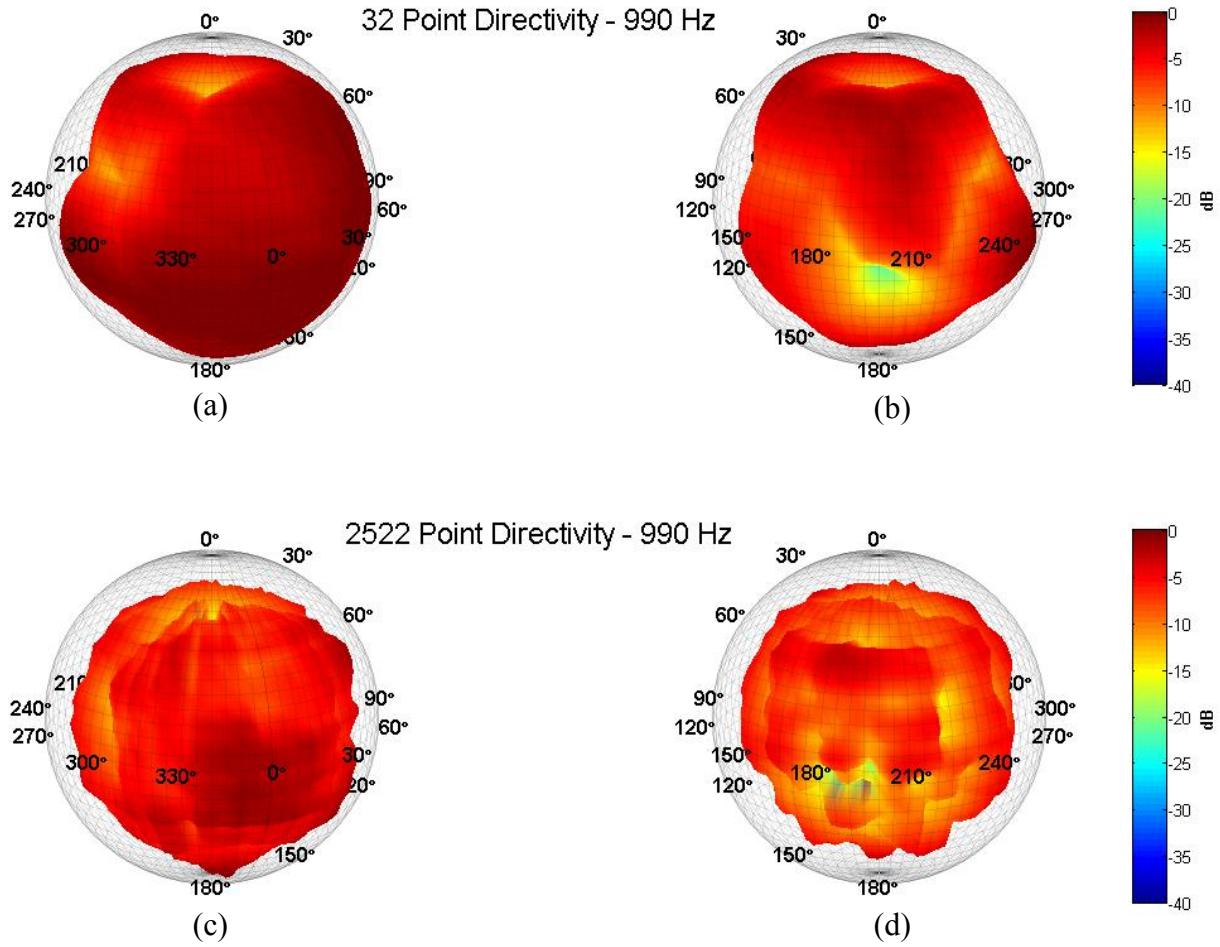

Figure 4.9. Directivity of a Trumpet at 990 Hz. Plots (a) through (d) are arranged as described in Fig. 4.2.

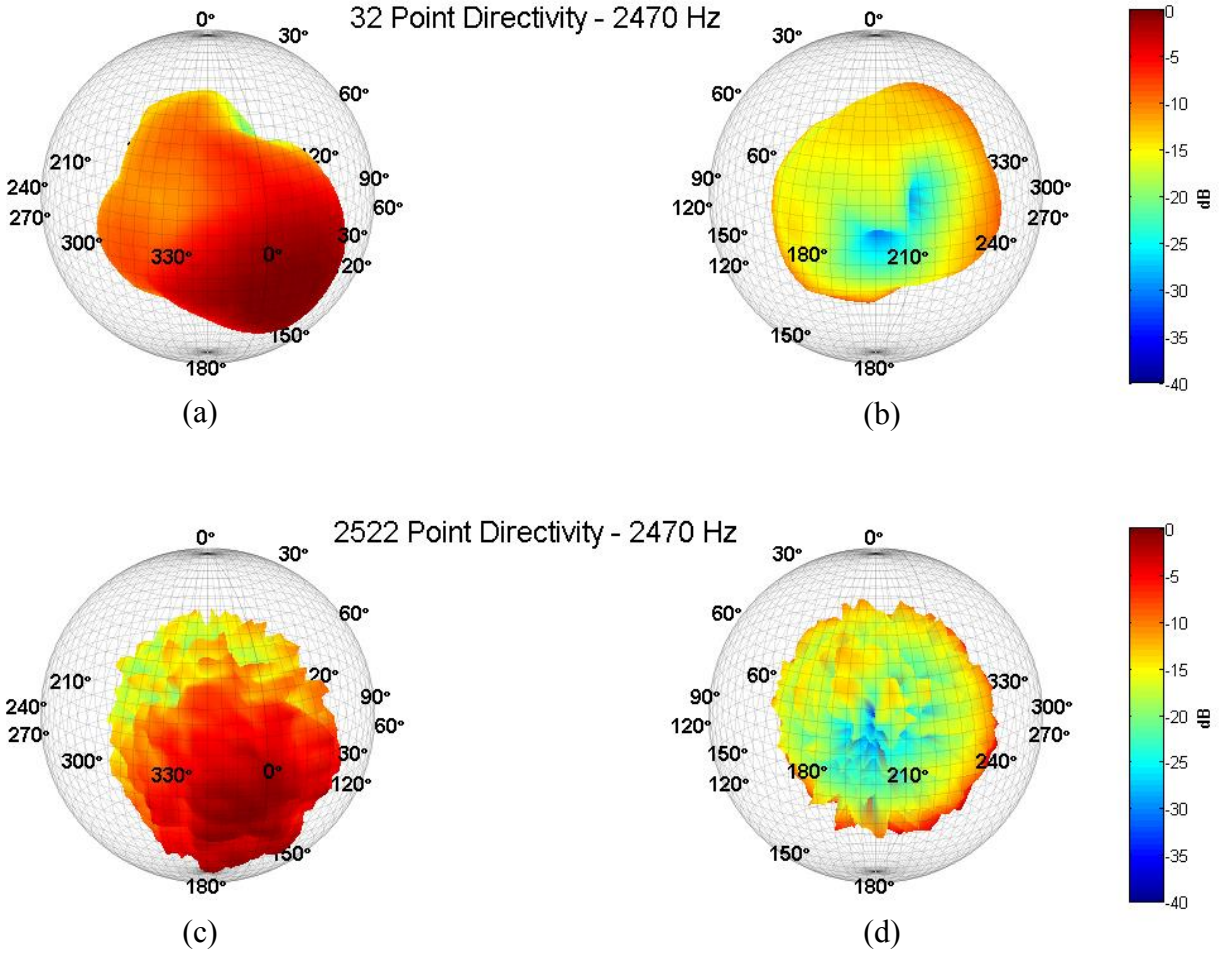

Figure 4.10. Directivity of a Trumpet at 2,470 Hz. Plots (a) through (d) are arranged as described in Fig. 4.2.

Table 4.2. Comparison of average musician recording session times, file sizes, and processing times for a single-capture system and repeated-capture system.

System	Avg. Recording Time	Avg. Recordings File Size	Avg. Computational Period
Single-capture	29 s	800 MB	288 s
Repeated-capture	4.8 hrs.	65 GB	5 hrs.

calculations. While less noticeable at lower frequencies where the radiation pattern is relatively omnidirectional, higher frequencies with more complex directivity patterns show significant deviation from one system to the other. Both loudspeakers show small RMS errors at low frequencies, which then increase with frequency.

The RMS error for the Mackie peaks around 1.6 kHz due in part to the crossover region being well defined in the high-resolution system with deep nulls in the directivity pattern. These are not present in the 32-point system (see Fig. 4.3). Because the RMS error exceeds 20 dB at some frequencies the results cast doubt on the value of using a single-capture system to provide sufficiently detailed results.

4.3.2 Instruments

The results for the musical instruments do not have a standard for comparison. It is for this reason and those outlined earlier that RMS error was not calculated. However, several key findings should be noted. First, in the higher-resolution system there are vertical bands present at higher frequencies. These are a result of playing variations that occur from rotation to rotation and have an associated error which was quantified in an example in Sec. 3.3. These errors would not be present in single-capture systems.

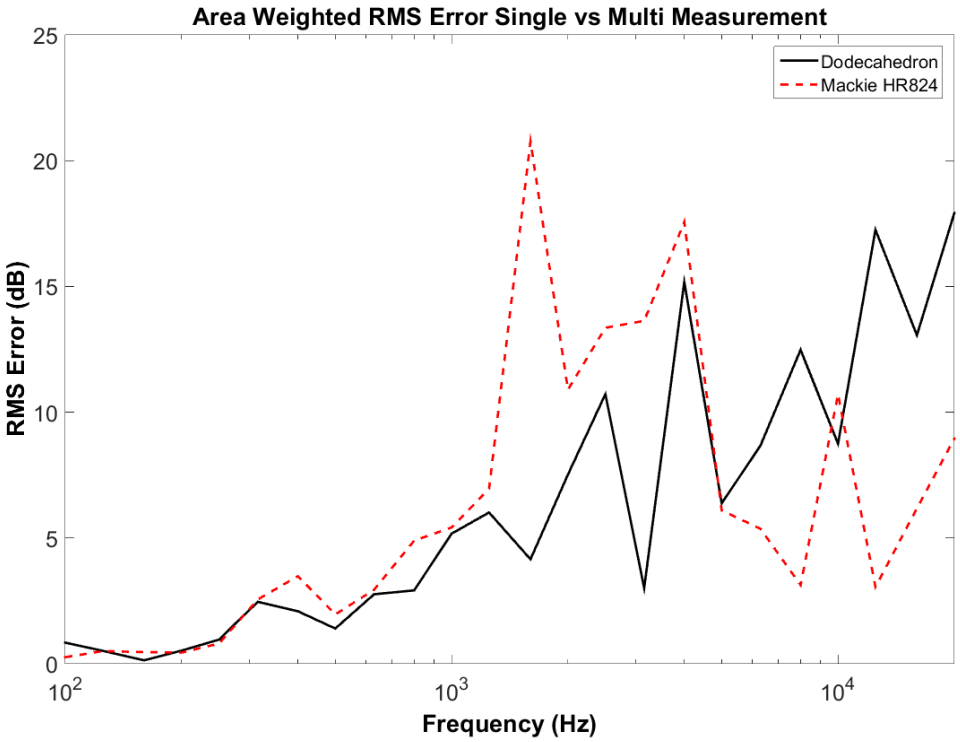

Figure 4.11. Area weighted root mean square error of the Mackie HR824 and Dodecahedron loudspeaker directivity measurements using the single-capture system relative to the 5° resolution multiple capture system.

With vertical banding aside, there are still distinct differences in the results of the two systems. While the general shapes of directivities are similar, the high-resolution system shows details that are misconstrued by the lower-resolution system. For example, results from the repeated-capture system show two significant symmetric "holes" in the directivity pattern at 740 Hz for the bass clarinet and 440 Hz for the trumpet [see Figs. 4.7(d) and 4.8(d)]. This is believed to be caused by sound diffracting around the musician and causing destructive interference. At the same locations, the low-resolution system results either do not contain the nulls or show only a single null in the directivity [see Figs. 4.7(b) and 4.8(b)].

Another concerning result from the single-capture system is the asymmetry of directivity patterns for these particular instruments. The trumpet in particular is assumed to be axisymmetric

in the medial plane due its relatively simple horn shape. However, the harmonics of the fundamental frequency depicted by the 32-point system do not show a symmetric directivity pattern.

Symmetry is present regardless of the choppy directivity in the high-resolution repeated-capture system, which increases confidence in its results. The significant amount of interpolation between microphone locations in the single-capture system seems to mask intuitive features in measured directivity patterns. Spherical harmonics could be utilized to reduce interpolation errors. However, more complex patterns at higher frequencies could be challenging to resolve accurately [9]. Due to the sparse resolution over the sphere in the 32-point system, spherical harmonics having an order above four could not be utilized to represent the sound field without spatial aliasing occurring and introducing errors in the results [10].

References

[1] J. Pätynen, V. Pulkki, and T. Lokki, “Anechoic recording system for symphony orchestra,” Acta Acust. United Acust. **94**, 856-865 (2008).

[2] M. Pollow, “Measuring directivities of musical instruments for auralization,” Fortschritte der Anustin: Tagungsband, **35**, 1471-1473 (2009).

[3] F. Hohl, “Kugelmikrofonarray zur Abstrahlungsvermessung von Musikinstrumenten” (“Spherical microphone array for radiation survey of musical instruments”), Master’s thesis, University of Music and Performing Arts, Graz, Austria (2009) [available at <http://old.iem.at/projekte/acoustics/musik/kugel/hohl.pdf > (last viewed December 7, 2015)].

[4] AES56-2008, “AES standard on acoustics – Sound source modeling – Loudspeaker polar radiation measurements,” Audio Eng. Soc. INC., New York, New York.

[5] N. J. Eyring, "Development and Validation of an Automated Directivity Acquisition System Used in the Acquisition, Processing, and Presentation of the Acoustic Far-Field Directivity of Musical Instruments in an Anechoic Space," MS Thesis, Brigham Young University, (2013), available online through Brigham Young University Electronic Theses & Dissertations at <http://etd.lib.byu.edu> (Last viewed December 7, 2015).

[6] A. Pérez Carrillo, J. Bonada, J. Pätynen, and V. Välimäki, “Method for measuring violin sound radiation based on bowed glissandi and its application to sound synthesis,” J. Acoust. Soc. Am. **130**, 1020-1029 (2011).

[7] T. W. Leishman, S. Rollins, and H. M. Smith, "An experimental evaluation of regular polyhedron loudspeakers as omnidirectional sources of sound," J. Acoust. Soc. Am. **120**, 1411-1422 (2006).

[8] A. Holden, *Shapes, space, and symmetry,* (Columbia University Press, New York, 1971)

[9] M. Pollow, G. Behler, and M. Vorlander, “Post-processing and center adjustment of measured directivity data of musical instruments,” Acoustics 2012 Nantes (2012) [available online at <https://hal.archives-ouvertes.fr/hal-00811212/> (Last viewed December 7, 2015)].

[10] T. D. Abhayapala and D. B. Ward. “Theory and design of high order sound field microphones using spherical microphone array,” *Proc. of ICASSP* **2**, 1949-1952 (2002).

Chapter 5

Evidences of Nonanechoic Fields in Anechoic Chambers

Anechoic chambers have been used for years to simulate free-field acoustic conditions in laboratory settings. Chambers are typically qualified in accordance with international standard ISO 3745:2012 [1], which describes the procedure and requirements for a suitable chamber. There has been some concern in the literature as to whether the standard needs improvement to satisfy the demands of modern data collection. Luykx found that low-level reflections, especially from practical features such as lights and flooring elements, can cause deviations above the prescribed limits of the standard, even in rooms which had been previously qualified as anechoic [2]. Others have found that the use of different excitation signals, such as single tones, noise, and impulses produce significantly different measurements when compared to one another [3], [4], [5]. The ISO standard itself alludes to this possibility, stating that a room qualified using “pure tones will be more costly both to construct and qualify than one to be qualified for one-third-octave band random noise” [1].

The standard requires that a series of five linear traverse measurements be made away from a nominally omnidirectional source, recording pressures at either continuous or discrete increments. Measurements along a single traverse must be made in 0.1 m or shorter increments. No fewer than 50 locations may be used to represent the entire qualification data set of 5 total traverses. These measurements are subsequently compared to the inverse-square law. The chamber is considered "anechoic" for frequencies that fall within prescribed deviation tolerances as shown in Table 5.1. The source signal should utilize pure tones at third octave frequencies where possible, with noise being permissible if the source is unable to produce tonal signals.

At the outset, this procedure has several limiting factors which could impact the value of qualification. Firstly, both the output signals and measured tolerances are determined using $1/3^{rd}$ octave band data rather than narrow band. Placing data into $(1/N)^{th}$ octave bands has the effect of smoothing what would otherwise be more sporadic with a finer resolution. This could mean that calculations and measurements using a narrow band frequency resolution in an anechoic chamber may not truly be in an anechoic environment.

Secondly, linear traverses, while effectively providing details for inverse-square law comparisons, are not a typical form of measurement in many studies. It is often the case that a source is placed in an anechoic environment to understand the sound field *surrounding* that object.

Table 5.1 Allowable deviations for linear traverse measurements in the anechoic chamber qualification standard.

One-third-octave band frequency (Hz)	Allowable deviation (dB)
≤ 630	± 1.5
800 to 5000	± 1.0
≥ 6300	± 1.5

Measurement positions would therefore surround the source. If a source is omnidirectional, as ISO 3745:2012 requires [1], pressure should remain constant for any angle at a fixed radius in a free-field environment. A linear traverse does not sufficiently demonstrate this supposition accurately enough to consider a chamber to be anechoic in this respect. In fact, if one were to take the minimum number of linear traverse measurements for qualification in an anechoic chamber with dimensions of 8.6 m × 5.7 m × 5.7 m (the size of the BYU anechoic chamber), this would equate to approximately 293 total linear traverse locations. This number, even if equally distributed around the room, equates to each microphone location representing approximately 1 m^3 of volume. This is an incredibly sparse resolution considering that directivity measurements require a 5^o angular resolution at a fixed 1 m radius if measured according to the AES standard [6].

5.1 Motivations

Concerns about this matter have developed in the course of work completed for this thesis. During the validation of the DMS for musical instruments, measurements were conducted in a qualified anechoic chamber to a low-frequency cutoff of approximately 80 Hz. To determine the accuracy of musical instrument results, loudspeakers were measured by rotating them relative to the fixed array in order to measure 2,522 unique points over a sphere. Measurements were taken using a series of linear chirps at a 48 kHz sampling frequency. Directivity was subsequently plotted as a function of frequency with a resolution ranging from 1 Hz to 10 Hz.

One of the loudspeakers tested was a 20 cm dodecahedron loudspeaker similar to those commonly used in architectural acoustics measurements (see Fig. 5.1). These loudspeakers behave as omnidirectional sources up to a certain cutoff frequency that is determined by the size and shape of the loudspeaker [7]. When the directivity was plotted, the general shape below the cutoff was

omnidirectional. However, several latitudinal bands appeared in the results, some of which ranged up to 4 dB in amplitude. More curiously, these bands seem to smoothly shift and increase in numbers with frequency (See Fig. 5.2).

To ensure that these bands were not somehow an artifact from the loudspeaker itself, a Tannoy System 800 loudspeaker was also measured both in upright and sideways orientations. The directivity bands remained present in the same locations, regardless of the source type and configuration (see Fig. 5.3), thus eliminating the possibility of error due to the source. Several array microphone calibrations and calibration methods were applied and all yielded similar results. This, coupled with the frequency-dependent motion of the bands across multiple microphone locations eliminated microphone calibration error as a cause of the banding (see Sec. 2.7).

As a result, a hypothesis that qualified anechoic chambers may not be sufficiently anechoic for high spatial and spectral resolution data collection was developed and investigated as part of this work. While tests were performed in a single chamber, the results potentially affect data collected in all anechoic chambers qualified under the conventional standard. This study reports only on preliminary findings and results, leaving conclusions about the necessity of improved standards for further research.

5.2 Methods

In order to investigate spatial variations in the anechoic chamber, a measurement system was needed that would move but provide repeatable pressure levels over frequency in a perfect free field. A point source or an omnidirectional source would have been ideal. However, these do

not exist in practice across all frequencies of interest, so a more complex but equally effective system was developed. This consisted of a rotatable loudspeaker with a microphone attached to an

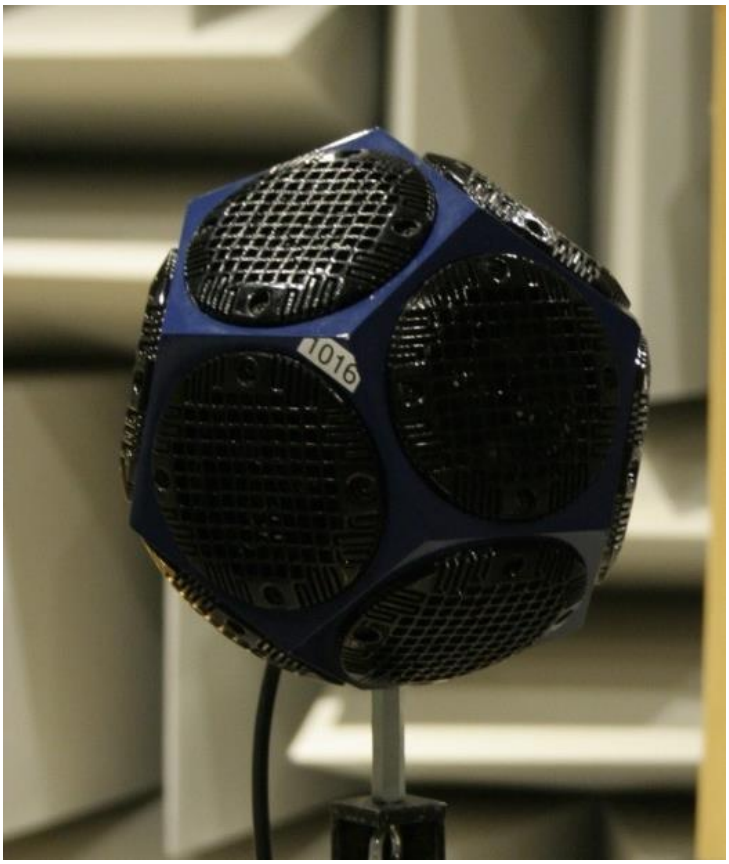

Figure 5.1. A 20 cm dodecahedron loudspeaker used in directivity measurements.

adjustable radius boom arm that remained fixed in the loudspeaker reference frame. A Tannoy System 800 loudspeaker was initially chosen as the source. A series of acoustically treated rods with a 1.2 cm square cross section were attached to the loudspeaker support system which held a GRAS 40AE 1.27 cm microphone in the same on-axis location relative to the loudspeaker, regardless of orientation (see Fig. 5.4). A removable laser mounting system was also used to ensure the microphone did not deviate from its on-axis position.

The loudspeaker was aligned with the center of the DMS microphone array and polar data were collected in three orthogonal planes with 5º resolution. Recordings were completed using a Gaussian noise signal generated from the loudspeaker with a duration of 30 seconds. The first ten seconds of noise was used to excite the room fully. The final 20 seconds were recorded and processed as a FRF using the digital loudspeaker input signal as reference. The entire apparatus was rotated after each measurement by 5º and the measurements were repeated. For consistency, the same 30 second sampling of random noise was used in every recording.

Recordings were measured over a full 360º in the azimuthal plane at radii ranging from 0 m to 1.83 m in 30.5 cm increments. Vertical planes were measured only at 1.83 m and 1.22 m radii with the limited polar-angle range of 0º to 135º due to the physical barrier of the cable floor. One of the vertical planes corresponded with the DMS array plane. The second was orthogonal.

5.3 Results

In a perfectly anechoic room, the magnitudes of the FRF between the digital input signal and the microphone signal at every measurement location should be identical for each measurement position. To determine the deviation from this ideal, the frequency-dependent standard deviation was computed as

$$\sigma(f) = \sqrt{\frac{1}{N}\sum_{i=1}^{N}[|H_i(f)| - \mu(f)]^2}\ , \tag{5.1}$$

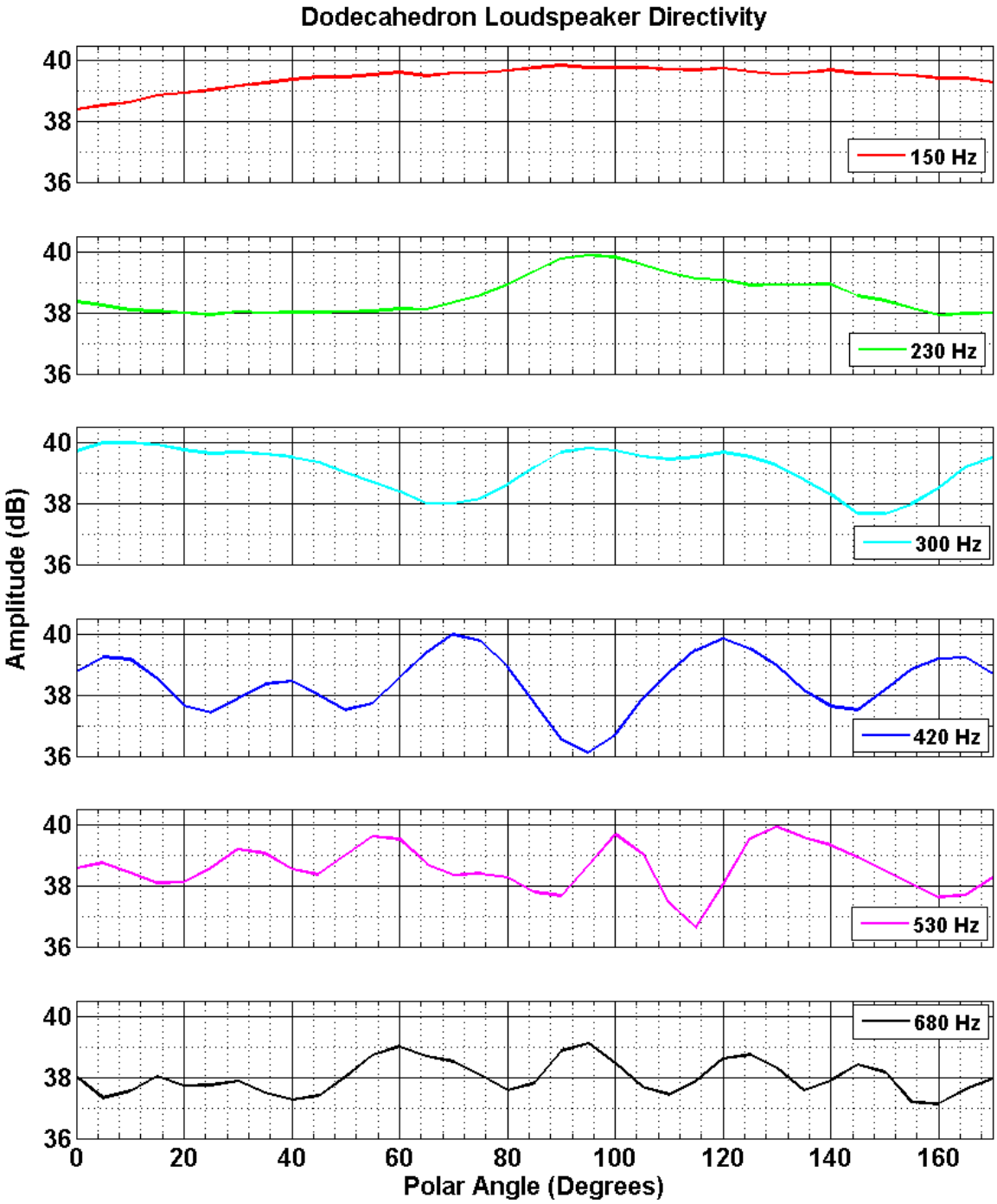

Figure 5.2. Normalized directivity of a 20 cm dodecahedron loudspeaker at several frequencies. The directivity represents the medial half plane at $\phi = 0^o$. Each plot has been normalized to the maximum value depicted at that respective frequency.

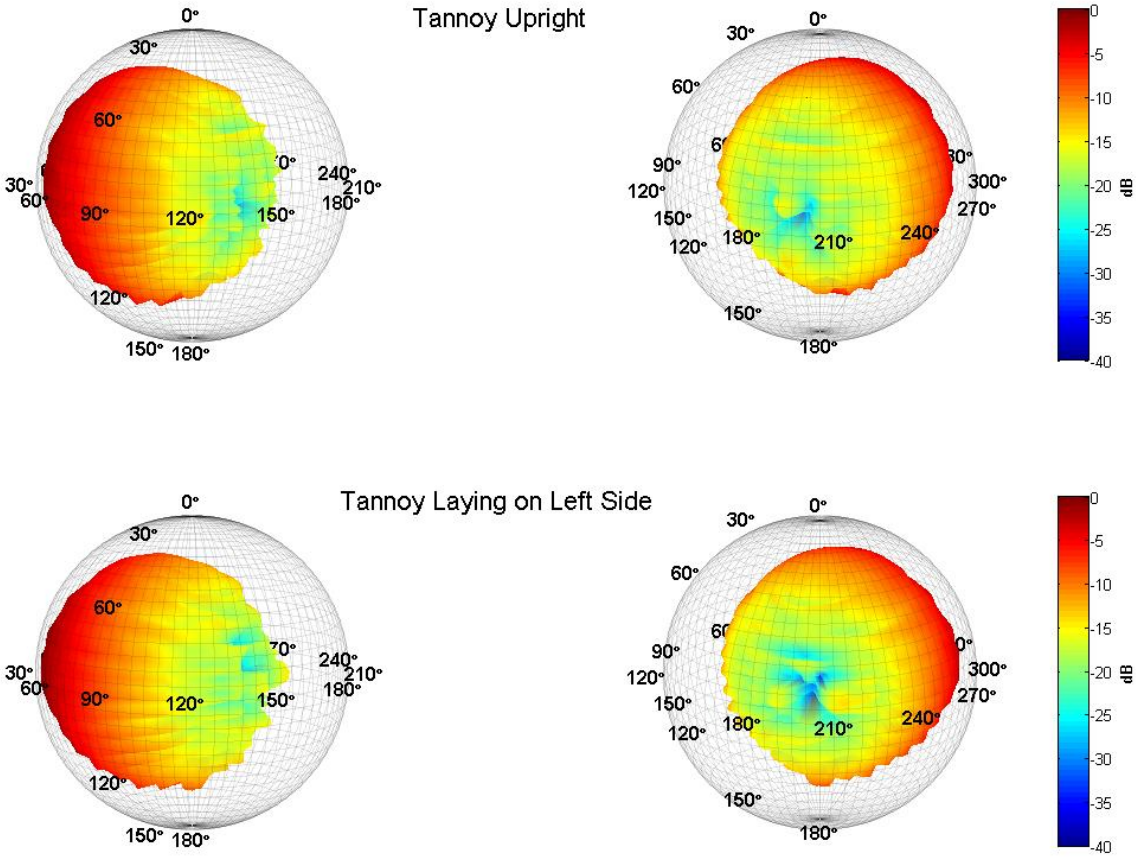

Figure 5.3. Directivity of a Tannoy System 800 loudspeaker at 1.8 kHz. (a) Left-rear view with the speaker placed upright. (b) Right-rear view of the speaker placed upright. (c) Left-rear view of the speaker laying on its left side. (d) Right-rear view of the speaker laying on its left side.

where

$$\mu(f) = \frac{1}{N}\sum_{i=1}^{N}|H_i(f)| \tag{5.2}$$

and $|H_i(f)|$ is the magnitude of the i^{th} frequency response. Standard deviations are plotted as functions of frequency in Fig. 5.5 for azimuthal rotations at different radii. Similar plots are shown in Fig. 5.6 with third-octave smoothing applied to power spectral density data.

In order to more fully understand the physical meaning of these standard deviations they are represented by a computed level variation range from the average by

$$\sigma_{\mathrm{dB_{diff}}}(f) = 2\,\{20\ log_{10}[m_\sigma \sigma(f) + \mu(f)] - 20\log_{10}[\mu(f)]\}, \tag{5.3}$$

where m_σ symbolizes the number of standard deviations used. Simplification yields

$$\sigma_{\mathrm{dB_{diff}}}(f) = 40\ log_{10}\left[\frac{m_\sigma \sigma(f) + \mu(f)}{\mu(f)}\right]. \tag{5.4}$$

In these expressions, $\sigma_{\mathrm{dB_{diff}}}(f)$ represents the difference in dB of computed maximum and minimum values from the mean. Because standard deviation is calculated based on a mean value, it was necessary to include the mean in level calculations rather than computing the logarithm using only $\sigma(f)$. This addition enables data sets with different means to be compared. A Gaussian distribution is assumed so the use of the factor of 2 in Eq. (5.3) is required to compute the full range of deviation caused by nonanechoic field effects.

Assuming the data has a Gaussian distribution, the use of ±3 standard deviations considers 99.7% of the total number of samples and would theoretically contain the extreme values of variance. Figure 5.7 depicts the calculation form Eq. (5.4) vs. frequency at several different radii. Maximum level differences are also plotted in Fig. 5.8 from measured values to provide validation to the standard deviation level difference calculations. Differences in these plots are attributed to the use of a mean in standard deviation calculations, which can be significantly influenced by

outliers in data. Further statistical analyses to investigate the possibility of removing outliers and other artifacts were beyond the scope of this thesis.

Standard deviations are also plotted in Figs. 5.9 and 5.10 for data collected in the medial and frontal planes at 1.2 m and 1.83 m radii. As indicated earlier, these standard deviations calculated in Eq. (5.4) were measured over 0^o to 135^o due to the cable flooring interfering with the measurement apparatus. Maximum level differences at each radius have also been calculated to gain a more concrete understanding of standard deviation values (see Figs. 5.11 and 5.12).

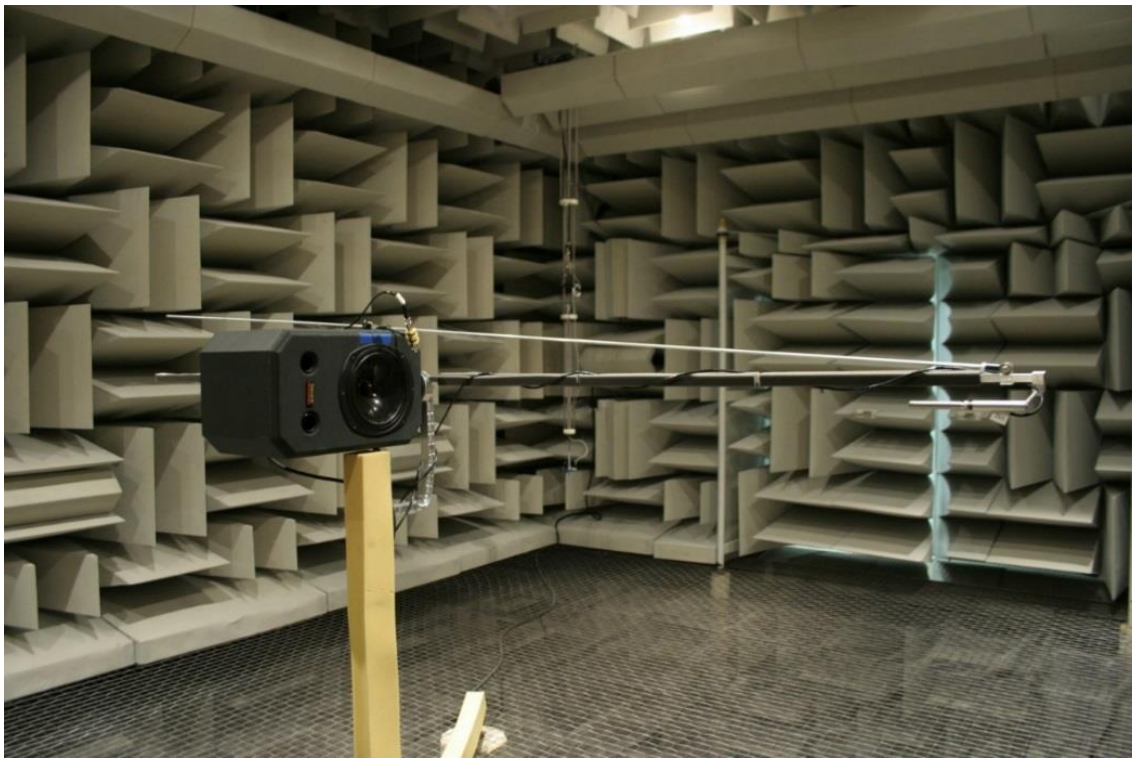

Figure 5.4. Tannoy System 800 loudspeaker outfitted with an adjustable rotating boom arm used to fix a microphone on axis with the loudspeaker, regardless of loudspeaker orientation.

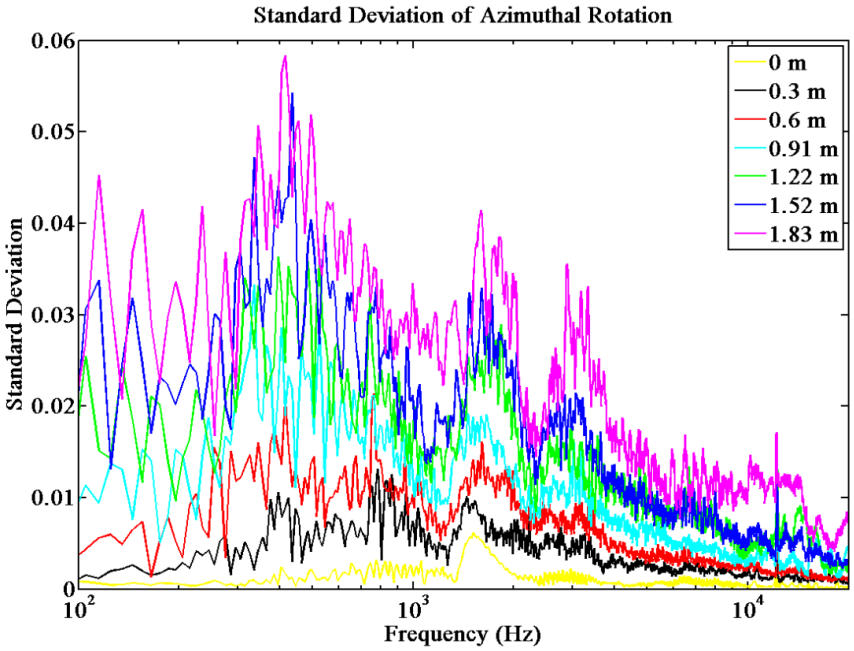

Figure 5.5. Standard deviation of measurements taken in the transverse plane for different radii using a 10 Hz bin width. Each radius contained 72 measurements in 5° increments from which the standard deviation was calculated.

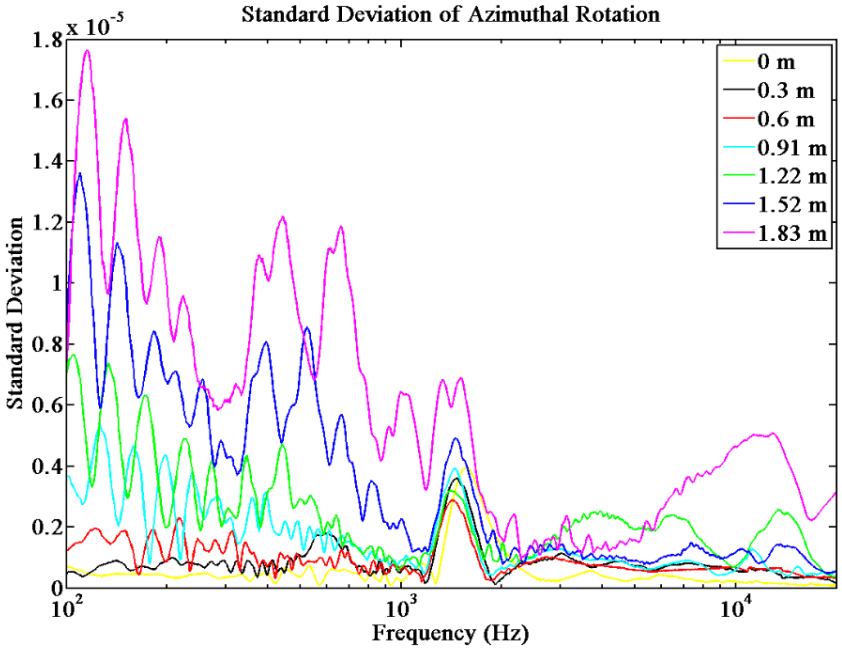

Figure 5.6. Standard deviation of measurements taken in the transverse plane for different radii using proportional third octave bands of the power spectral density. Each radius contained 72 measurements in 5° increments from which the standard deviation was calculated.

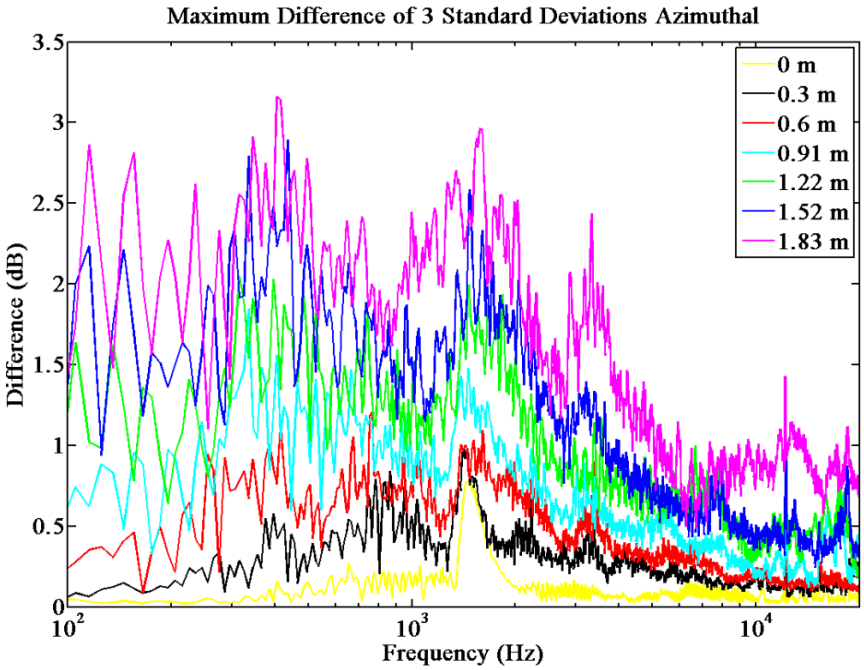

Figure 5.7. Difference in level over three standard deviations above and below the mean [see Eq. (5.4)] over a circle with 5° resolution at several radii in the transverse plane.

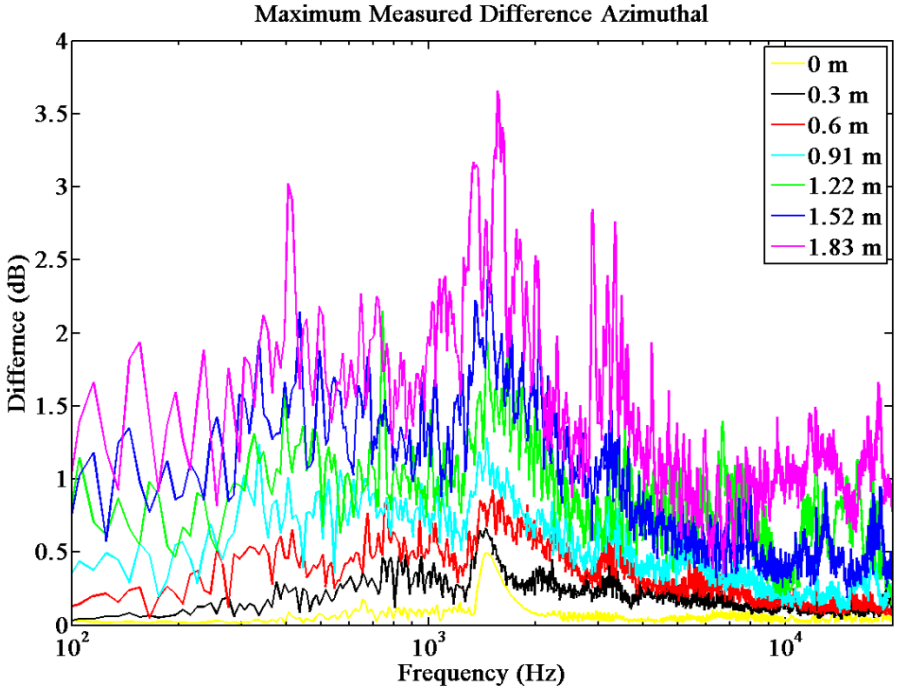

Figure 5.8. Difference between measured maximum and minimum levels recorded over a circle with 5° resolution in the transverse plane at several radii.

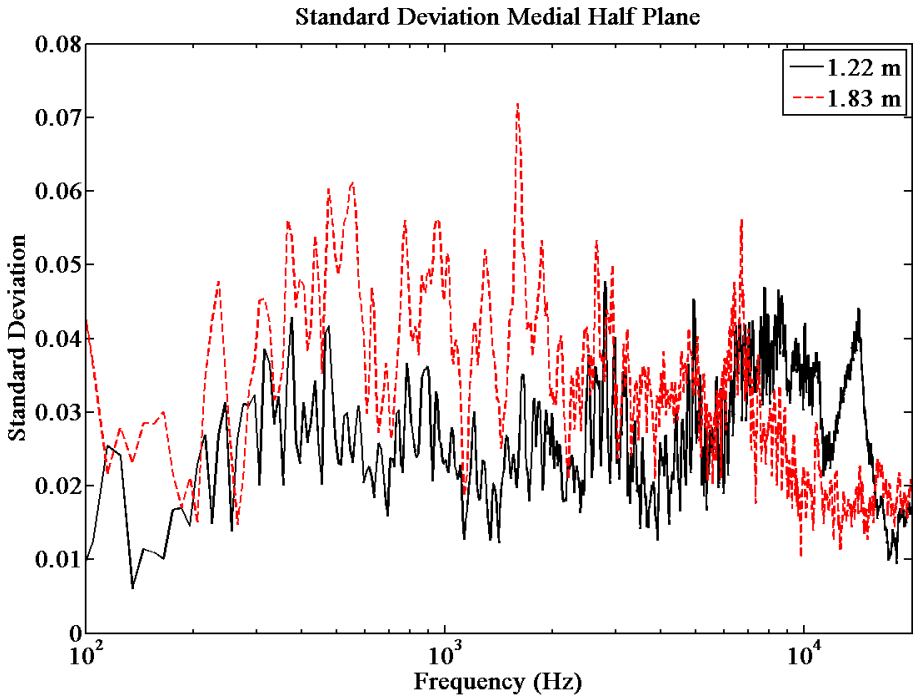

Figure 5.9. Standard deviation of measurements taken in the medial plane for different radii using a 10 Hz bin width. Each radius contained 28 measurements in 5° increments over $\theta = 0°$ to 135° from which the standard deviation was calculated.

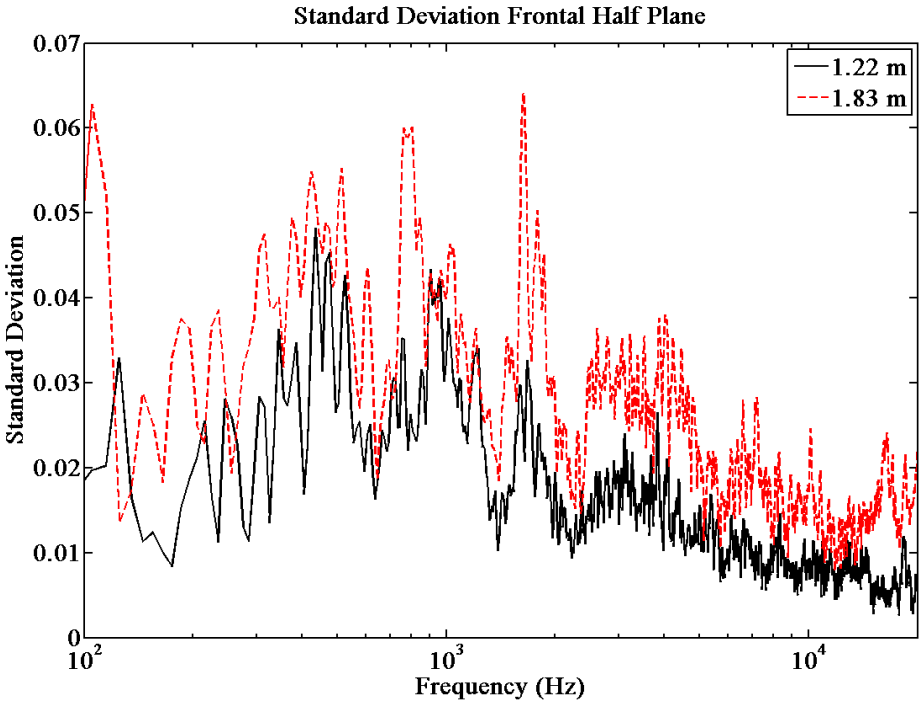

Figure 5.10. Standard deviation of measurements taken in the frontal plane for different radii using a 10 Hz bin width. Each radius contained 28 measurements in 5° increments over $\theta = 0°$ to 135° from which the standard deviation was calculated.

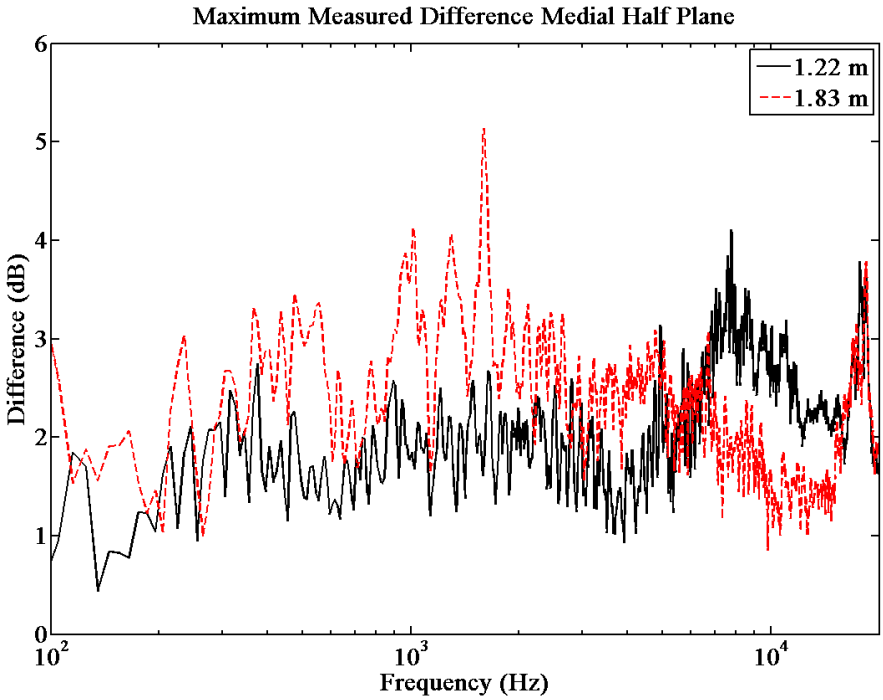

Figure 5.11. Difference between maximum and minimum levels due to chamber effects over $\theta = 0^o$ to 135^o with 5^o resolution in the medial plane over frequency at a 1.22 m and 1.83 m distance.

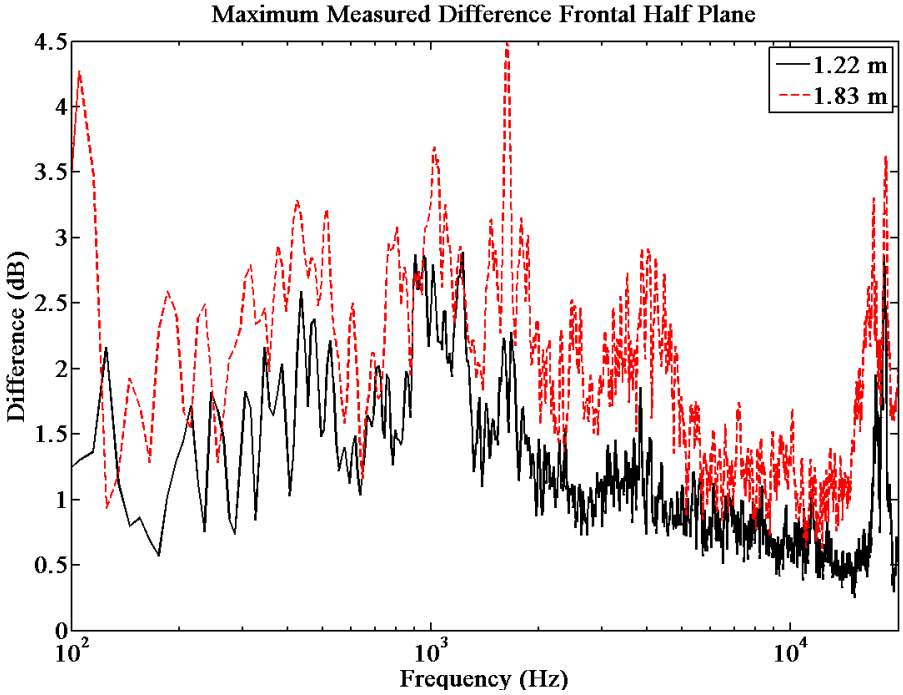

Figure 5.12. Difference between measured maximum and minimum levels due to chamber effects over $\theta = 0^o$ to 135^o with 5^o resolution in the frontal plane over frequency at a 1.22 m and 1.83 m distance.

5.4 Analysis and Discussion

As seen in Figs. 5.5, 5.9, and 5.10, the broadband standard deviation tends to increase with distance from the source. On average, the relative difference in standard deviation appears to increase roughly proportional to changes in distance. In fact, when all frequencies are averaged together, the standard deviation does not appear to plateau over distance (see Fig. 5.13). Interestingly, narrow-band data with a 10 Hz resolution show the largest standard deviations occurring for this chamber at low to mid-range frequencies with σ tapering off at all distances as frequency increases (see Fig. 5.5). This seems to reflects the fact that it is increasingly difficult for the wedges in the anechoic chamber to fully absorb sound energy as frequency decreases. As wavelength increases, the amount and depth of absorptive structure must be increased to maintain the same level of absorption.

There is a significant jump at all azimuthal radii in standard deviation near 1.5 kHz that is not attributed to room effects (see Figs. 5.5 through 5.12). This may be in partially due to the arc array structure scattering more reflections in the frequency range of 1 kHz to 2 kHz. When the data are shown as polar plots at a single frequency in this region the greatest deviations seem to occur near the arc (see Fig. 5.14). Additionally, the patterns seem to be relatively symmetric about the arc as would be expected due to the arc's symmetry.

However, it was recently discovered that the loudspeaker used to produce these results was not time invariant over the 1 kHz to 2 kHz frequency range. Over time, the amplitude increased in this ranged by up to 0.6 dB. The amplitude of the signal increased for these frequencies with time, which significantly impacted standard deviations over this frequency range. Further investigation

is required to determine the relative impact of scattering vs. loudspeaker effects on overall standard deviation results.

Figures. 5.9 and 5.11 depict measurements taken using methods outlined in Sec. 5.2 in the medial plane. Figures 5.8 and 5.12 represent polar angle measurements taken 90^{o} away from the arc in the frontal half plane of the loudspeaker. There is little change in overall maximum difference levels between the two planes when comparing similar radii. There is roughly 0.5 dB increase for measurements near the arc.

On the whole, the 1.83 m radius has a higher standard deviation than the 1.22 m radius, with a noticeable exception above 5 kHz when measured near the arc. During the period when these measurements were taken, microphones on the DMS array had been extended away from the arc to a radius of 1.22 m. As a result measurement locations at this radius were within 2 cm of the DMS microphones. Scattering from the DMS mirophones is believed to be the reason that the 1.22 m radius has a higher standard deviation than at 1.83 m above 5 kHz. Further investigation is currently in progress to understand the validity of this hypothesis.

Even though further investigation is required on nonanecoic fields in anechoic chambers there appears to be significant correlation between the horizontal banding measured in directivity data (see Fig. 3.2) and the results from this chapter. The normalized plots in Fig. 5.2 were taken from a complete directivity measurement of a 20 cm dodecahedron loudspeaker. As discussed in Sec. 4.2.2 the frequencies presented should be omnidirectional. This would be visualized as a flat line when represented in Fig. 5.2. There are clearly deviations from this at all frequencies with extreme amplitude ranges in excess of 3 dB at some frequencies. When compared to results from

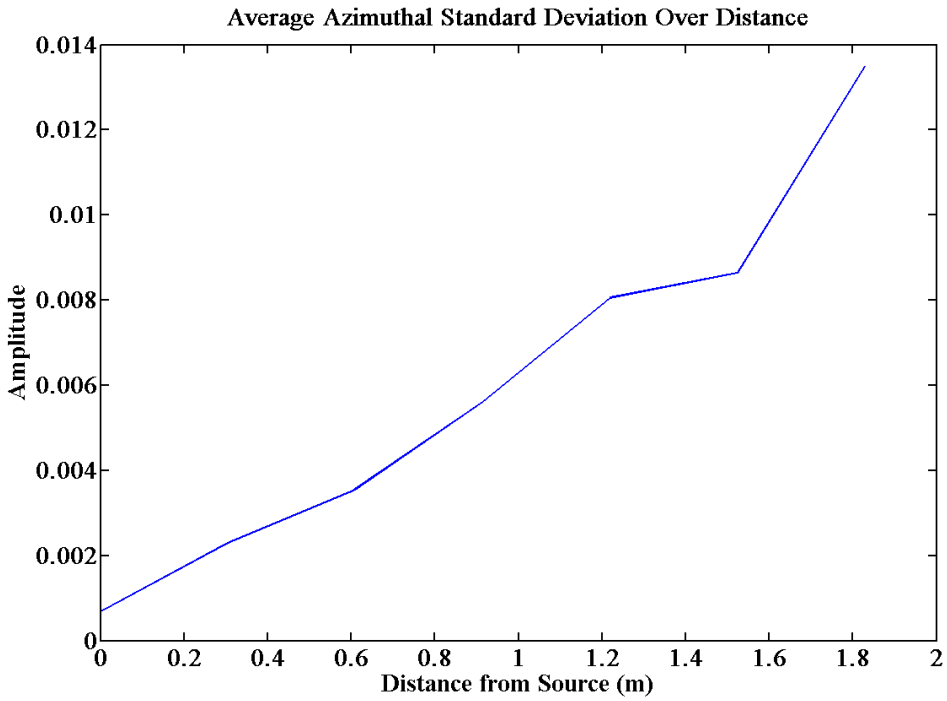

Figure 5.13. Spectrally averaged standard deviation of circular measurements at different radii in the transverse plane.

methods described in Sec. 5.2, the amplitudes in Fig. 5.2 are comparable to those measured as nonanechoic field effects (see Fig. 5.11). These similar deviations in the DMS measurements and the rotating microphone measurements in this chapter provide convincing evidence that the latitudinal bands measured using BYUs DMS system are representative of the actual sound field rather than an artifact of the DMS itself.

5.5 Conclusion

After conducting initial measurements in the BYU anechoic chamber, it appears that standard deviations of similar loudspeaker measurements taken at different angular locations and measurement radius are highly correlated. When both a dense spectral resolution and sampling field are used, it becomes apparent that there is significant variation from a perfectly anechoic

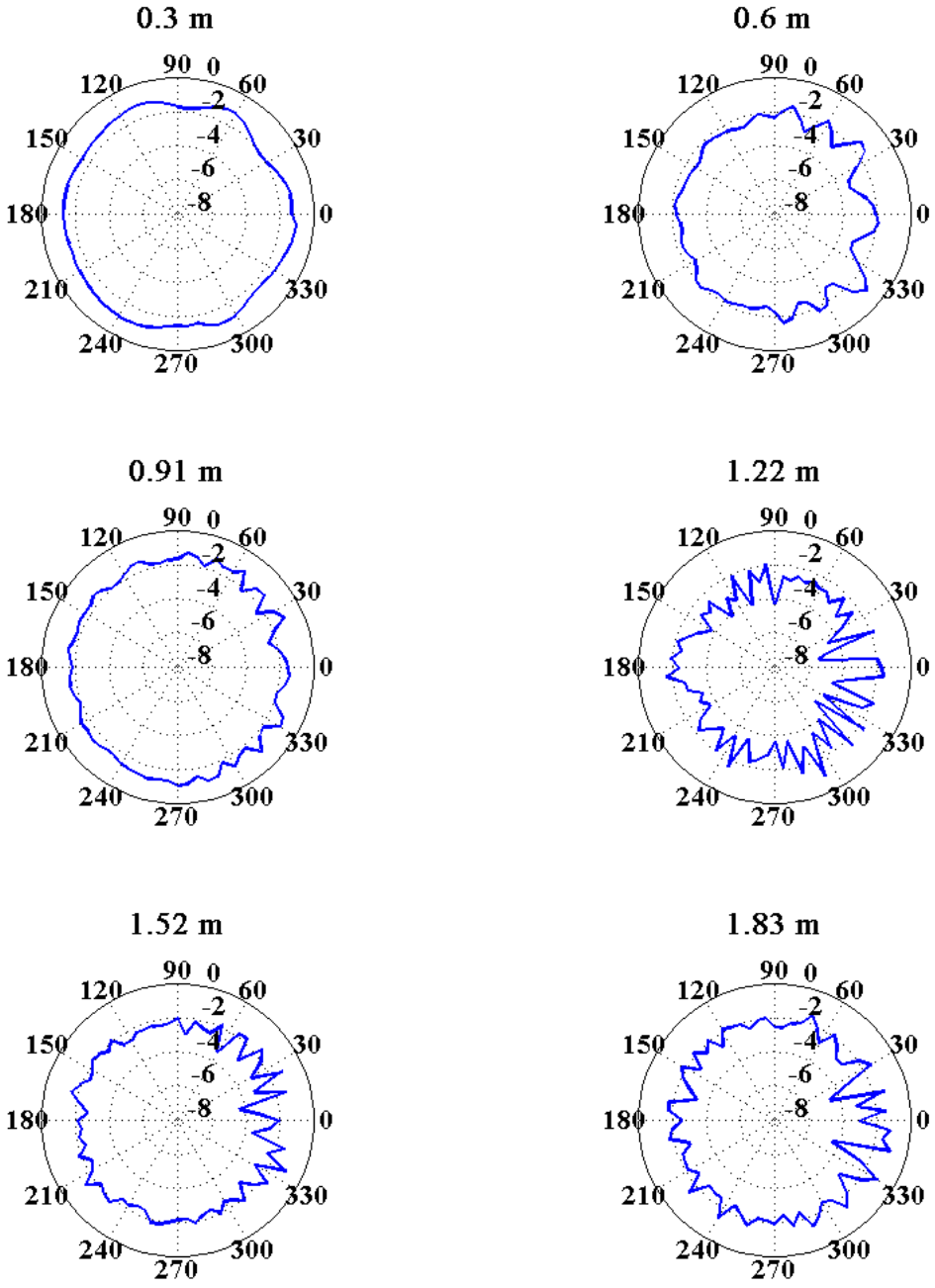

Figure 5.14. Normalized frequency responses of azimuthal measurements of a Tannoy Series 800 loudspeaker in the transverse plane of the DMS at 1.7 kHz. Different measurement radii are represented in plots (a) through (f) ranging from 0 m to 1.83 m as indicated in approximate increments of 30 cm. The measurement arc of the DMS is oriented through the page at the 0^{o} maker in each plot.

environment due to nonanechoic effects. The main causes of these variations are still unknown and will continue to be investigated through further study. Results of this chapter also seem to reflect that the cause of latitudinal banding, as seen in directivity balloons measured with the BYU DMS, are due to nonanechoic field effects in the anechoic chamber. In the future, it may be necessary to alter current standards for anechoic chamber qualification to accommodate high-resolution directivity measurements.

References

[1] ISO 3745:2012: *Acoustics-Determination of sound power levels of noise sources – Precision methods for anechoic and semi-anechoic rooms* (International Organization for Standardization, Geneva, Switzerland).

[2] M.P.M. Luykx, "Reflections in anechoic rooms," *Proc. Inter-noise and Noise-Con Congress,* 2534-2537 (2001).

[3] K. A. Cunefare, J. Badertscher, and V. Wittstock, "On the qualification of anechoic chambers; Issues related to signals and bandwidth," J. Acoust. Soc. Am. **120**, 820-829 (2006).

[4] K. A. Cunefare, V. B. Biesel, J. Tran, R. Rye, A. Graf, M. Holdhusen, and A. M. Albanese, "Anechoic chamber qualification: Traverse method, inverse square law analysis method, and nature of test signal," J. Acoust. Soc. Am. **113**, 881-892 (2003).

[5] R. J. Fridrich, "Is This Room Anechoic? A New Anechoic Room Qualification Standard May Be Needed for Impulsive Sound Quality Tests," SAE International Technical Paper No. 2007-01-2217 (2007).

[6] AES56-2008 AES standard on acoustics – Sound source modeling – Loudspeaker polar radiation measurements (Audio Eng. Soc. Inc., New York, 2008).

[7] T. W. Leishman, S. Rollins, and H. Smith, "An experimental evaluation of regular polyhedron loudspeakers as omnidirectional sources of sound," J. Acoust. Soc. Am. **120**, 1411-1422 (2006).

Chapter 6

Musical Instrument Directivity Results

Several directivity results for 16 musical instruments are shown in the sections below. The instruments include violin, viola, cello, double bass, trumpet, trombone, French horn, euphonium, tuba, baritone saxophone, tenor saxophone, flute, oboe, bassoon, clarinet, and bass clarinet. Photographs of the musicians sitting in the DMS and directivities of discrete partials are shown for each instrument in Figs. 6.1 through 6.112. Plots included in this body of text were chosen for each instrument to demonstrate several octaves of directivity patterns. The chosen plots all maintain high coherence values over all measurement locations.

Directivity balloons, coherence balloons, and polar plots were chosen to represent the directivity data and coherence. In each balloon, the musician was oriented toward $\phi = 0^o$ with the radiating portion of the instrument centered at $\theta = 90^o$. Distinct polar plots are presented and color coded to match the transverse, medial, and frontal planes, indicated on the directivity balloons. These multiple-plot figures are shown throughout the chapter as some of the standard

plotting options available from the DMS system. Each figure represents a single partial of a single note using one of three reference microphone signals.

Coherence balloons, calculated using Eq. (2.6), are useful to visualize the quality of the directivity measurements. As previously described, coherence demonstrates a linear cause and effect between the reference microphone and measurement arc signals. A perfect coherence value of 1 would indicate that the measured signal resulted from the instrument output, as measured by a reference microphone. This typically signifies a high signal-to-noise ratio and good time alignment of input and output signals during processing. Plots in this thesis have coherence scales set from 0.995 to 1, indicating the high standard set in the study. Values lower than 0.995 are represented by a consistent dark blue color and use only balloon radius to represent amplitude. Coherence can be converted into a decibel signal-to-noise ratio value using

$$S/N = 10\log_{10}\left[\frac{\gamma^2_{\mathrm{ab}lmn}(f)}{\left(1-\gamma^2_{\mathrm{ab}lmn}(f)\right)}\right] \quad . \tag{6.1}$$

This equates the coherence scale used in this thesis to a signal-to-noise ratio scale ranging from 23 dB to infinity. Coherence values below 0.995, or equivalently below a 23 dB signal-to-noise ratio, were generally treated with suspicion. However, regions with low coherence can also be indicative of actual nulls in directivity patterns where low signal-to-noise ratios inherently exist. (See Fig. 6.71 for the baritone saxophone and Fig. 6.84 for the flute as examples.)

After recording and fully processing the data of each instrument, a complete results package was produced that included (1) 2,522 unique recordings of every note played (saved in a *.wav file format), (2) associated coherence and directivity balloon plots (as shown in this chapter),

(3) associated directivity balloons with three polar plots (as shown in this chapter), and (4) associated rotating directivity animations using each of the three reference microphones as the input signal to the FRF. The plots and animations were made for each of the first 5 partials of every note. This resulted in a set of 33 plots and animations for every note played by each instrument, in addition to their audio files. The plots in this chapter represent a small sampling of those generated in the study. The animations consisted of a balloon plot viewed from both the front and rear hemispheres that rotated while periodically jumping by one partial every half rotation for each note. Examples of these and other results not displayed in the body of the thesis may be found digitally in the supplemental materials [1].

6.1 Violin

Figure 6.1. Violinist seated in directivity measurement system.

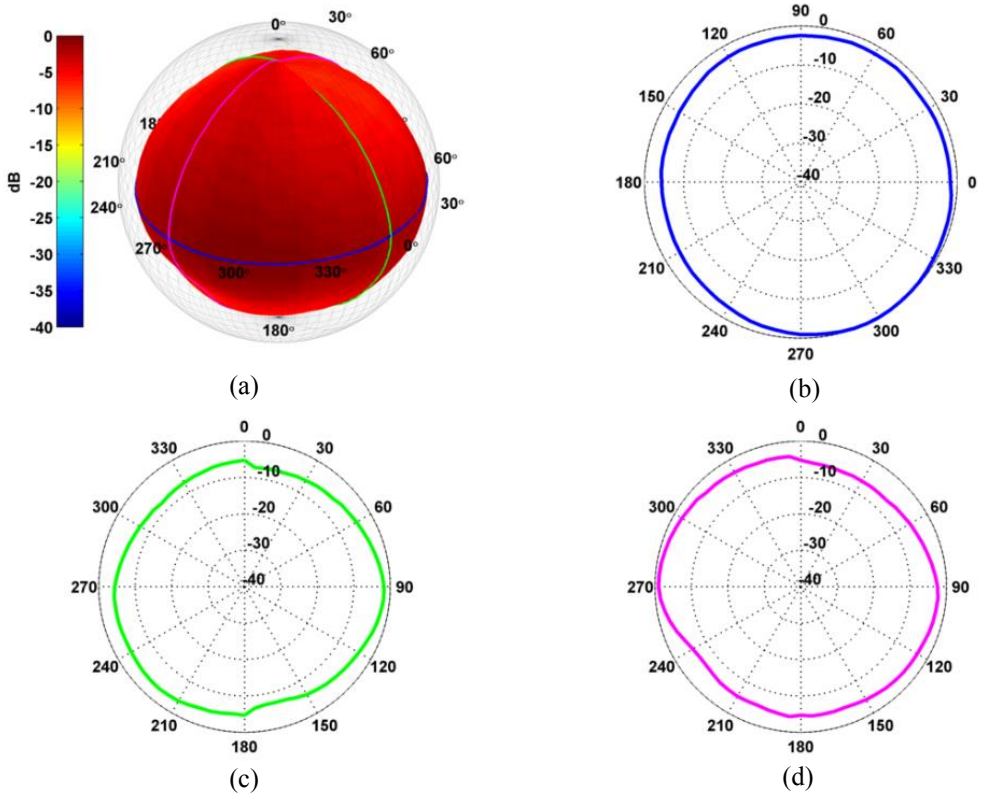

Figure 6.2. Violin directivity of the fundamental frequency for a B♭3. (a) Directivity balloon. (b) Directivity in the transverse plane. (c) Directivity in the medial plane. (d) Directivity in the frontal plane.

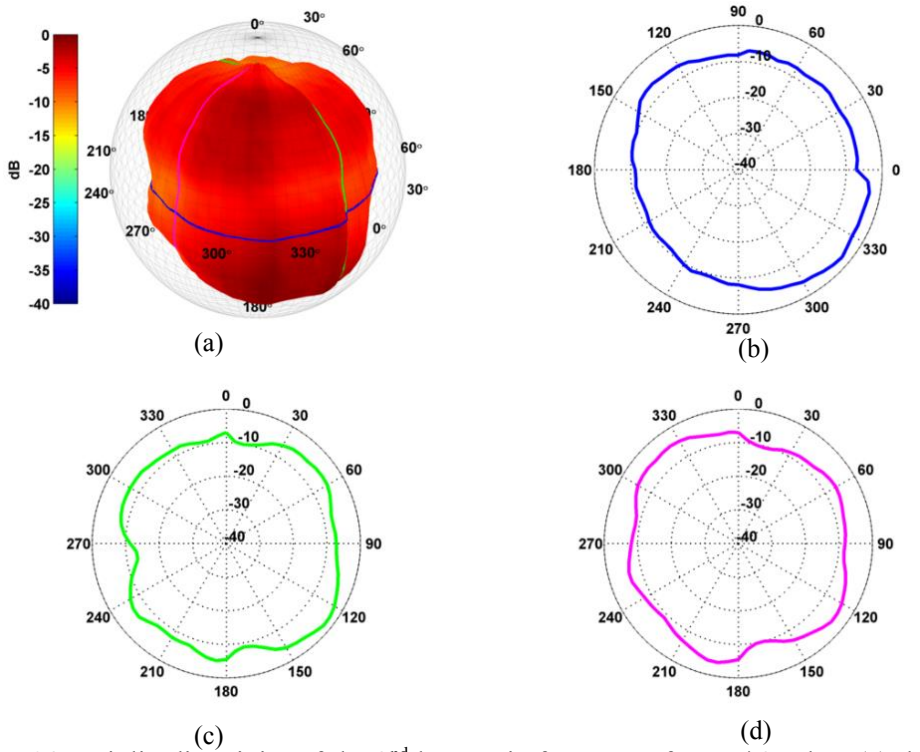

Figure 6.3. Violin directivity of the 2nd harmonic frequency for a B♭3. Plots (a) through (d) are arranged as described in Fig. 6.2.

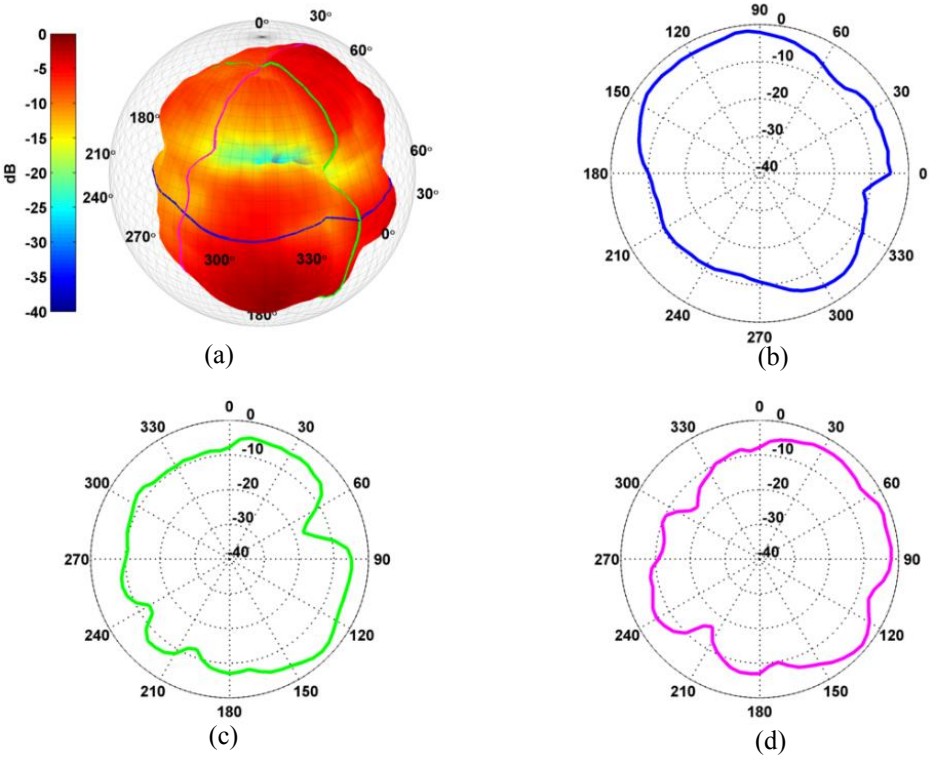

Figure 6.4. Violin directivity of the 3rd harmonic frequency for a B♭3. Plots (a) through (d) are arranged as described in Fig. 6.2.

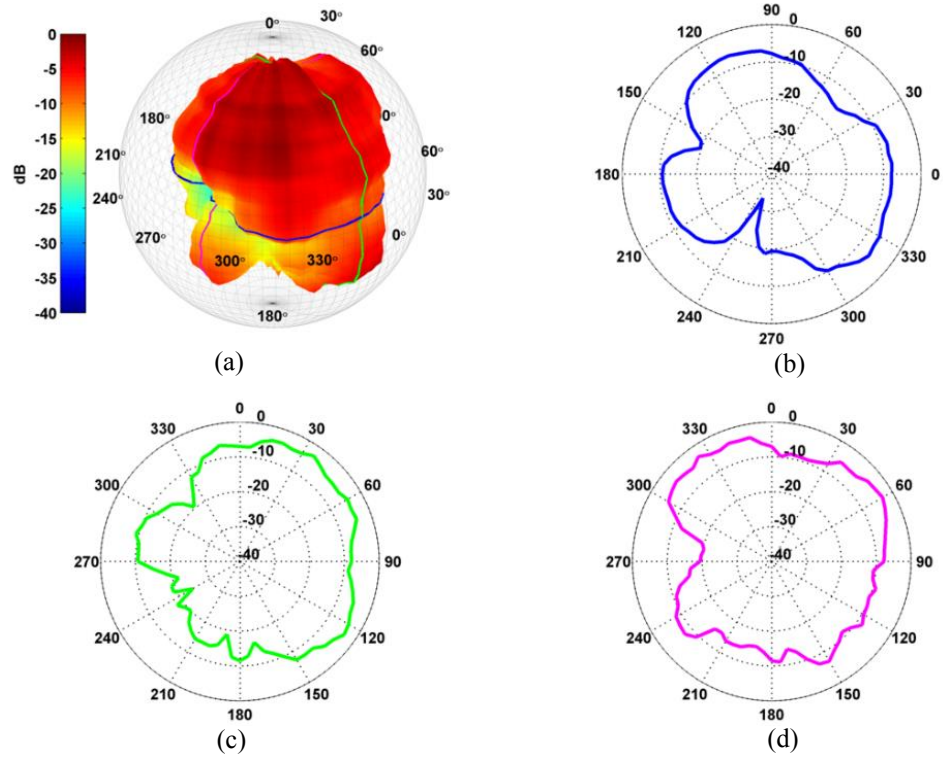

Figure 6.5. Violin directivity of the 4th harmonic frequency for a B♭3. Plots (a) through (d) are arranged as described in Fig. 6.2.

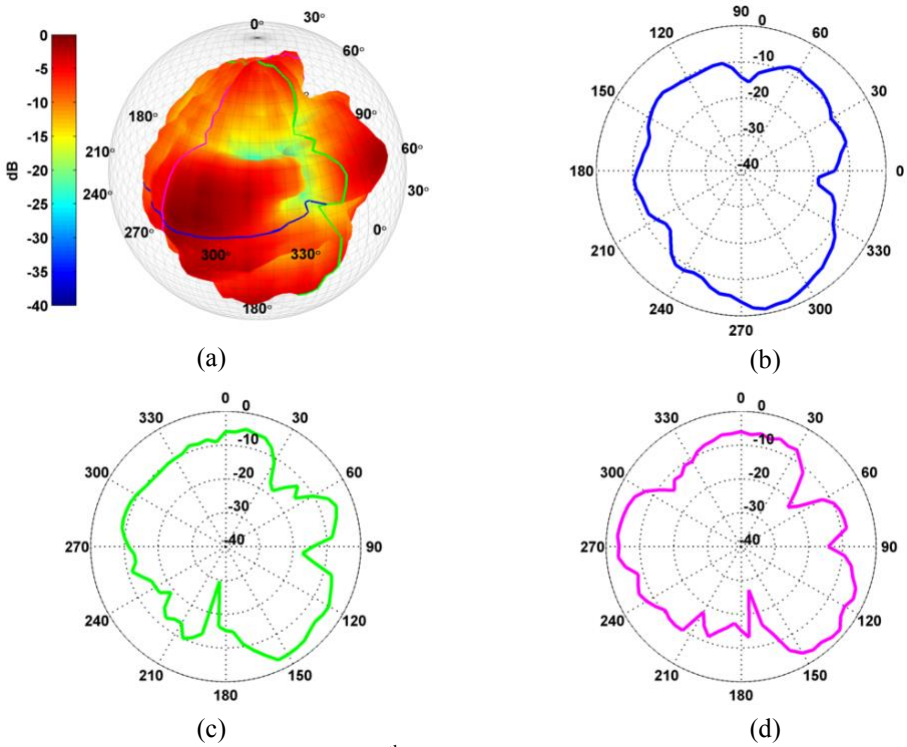

Figure 6.6. Violin directivity of the 5th harmonic frequency for a B♭3. Plots (a) through (d) are arranged as described in Fig. 6.2.

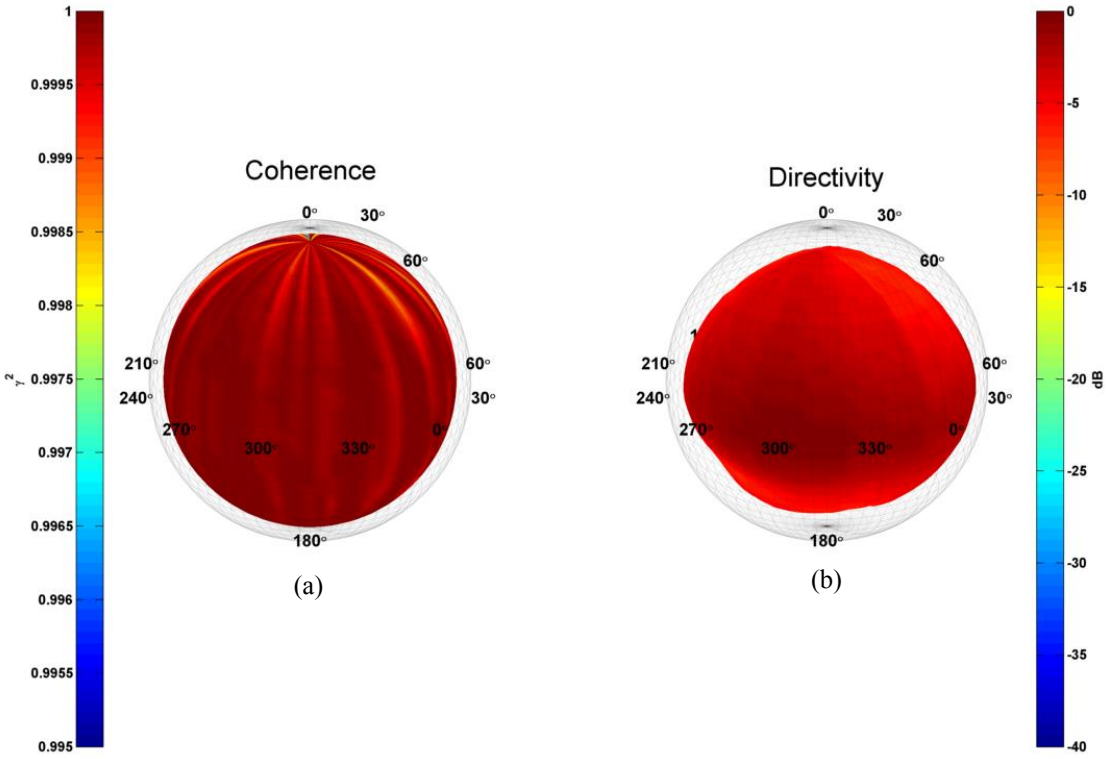

Figure 6.7. Violin plots of the fundamental frequency for a B♭3. (a) Coherence balloon. (b) Directivity balloon.

6.2 Viola

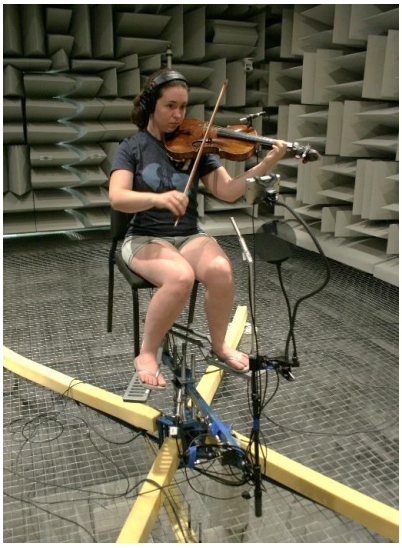

Figure 6.8. Violist seated in the DMS.

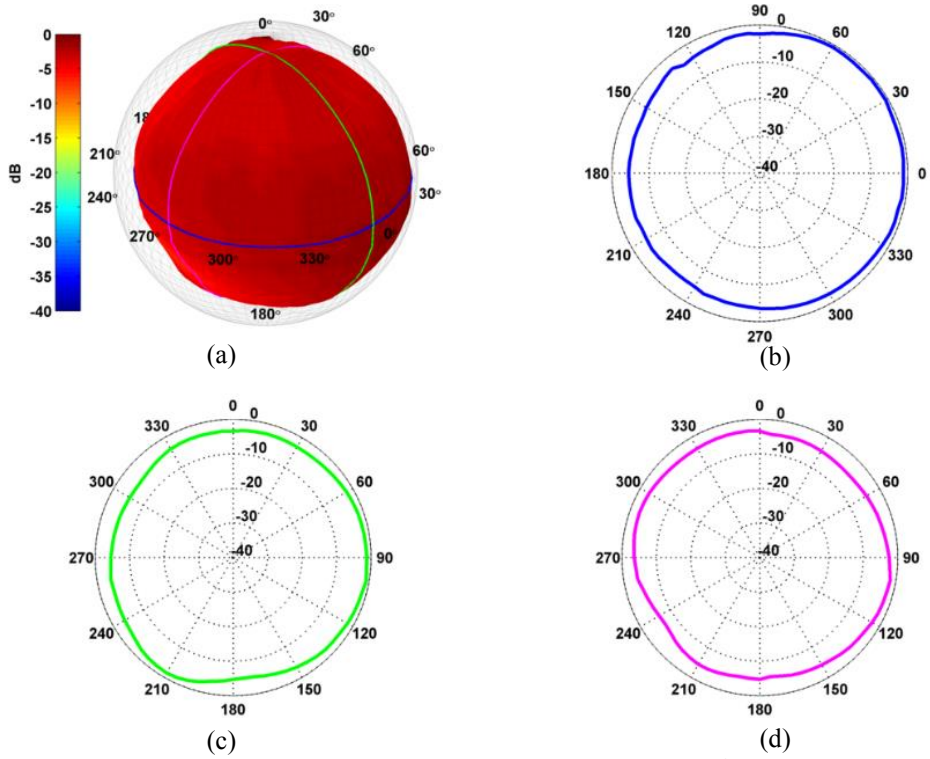

Figure 6.9. Viola directivity of the fundamental frequency for a C♯4. Plots (a) through (d) are arranged as described in Fig. 6.2.

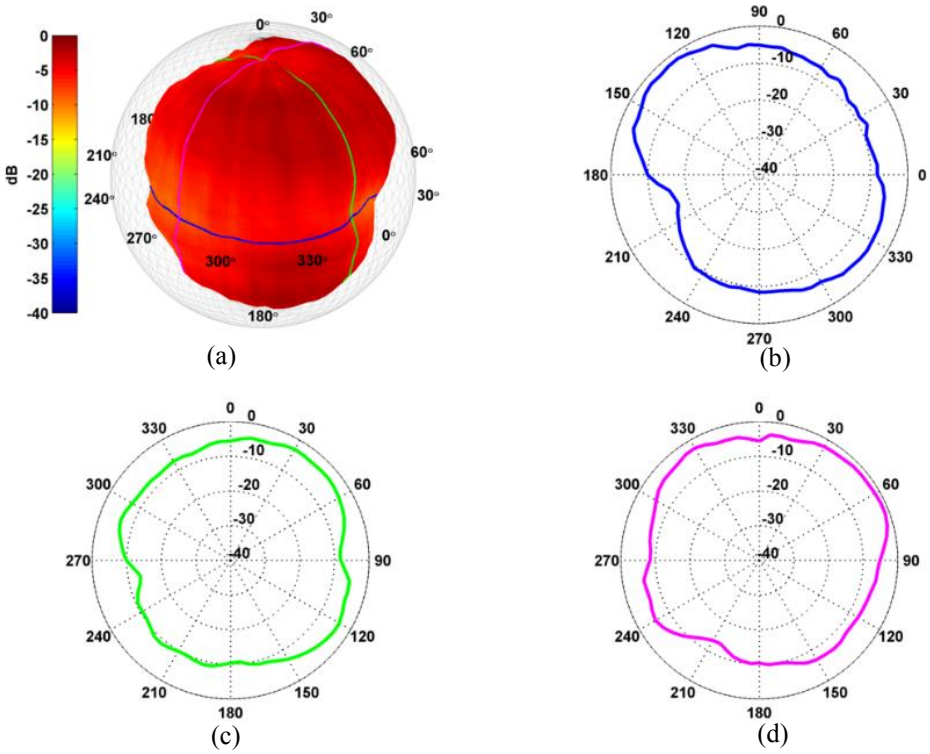

Figure 6.10. Viola directivity of the 2nd harmonic frequency for a C♯4. Plots (a) through (d) are arranged as described in Fig. 6.2.

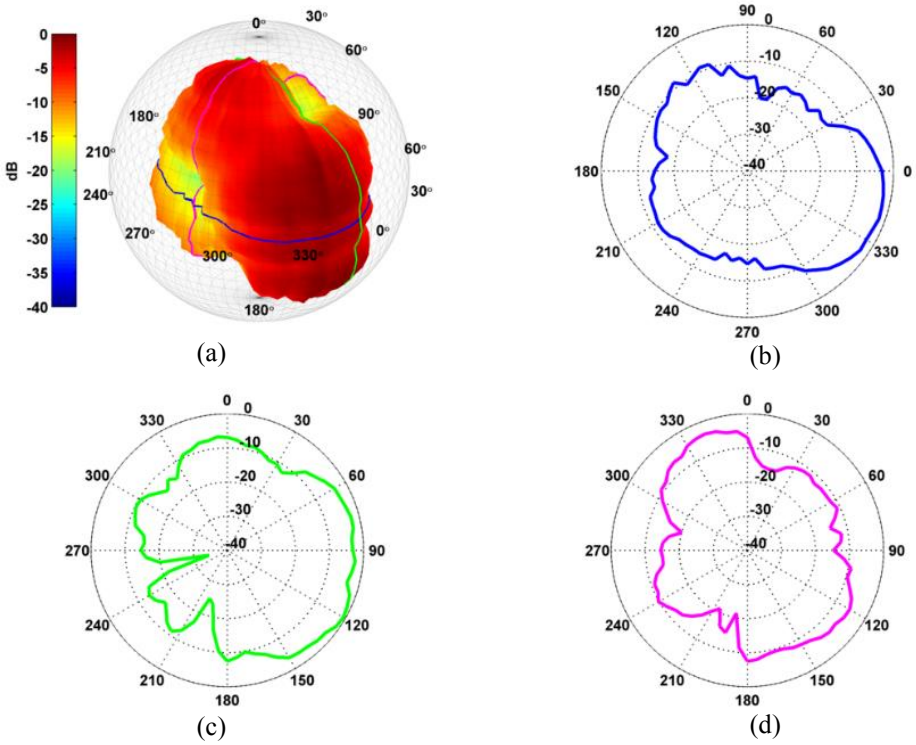

Figure 6.11. Viola directivity of the 3rd harmonic frequency for a C♯4. Plots (a) through (d) are arranged as described in Fig. 6.2.

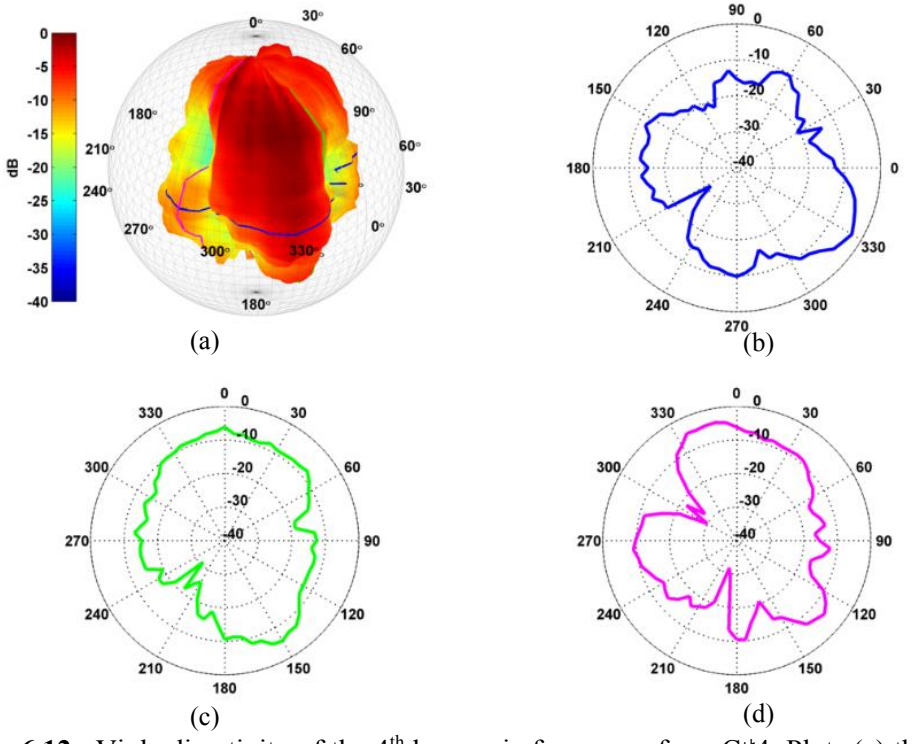

Figure 6.12. Viola directivity of the 4th harmonic frequency for a C♯4. Plots (a) through (d) are arranged as described in Fig. 6.2.

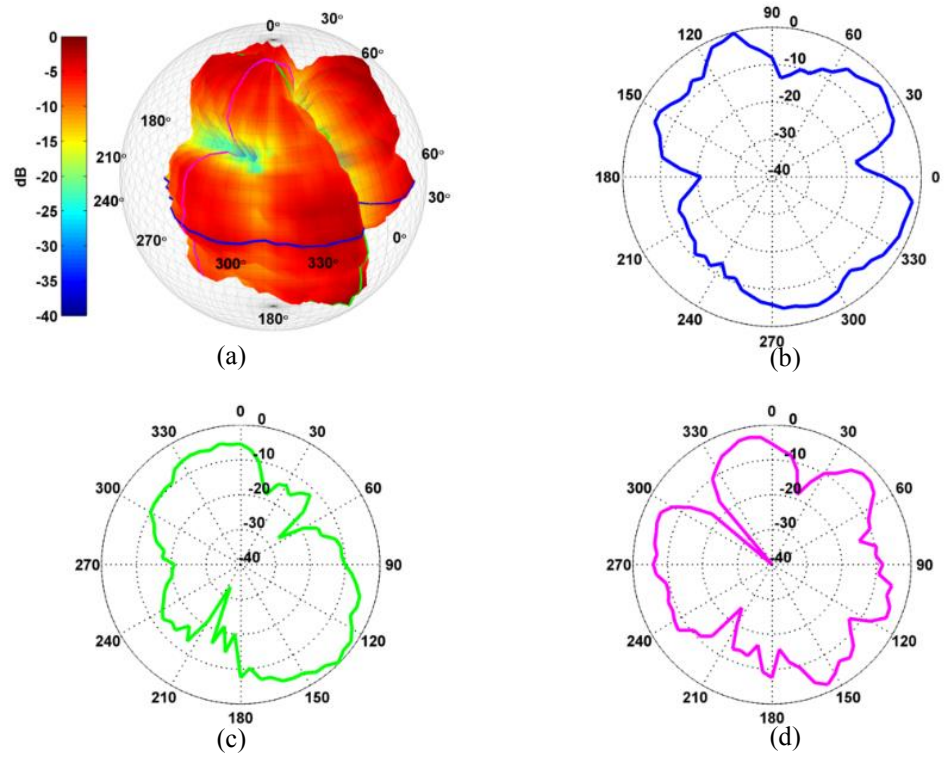

Figure 6.13. Viola directivity of the 5th harmonic frequency for a C♯4. Plots (a) through (d) are arranged as described in Fig. 6.2.

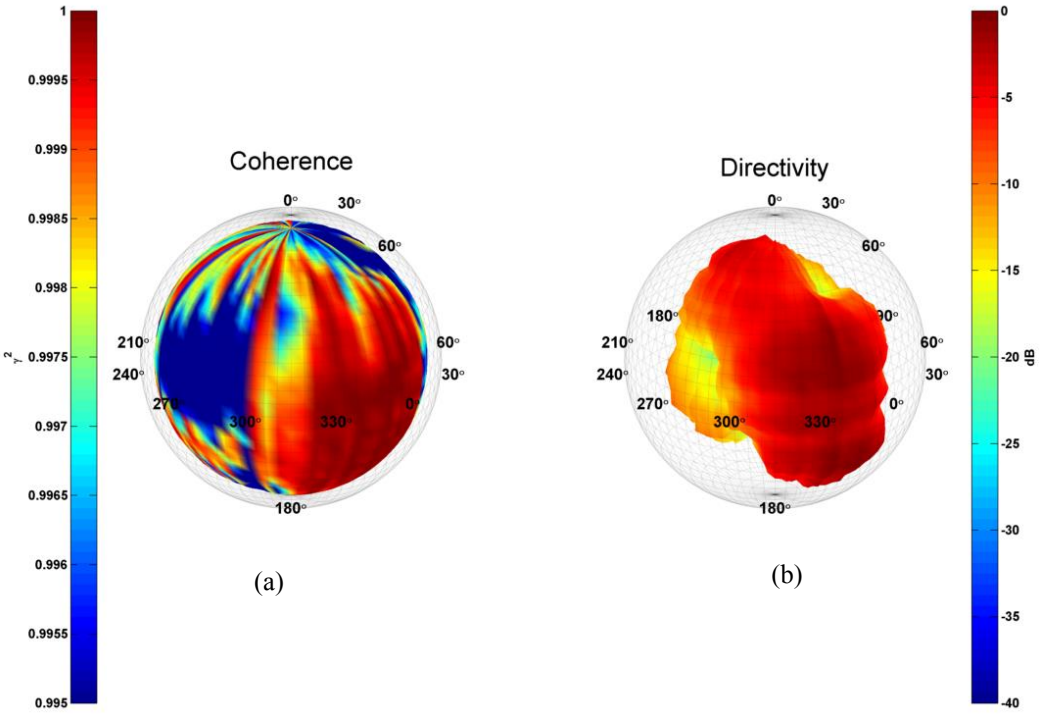

Figure 6.14. Viola plots of the 3rd harmonic frequency for a C♯4. (a) Coherence balloon. (b) Directivity balloon.

6.3 Cello

Figure 6.15. Cellist seated in the DMS.

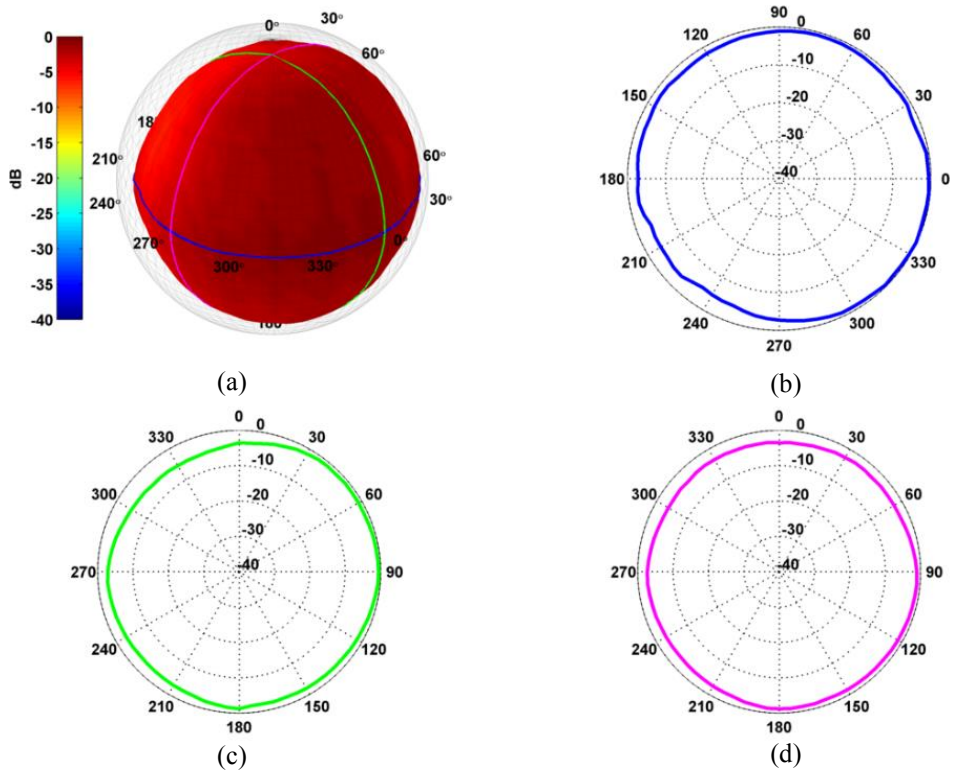

Figure 6.16. Cello directivity of the fundamental frequency for a F3. Plots (a) through (d) are arranged as described in Fig. 6.2.

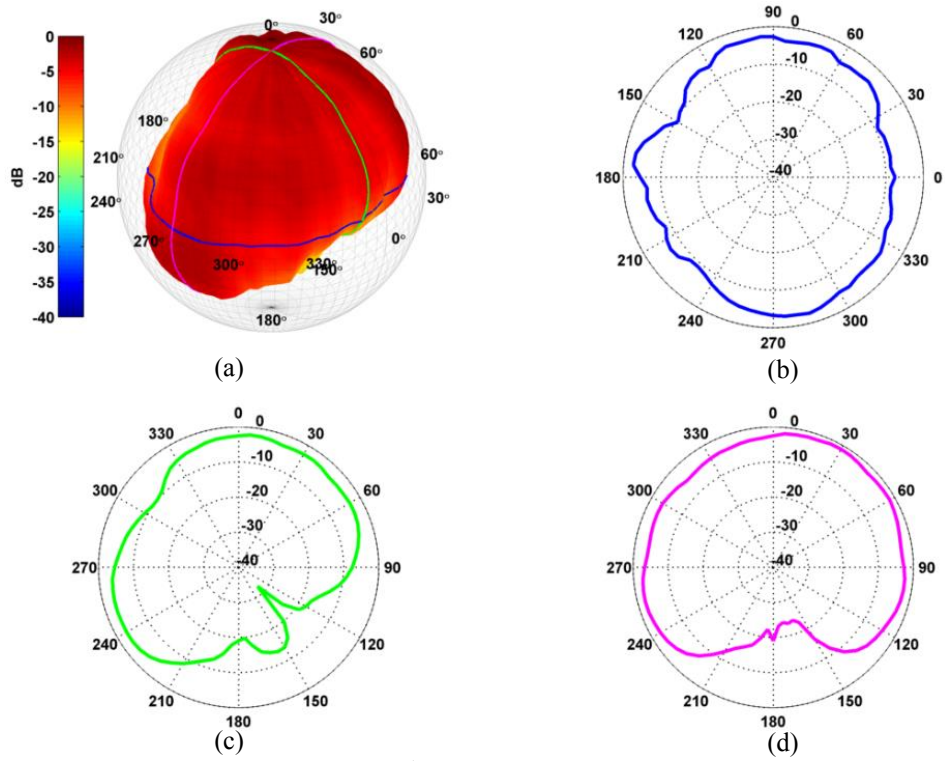

Figure 6.17. Cello directivity of the 2nd harmonic frequency for a F3. Plots (a) through (d) are arranged as described in Fig. 6.2.

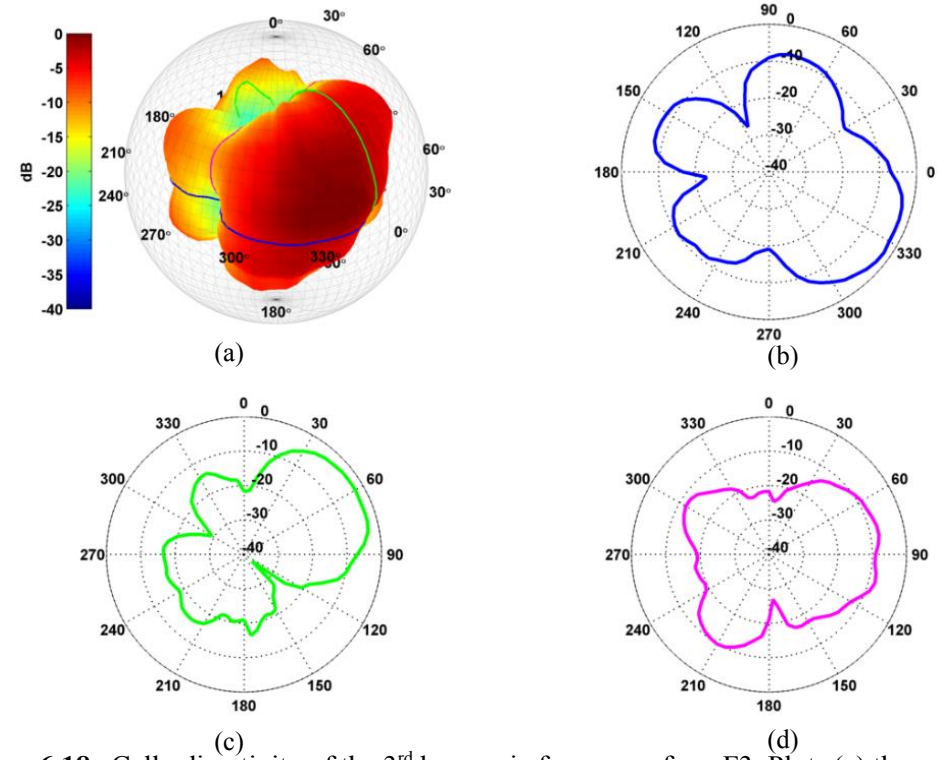

Figure 6.18. Cello directivity of the 3rd harmonic frequency for a F3. Plots (a) through (d) are arranged as described in Fig. 6.2.

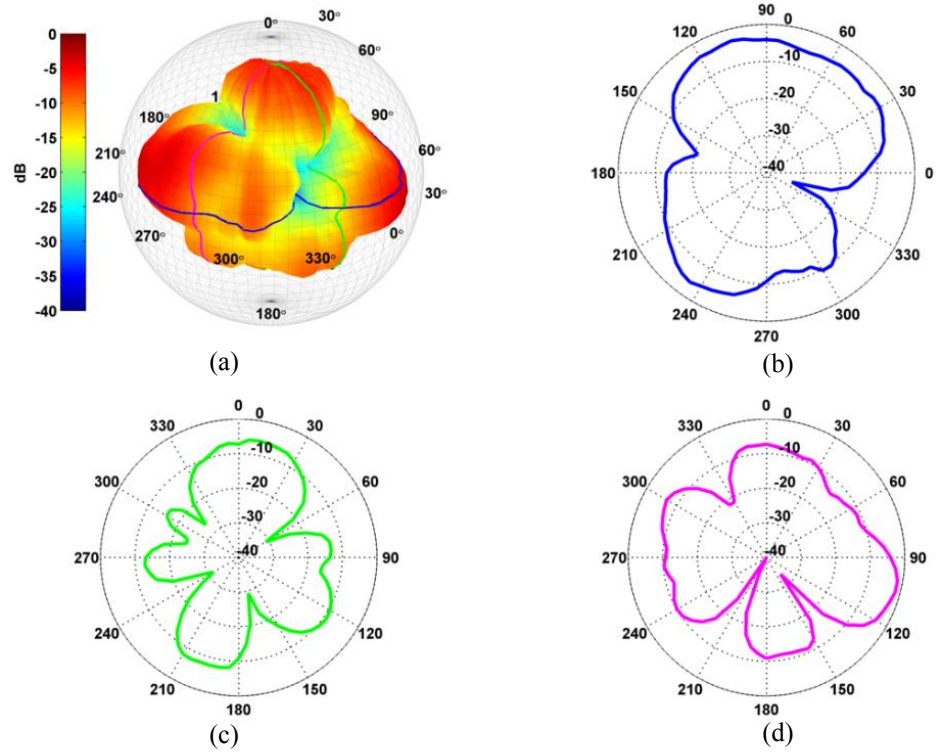

Figure 6.19. Cello directivity of the 4th harmonic frequency for a F3. Plots (a) through (d) are arranged as described in Fig. 6.2.

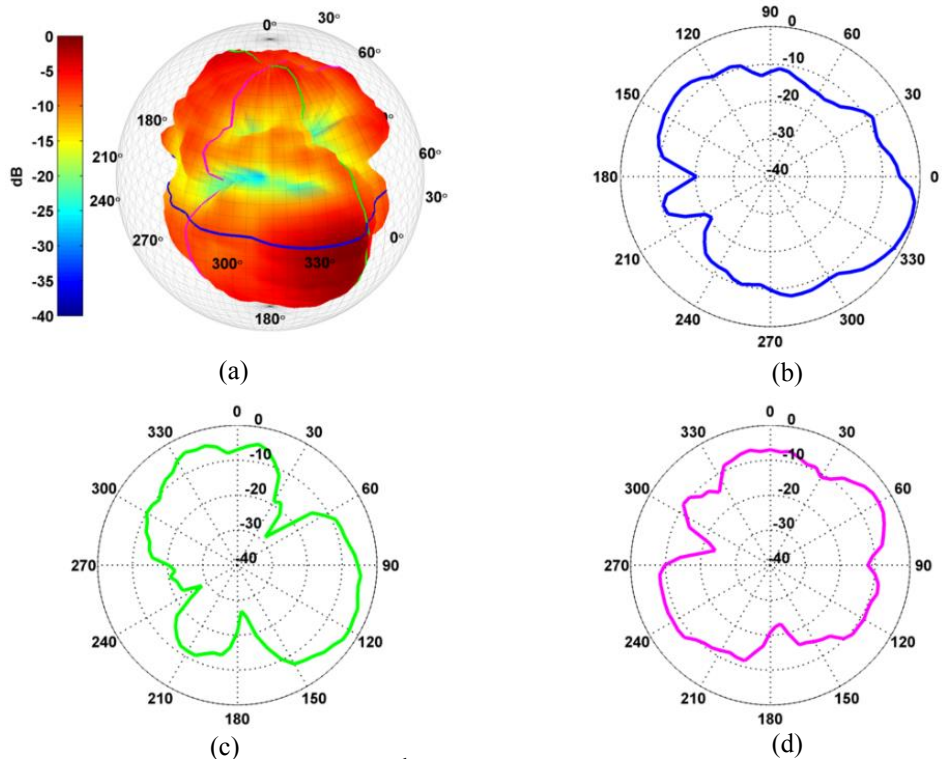

Figure 6.20. Cello directivity of the 5th harmonic frequency for a F3. Plots (a) through (d) are arranged as described in Fig. 6.2.

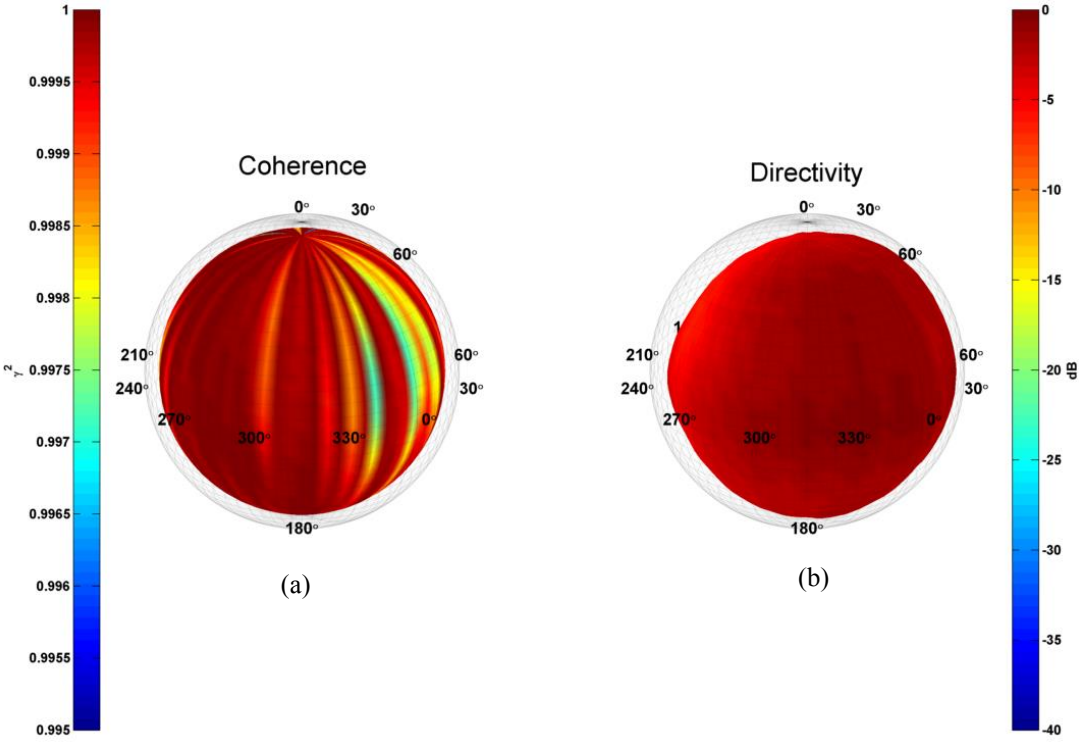

(a) (b)

Figure 6.21. Cello plots of the fundamental frequency for a F3. (a) Coherence balloon. (b) Directivity balloon.

6.4 Double Bass

Figure 6.22. Bassist seated in the DMS.

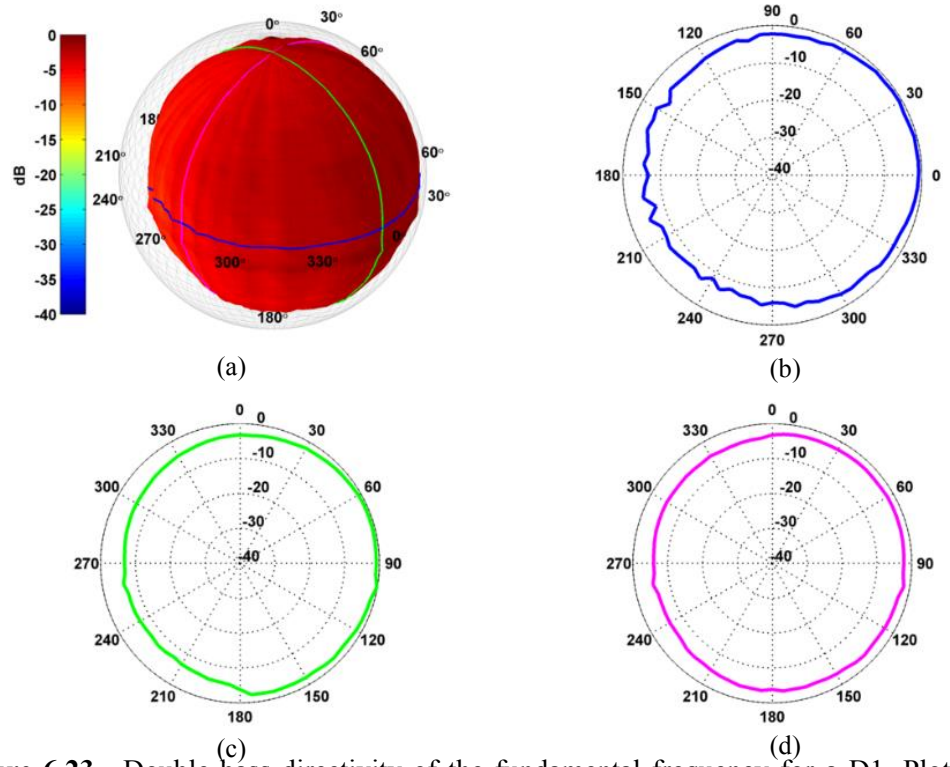

Figure 6.23. Double bass directivity of the fundamental frequency for a D1. Plots (a) through (d) are arranged as described in Fig. 6.2.

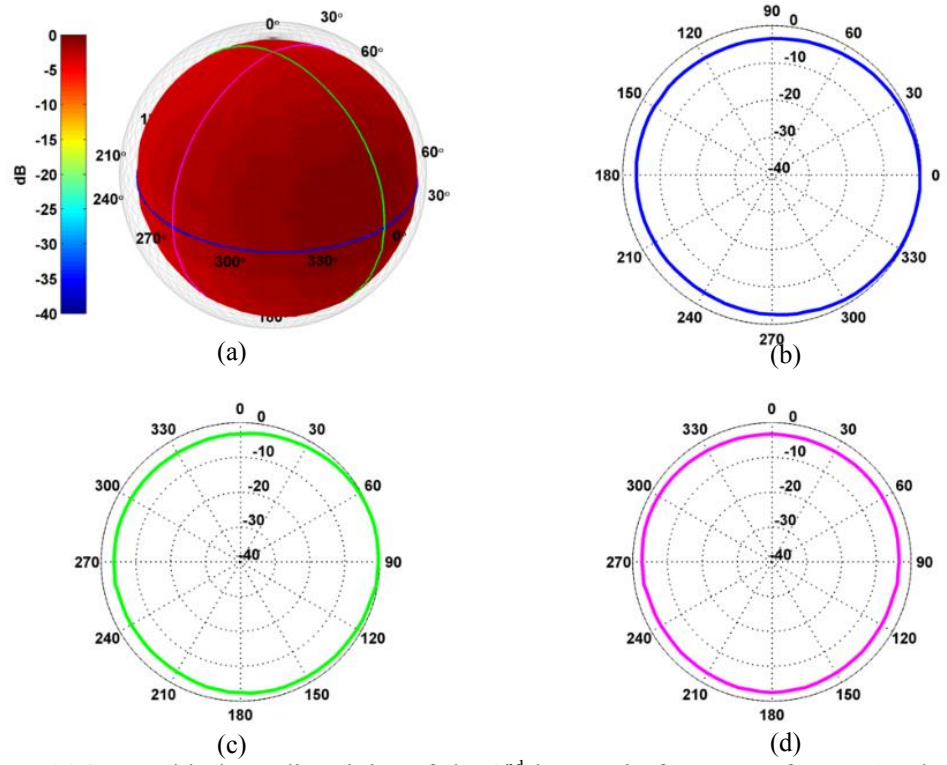

Figure 6.24. Double bass directivity of the 2nd harmonic frequency for a D1. Plots (a) through (d) are arranged as described in Fig. 6.2.

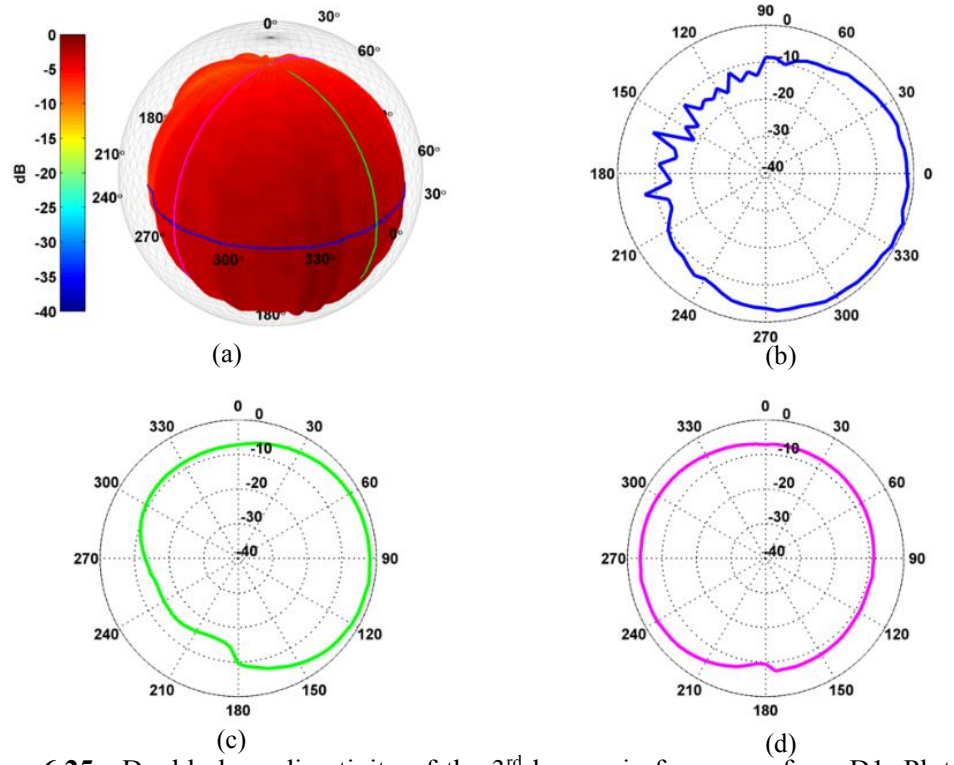

Figure 6.25. Double bass directivity of the 3rd harmonic frequency for a D1. Plots (a) through (d) are arranged as described in Fig. 6.2.

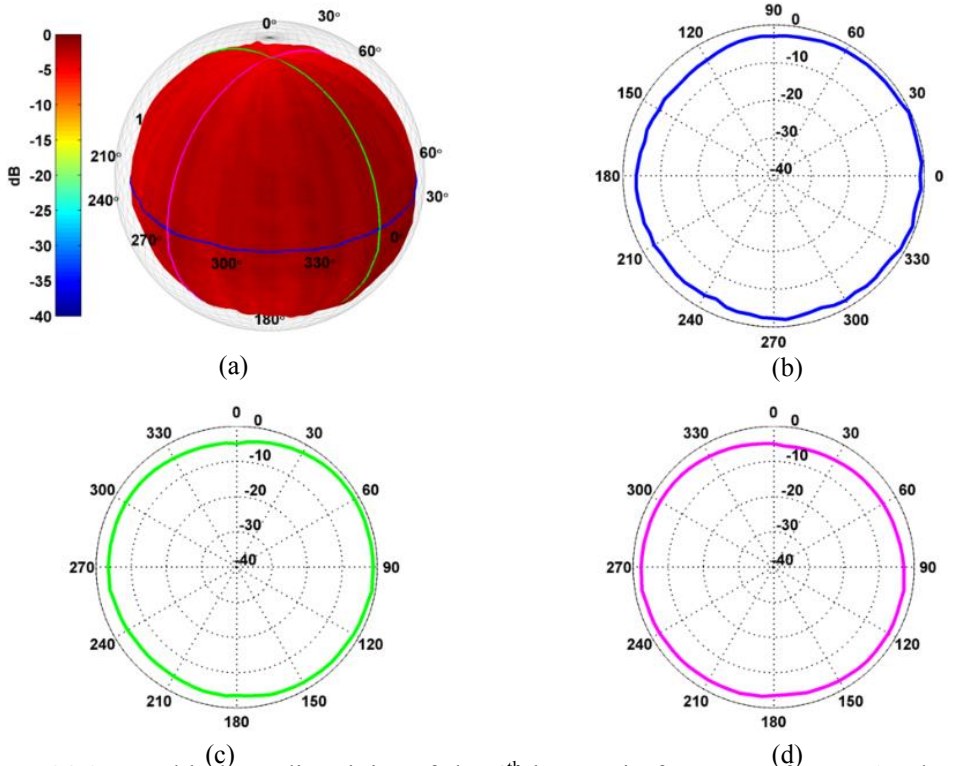

Figure 6.26. Double bass directivity of the 4th harmonic frequency for a D1. Plots (a) through (d) are arranged as described in Fig. 6.2.

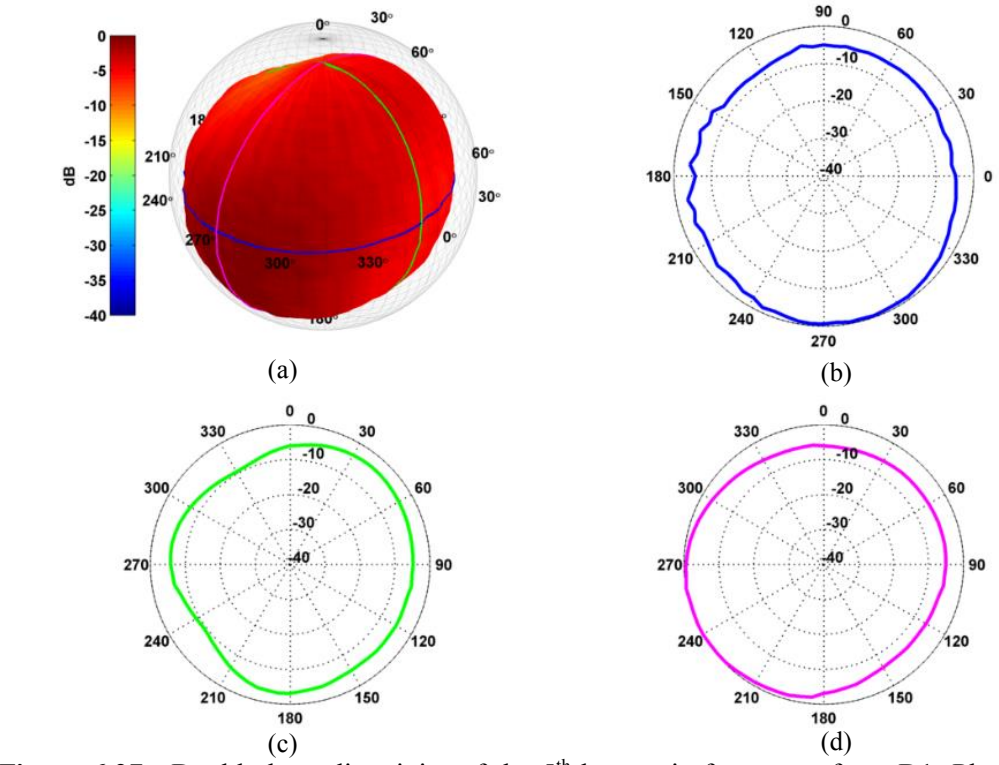

Figure 6.27. Double bass directivity of the 5th harmonic frequency for a D1. Plots (a) through (d) are arranged as described in Fig. 6.2.

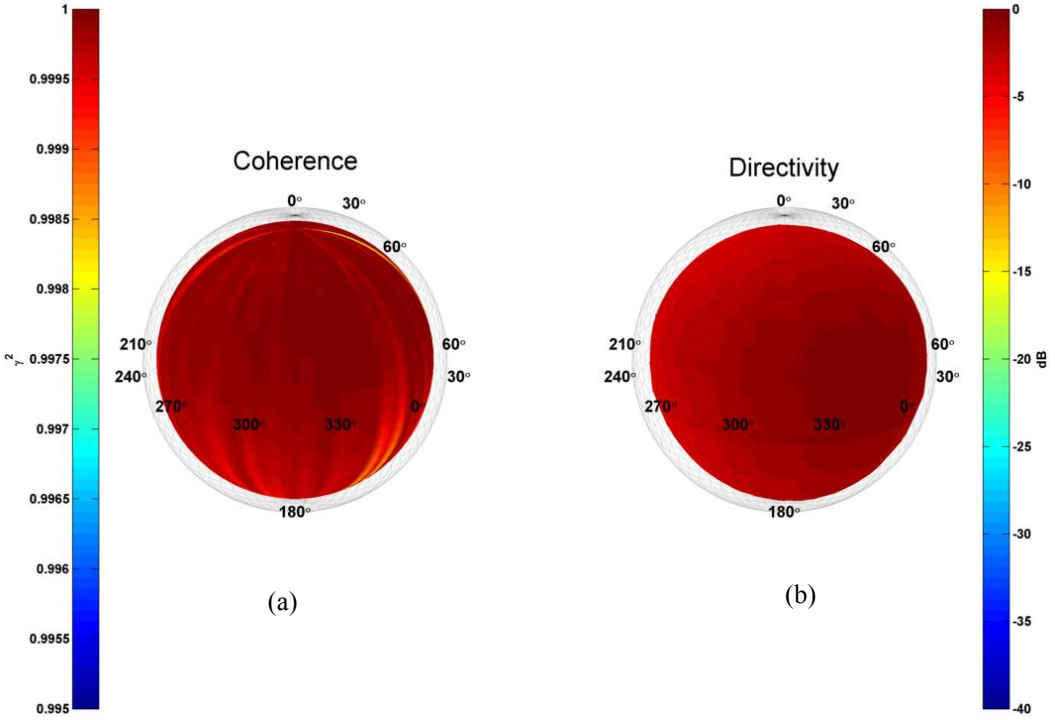

Figure 6.28. Double bass plots of the 2nd harmonic frequency for a D1. (a) Coherence balloon. (b) Directivity balloon.

6.5 Trumpet

Figure 6.29. Trumpeter seated in the DMS.

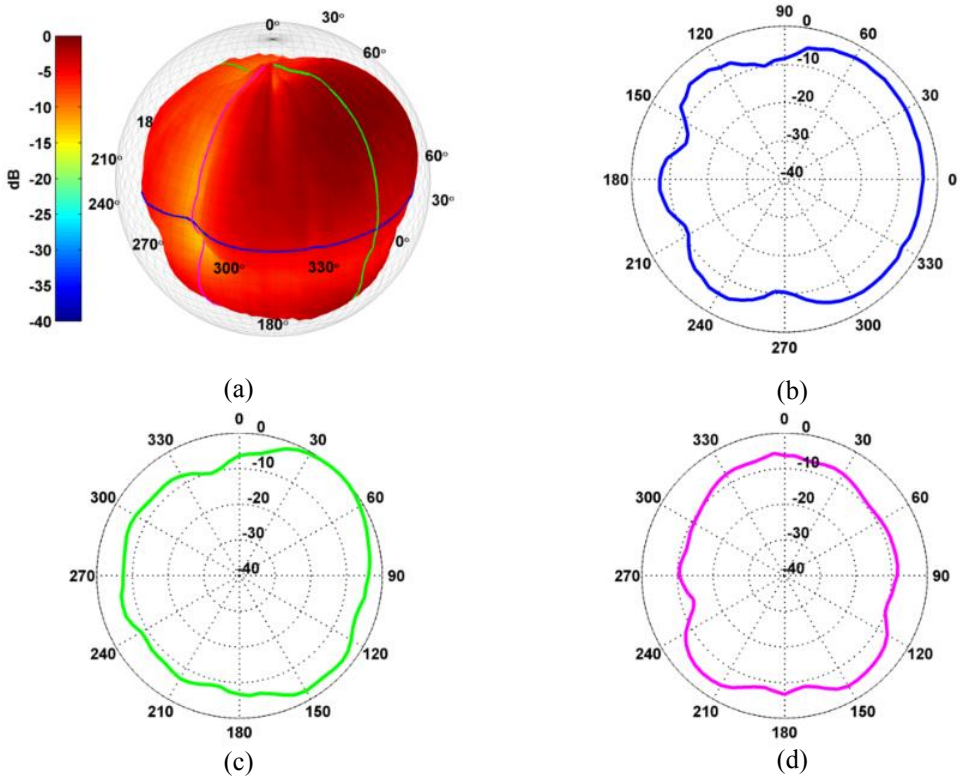

Figure 6.30. Trumpet directivity of the fundamental frequency for an A♯4. Plots (a) through (d) are arranged as described in Fig. 6.2.

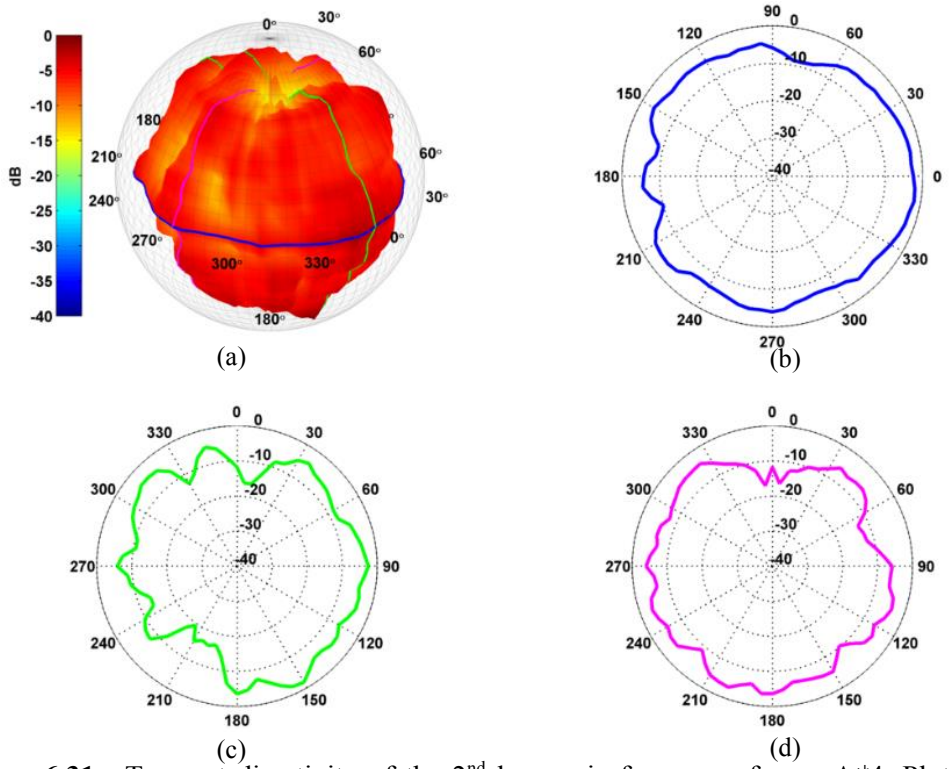

Figure 6.31. Trumpet directivity of the 2nd harmonic frequency for an A♯4. Plots (a) through (d) are arranged as described in Fig. 6.2.

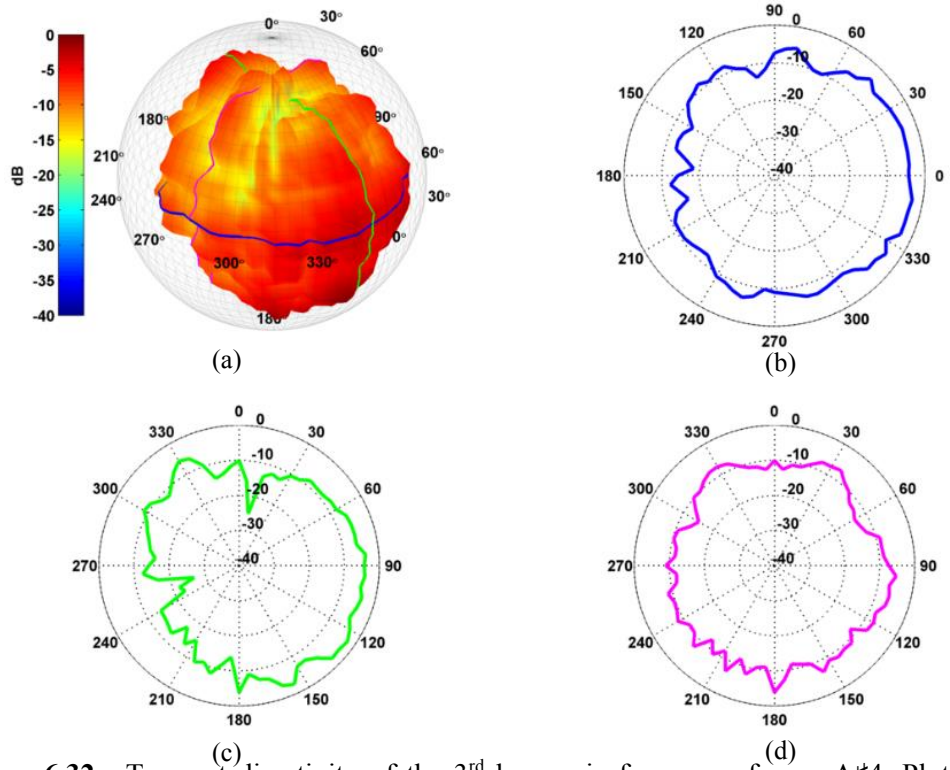

Figure 6.32. Trumpet directivity of the 3rd harmonic frequency for an A♯4. Plots (a) through (d) are arranged as described in Fig. 6.2.

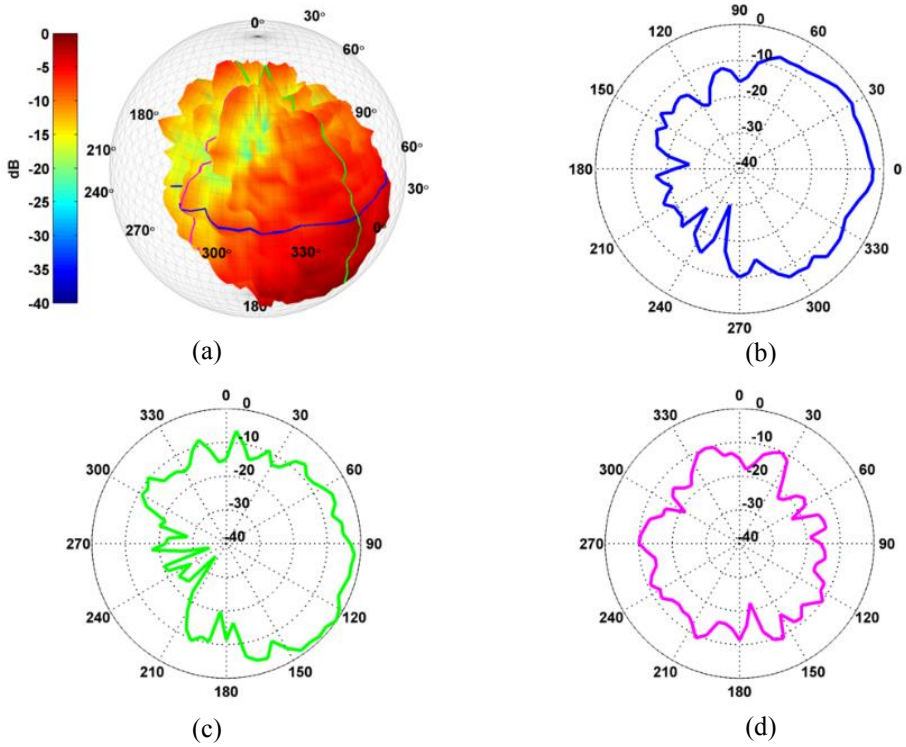

Figure 6.33. Trumpet directivity of the 4th harmonic frequency for an A♯4. Plots (a) through (d) are arranged as described in Fig. 6.2.

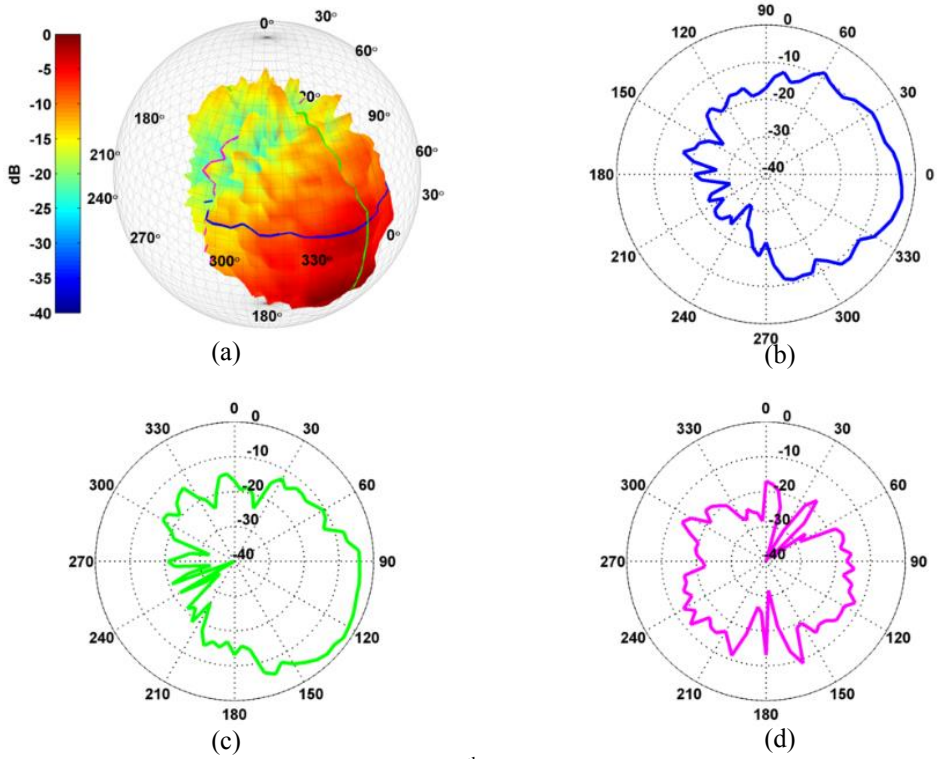

Figure 6.34. Trumpet directivity of the 5th harmonic frequency for an A♯4. Plots (a) through (d) are arranged as described in Fig. 6.2.

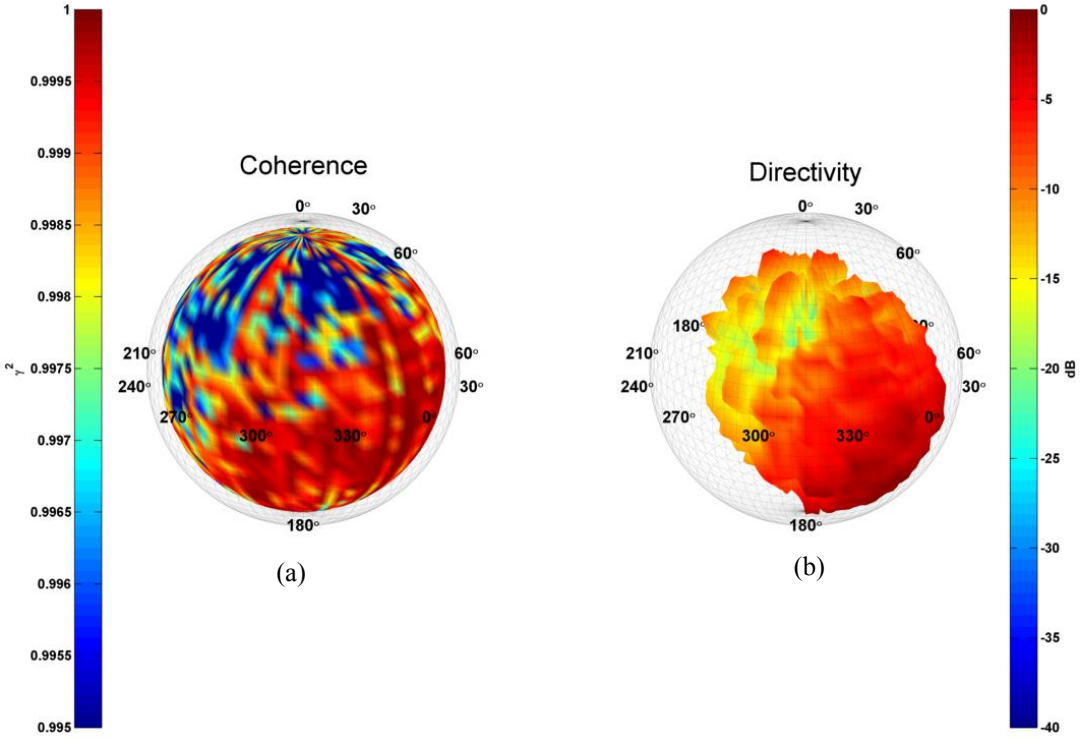

Figure 6.35. Trumpet plots of the 4th harmonic frequency for a A♯4. (a) Coherence balloon. (b) Directivity balloon.

6.6 Trombone

Figure 6.36. Trombonist seated in the DMS.

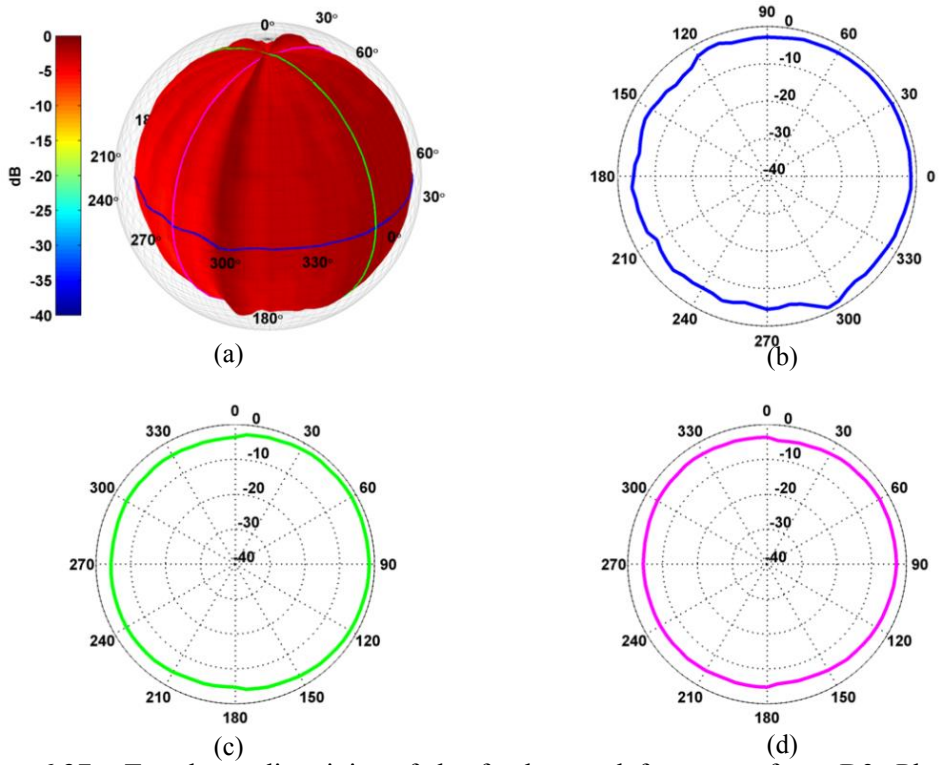

Figure 6.37. Trombone directivity of the fundamental frequency for a D3. Plots (a) through (d) are arranged as described in Fig. 6.2.

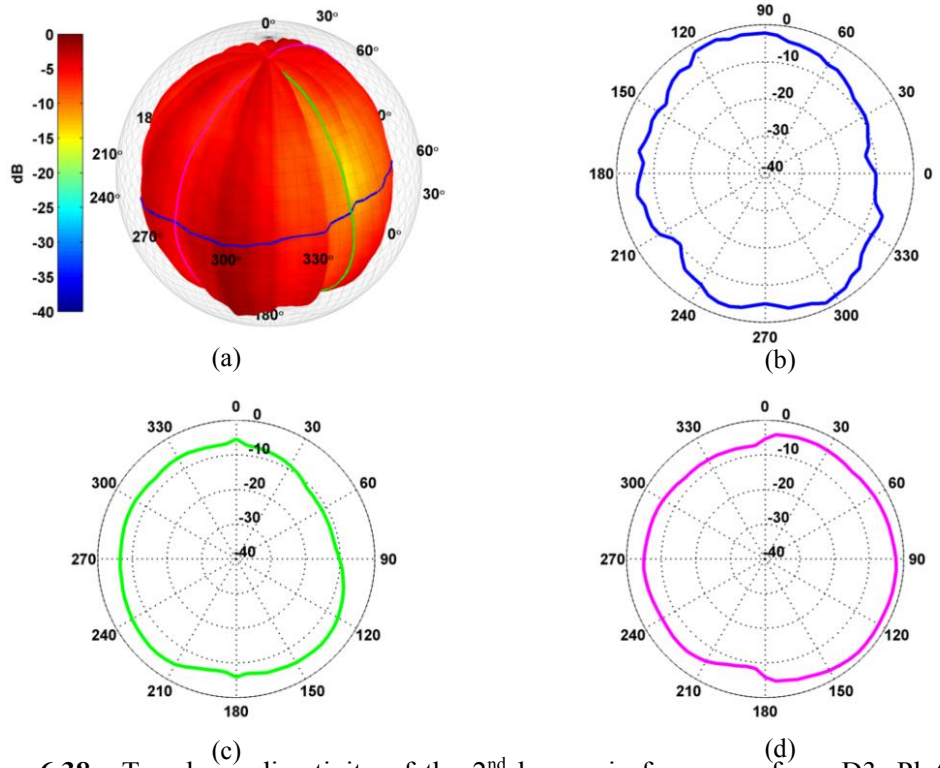

Figure 6.38. Trombone directivity of the 2nd harmonic frequency for a D3. Plots (a) through (d) are arranged as described in Fig. 6.2.

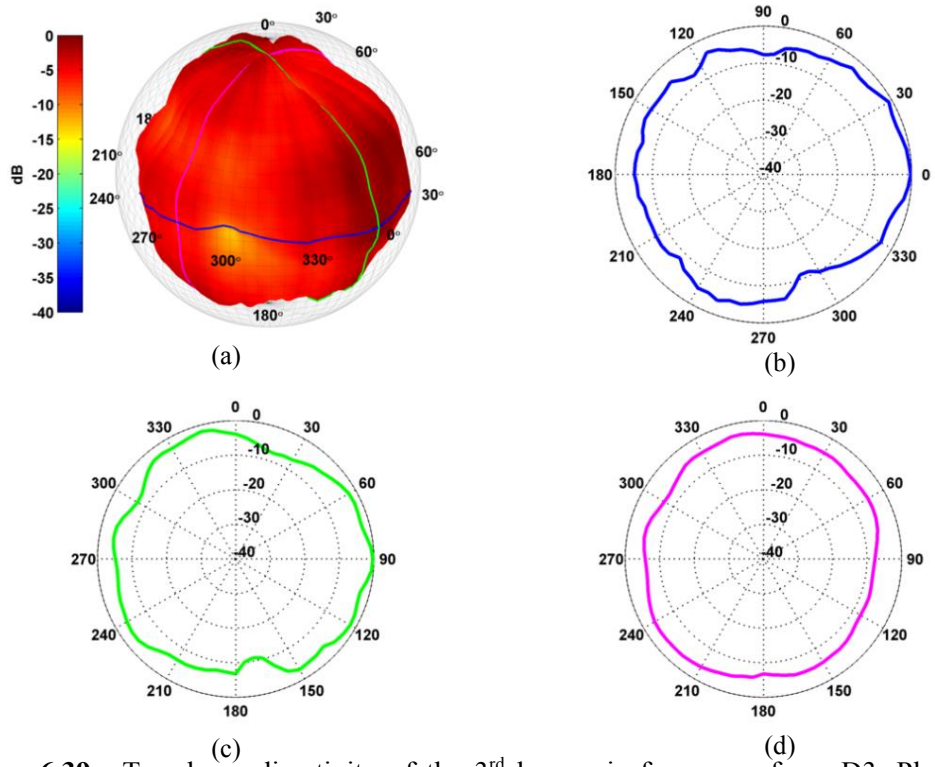

Figure 6.39. Trombone directivity of the 3rd harmonic frequency for a D3. Plots (a) through (d) are arranged as described in Fig. 6.2.

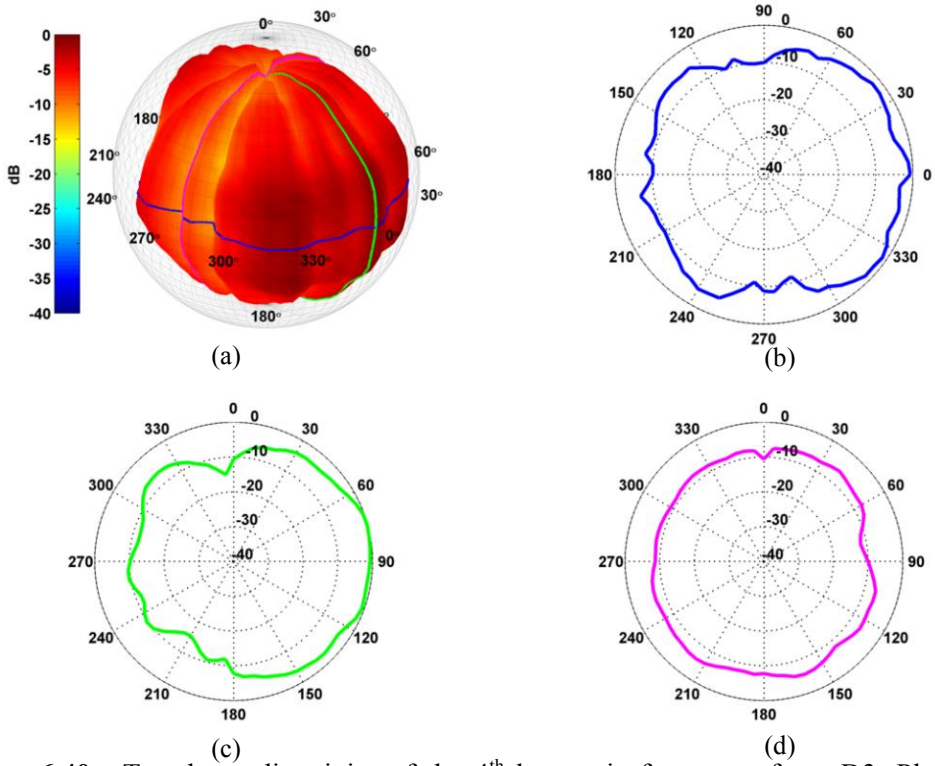

Figure 6.40. Trombone directivity of the 4th harmonic frequency for a D3. Plots (a) through (d) are arranged as described in Fig. 6.2.

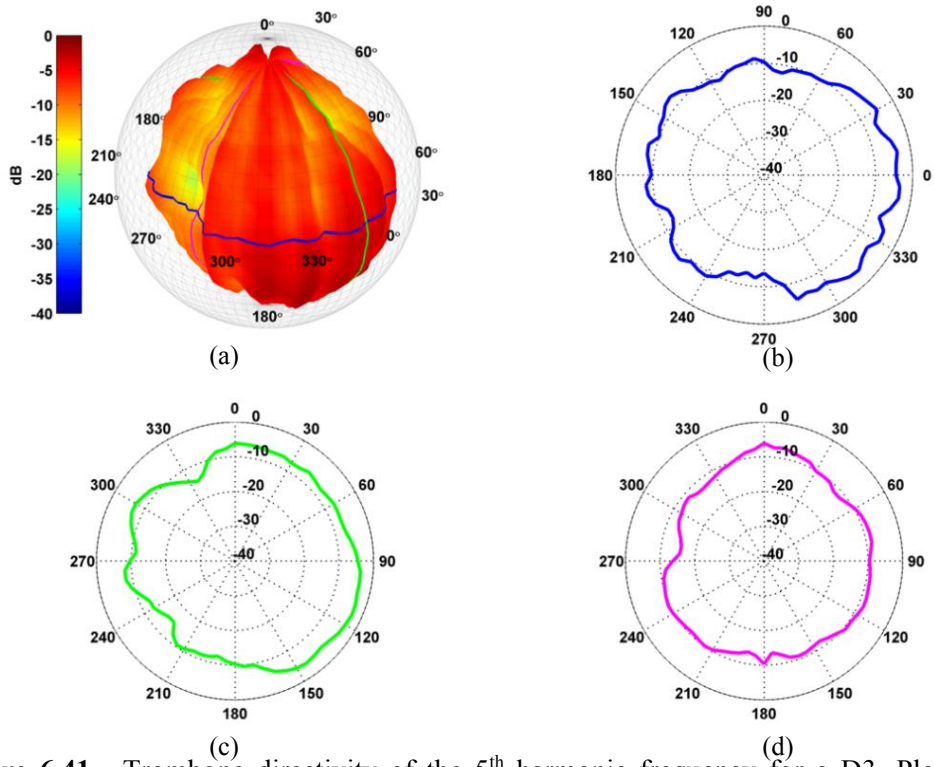

Figure 6.41. Trombone directivity of the 5th harmonic frequency for a D3. Plots (a) through (d) are arranged as described in Fig. 6.2.

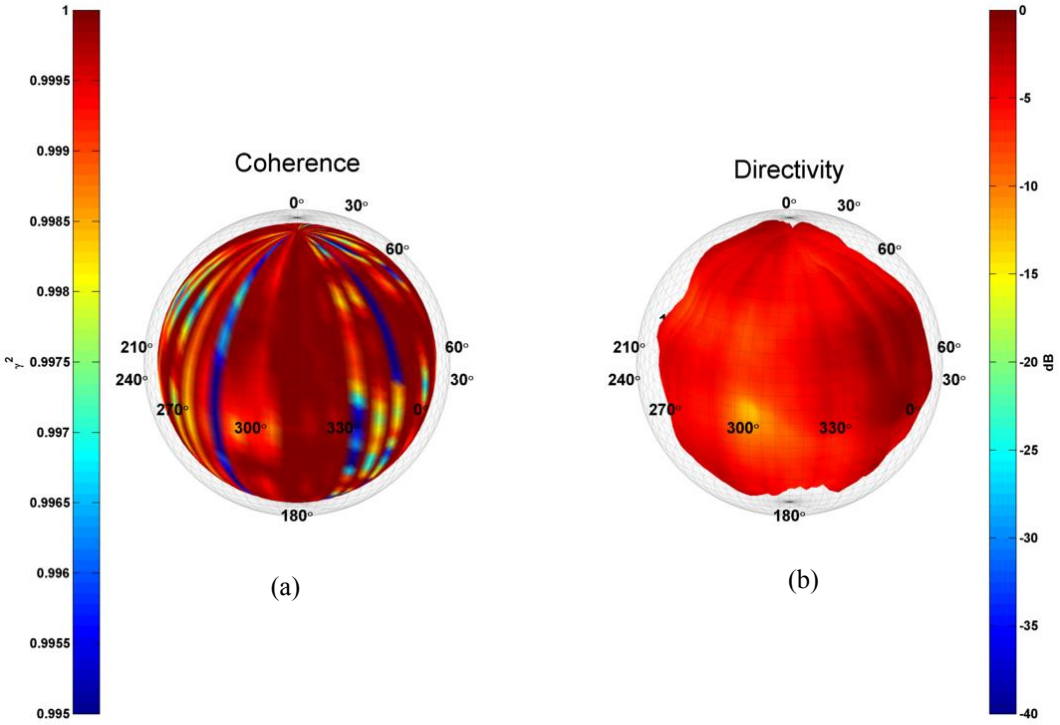

Figure 6.42. Trombone plots of the 3rd harmonic frequency for a D3. (a) Coherence balloon. (b) Directivity balloon.

6.7 French horn

Figure 6.43. French horn player seated in the DMS.

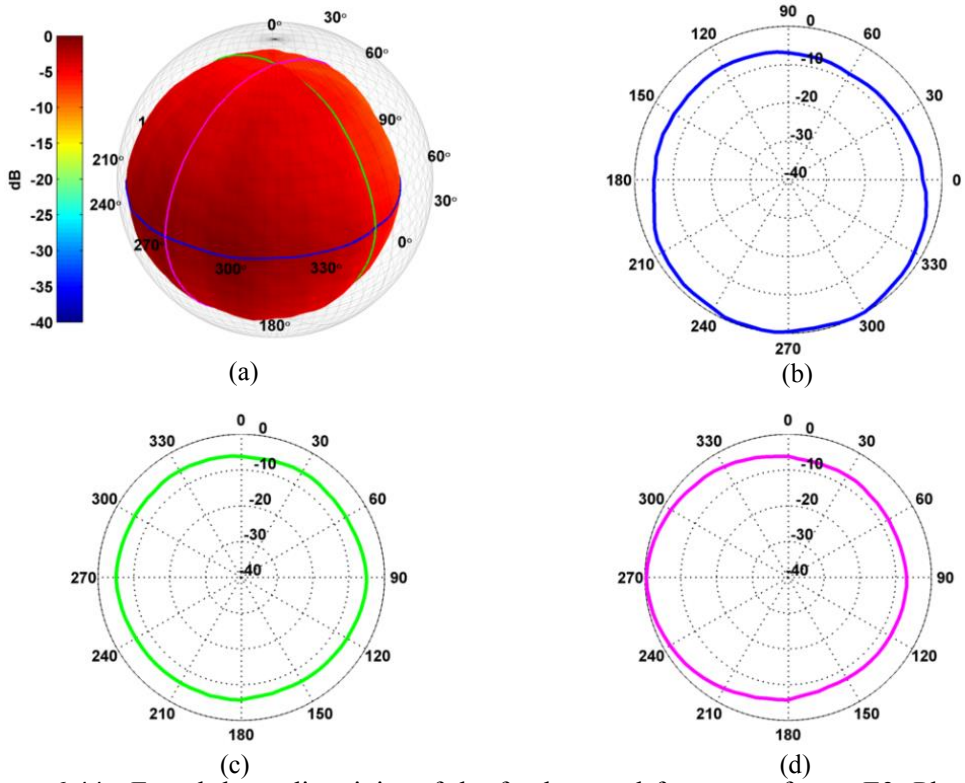

Figure 6.44. French horn directivity of the fundamental frequency for an E3. Plots (a) through (d) are arranged as described in Fig. 6.2.

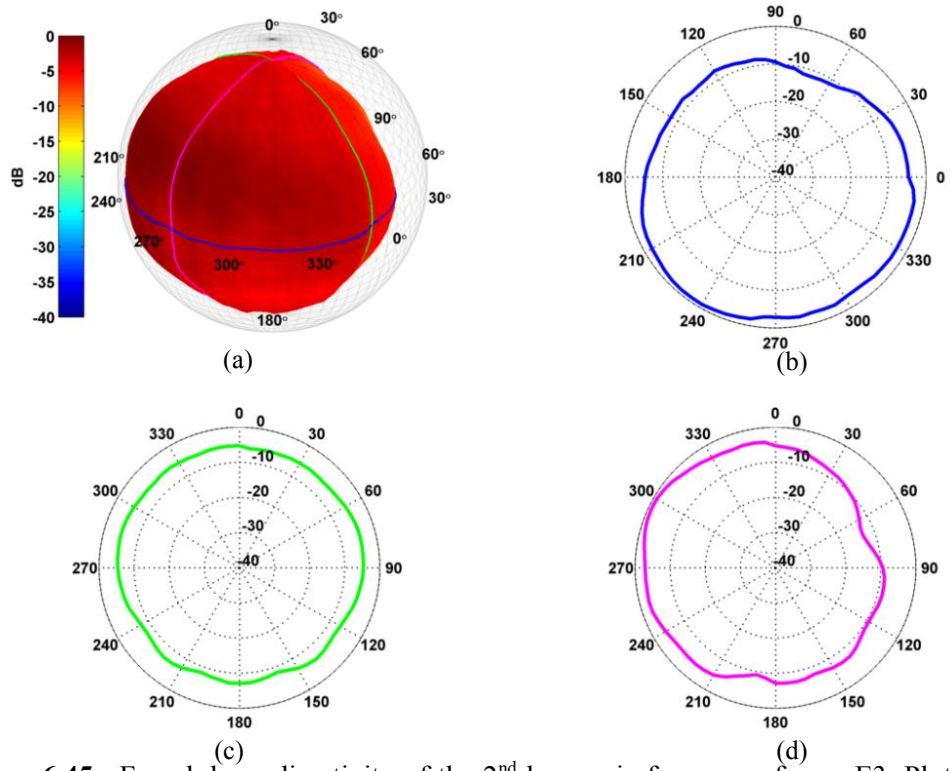

Figure 6.45. French horn directivity of the 2nd harmonic frequency for an E3. Plots (a) through (d) are arranged as described in Fig. 6.2.

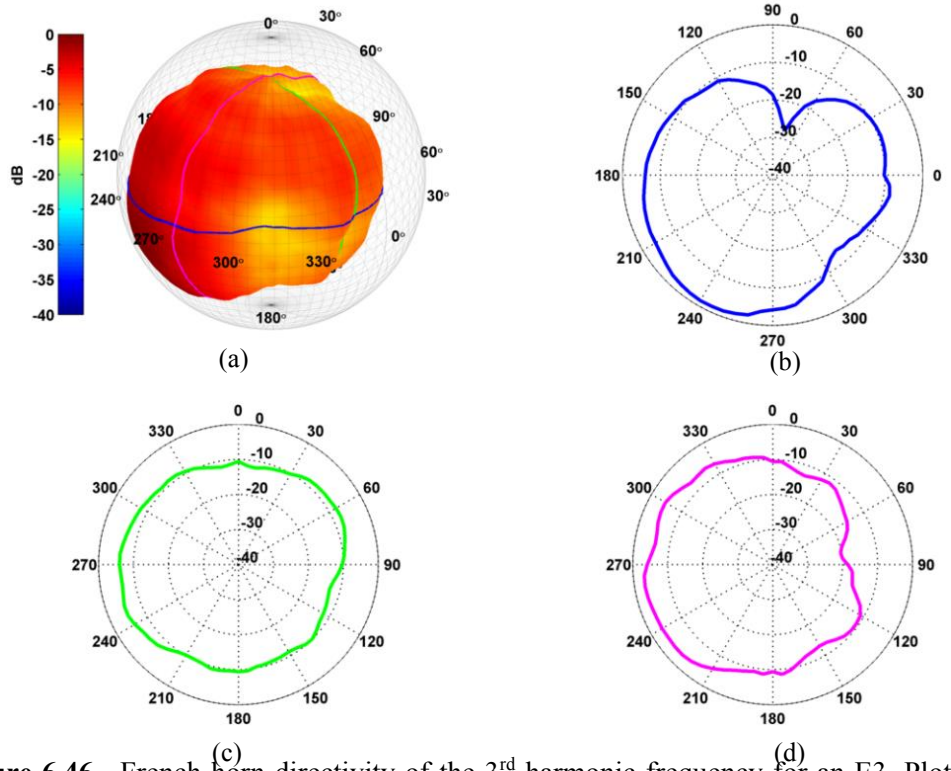

Figure 6.46. French horn directivity of the 3rd harmonic frequency for an E3. Plots (a) through (d) are arranged as described in Fig. 6.2.

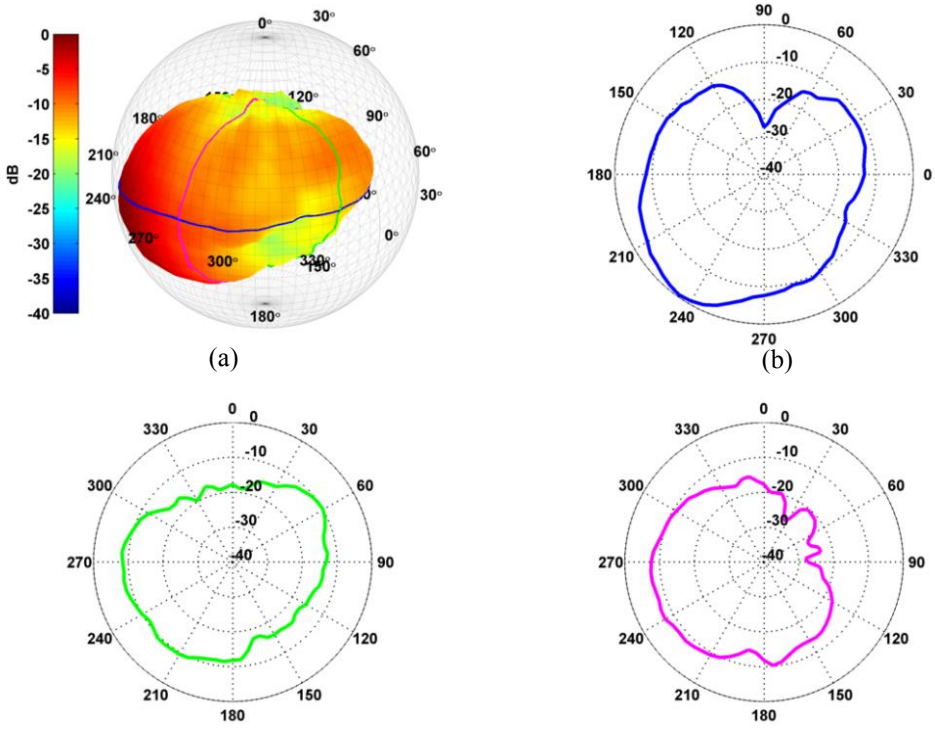

Figure 6.47. French horn directivity of the 4th harmonic frequency for an E3. Plots (a) through (d) are arranged as described in Fig. 6.2.

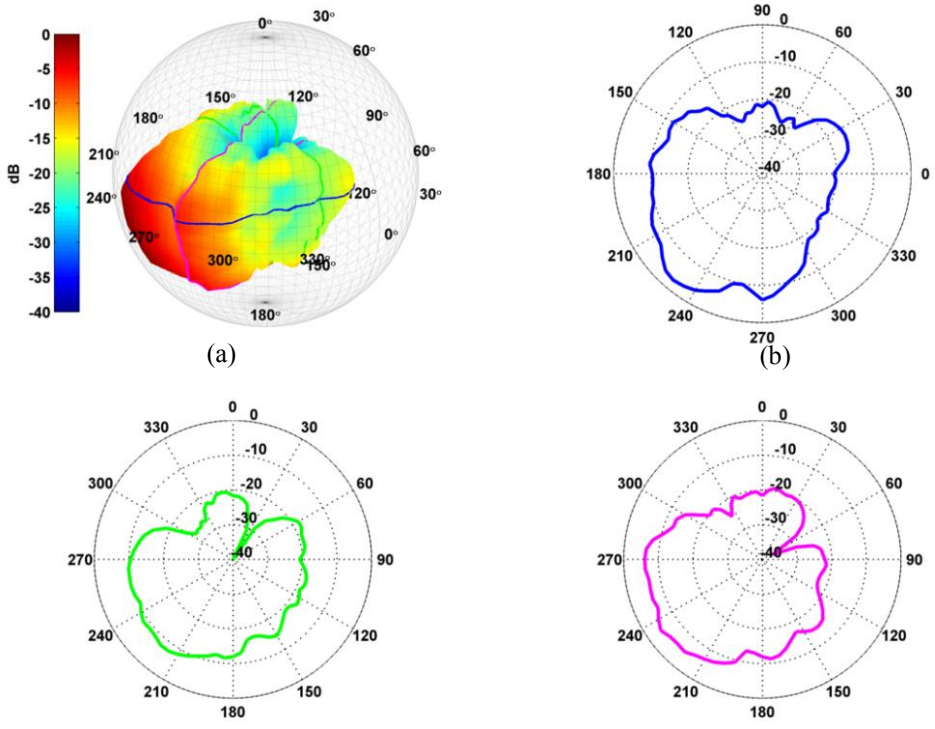

Figure 6.48. French horn directivity of the 5th harmonic frequency for an E3. Plots (a) through (d) are arranged as described in Fig. 6.2.

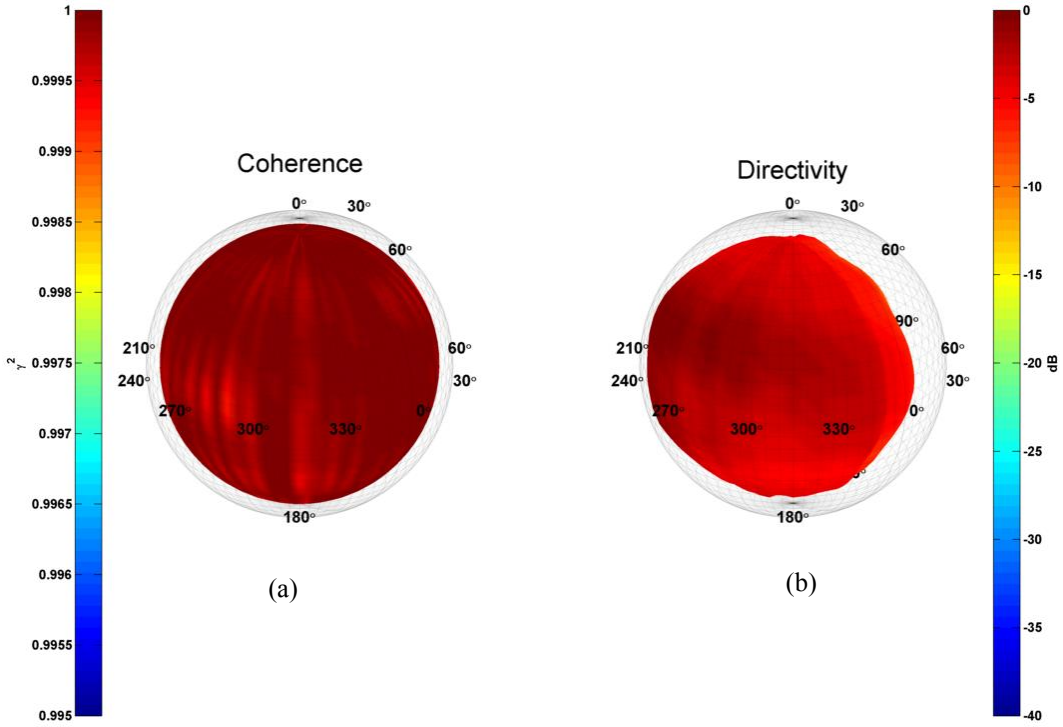

Figure 6.49. French horn plots of the 2nd harmonic frequency for a E3. (a) Coherence balloon. (b) Directivity balloon.

6.8 Euphonium

Figure 6.50. Euphonium player seated in the DMS.

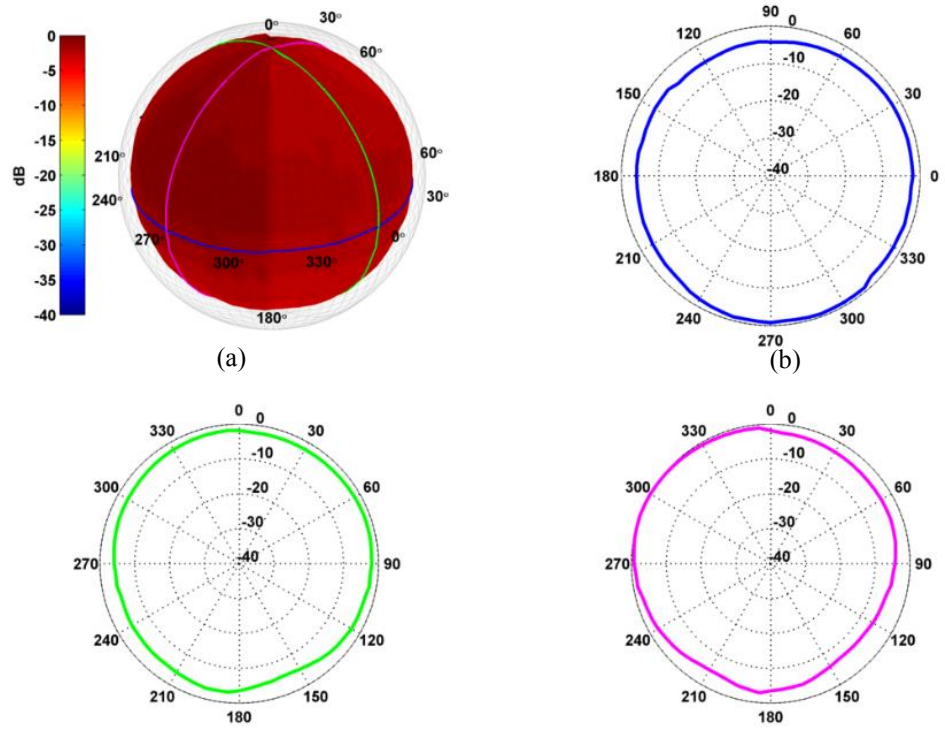

Figure 6.51. Euphonium directivity of the fundamental frequency for a G3. Plots (a) through (d) are arranged as described in Fig. 6.2.

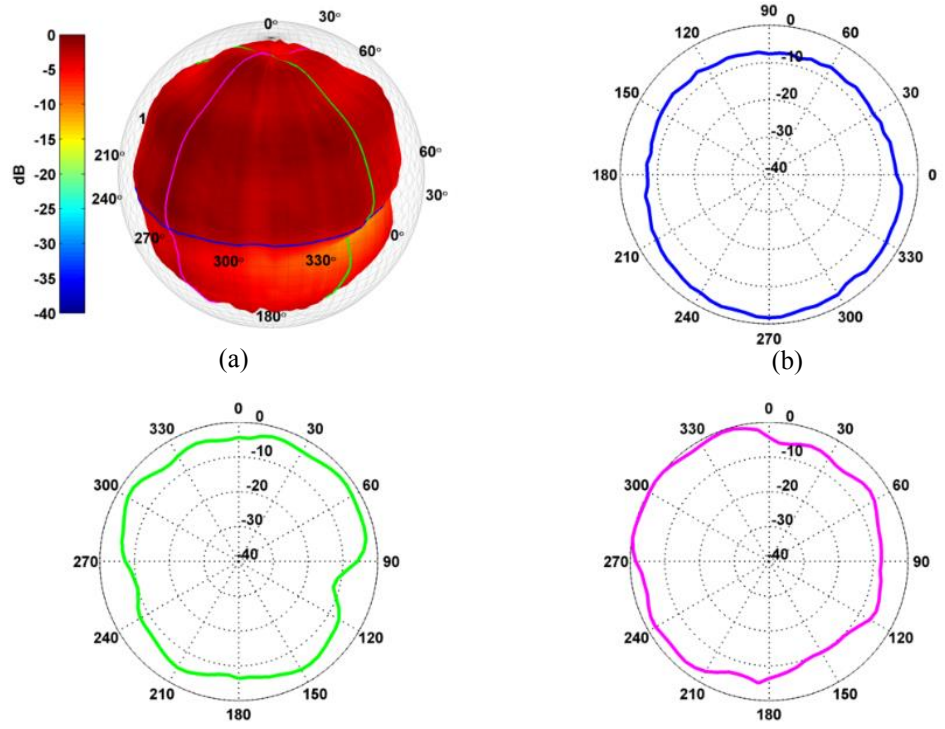

Figure 6.52. Euphonium directivity of the 2nd harmonic frequency for a G3. Plots (a) through (d) are arranged as described in Fig. 6.2.

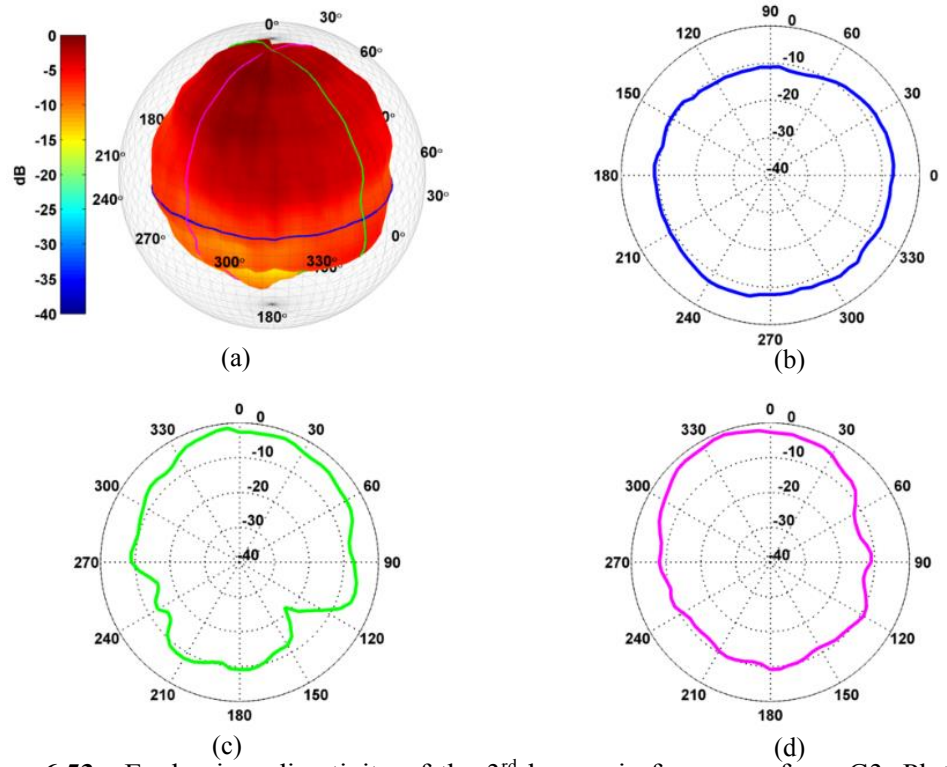

Figure 6.53. Euphonium directivity of the 3rd harmonic frequency for a G3. Plots (a) through (d) are arranged as described in Fig. 6.2.

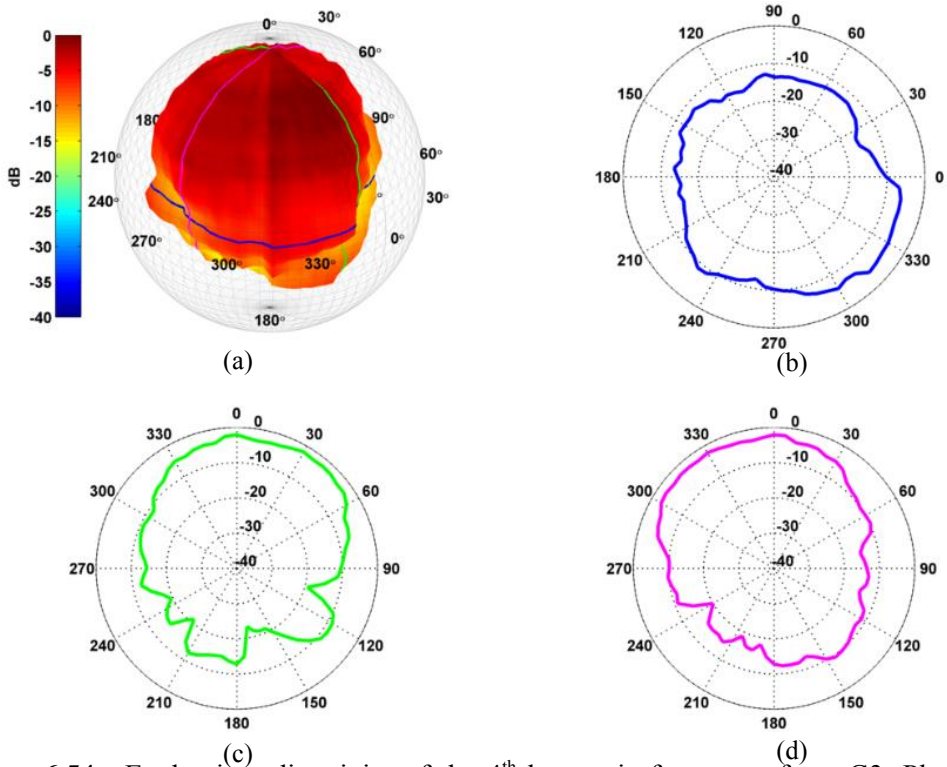

Figure 6.54. Euphonium directivity of the 4th harmonic frequency for a G3. Plots (a) through (d) are arranged as described in Fig. 6.2.

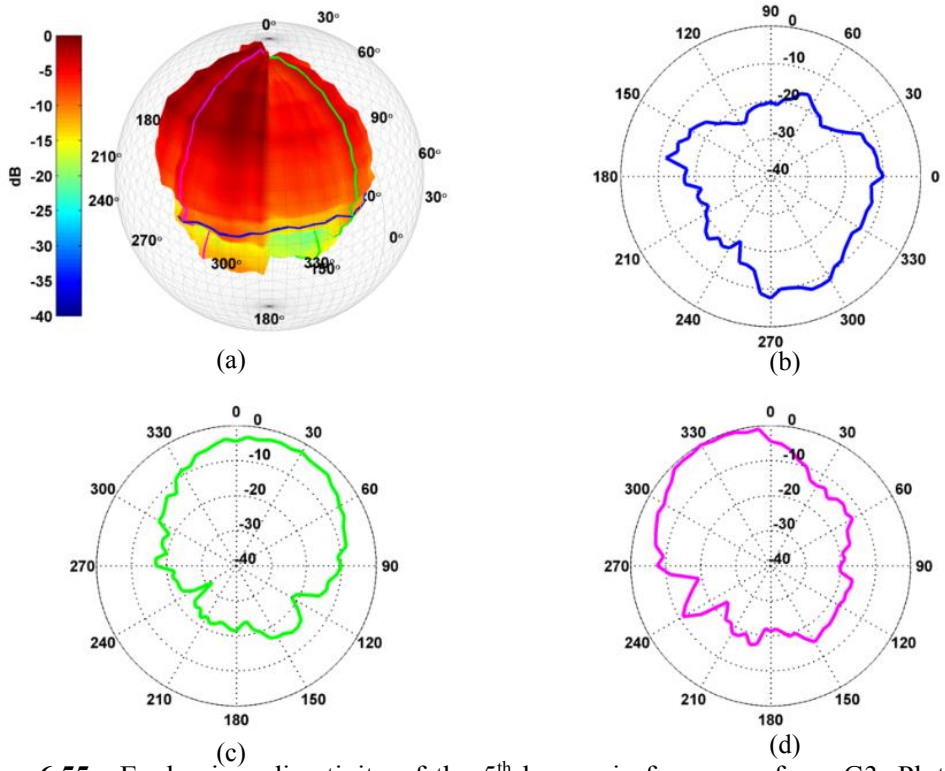

Figure 6.55. Euphonium directivity of the 5th harmonic frequency for a G3. Plots (a) through (d) are arranged as described in Fig. 6.2.

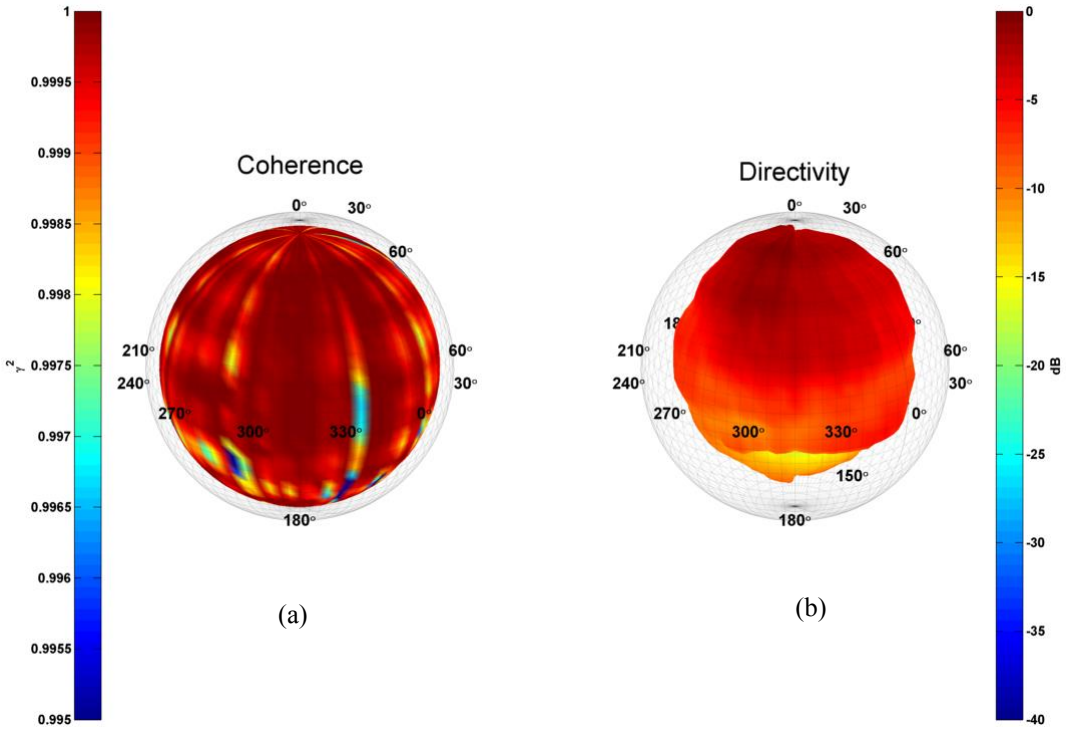

Figure 6.56. Euphonium plots of the 3rd harmonic frequency for a G3. (a) Coherence balloon. (b) Directivity balloon.

6.9 Tuba

Figure 6.57. Tuba player seated in the DMS.

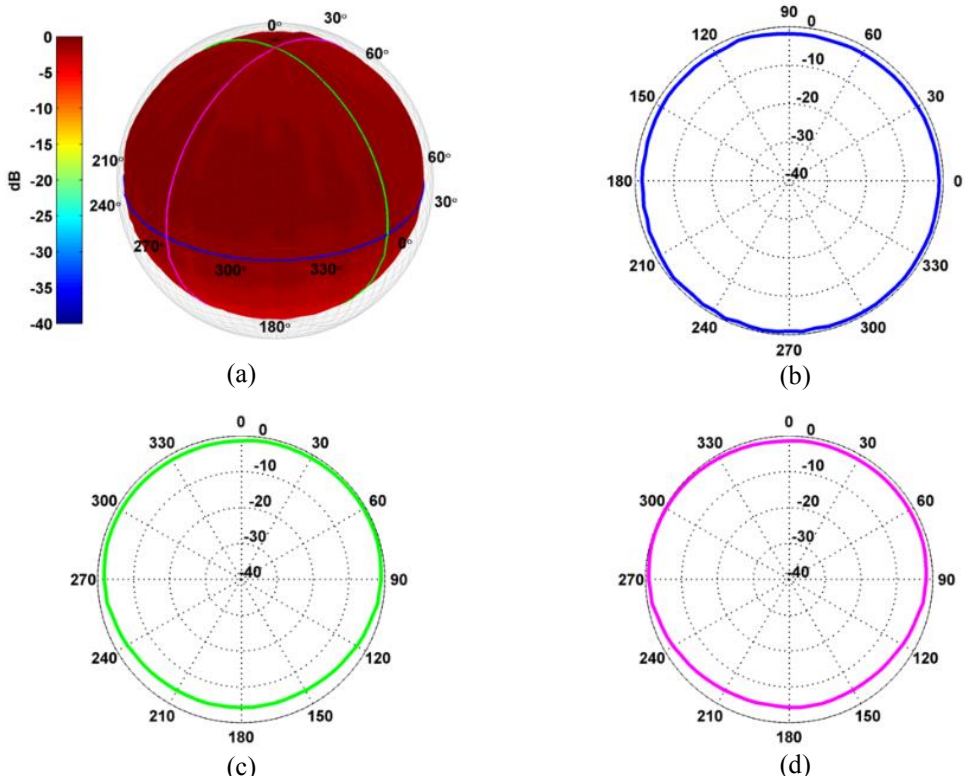

Figure 6.58. Tuba directivity of the fundamental frequency for an F♯2. Plots (a) through (d) are arranged as described in Fig. 6.2.

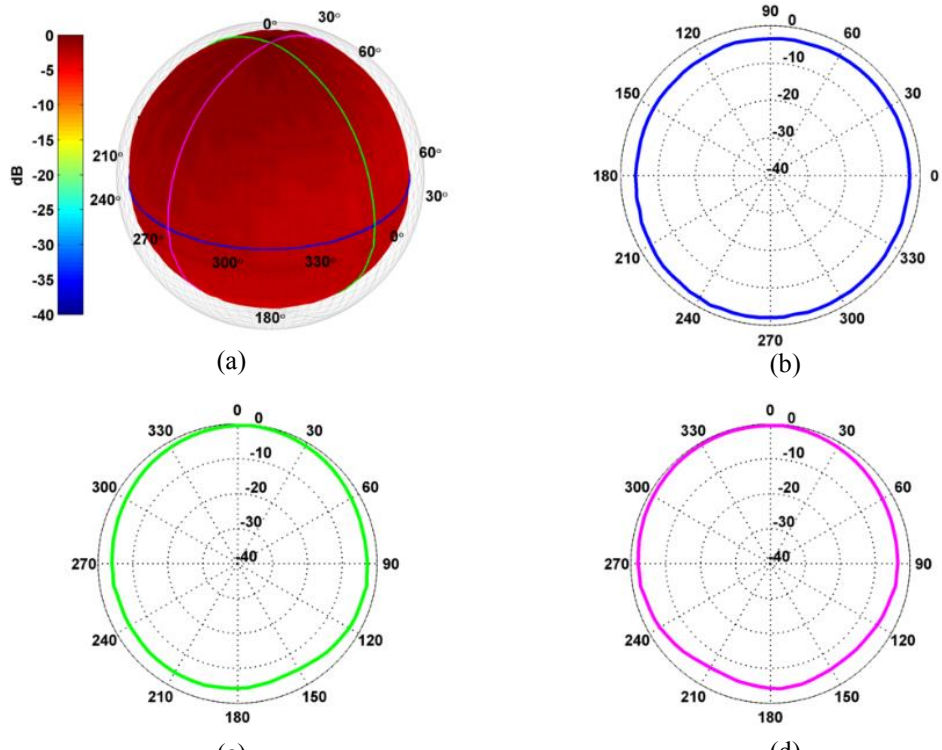

Figure 6.59. Tuba directivity of the 2nd harmonic frequency for an F♯2. Plots (a) through (d) are arranged as described in Fig. 6.2.

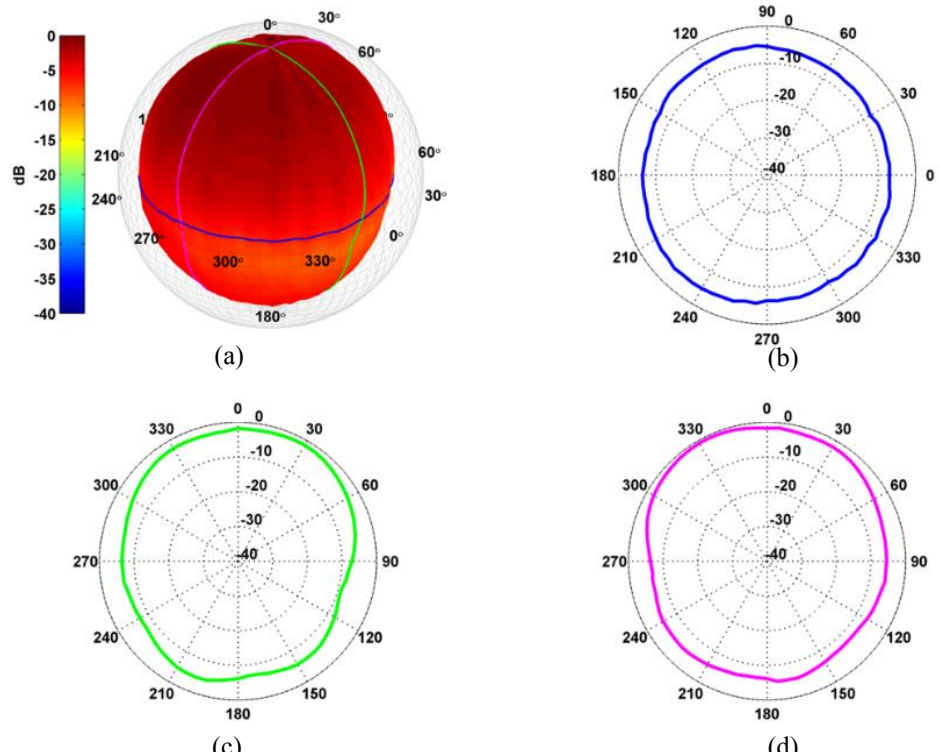

Figure 6.60. Tuba directivity of the 3rd harmonic frequency for an F♯2. Plots (a) through (d) are arranged as described in Fig. 6.2.

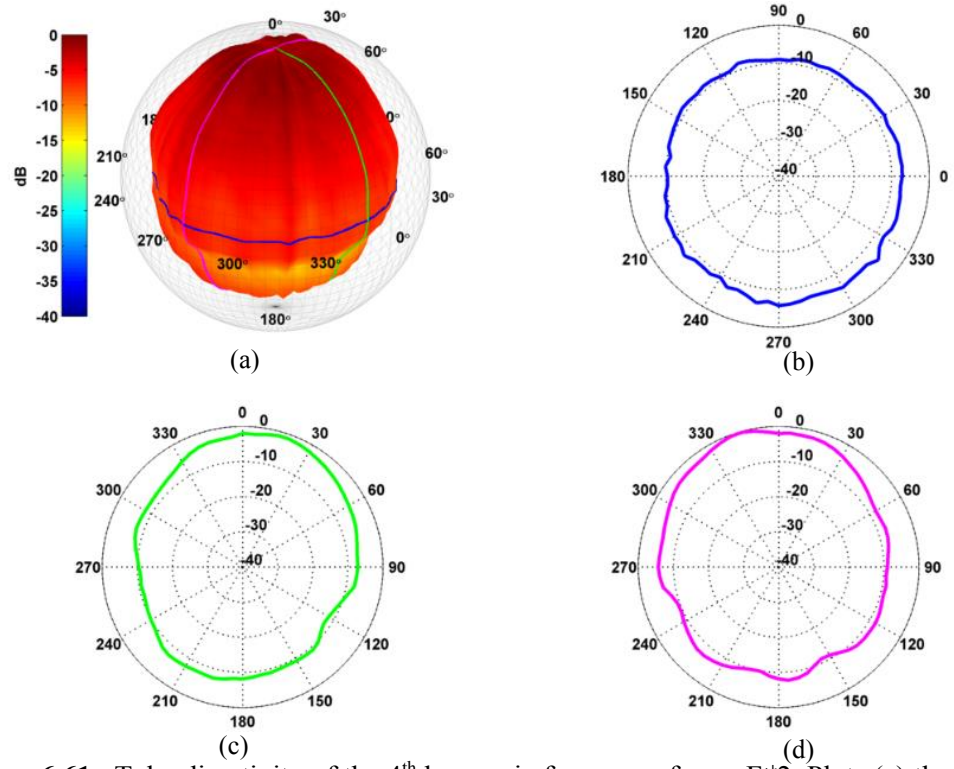

Figure 6.61. Tuba directivity of the 4th harmonic frequency for an F♯2. Plots (a) through (d) are arranged as described in Fig. 6.2.

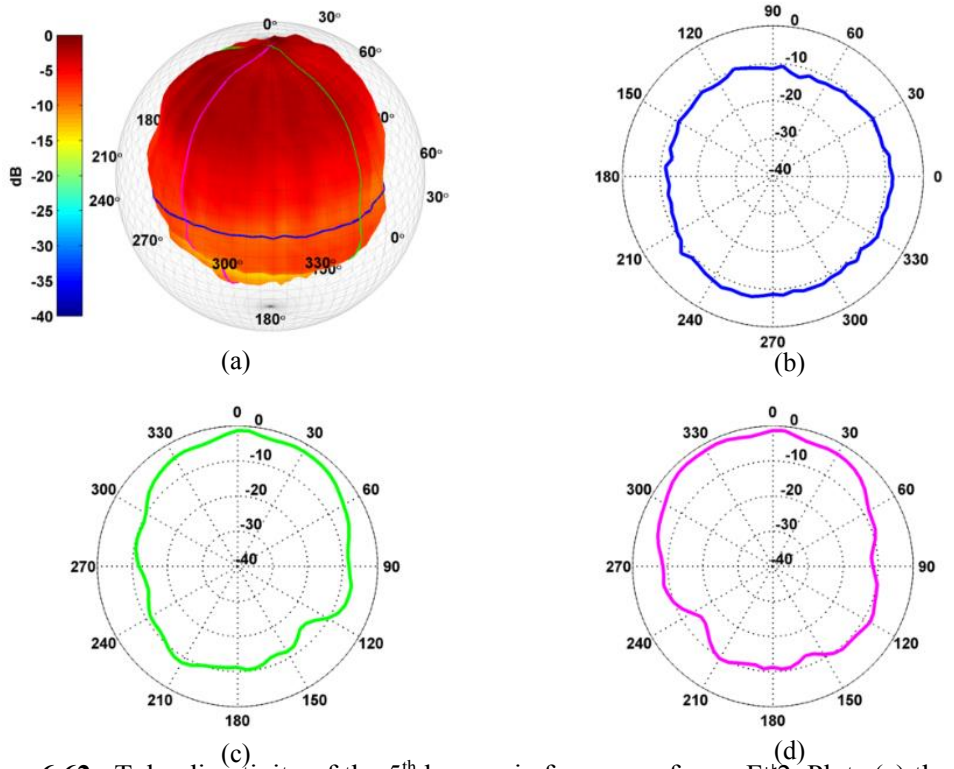

Figure 6.62. Tuba directivity of the 5th harmonic frequency for an F♯2. Plots (a) through (d) are arranged as described in Fig. 6.2.

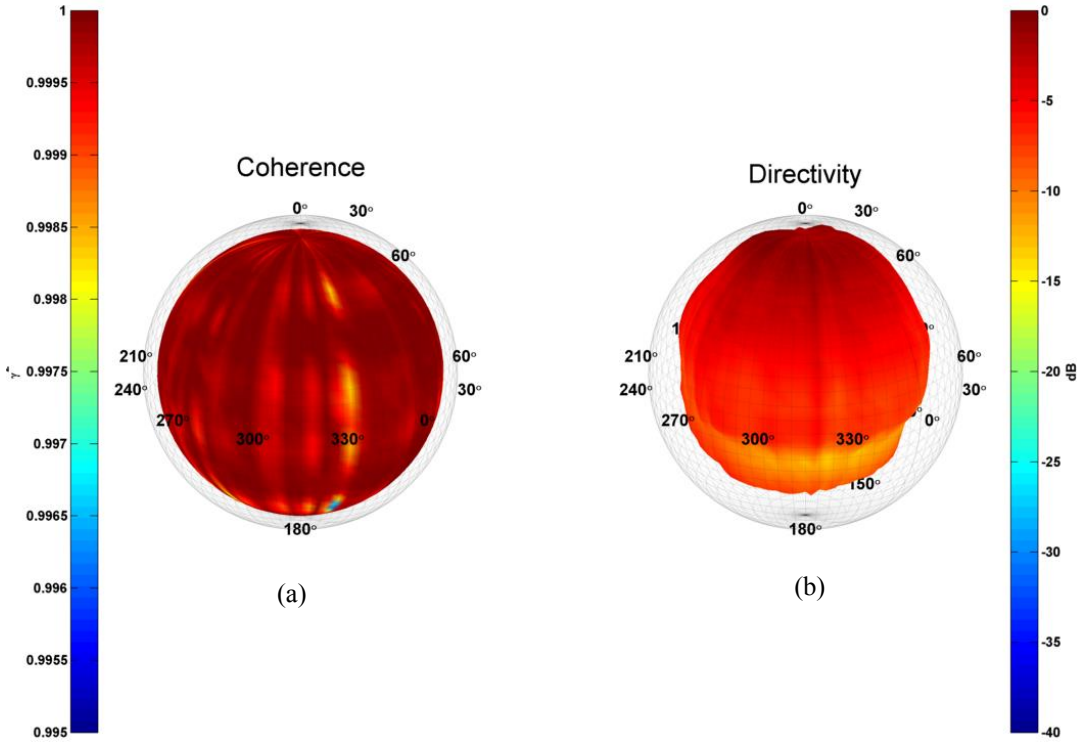

Figure 6.63. Tuba plots of the 4th harmonic frequency for a F♯2. (a) Coherence balloon. (b) Directivity balloon.

6.10 Baritone Saxophone

Figure 6.64. Baritone Saxophonist seated in the DMS.

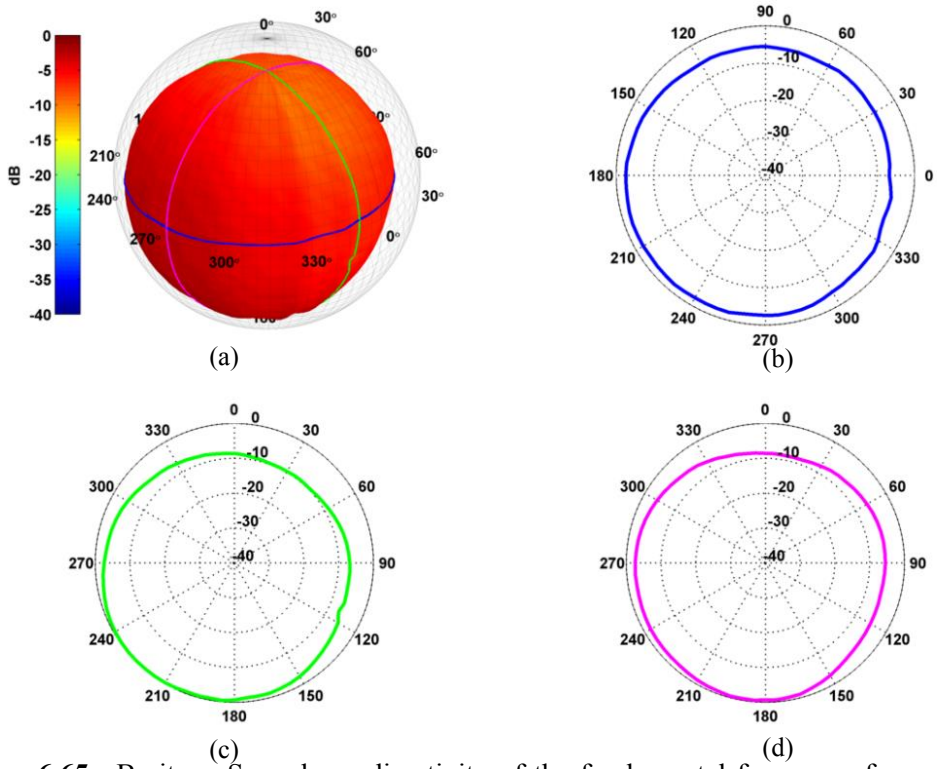

Figure 6.65. Baritone Saxophone directivity of the fundamental frequency for an F♯3. Plots (a) through (d) are arranged as described in Fig. 6.2.

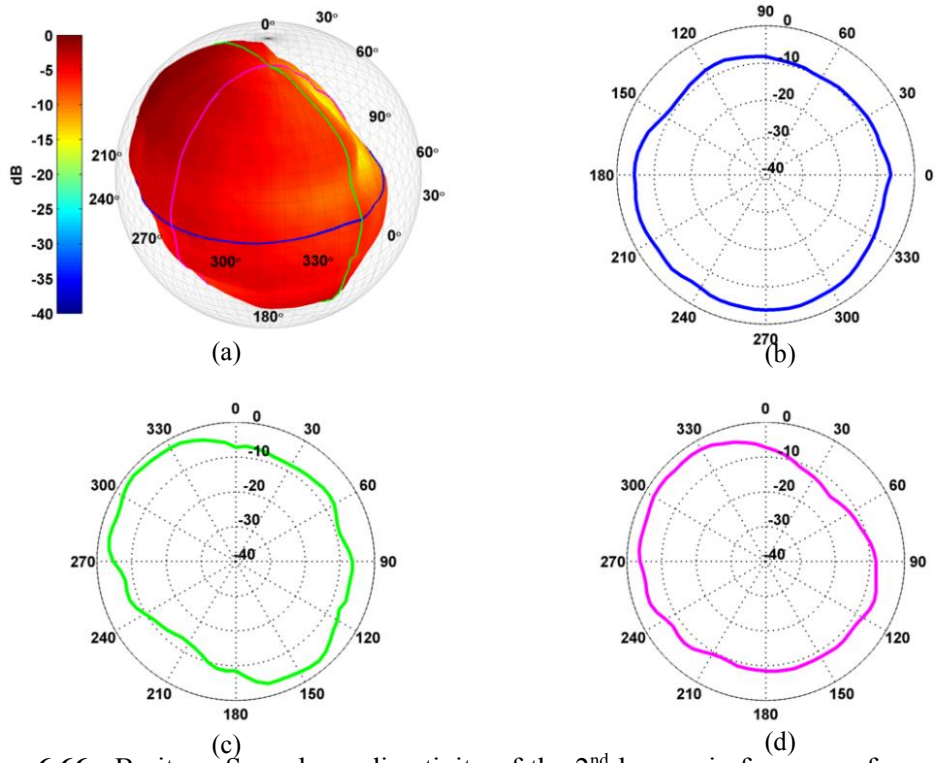

Figure 6.66. Baritone Saxophone directivity of the 2nd harmonic frequency for an F♯3. Plots (a) through (d) are arranged as described in Fig. 6.2.

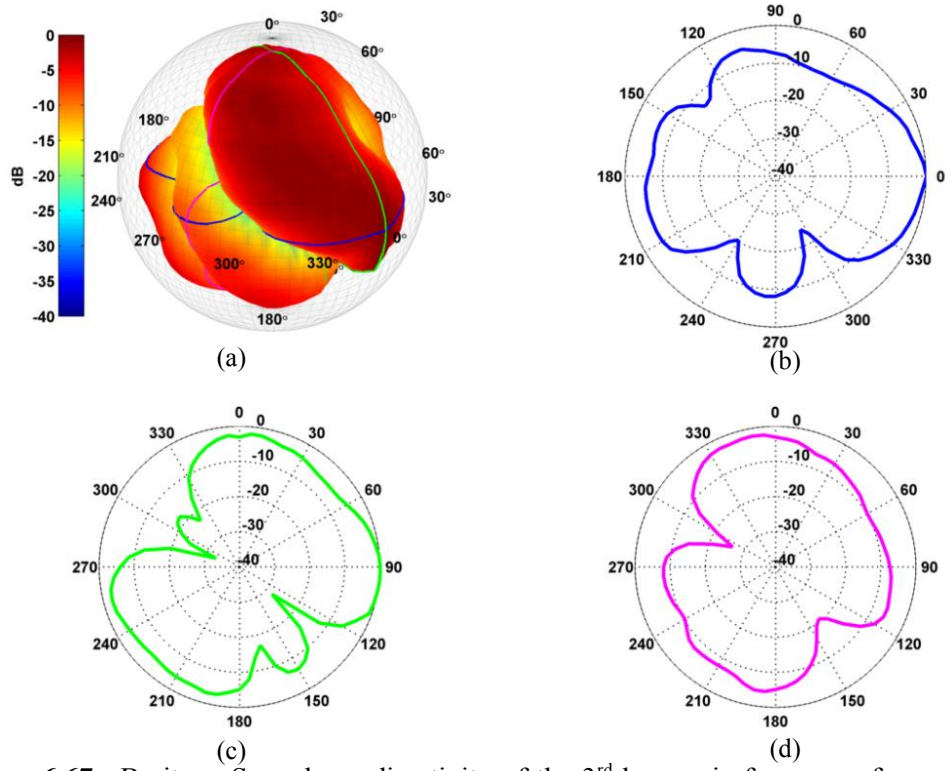

Figure 6.67. Baritone Saxophone directivity of the 3rd harmonic frequency for an F♯3. Plots (a) through (d) are arranged as described in Fig. 6.2.

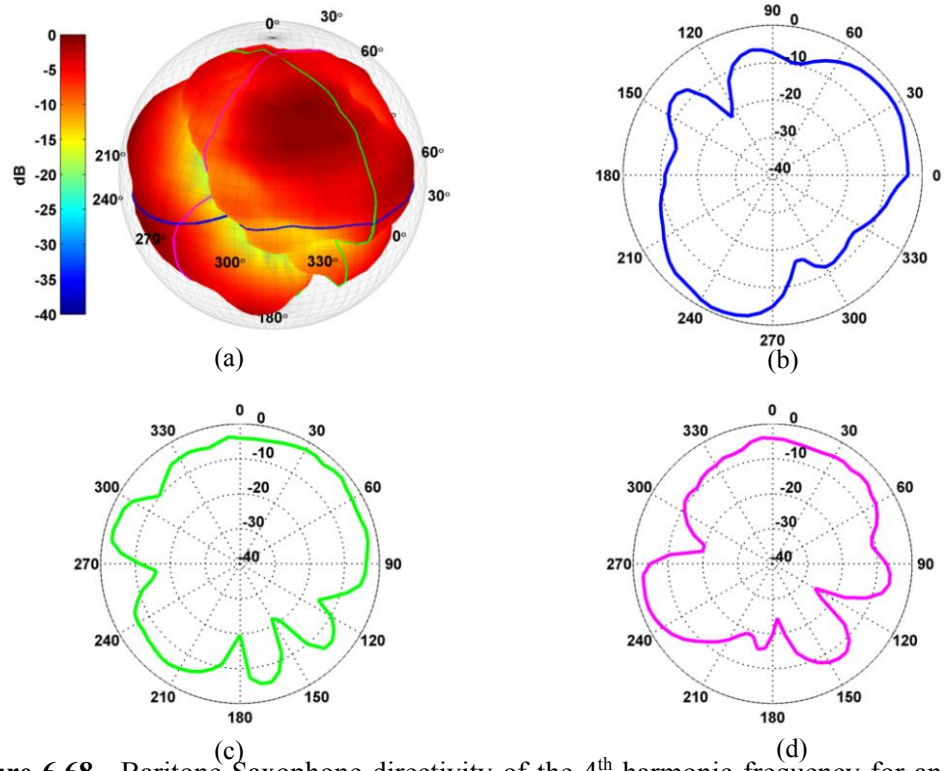

Figure 6.68. Baritone Saxophone directivity of the 4th harmonic frequency for an F♯3. Plots (a) through (d) are arranged as described in Fig. 6.2.

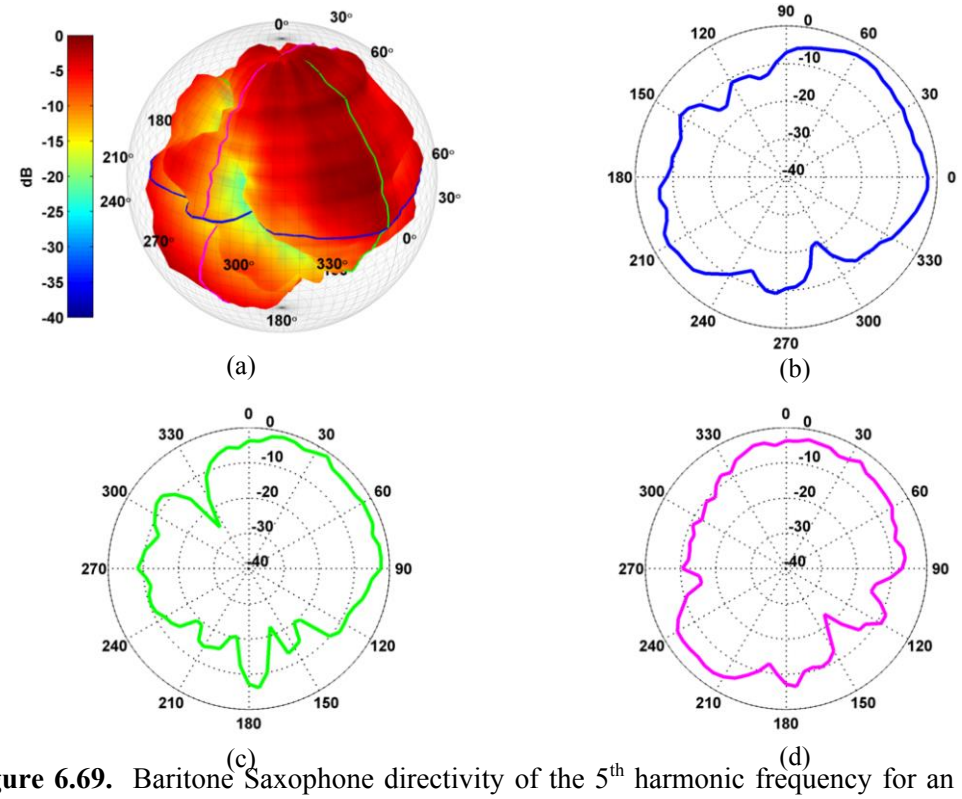

Figure 6.69. Baritone Saxophone directivity of the 5th harmonic frequency for an F♯3. Plots (a) through (d) are arranged as described in Fig. 6.2.

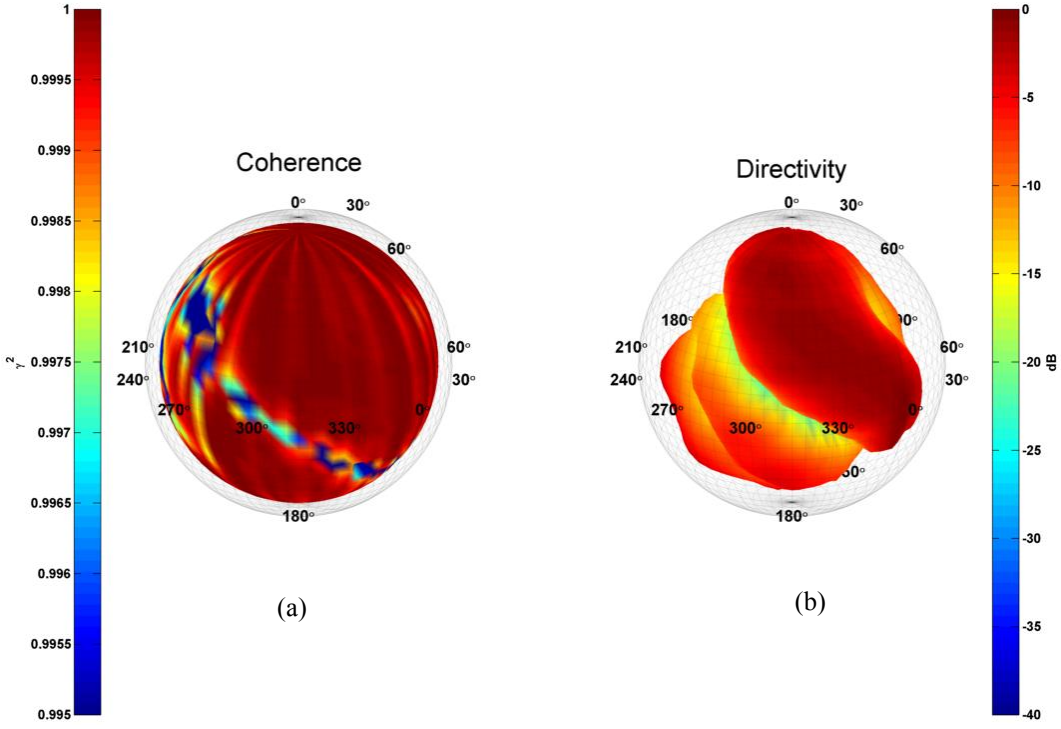

Figure 6.70. Baritone saxophone plots of the 3rd harmonic frequency for a F♯3. (a) Coherence balloon. (b) Directivity balloon.

6.11 Tenor Saxophone

Figure 6.71. Tenor Saxophonist seated in the DMS.

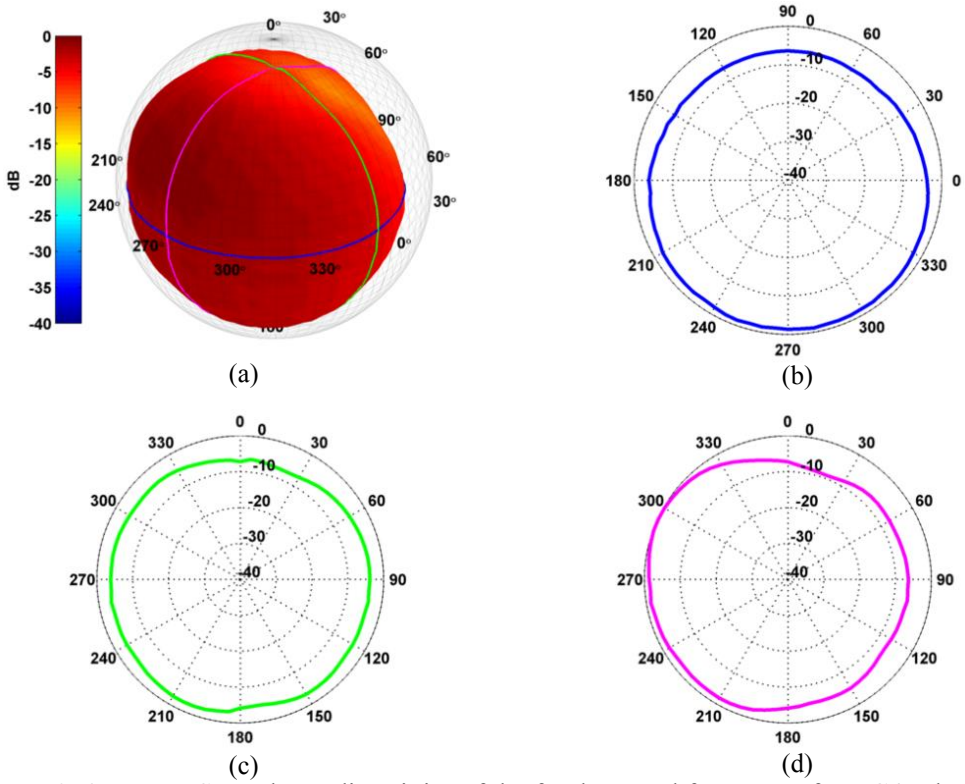

Figure 6.72. Tenor Saxophone directivity of the fundamental frequency for a C4. Plots (a) through (d) are arranged as described in Fig. 6.2.

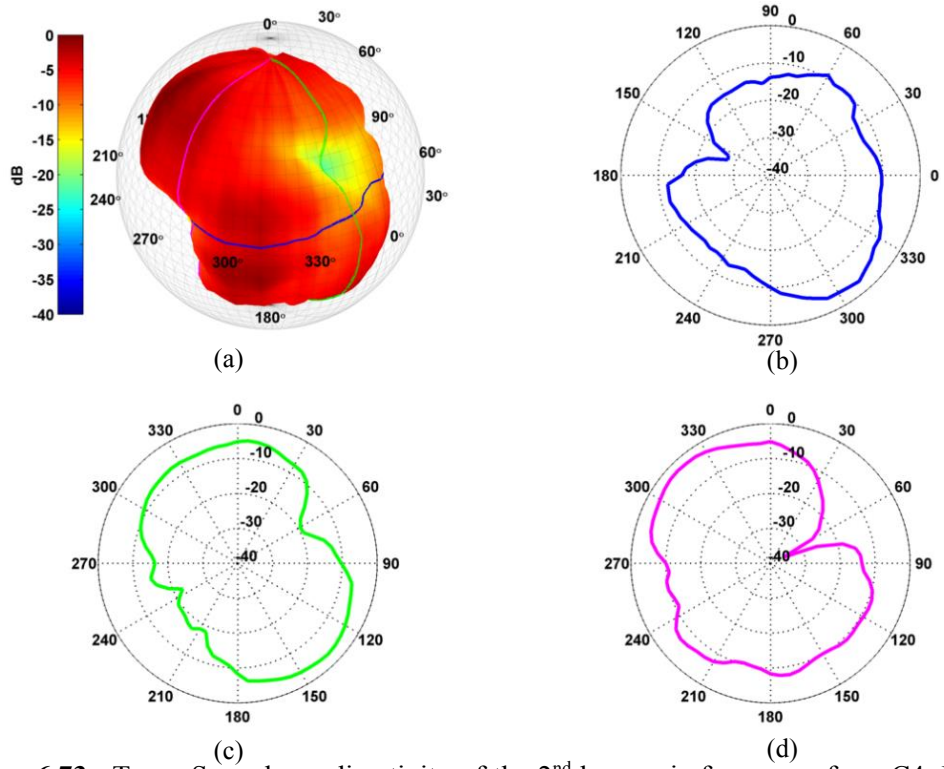

Figure 6.73. Tenor Saxophone directivity of the 2nd harmonic frequency for a C4. Plots (a) through (d) are arranged as described in Fig. 6.2.

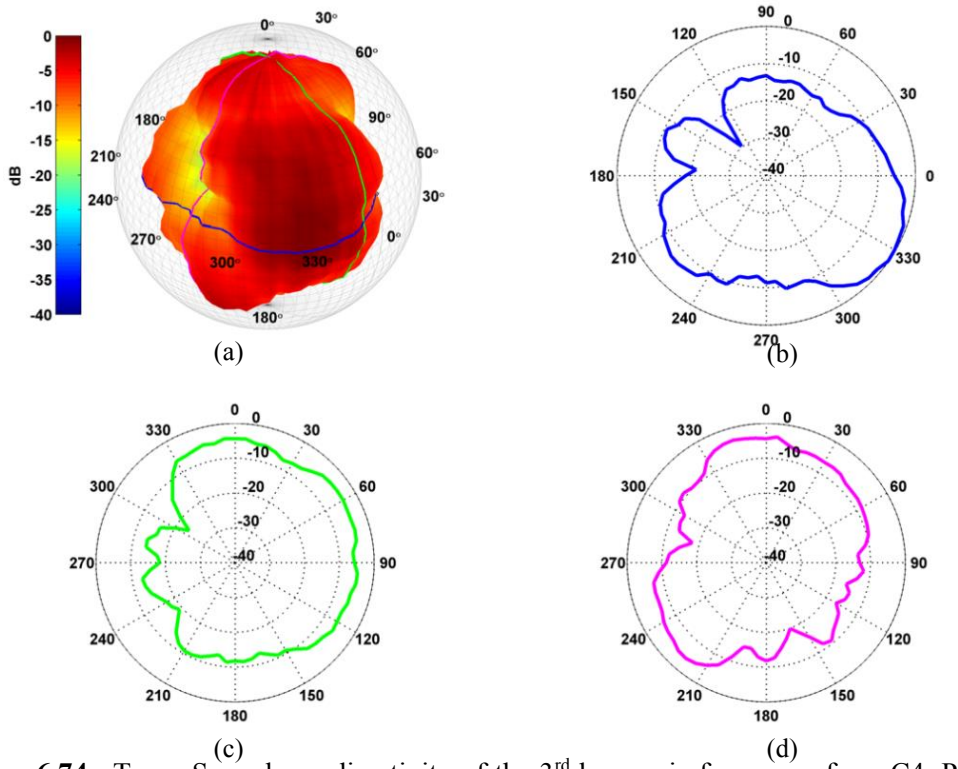

Figure 6.74. Tenor Saxophone directivity of the 3rd harmonic frequency for a C4. Plots (a) through (d) are arranged as described in Fig. 6.2.

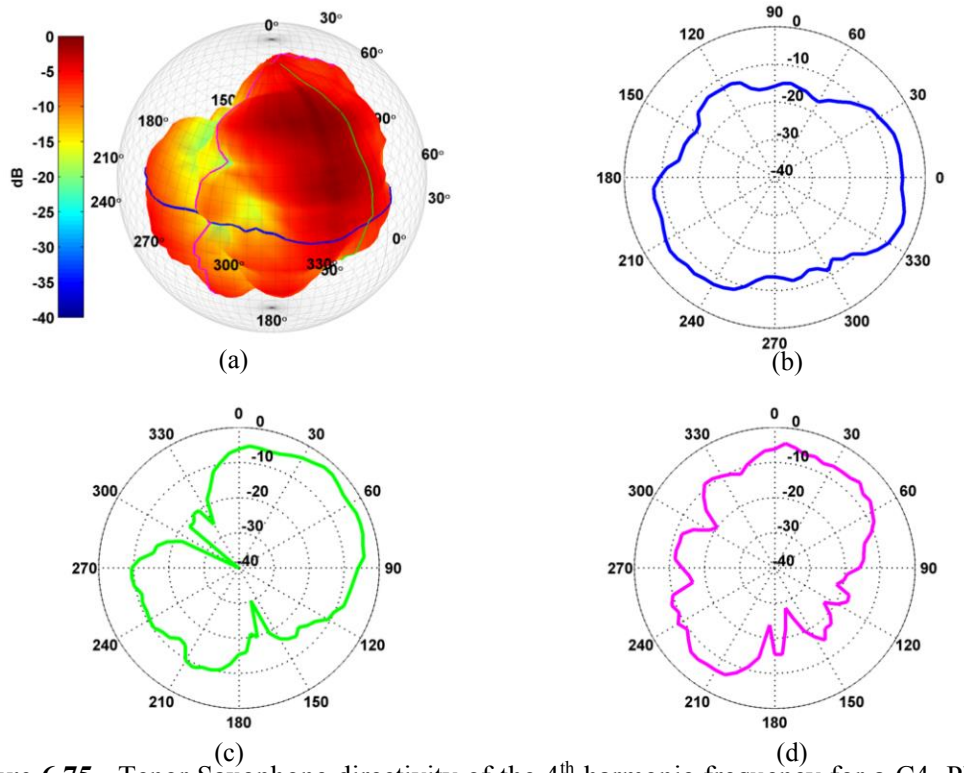

Figure 6.75. Tenor Saxophone directivity of the 4th harmonic frequency for a C4. Plots (a) through (d) are arranged as described in Fig. 6.2.

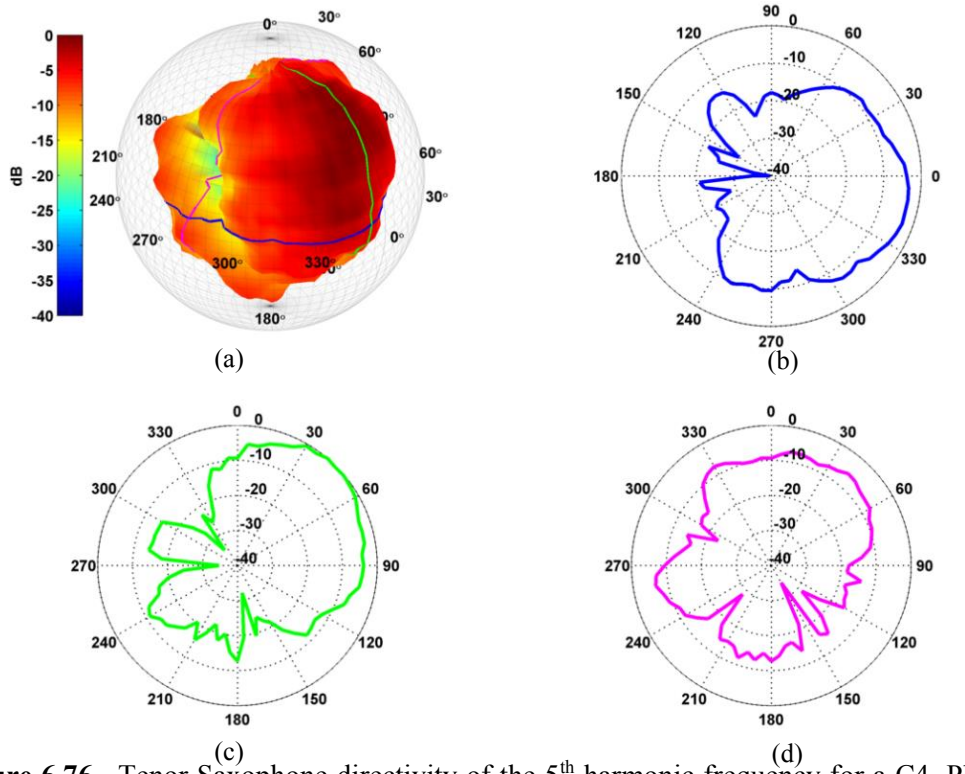

Figure 6.76. Tenor Saxophone directivity of the 5th harmonic frequency for a C4. Plots (a) through (d) are arranged as described in Fig. 6.2.

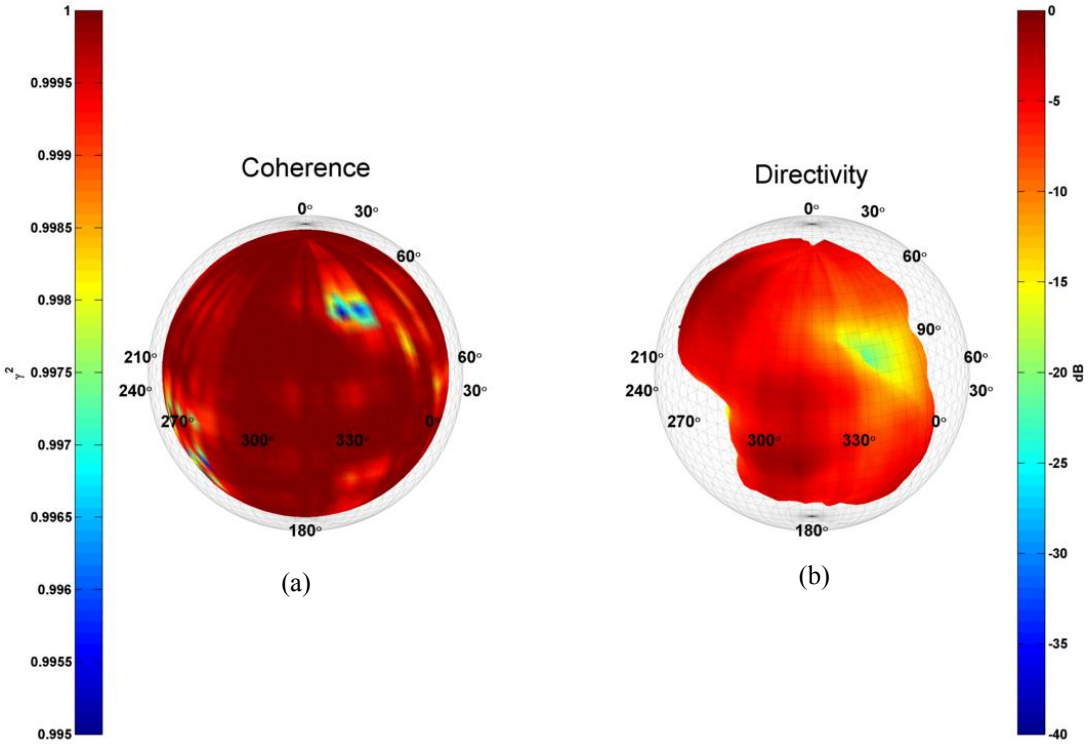

Figure 6.77. Tenor saxophone plots of the 2nd harmonic frequency for a C4. (a) Coherence balloon. (b) Directivity balloon.

6.12 Flute

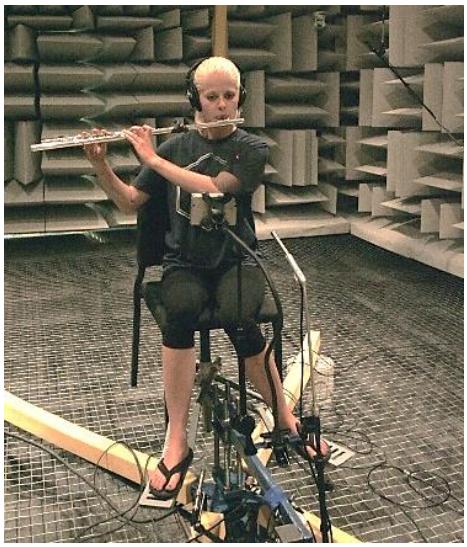

Figure 6.78. Flutist seated in the DMS.

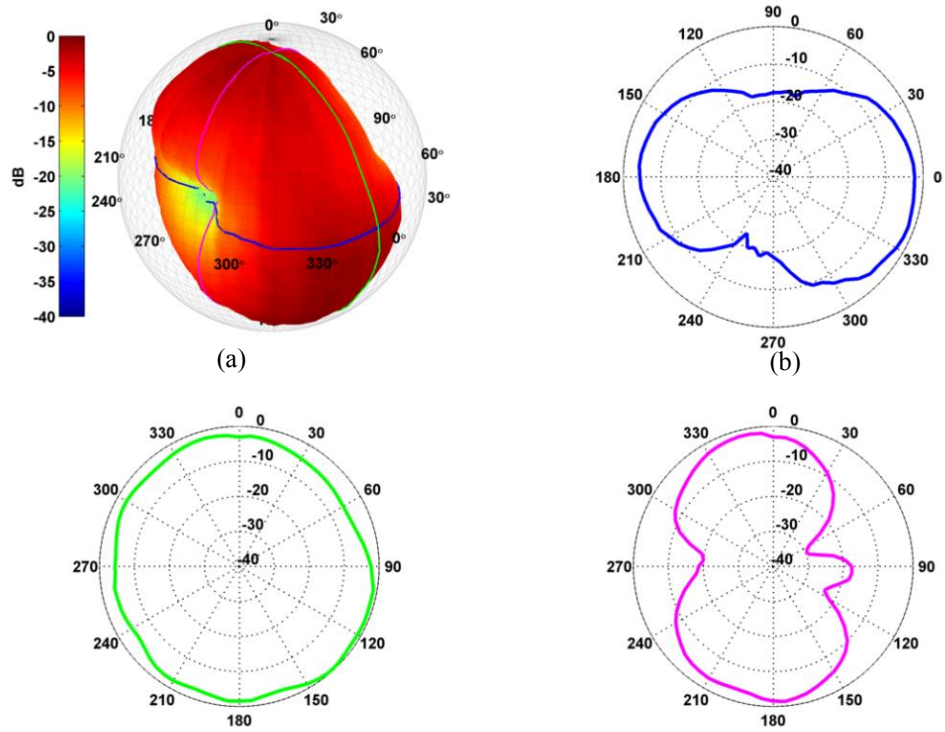

Fi**gure 6.79.** Flute directivity of the fundamental frequency for an E4. Plots (a) through (d) are arranged as described in Fig. 6.2.

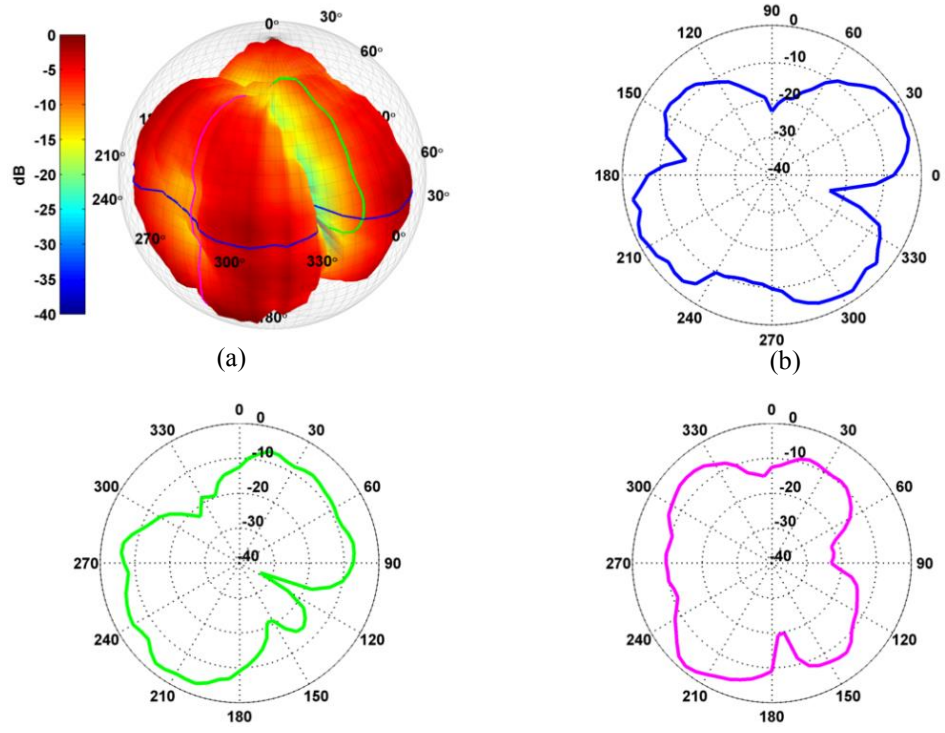

Figure 6.80. Flute directivity of the 2nd harmonic frequency for an E4. Plots (a) through (d) are arranged as described in Fig. 6.2.

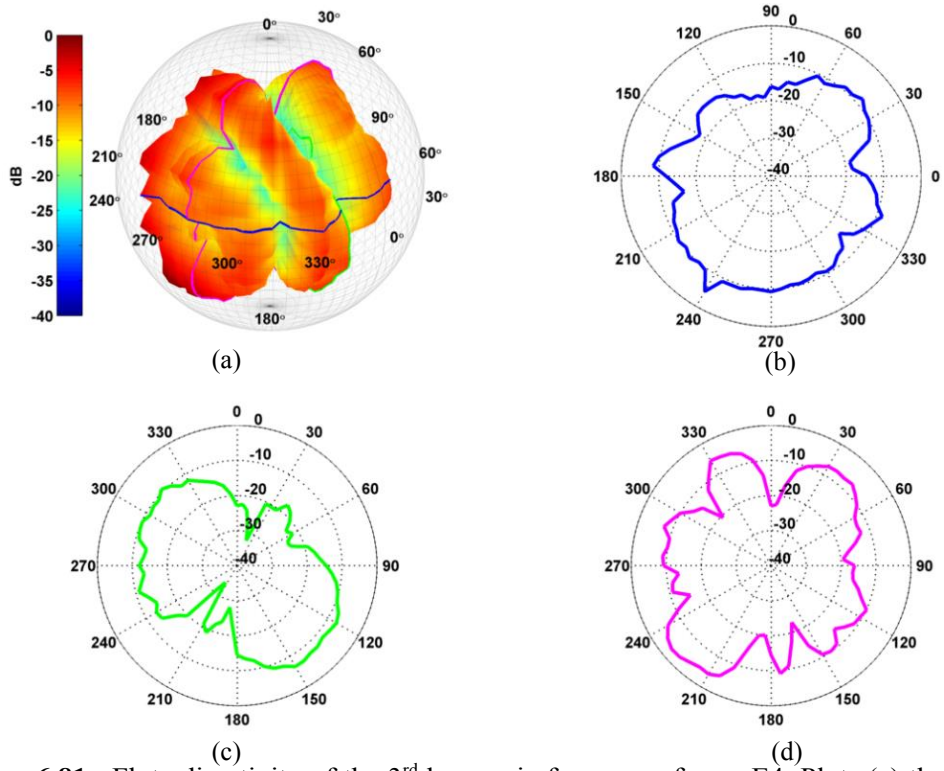

Figure 6.81. Flute directivity of the 3rd harmonic frequency for an E4. Plots (a) through (d) are arranged as described in Fig. 6.2.

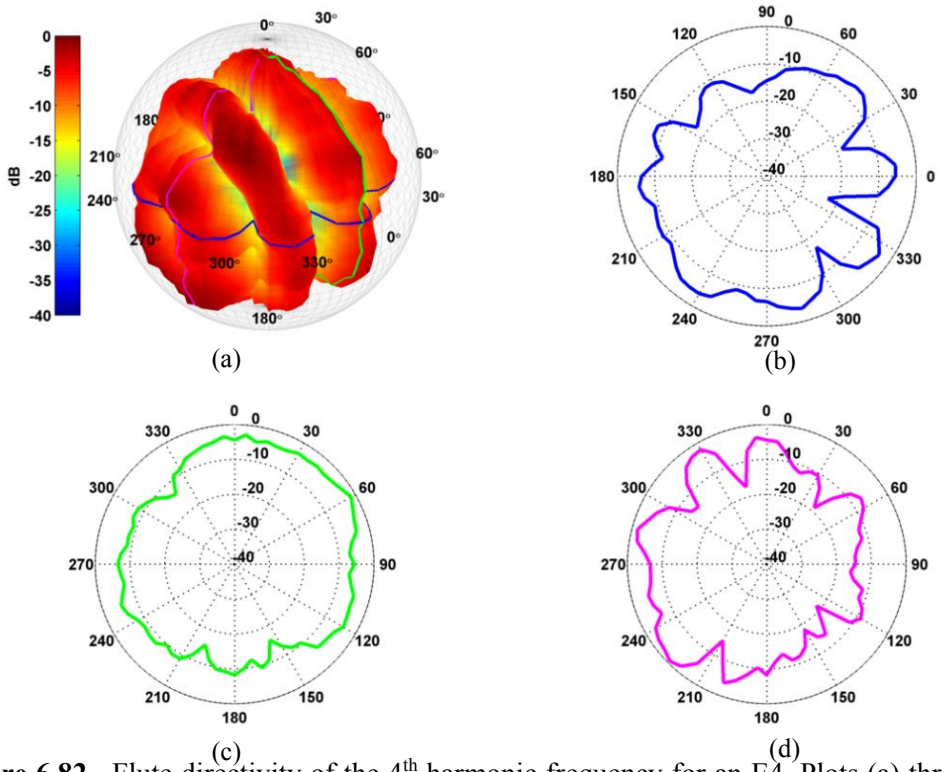

Figure 6.82. Flute directivity of the 4th harmonic frequency for an E4. Plots (a) through (d) are arranged as described in Fig. 6.2.

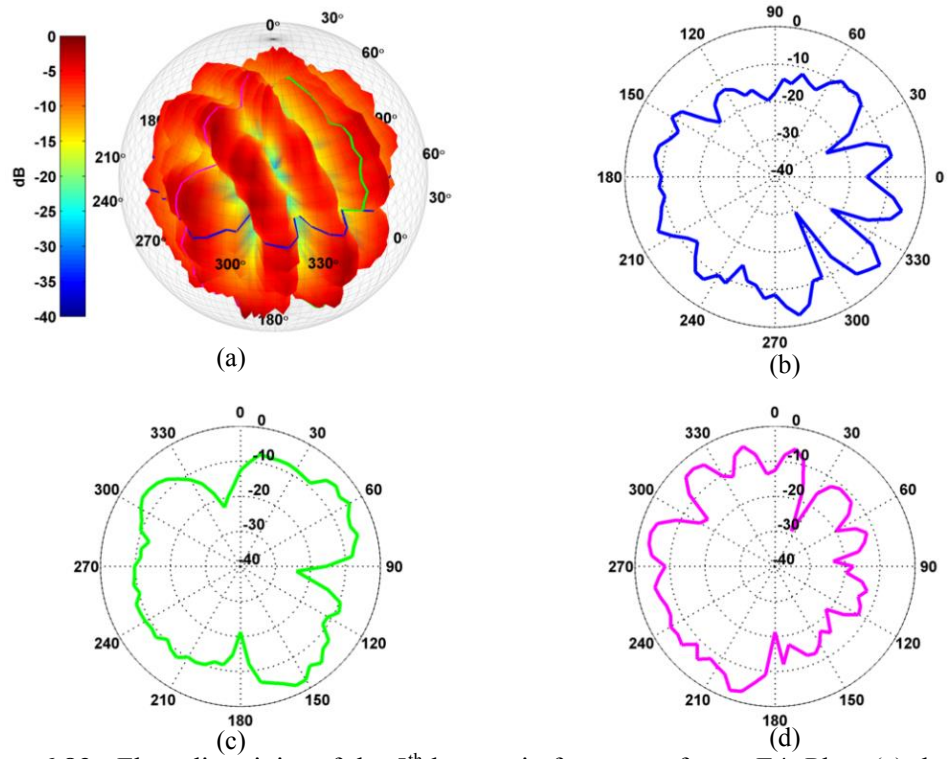

Figure 6.83. Flute directivity of the 5th harmonic frequency for an E4. Plots (a) through (d) are arranged as described in Fig. 6.2.

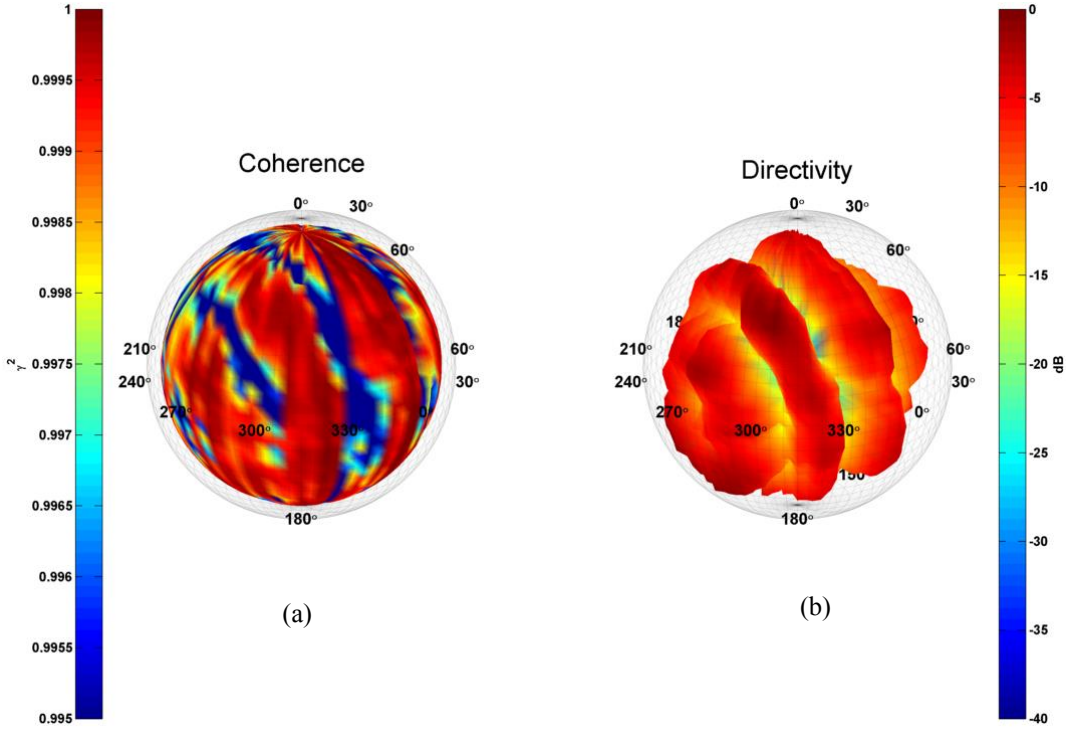

Figure 6.84. Flute plots of the 4th harmonic frequency for a E4. (a) Coherence balloon. (b) Directivity balloon.

6.13 Oboe

Figure 6.85. Oboist seated in the DMS.

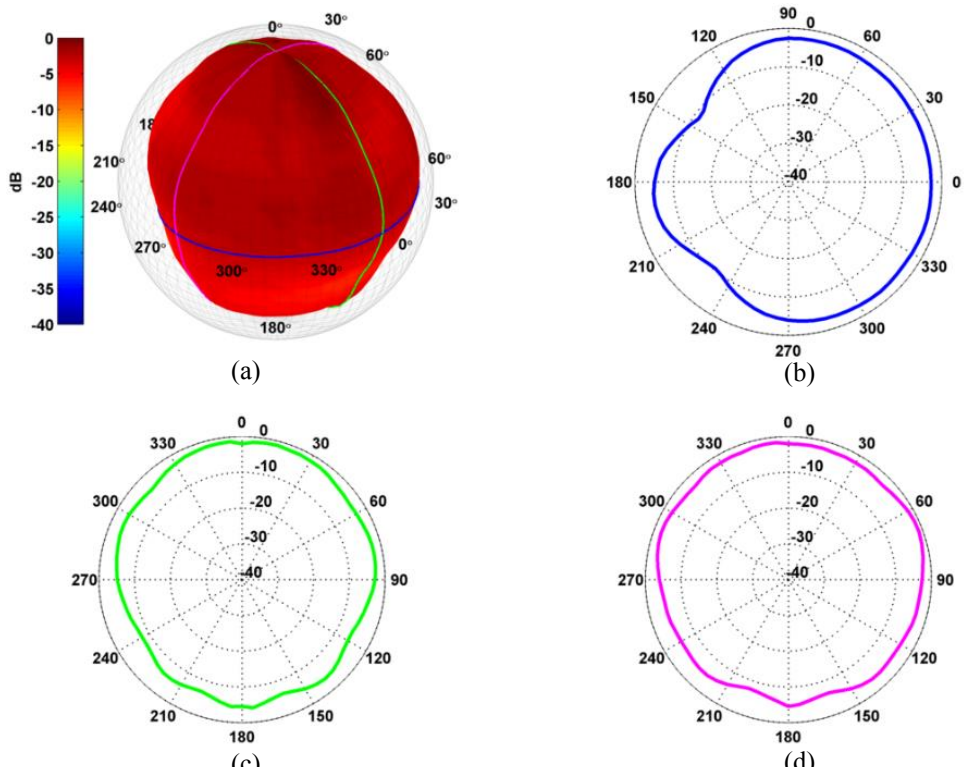

Figure 6.86. Oboe directivity of the 2nd harmonic frequency for an E3. Plots (a) through (d) are arranged as described in Fig. 6.2.

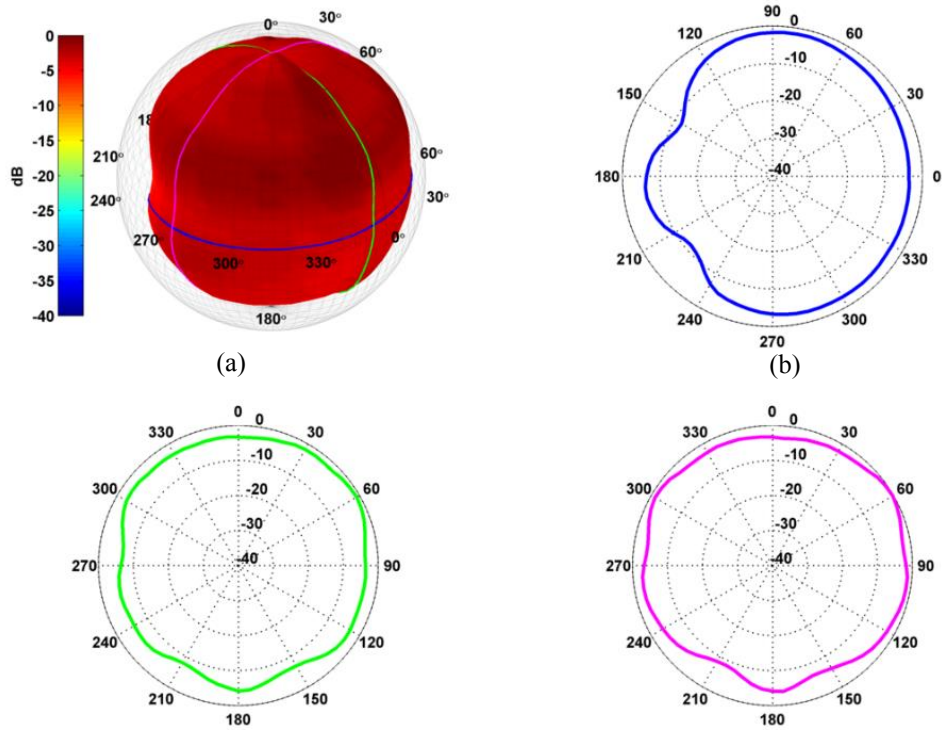

Figure 6.87. Oboe directivity of the 2nd harmonic frequency for an F3. Plots (a) through (d) are arranged as described in Fig. 6.2.

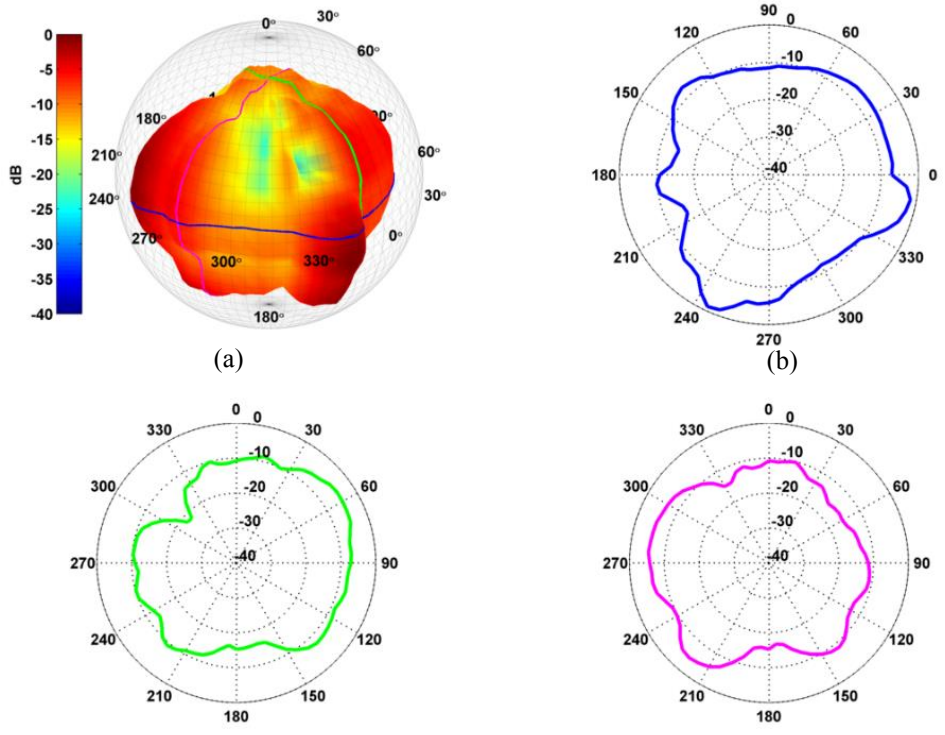

Figure 6.88. Oboe directivity of the 2nd harmonic frequency for an E4. Plots (a) through (d) are arranged as described in Fig. 6.2.

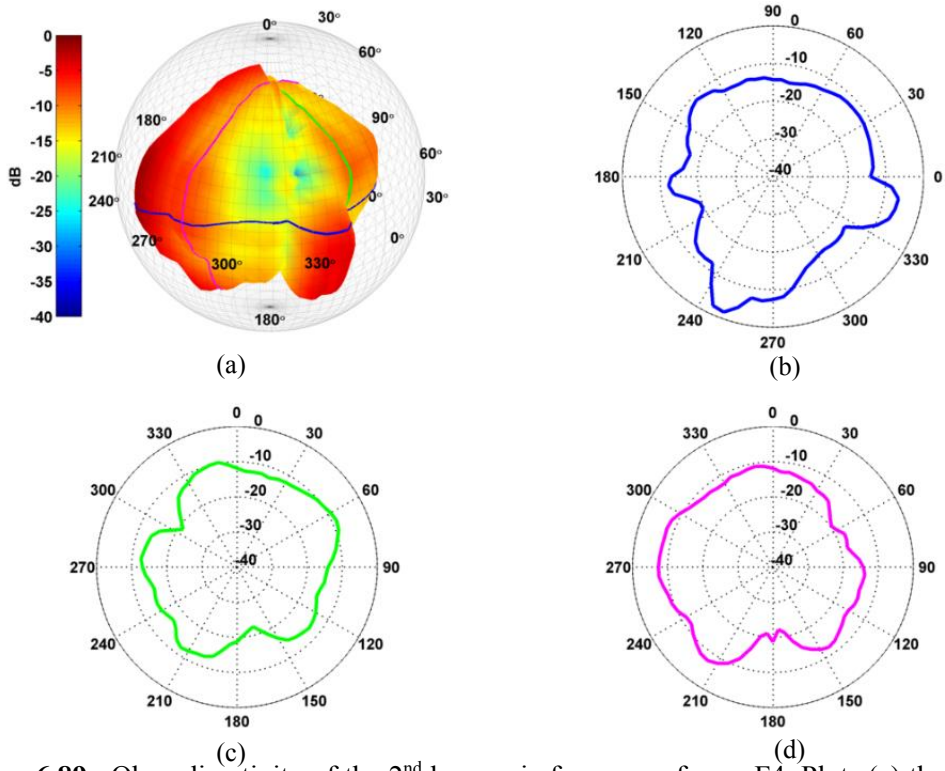

Figure 6.89. Oboe directivity of the 2nd harmonic frequency for an F4. Plots (a) through (d) are arranged as described in Fig. 6.2.

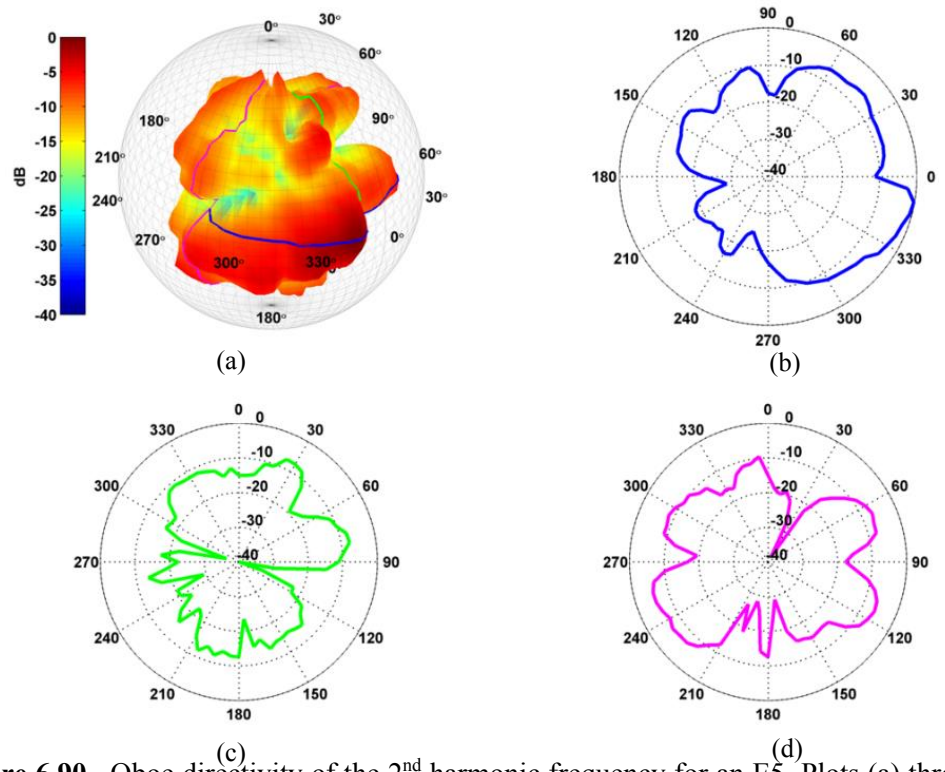

Figure 6.90. Oboe directivity of the 2nd harmonic frequency for an E5. Plots (a) through (d) are arranged as described in Fig. 6.2.

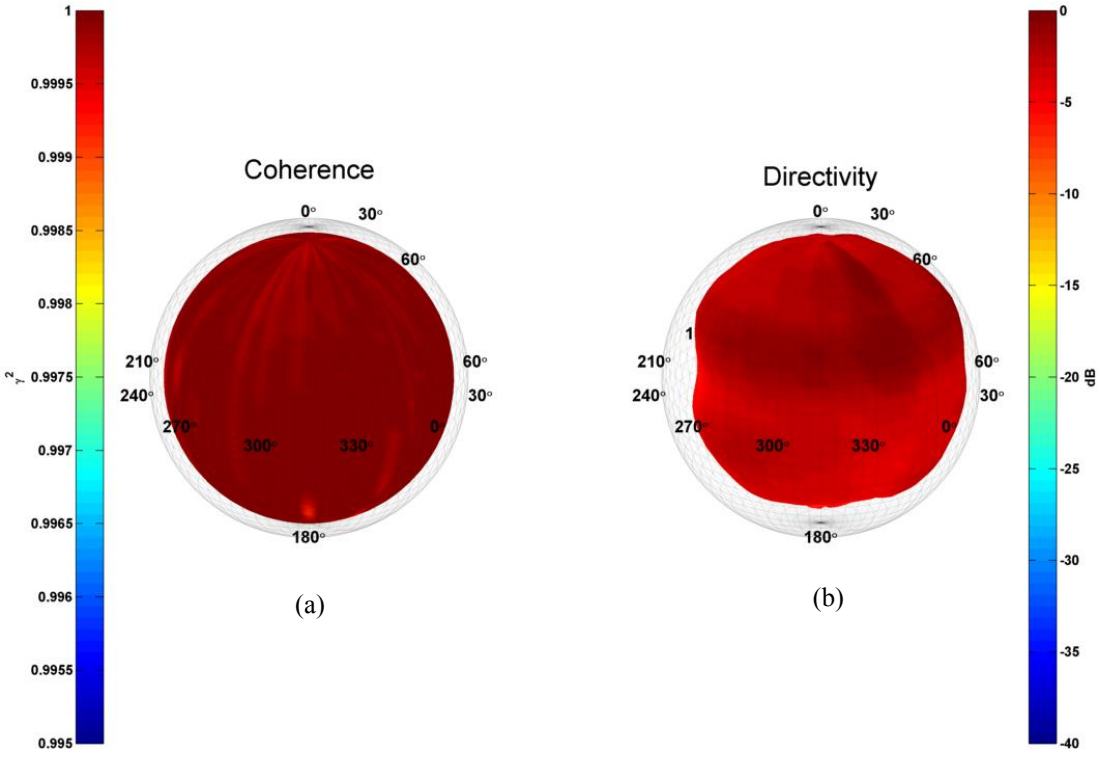

Figure 6.91. Oboe plots of the 2nd harmonic frequency for a E3. (a) Coherence balloon. (b) Directivity balloon.

6.14 Bassoon

Figure 6.92. Bassoonist seated in the DMS.

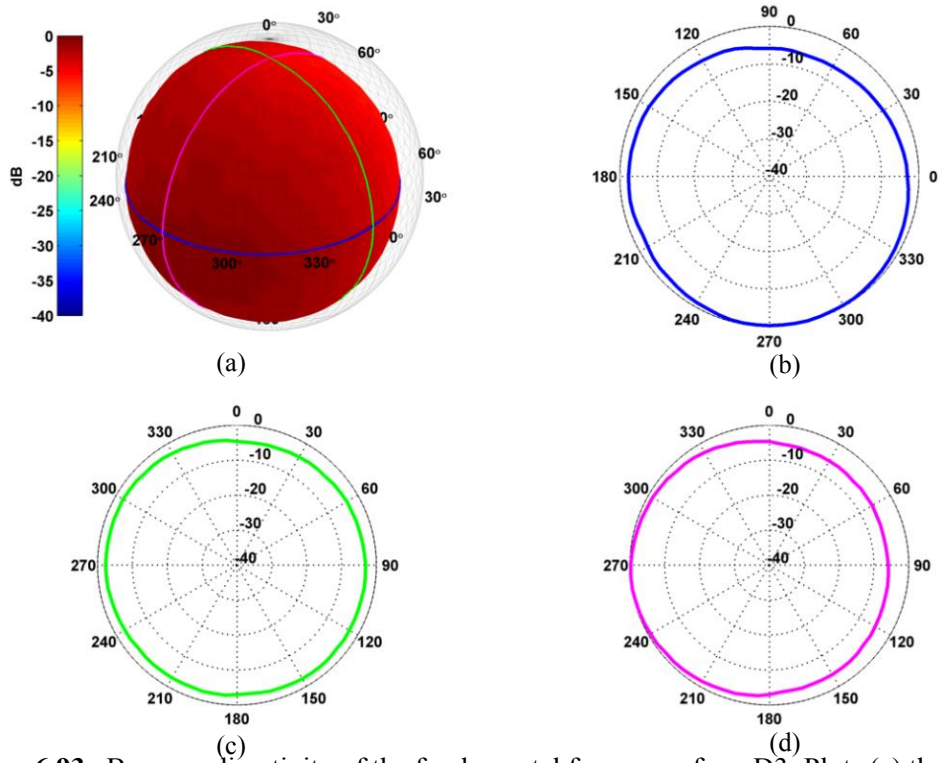

Figure 6.93. Bassoon directivity of the fundamental frequency for a D3. Plots (a) through (d) are arranged as described in Fig. 6.2.

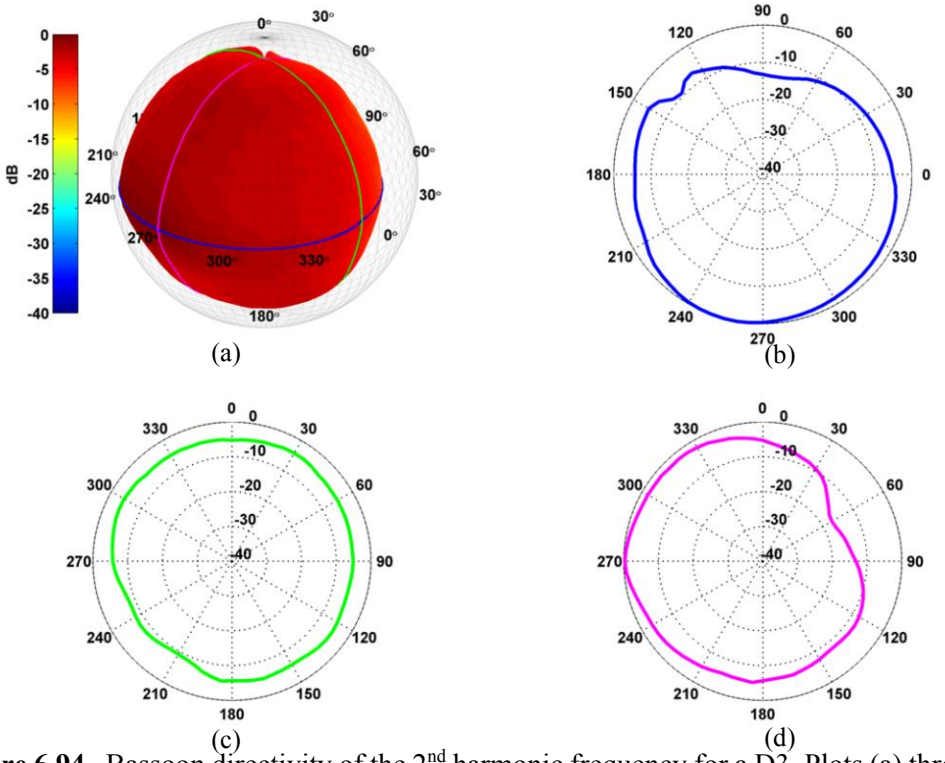

Figure 6.94. Bassoon directivity of the 2nd harmonic frequency for a D3. Plots (a) through (d) are arranged as described in Fig. 6.2.

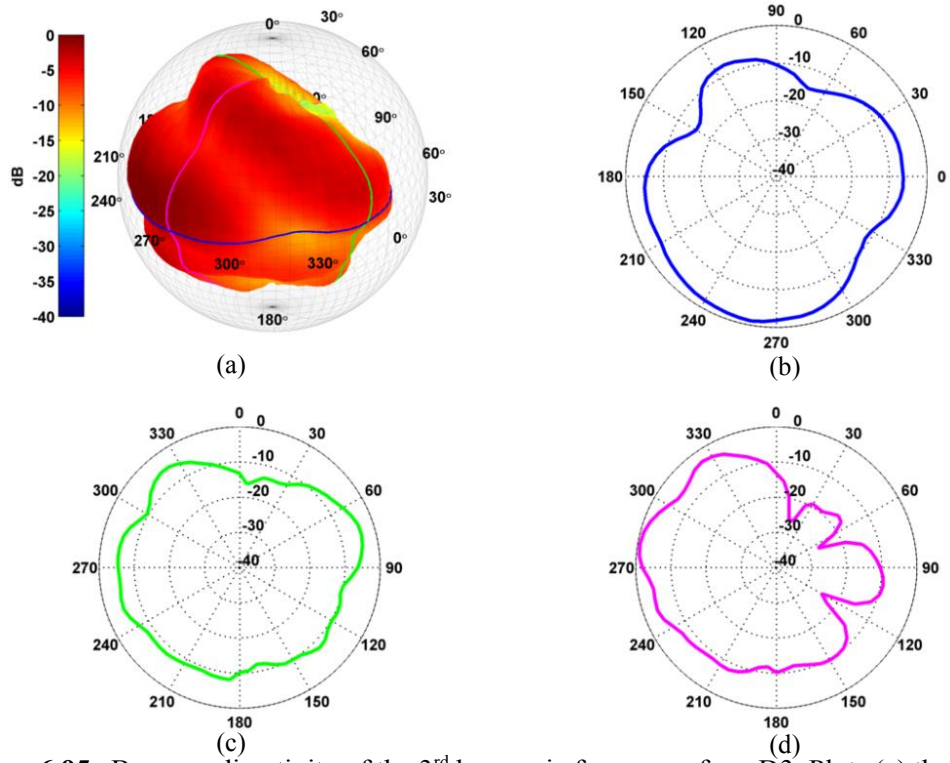

Figure 6.95. Bassoon directivity of the 3rd harmonic frequency for a D3. Plots (a) through (d) are arranged as described in Fig. 6.2.

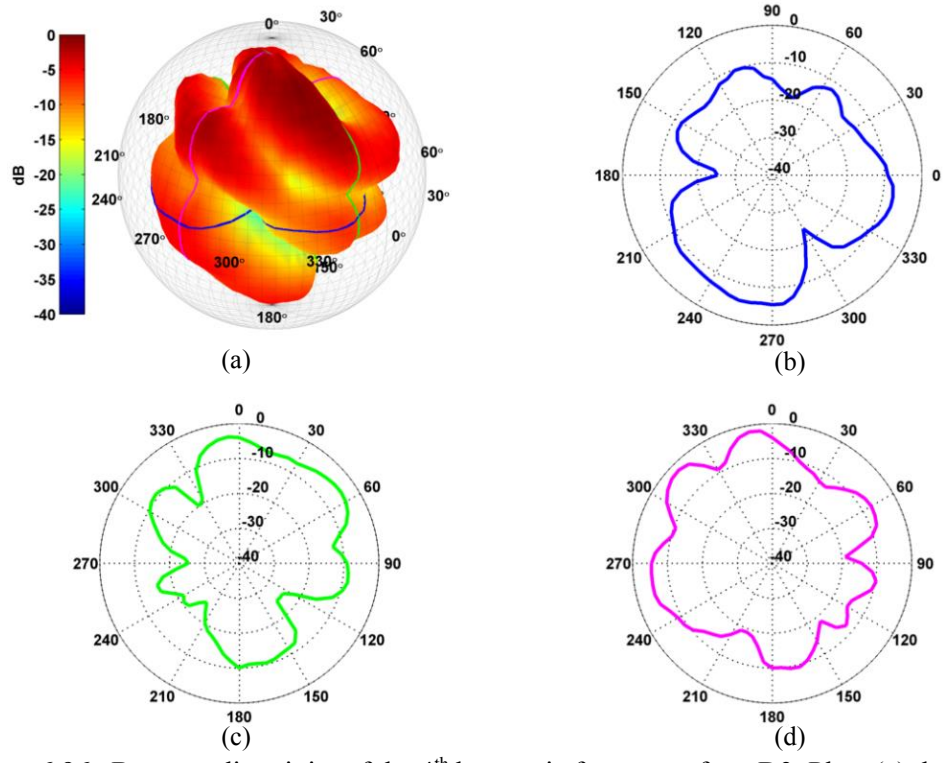

Figure 6.96. Bassoon directivity of the 4th harmonic frequency for a D3. Plots (a) through (d) are arranged as described in Fig. 6.2.

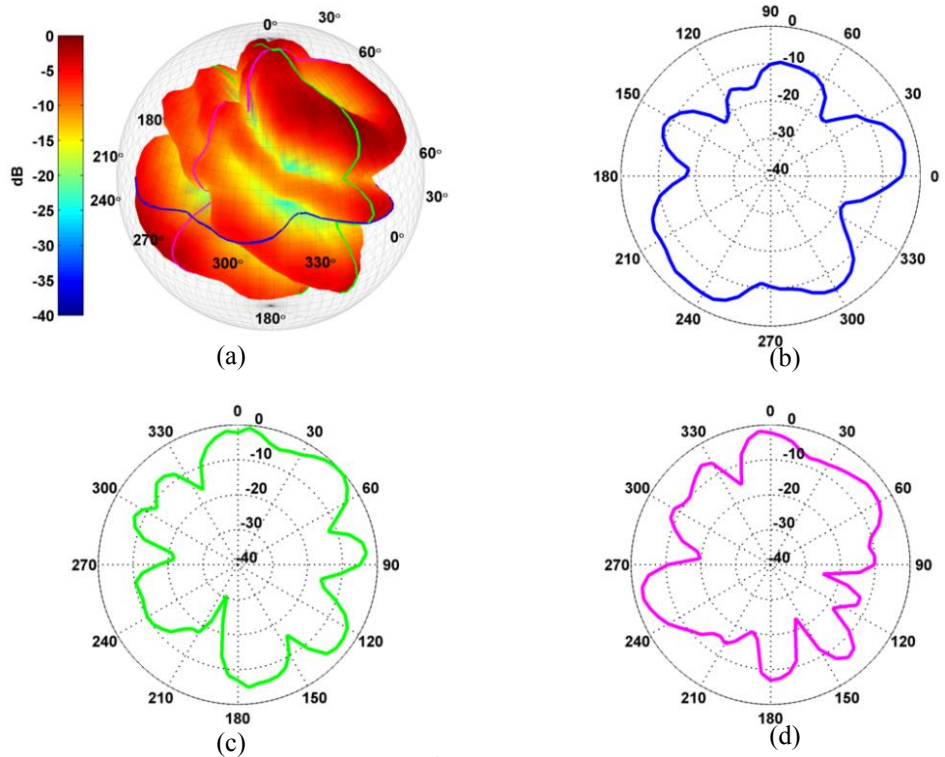

Figure 6.97. Bassoon directivity of the 5th harmonic frequency for a D3. Plots (a) through (d) are arranged as described in Fig. 6.2.

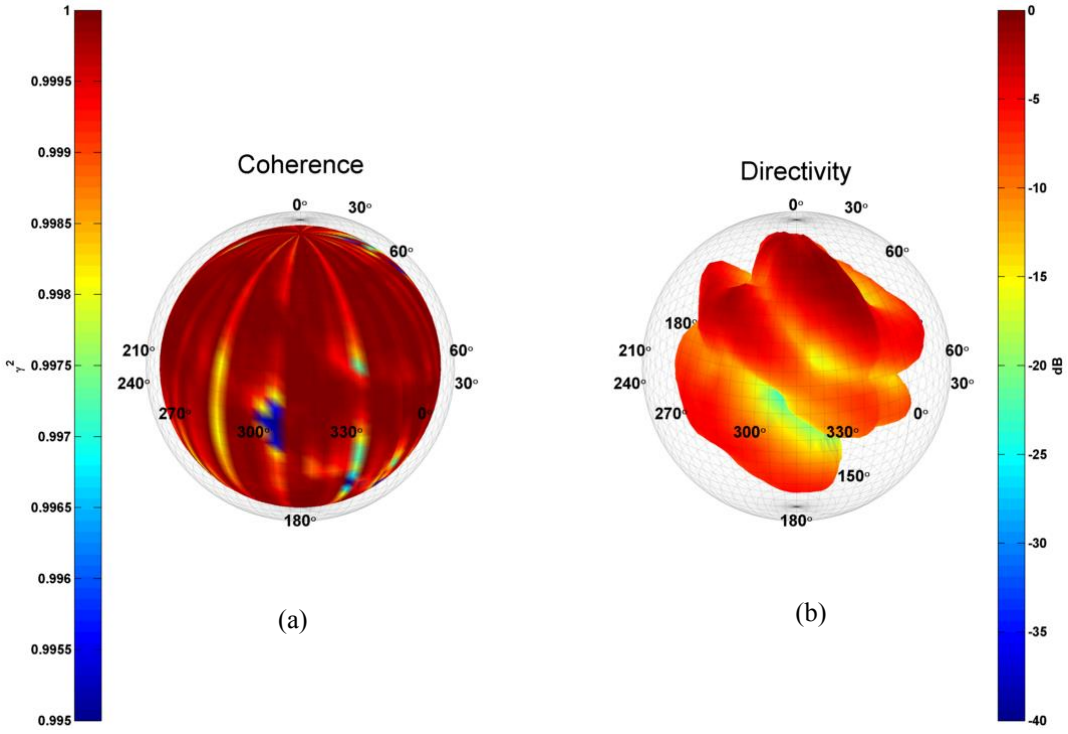

Figure 6.98. Bassoon plots of the 4th harmonic frequency for a D3. (a) Coherence balloon. (b) Directivity balloon.

6.15 Clarinet

Figure 6.99. Clarinet player seated in the DMS.

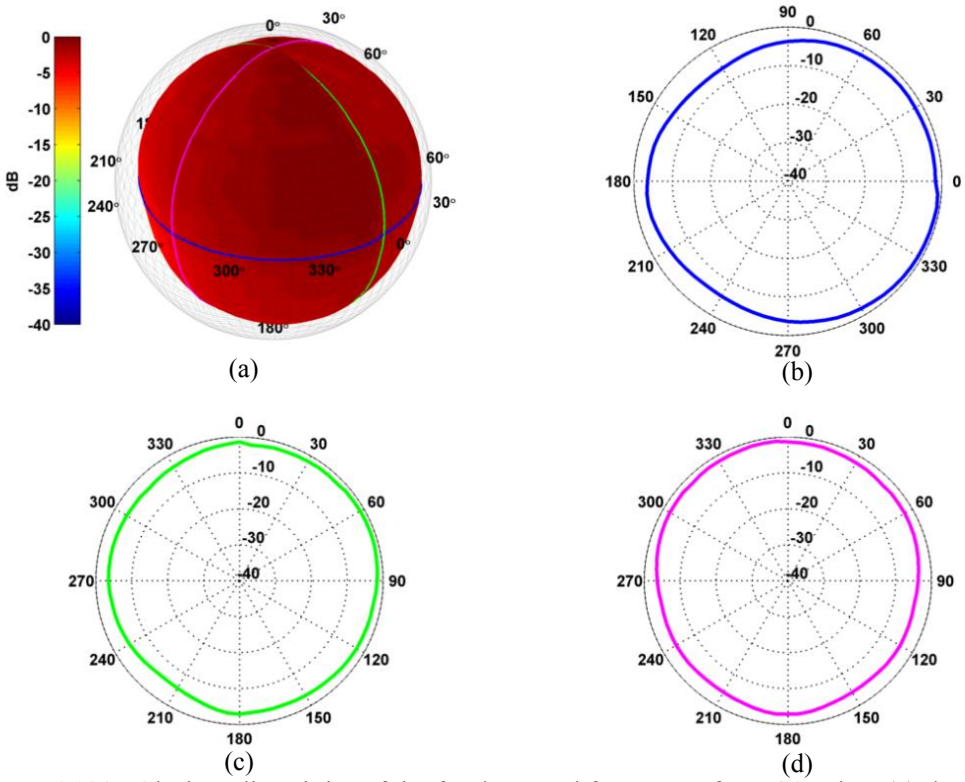

Figure 6.100. Clarinet directivity of the fundamental frequency for a G3. Plots (a) through (d) are arranged as described in Fig. 6.2.

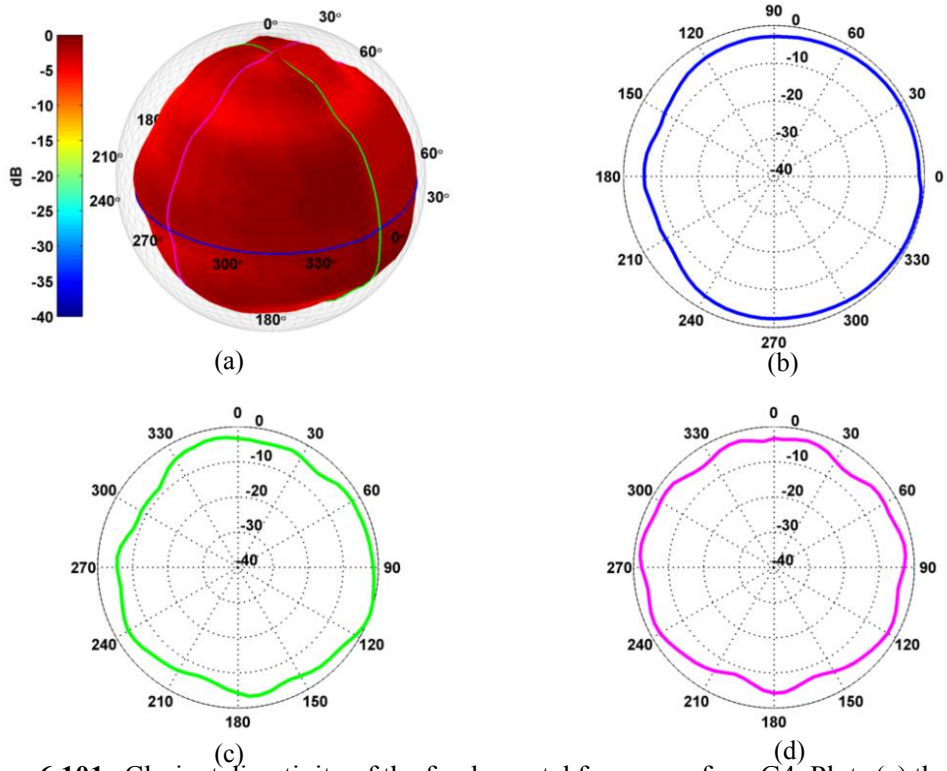

Figure 6.101. Clarinet directivity of the fundamental frequency for a G4. Plots (a) through (d) are arranged as described in Fig. 6.2.

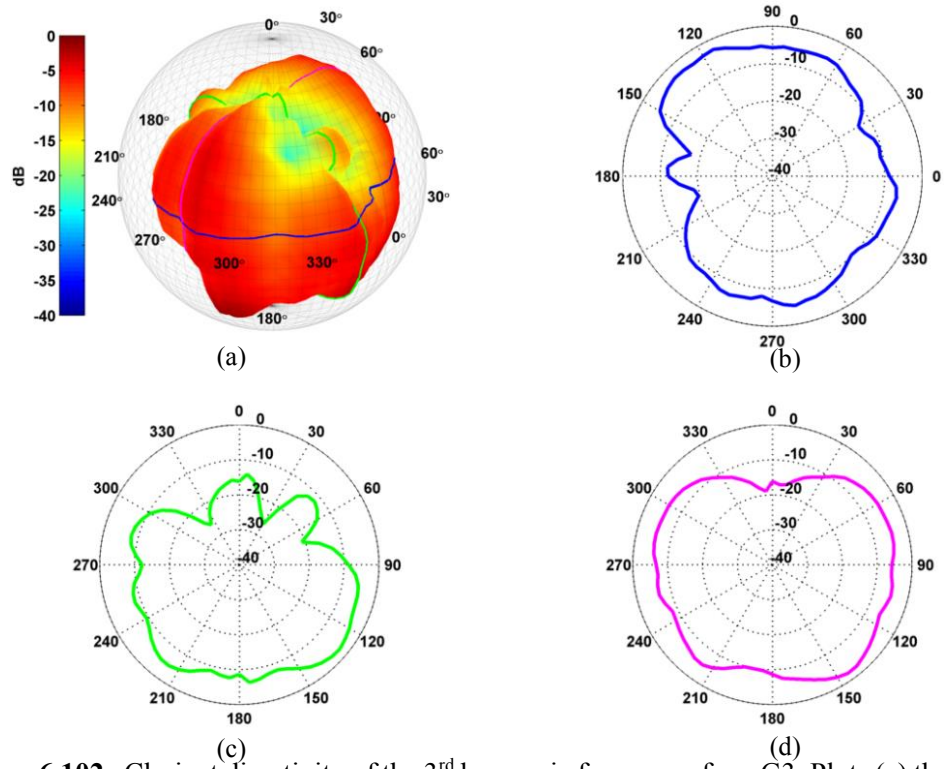

Figure 6.102. Clarinet directivity of the 3rd harmonic frequency for a G3. Plots (a) through (d) are arranged as described in Fig. 6.2.

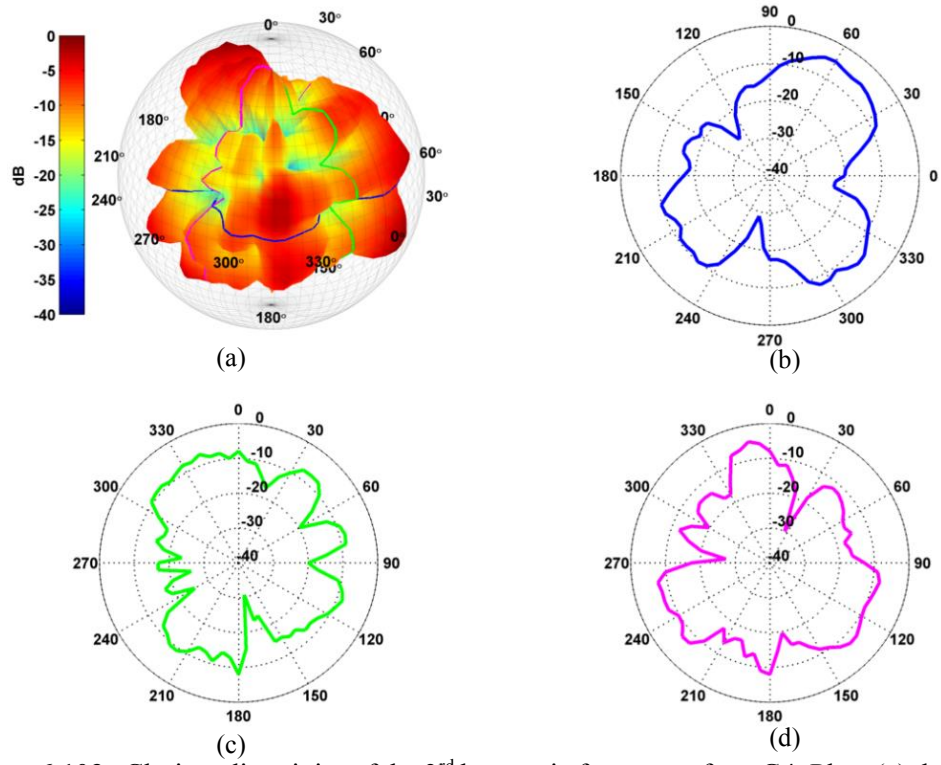

Figure 6.103. Clarinet directivity of the 3rd harmonic frequency for a G4. Plots (a) through (d) are arranged as described in Fig. 6.2.

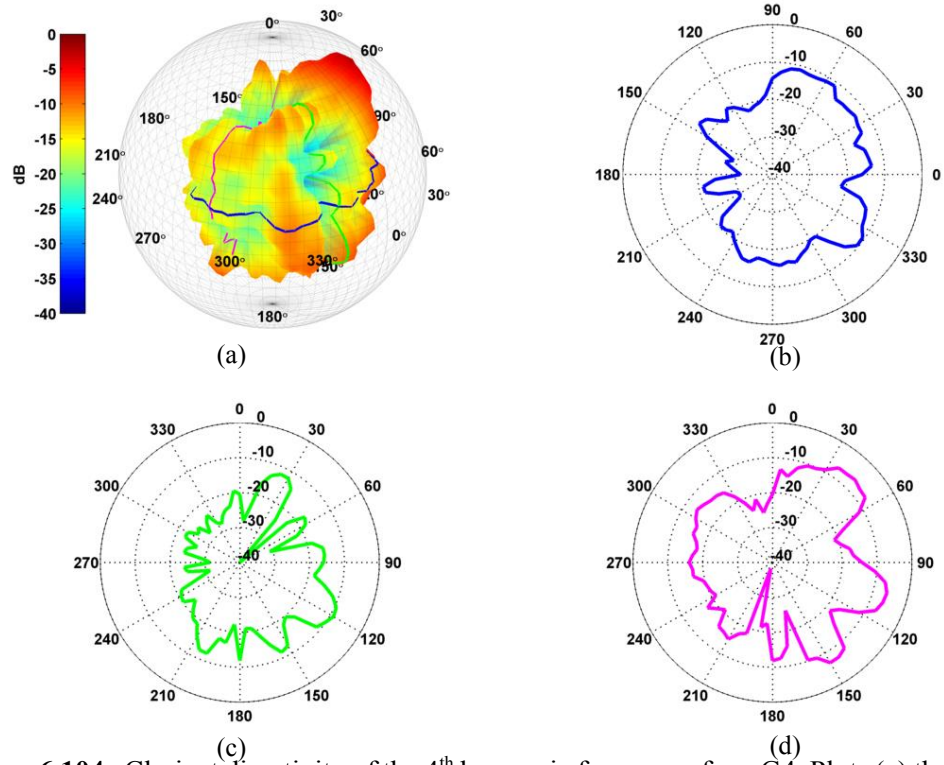

Figure 6.104. Clarinet directivity of the 4th harmonic frequency for a G4. Plots (a) through (d) are arranged as described in Fig. 6.2.

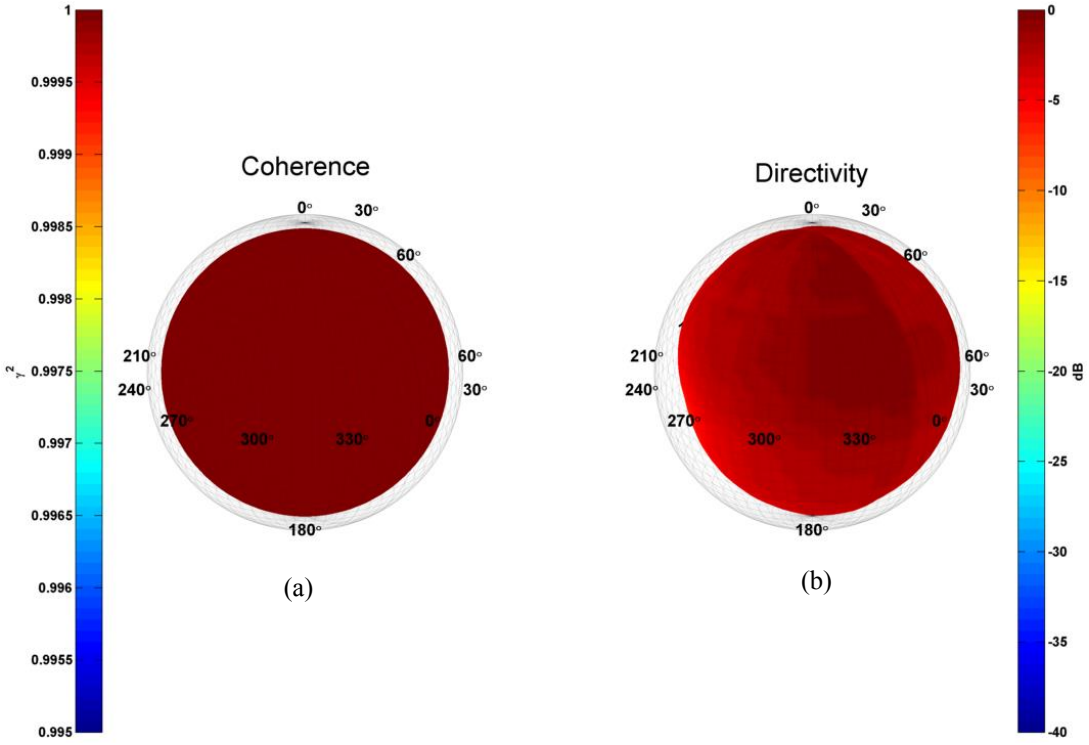

(a) (b)

Figure 6.105. Clarinet plots of the fundamental frequency for a G3. (a) Coherence balloon. (b) Directivity balloon.

6.16 Bass Clarinet

Figure 6.106. Bass clarinet player seated in the DMS.

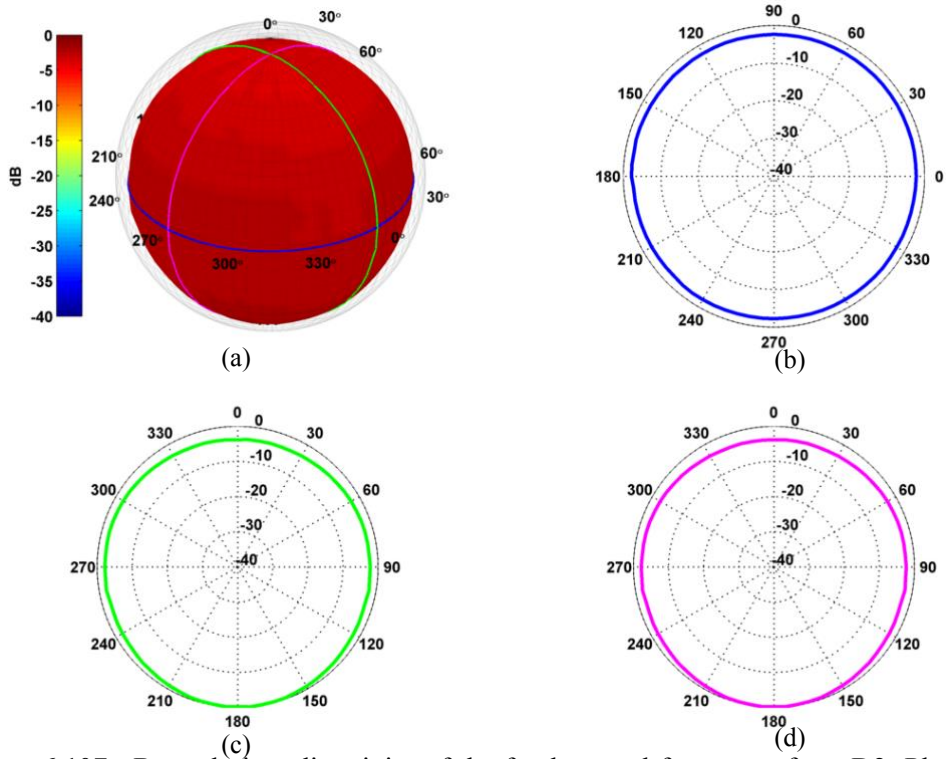

Figure 6.107. Bass clarinet directivity of the fundamental frequency for a D2. Plots (a) through (d) are arranged as described in Fig. 6.2.

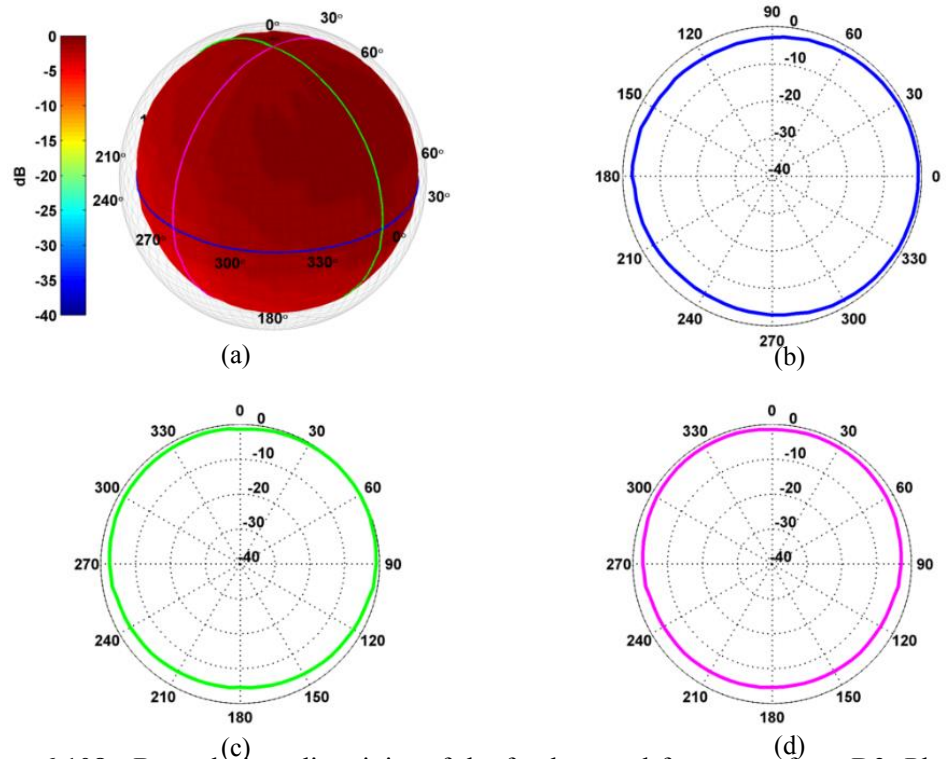

Figure 6.108. Bass clarinet directivity of the fundamental frequency for a D3. Plots (a) through (d) are arranged as described in Fig. 6.2.

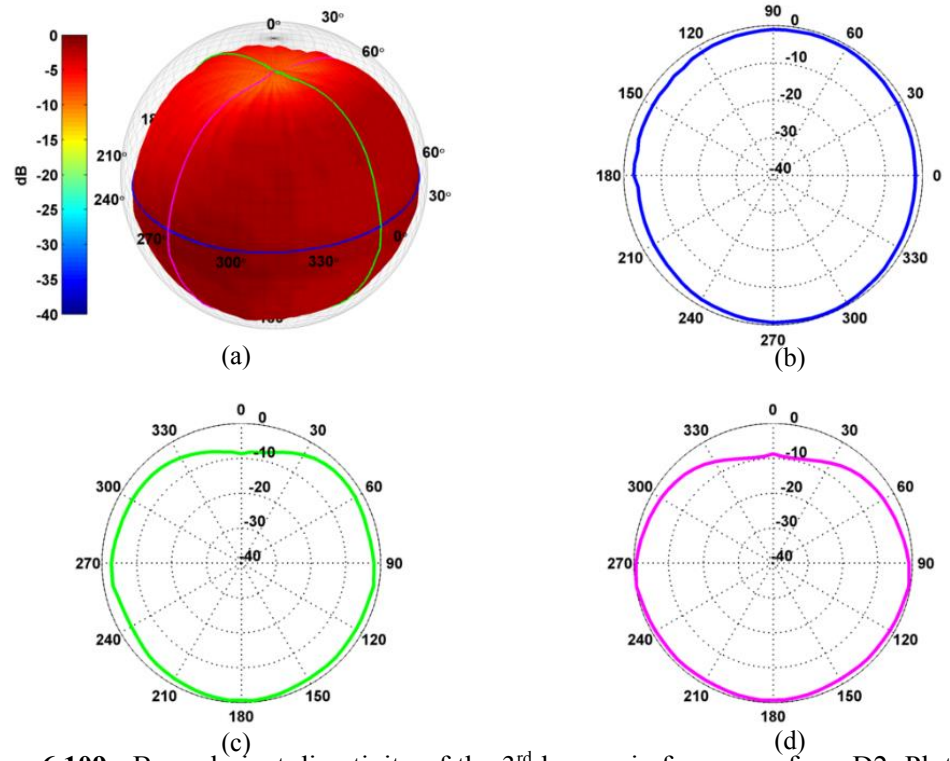

Figure 6.109. Bass clarinet directivity of the 3rd harmonic frequency for a D2. Plots (a) through (d) are arranged as described in Fig. 6.2.

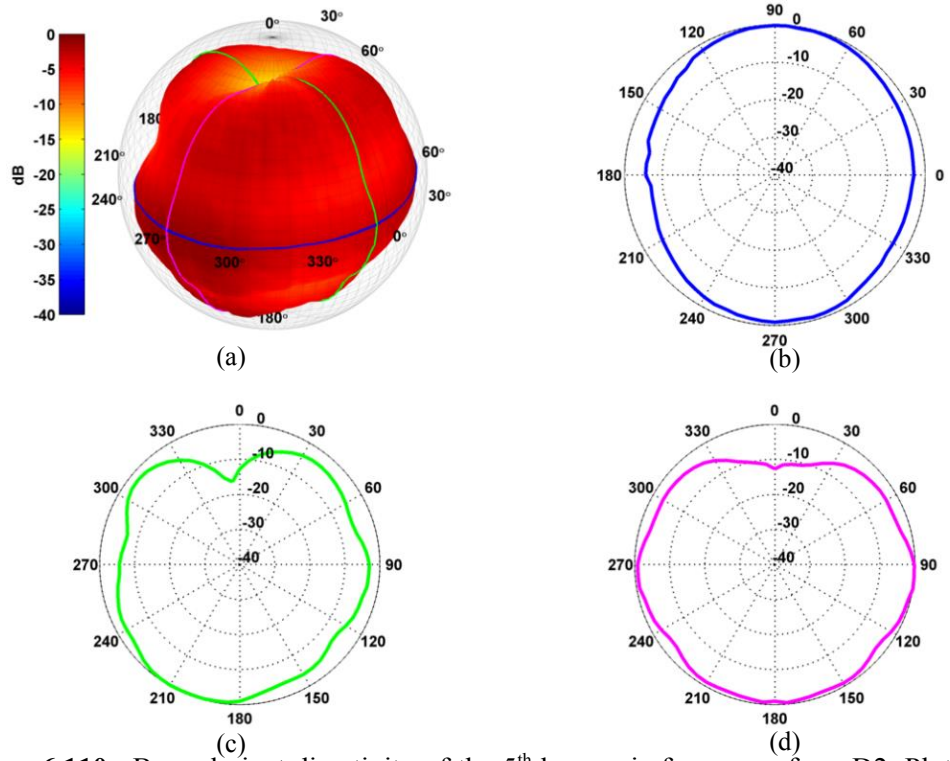

Figure 6.110. Bass clarinet directivity of the 5th harmonic frequency for a D2. Plots (a) through (d) are arranged as described in Fig. 6.2.

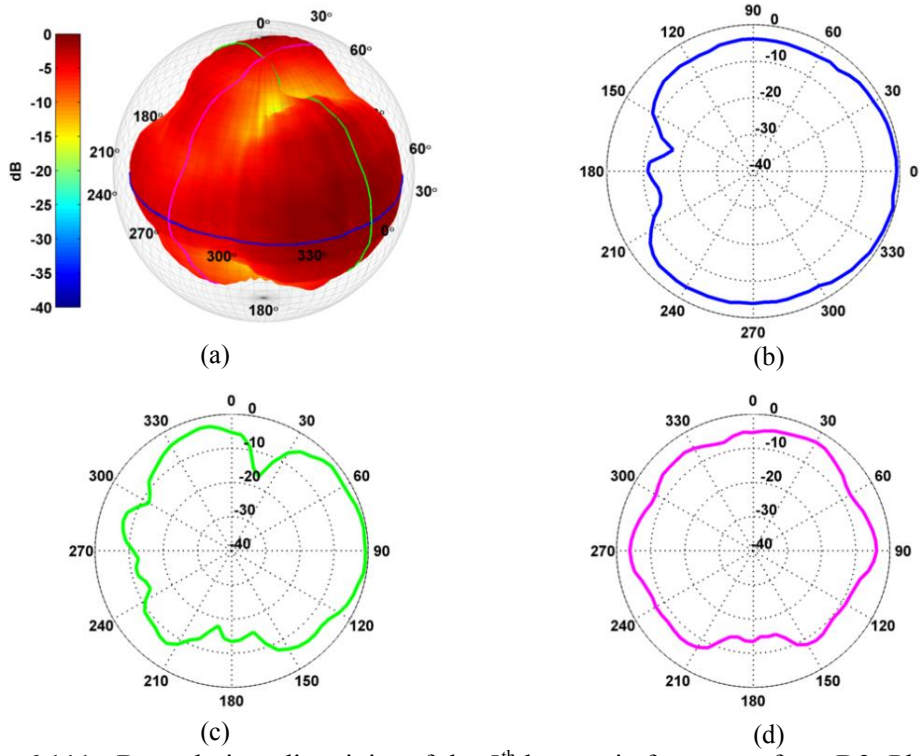

Figure 6.111. Bass clarinet directivity of the 5th harmonic frequency for a D3. Plots (a) through (d) are arranged as described in Fig. 6.2.

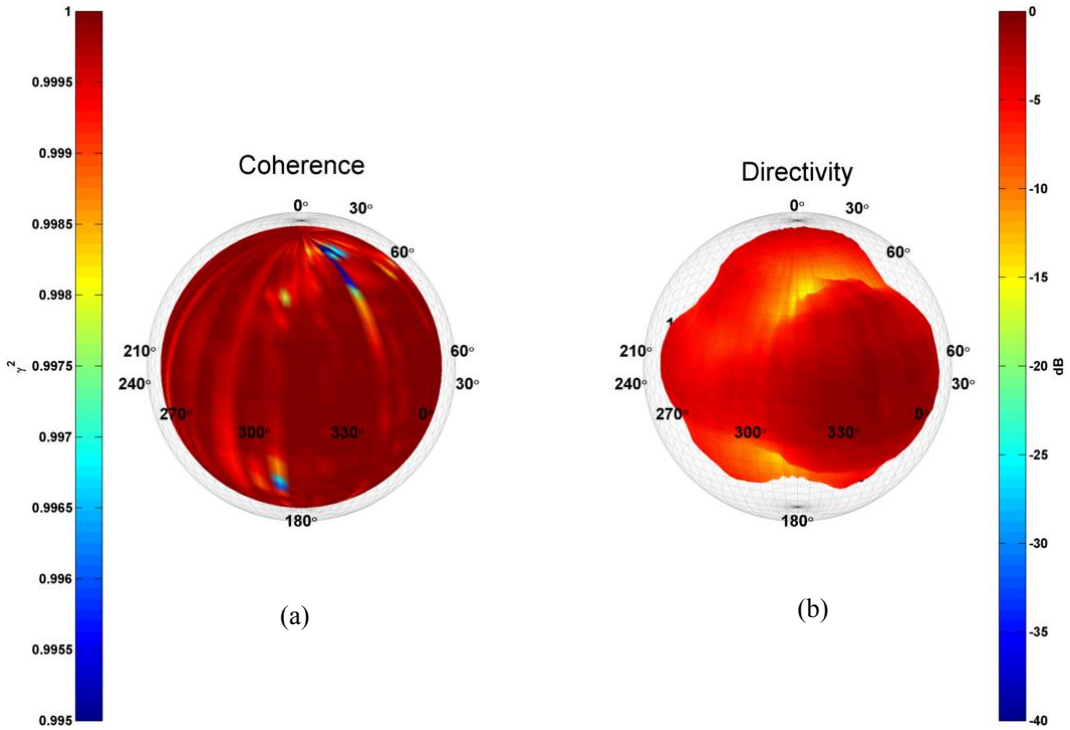

Figure 6.112. Bass clarinet plots of the 5th harmonic frequency for a D3. (a) Coherence balloon. (b) Directivity balloon.

References

[1] K. J. Bodon, “Masters Thesis Supplemental Materials,” Brigham Young University (2016) [available at <http://scholarsarchive.byu.edu/etd/5653/>]

Chapter 7

Conclusions

The previously existing DMS at BYU has been updated and improved in many ways. As a result of the work reported in this thesis it now incorporates acoustical treatments of the arc array, a positioning laser, and high-quality digital audio interfaces. New directivity processing algorithms have also been developed using MATLAB to calculate and plot directivities in a number of ways. To the knowledge of the author, the BYU DMS is currently the highest-resolution systems for musical instruments, incorporating 2,522 unique measurement locations over a sphere and 5^{o} angular resolution. It has been streamlined in efficiency to allow for complete measurement and data processing to occur for an instrument in under 24 hours. It is also flexible enough to accommodate many different types of instruments as well as loudspeakers and other sources of sound.

Loudspeakers were used to simulate played musical instruments. Directivities at individual frequencies were compared to those of standard loudspeaker measurements. The RMS errors, when random amplitude, pitch, and positioning errors were intentionally introduced, ranged from 0 dB to 1.5 dB, falling within allowable tolerances of anechoic chamber qualifications.

Nonanechoic spatial field variances are also present for other types of DMSs, but are not typically reported.

The spatial resolution of the BYU DMS matches the AES56-2008 standard for Type A loudspeaker directivity measurements and provides high levels of detail. Results shown in Ch. 3 validate the use of a repeated-capture system, when used with the stated methods, for musical instrument directivity. This work provides important steps toward standardizing played musical instrument directivity measurements in a way that approaches the AES standard for loudspeaker measurements.

Measuring the complete directivity of played musical instruments is not a simple matter. With no current standard, many groups have taken different approaches to the problem. Most DMSs fall under two general types of systems: single-capture or repeated-capture. Single-capture systems measure directivity using spherical arrays with sparse sampling and quite limited resolution. Repeated-capture systems usually involve single-dimensional arrays, which collect spherical data through rotation of either the array or the musicians and instruments, with subsequent stitching of the measurements together into a sphere of data for high-resolution directivity.

After comparing these two system types, it was found that single-capture systems provide a relatively simple, rapid, and efficient method to determine directivity. Errors due to musician playing deviations are not present for these systems. They produce smooth directivity patterns through interpolation or low-order spherical harmonic expansions. However, with their low spatial resolution, the directivities they produce may not accurately represent the important details of complex radiation patterns especially at higher frequencies.

Repeated-capture systems provide rich detail but suffer from errors and inconsistencies produced by inconsistencies of live musicians. In some cases, resulting directivity patterns appear to have longitudinal bands with up to 1.3 dB of error. However, this margin again falls within the tolerances outlined in the anechoic chamber qualification standards. Additionally, the time taken to record musicians and the complexity of the system are significant. Despite these challenges, the BYU DMS currently provides what appears to be the highest resolution directivity measurements of any system discussed in the literature.

In order to accurately represent directivity, it may be necessary to use repeated-capture systems with a high spatial resolution similar to those used for loudspeaker standards. High-resolution directivity patterns may contain some quantifiable errors, while the errors associated with low-resolution systems remain unknown. An ideal system would combine the resolution of a repeated-capture system with the simple measurement technique of a single-capture system. However, as it is not practical to implement a spherical array with 2,522 microphones, repeated-capture systems are required to achieve feature-rich details of directivity patterns with some degree of quantifiable error.

7.1 Project Results and Contributions

Sixteen musical instruments were recorded playing chromatic scales over their repeatable working ranges. These included violin, viola, cello, double bass, trumpet, trombone, French horn, euphonium, tuba, baritone saxophone, tenor saxophone, flute, oboe, bassoon, clarinet, and bass clarinet. Audio recordings of each chromatic scale were recorded above CD quality for each of the 2,522 unique microphone locations. The directivities of the first five harmonics for each chromatic note have been calculated, plotted, and animated as directivity balloons with 5^{o} angular resolution.

Additionally, loudspeakers used for system validations have been successfully measured with the DMS at 1 Hz resolution. Directivity balloons and animations were also generated for these sources.

Building on the work of Eyring, this thesis has developed many improvements to musical instrument directivity measurements. These include (1) updating and improving the BYU DMS, (2) creating an efficient measurement procedure and processing algorithms in MATLAB, (3) measuring 16 musical instruments over their complete working ranges, (4) validating and quantifying errors from the use of the repeated-capture DMS at BYU using simulated musicians, (5) providing an analysis of using repeated-capture systems vs. single-capture systems, and (6) providing a preliminary analysis of nonanechoic field effects discovered using the DMS.

7.2 Future Work

Although much has been accomplished in this study, there are several items that remain for future work. A primary focus for future study might involve the determination of ideal directivity presentation formats for different applications. This study utilized a 10 Hz bandwidth to present directivities for individual harmonics of each note. This could be modified to represent overall directivity by note or general $(1/N)^{th}$ octave directivities for instruments. Current loudspeaker directivity data for architectural acoustics simulation packages conforms to this latter approach. To produce this format, current directivity data will need to be converted to match the desired spectral bands. Due to the spectrally sparse nature of chromatic scales, this conversion would require special attention to avoid nonharmonic frequencies with poor signal-to-noise ratios.

Beyond spectral issues, considerations for directivity information in the radial direction might be considered. Measurements in this study were taken at a 1.83 m radius from the presumed

center of the source. For many frequencies, this would be considered a far-field measurement. Directivity effects in the near fields of musical instruments still remain largely unknown and might be investigated using a smaller measurement radius and implementing spherical near-field acoustical holography to propagate directivity patterns to any finite radius of interest.

Appendix A

Previous Work on Acoustic Directivity Measurement Systems

Documenting the radiation of acoustic sources is not a new field of acoustical research. In fact, there have been many studies conducted on directivity patterns for over 50 years. The methods of obtaining and presenting directivities have varied greatly over time. In order to learn from the successes and failures of others, a knowledge of what has already been accomplished is required. The following sections outline work that has been done in different categories of directivity measurements over the last half century. The strengths and shortcomings of various methods are given to provide a basis for the reader and aid in categorizing and evaluating the present work. The material is not intended to provide a comprehensive listing, but it touches on important developments and methods that are relevant to the current research. The information is grouped by acoustic source type.

A.1 General Directivity

There are many considerations to take into account when attempting to design a DMS and subsequently measure the spatial dependence of sources of acoustic radiation. The type of source being measured, the spatial resolution desired, the type of analyses to be run, the presentation method, and other logistical considerations are just a few major concerns that must be addressed. Each decision that is made will either expand or limit the flexibility and capability of each measurement system and its results.

Typically, systems have been designed to target the single-source category. The three most common sources for directivity measurements include loudspeakers, the human voice, and musical instruments. The latter two provide additional challenges due to the human excitation factor affecting radiation patterns. Different methods of measuring the directivity, of all three source types, are detailed in subsequent sections.

The angular resolution of measurements is highly varied between research groups and is greatly influenced by logistical constraints. A large number of measurement locations can provide a great level of detail in directivity patterns, but it also requires large data sets, which can be computationally expensive. In addition, high-resolution systems usually require extended measurement sessions due to repeated-capture methods.

Directivity is typically reported using frequency-dependent energetic values normalized to that of the strongest geometric measurement location. Using multiple microphones in a system requires relative calibrations to ensure that microphone responses do not affect these results. Beyond collection and processing data, directivity research groups must determine how to present

their results. Common graphical methods include polar plots in various planes, isobar plots, and directivity balloons [1].

A.2 Loudspeaker Directivity

Of the three source types presented here, loudspeakers provide the fewest challenges, due to their precisely repeatable excitations. Several private and publicly marketed measurement systems for loudspeakers exist. Two variants are presented here to provide a comparison to live-source measurement systems to be discussed later.

A.2.1 Hughes

Charles Hughes has detailed the DMS that was once in place in the anechoic chamber at NWAA Labs [2]. The system was based on a 4.4 m inner-radius, quarter-circle microphone array, consisting of 19 evenly spaced, 0.63 cm precision microphones placed at 5° polar-angle increments. The chamber floor consisted of a heavy metal grating, which caused significant reflections for higher frequencies. These floor panels were removed as much as possible for measurements. The arc was also acoustically treated with absorptive material wrapped around the support structure. Due to the chambers location in the side of a hill, large temperature gradients occurred in the chamber from floor to ceiling. These gradients, which would affect arrival times of the signal, were corrected during processing.

All microphones were calibrated over frequency using a substitution technique with an off-axis loudspeaker as a source in a large parking lot. The microphones are accurately placed to within 4.3 mm of the exact location of an ideal arc using a rotating laser positioning system. The loudspeakers were placed in the circular center of the arc and the measurements were conducted

by measuring and rotating the loudspeaker by 5° azimuthal angle-increments until a complete revolution occurred. The loudspeaker was then flipped over, top to bottom, and the rotation process was repeated. Upon completion, a complete sphere of data were collected, with a recording time of just over 30 minutes. The recordings were taken using the EASERA software package.

A.2.2 Leishman et al.

Leishman et al. used a similar system in an anechoic chamber at BYU to measure various multiple-driver loudspeakers with different platonic solid geometries [3]. Loudspeakers were mounted on a thin stand connected to a turntable in the center of a quarter-circle array with a 2.1 m radius. Nineteen electret free-field precision microphones were mounted on the arc and evenly spaced in 5° polar-angle increments to record the radiation. Measurements were repeated 73 times, rotating azimuthally by 5° increments to complete a full circle. The first location was repeated as a consistency check. The loudspeakers were then flipped over and the process was repeated. Initially, all microphones were calibrated using a single-frequency 1 kHz tone.

Signal processing was done over a frequency range of 0 Hz to 20 kHz, with 12.5 Hz spectral resolution. Only frequencies over 100 Hz were in the range of interest for the study. Directivity was conveyed using single-bin balloon plots and could be animated as frequency increased to show the evolution of directivity over frequency.

Rather than using a strict power-spectrum or magnitude-based method for calculating directivity, as had been common, a complex frequency response was calculated instead as

$$H_1 = \frac{G_{ab}}{G_{aa}}, \tag{8.1}$$

where G_{ab} denotes the single sided cross-spectrum between input and output and G_{aa} denotes the single-sided input auto-spectrum. By choosing this method, phase information was preserved in the frequency response.

A.3 Human Voice

The directivity of the human voice is not under direct study in this thesis, but there have been many attempts to measure it under varied circumstances. As a live imperfectly repeatable source of sound it provides enough similarity to musical instruments to be of importance.

A.3.1 Marshall and Meyer

A study at the University of Auckland investigated the directivity of the human voice using a sung vocal selection as the signal [4]. Measurements were made in an anechoic chamber in three orthogonal planes (two vertical and one horizontal). While azimuthal angles were measured in approximately 10° increments over an entire circle, the vertical planes suffered from a more sparse 20° resolution spanning from 0° to 130° in the polar direction. Single notes over three separate octaves were recorded at two amplitudes and data were processed using fractional octave bands. Normalized sound pressure level (SPL) polar plots were created in all three planes at standard octave bands. Additionally, polar plots containing multiple frequency ranges were presented in a contour fashion, using 0 dB, 3 dB and 10 dB down contour colors.

A.3.2 Kob and Jers

Kob and Jers, at the Institute of Technical Acoustics, used only two microphones to complete their measurements [5]. A musician stood on a turntable and had microphone taped to

their nose to provide a reference signal while a second mic was placed on a nearly semicircular vertical arc, which allowed movement for the microphone from 0º to 130°. The chamber used in the study did not appear to be fully anechoic, which could create unwanted reflections and significantly influence results.

A vocalist would sing a glissando (a single vowel that increased pitch with time) repeatedly and as consistently as possible. Detail is not given regarding the spatial resolution of the measurement. The data were processed using 1/3rd octave bands and used normalized sound pressure level (SPL) values relative to the reference. The data were represented as balloon plots at standard 1/3rd octave band center frequencies, with radius as well as color denoting amplitude. The process was also repeated with an artificial singer, similar to a Head and Torso Simulator (HATS) system, to validate that the process was accurate for a repeatable source.

A.3.3 Bazzoli et al.

Bazzoli et al. recorded 10 male talkers to determine the directivity of male speech [6]. This was accomplished using a vertical circular arc with 3 microphones, located at 60° intervals, starting at 0° directly overhead as well as a microphone at polar 90º. An additional microphone was placed in front of the talker, level with the mouth, and was not moved during measurements. All microphones were placed at a 1 m radius from the mouth. The microphone array was rotated azimuthally in 15° increments around the talker after every vocal repetition. The data were analyzed using octave bands and presented using polar plots. A similar experiment was completed using a HATS system for validation of the live source vocal directivity measurements.

A.3.4 Halkosaari et al.

Halkosaari et al. investigated human speech directivity, but did not fully clarify their methods [7]. It was reported that the recordings were accomplished using a 32 kHz sampling frequency and a 16 bit depth. Spectral analysis was done using a 1024 sample block size and 50% overlap averaging. Rather than reporting directivity in a typical method, the frequency response plots were overlaid from various recording locations. Additionally, the quality of the recordings was measured using the coherence function, to ensure that all data collected was valid. The comparison between an artificial mouth and the live human talkers were compared using similar frequency response plots.

A.3.5 Katz and d'Allessandro

Katz and d'Allessandro also used a rotational method to measure directivity of a human voice [8]. Measurements were taken in an anechoic chamber using 24 equally spaced microphones on a horizontal semicircular array. Two additional microphones were used as references. The first was placed on the subject's head and the second in front of the subject. The microphone array was rotated in the polar angle after each measurement, from 0^o to 135^o.

Two types of vocal excerpts were used in determining directivity: running speech and specific phonemes. Directivity was reported in a $1/3^{rd}$ octave band resolution, using half polar plots. The required calibrations were attained by positioning the arc horizontally and placing a loudspeaker at the center. Pink noise was emitted from the loudspeaker and the levels were matched in each band to be omnidirectional. No mention of level compensation for the loudspeakers directivity pattern was mentioned when calculating the calibration adjustments for

each microphone. Several efforts were made to reduce variations from rotation to rotation. These included the use of a digital tuner visible to the subject and a laser alignment system to place the talker in the center of the arc. In addition to the static polar plots mentioned, videos of running speech directivity using short-time averages were generated by the researchers. These consisted of overall directivity, using amplitude-weighted frequency averaging, to compute the general directivity of the talker.

A.3.6 Chu and Warnock

Chu and Warnock undertook a study to determine the directivity of human conversational speech [9]. Their approach was to use two semicircular arcs, each 1 m in radius, arranged orthogonally, with microphones placed approximately 20° apart. The microphones were 1.2 cm Brüel and Kjær free-field condenser microphones. The arcs covered a polar angle from 0° to 140° and the subject was rotated to six positions, covering azimuthal angles from 0° to 180°, with the 0^o angle located directly in front of the musician. An assumption was made that directivity for a human is symmetric through the medial plane, and the data were simply duplicated for the opposite hemisphere.

During the recordings a microphone was placed on the talkers' head to produce a reference signal. For each rotation, his or her mouth was placed at the origin of the arcs. Approximately 40 seconds of conversation was recorded, which was related, but not identical, at each location. Using a Brüel and Kjær real-time analyzer, $1/3^{rd}$ octave band spectral data between 160 Hz and 8 kHz were examined. The study was repeated with a HATS system. For validation and comparison, polar plots in the horizontal and vertical planes were depicted, showing the relative SPL measurements to that of the reference microphone.

A.4 Musical Instrument Directivity

Like human speech directivity measurements, directivity measurements of musical instruments require special consideration, due to lack of playing repeatability. There are numerous approaches that have been taken to resolve this issue, including artificial excitation, single-capture measurements, and repeated-capture measurement techniques. Methods for relying directivity data are even more broadly diverse than for human speech directivity, as outlined in the following sections. Several measurement systems have been designed for specific instruments, while others allow for recordings of various instruments.

A.4.1 Olson

The first documentation of musical instrument directivity found in this literature search comes from Olson [10]. Little is documented discussing methods used and therefore cannot be commented on here. Polar plots are given in one plane for eight instruments and the human voice at several frequencies.

A.4.2 Meyer

Widely acknowledged as the father of directivity measurements of musical instruments, Jürgen Meyer conducted work that dates back half a century [11], [12]. Facts and figures that he produced are still commonly used in textbooks and are bases for comparison in current studies. However, exact details of how his data were collected and processed is difficult to determine. Some details were given for the directivities of bowed stringed instruments [12].

In this case recordings were performed in an anechoic chamber with the instrument placed upright on a turntable. The instrument was then excited with an electrodynamic shaker attached to the bridge to help ensure a more repeatable result. A single microphone was place between 1 m and 3.5 m depending on the measured instrument, and was used to collect data. Pressure data were collected in a horizontal plane, and was averaged together with multiple recordings from different models of the same instrument, to obtain an average directivity.

Transverse and median planes of data were collected by rotating the source, and were plotted in polar coordinates over frequency bands marked with 3 dB down locations. Diagrams showing principle radiation directions were also included in several planes [12].

A.4.3 Štěpánek and Otčenašek

Štěpánek and Otčenašek used a slightly different method of recording and presenting directivity data than many other groups [13]. A violin was recorded with a 3.2 m diameter fully circular array, using 16 evenly spaced microphones and a secondary 1.6 m diameter array with nine microphones. The larger array was moved vertically in 0.5 m increments and the played selection was repeated at each of the array locations. The smaller array was placed only at the highest and lowest vertical distances measured by the 3.2 m array, resulting in 98 total microphone locations. The recordings were made using a sampling rate of 44.1 kHz and a 16 bit depth.

The data were not analyzed spectrally, but was subjectively analyzed by several people in a set of listening tests. Each microphone signal for the selected note was rated in descriptive terms, such as full, damped, dark, etc., and plotted with these categories as color contours. This did not provide any numerical values, but was nonetheless an interesting method of conveying directivity.

A.4.4 Wang

Measurement of the radiation from a bowed violin was investigated by Lily Wang [14]. A violin was supported in an open-frame structure and a mechanical bow was used to excite the instrument, in place of a musician. The frame was acoustically treated to prevent scattering as much as possible. A rotating boom with an attached Brüel and Kjær 1.2 cm microphone at a 2 m radius was used for data collection.

Measurements were taken in two planes: horizontal and vertical, relative to the upright instrument, at every 5°. The microphones were calibrated over frequency using a combination of plane wave tubes and an equal-excitation method. The files were then processed in the frequency domain with a 1.56 Hz resolution, over a 100 Hz to 5 kHz range. These data were then presented using polar plots, which contained overlaid curves of four harmonics from the same note. In addition to standard directivity measurements, near-field acoustical holography (NAH) was applied to the data taken with a planar microphone array to examine the pressure response at several distances from the violin.

A.4.5 Vos et al.

A different method was proposed by Vos et al., which used reciprocity to determine the directivity of a violin [15]. A violin was mounted in an anechoic chamber and fitted with a piezoelectric transducer at its bridge. A loudspeaker facing the violin was used as a source to excite it. The loudspeaker was elevated to different polar angles and the violin was also rotated to achieve a 10° angular resolution over an entire sphere.

Data were collected at a sampling rate of 48 kHz. Results had a spectral bin width of 6 Hz. Data above 2 kHz was of no interest for the study and the directivity was found using spatial Fourier decomposition. The authors assumed that up to 1.8 kHz, the directivity could be described by either the first or second spherical harmonic orders.

A.4.6 Carrillo et al.

Another method for measuring the directivity of a violin was outlined by Carrillo et al. [16]. Their method utilized a live musician to excite the instrument, which was mounted in a movable altazimuth stand. Twenty-one RØDE NT1-A microphones were arranged in a nearly hemispherical pattern, using several horizontal rings of microphones. A filter was applied to produce a reasonably flat response for each microphone. A bowed glissando, on a single string, was played over the course of 50 seconds to loosely approximate a logarithmic frequency sweep. It took 15 bows to complete. Measurements were repeated every 5° in the azimuthal angle, and at four different elevation angles. After the recordings were completed azimuthally, the violin was rotated by 30° in the polar direction and the measurements were repeated. The musician exciting the instrument did not rotate along with the instrument and thus was oriented differently relative to the instrument at each polar elevation.

When measurements were completed, a total of 1,260 nonuniformly spaced sampling locations had been represented over the surface of a sphere. The frequency response magnitude data were placed in high-resolution polar plots that were overlaid for multiple frequency ranges.

A.4.7 Pollow et al.

The Institute of Technical Acoustics at RWTH Aachen University has significantly contributed to the study of musical instrument directivity in recent years [17] - [20]. They have a system consisting of 32 microphones evenly spaced over the surface of a sphere, with a diameter of between 4.2 m to 4.4 m, depending on the report [17], [18]. Sennheiser KE 4-211-2 electret microphones were used for the array while two additional studio quality microphones were used, with a higher signal-to-noise ratio, to record audio tracks for auralizations. The preliminary round of measurements was recorded in a hemi-anechoic chamber with an acoustically treated floor. The second round was taken in a fully anechoic chamber rated down to a 63 Hz cutoff frequency [17].

Musicians were placed in a movable and height-adjustable chair to locate the instrument's expected acoustic center near the geometric center of the spherical array [17], [18]. Several instruments such as the pedal harp and timpani were too large to allow for this alignment. Musicians were asked to move as little as possible and play without vibrato [17]. Both single notes and a selected musical excerpt were recorded at two different dynamics: pianissimo and fortissimo [19], [20]. In order to aid the musician in playing in such an acoustically dead space, headphones were used to provide him or her with live feedback and artificial reverberation while playing [19]. A total of 41 instruments were recorded in this manner [20]. No musician rotation or repetition was required, as an entire sphere of data were collected simultaneously.

Acoustic center alignment estimates were not always accurate and consequently corrections were required to acoustically center the instrument in the array during processing utilizing spherical harmonic decomposition of the sound field. However, due to the spatial sampling of the sphere, harmonics must be limited to fourth order and below to accurately

represent the field [21]. A short-time Fourier transform was applied to the data in order to examine directivity in the frequency domain in 1/3rd octave bands [18]. Two methods were attempted in processing the data: magnitude only and complex data. The magnitude only approach assumes a $1/r$ decay rate and is more immune to inaccurately placed sources. The complex data processing method is more difficult and suffers greatly from misplaced sources due to phase differences. However, it could be used in both near and far field, as it does not depend solely on a $1/r$ decay rate [18], [19].

A.4.8 Comesana et al.

Comesana et al. decided on a unique approach by taking a scan of a musician playing a traditional musical selection [22]. The recordings were taken in an anechoic chamber with a grated metal floor, using both a fixed reference microphone and a single movable microphone. The latter recorded at several locations on a square plane over the course of 4 minutes. After each scan was completed, the musician was rotated 90° and the measurements were repeated. For measurement locations above and below the musician, the scanning system remained in its fixed location and recordings were taken with the musician lying on a table. Using the planar pressure data, NAH was used to map the sound onto a sphere, and thus determine the directivity in a spherical shell around the musician.

A.4.9 Jaques et al.

In the study done by Jacques et al., measurements were taken in both an anechoic environment, as well as a recording studio environment [23]. Five instruments from a brass quintet were recorded, each with eight microphones arranged in a horizontal circular array, at the level of

the musician's head. This achieved an angular resolution of 22.5° while omitting the 112.5° location, due to an insufficient number of microphones. The microphones were Sennheiser MKH 800, set to a figure eight pattern. From each of the instruments, a polar plot of normalized levels were presented using 6 frequency bands. All instruments played the same piece of music and resulted in a virtual recording of the entire quintet comprised of 40 microphone locations.

A.4.10 Gautier and Dauchez

The radiation of a concert harp was studied by Gautier and Dauchez [24]. Using a mechanical excitation of a single string, repeatable measurements of the harp's soundboard radiation was made using a 3-D intensity probe. Intensity measurements allowed for visualization of the magnitude, and directionality of energy flow from the soundboard. While this is not a traditional method of measuring or relaying directivity information, it does allow for directionality of the sound board to be examined over frequency. The results are plotted using vector arrows pointing in the direction of flow, with arrow length as an indicator of relative amplitude.

A.4.11 Le Carrou et al.

Le Carrou et al. similarly studied concert harp radiation but utilized a more traditional method [25]. Two separate measurement methods were used in this study. The first utilized a vertical arch of 35, 0.6 cm microphones spaced 0.2 m apart in a semi-anechoic room. A concert harp was placed in the center of the arch maintaining a 2 m minimum radial distance from the harp to each microphone. A shaker fixed with a short rod was attached to the soundboard of the harp and was used as the driving source with a white noise excitation signal. Directivity was calculated

using a frequency response function at discrete frequencies and was displayed in polar plots in both the medial and transverse planes.

The second method utilized a ring of 32 microphones in the transverse plane arranged evenly around the harp with a 2.35 m radius. In this setup a live musician plucked the strings and directivity was calculated for the fundamental and six other partials of several strings and were calculated based on sound levels using the first 125 ms of the signal. The directivities were displayed in the plane of the microphone ring as polar plots.

A.4.12 Pätynen et al.

The contributors from the Helsinki University of Technology had a goal of creating a directivity library for orchestral instruments by individually recording each instrument [26], [27], [28]. This was done by creating a 20 microphone array in a fully anechoic chamber arranged in a dodecahedron pattern, with an extra two microphones placed above, and directly in front, of the musician. This arrangement conformed roughly to ISO 3745 standard for sound power measurements. Due to some physical constraints of the room, all microphones were not placed at a fixed radius from the source, but ranged between 1.81m and 2.49 m, with the average being 2.13 m [26], [27]. The microphones used were RØDE NT1-A large diaphragm studio microphones [26]. Musicians sat in a chair, which rested on a metal grating floor, which was assumed to add scattering effects, even with acoustic treatments. These effects were ignored in the study.

Four separate styles of music were played and recorded by each musician. The musicians wore open-back headphones, allowing them to hear a prerecorded piano track that accompanied them. The open-back style was chosen to allow the musician to both hear themselves and the accompaniment. This raised the concern of signal leaking into the recordings from the headset. It

was reported that no signal was audible from the headphones in the recorded tracks [26]. Beyond the aid of a headphone track, a music stand, tuner, and small video monitor of a conductor were placed in front of the musician to help keep tempo and pitch consistent from instrument to instrument [28]. Measurement sessions lasted from 1.5 hrs. to 6 hrs. per musician [26]. The recordings were taken with 16 bits and a 48 kHz sampling rate, using the REAPER audio software package.

A relative calibration was applied to all microphones during this test. A substitution technique was applied, by first placing a Brüel and Kjær microphone on axis with a Genelec loudspeaker and playing the sine sweep signal. Subsequent microphones were laser positioned to be in the same location and the measurement was repeated. From this data, filters were created to match the microphone responses over frequency between 1 dB and 2 dB [28].

After data collection, frequency responses were computed using MATLAB in 1/3rd octave bands [26]. Gain settings remained fixed during the recording of all instruments. As a result, a low signal-to-noise ratio was measured for several instruments. The directivities of the instruments were presented both, by normalized polar plots, with several overlaid frequency band lines, and note-based normalized contour plots over frequency and angle [27]. Many of the results for directivity were converted into CLF of type 1 and type 2 directivity data through interpolation for use in acoustic auralization, and architectural modeling programs [26].

A.4.13 Hole et al. and Nachbar et al.

The University of Performing Arts, in Graz Austria, used the highest resolution single-capture measurement system of this literature review, with 64 microphones arranged spherically [29], [30], [31]. The array used a 2.7 m diameter frame with “acoustically transparent” braces,

arranged triangularly, with microphones placed at the apexes of each triangle [29]. The microphones used were Behringer ECM8000. They were mounted in holsters designed for minimal scattering. Microphones were calibrated using a 1 kHz amplitude calibrator on each microphone [30].

For the recordings, a musician would be seated on a chair placed on a raised square platform, and would play two octaves of a chromatic scale, as well as a musical excerpt. The recording conditions were not explicitly stated, but due to a 4 kHz upper-frequency limit, before aliasing, an 8 kHz sampling frequency can be inferred [29]. The room conditions were nonanechoic, but room modes and reflections were neglected for this study.

The data were processed using a developed, vMIC hyper-interpolation software, which uses spherical harmonic decomposition to increase spatial resolution. The harmonic order was severely limited by the spatial resolution of the microphone array, and a maximum order of 7 was implemented to prevent spatial aliasing [29]. The results were presented as two angles of a specific frequency balloon, as well as a comparison contour between partials of various notes [29].

A.4.14 Otondo and Rindel

At the Technical University of Denmark, three instruments were measured for directivity, including the clarinet, trumpet, and French horn [32]. This was accomplished by placing 13 flat-response microphones arranged circularly in the transverse and median planes, with a spacing of 45° between microphones. The polar angle of 180°, located directly below the musician, was omitted for practical reasons. The microphones on the arrays were placed with a constant radius of 1.5 m. Each musician was asked to play short tones over the entire pitch range of the instrument,

while seated in a normal performance posture, with as little physical movement as possible. The recordings were taken with 24 bits and a sampling frequency of 44.1 kHz.

After collection, the data were processed using 700 ms of recording time from each played note. Spectral data with an octave band resolution was produced. The octave bands were then logarithmically averaged to achieve an overall directivity for the entire instrument. Both were represented graphically using normalized polar plots.

A.4.15 Grothe and Kob

Grothe and Kob focused their efforts on the directivity of the bassoon [33]. In their study, a bassoon was mounted to a turntable and fitted with a blowing mechanism to provide an artificial musician excitation. Specific tones were achieved by taping down tone holes. Two Brüel and Kjær microphones were used in data collection, with one being placed at 1.2 m and the other at 3.5 m from the source. There was no mention regarding the placement angles of the microphones relative to the bassoon. However, an image of the setup appears to have them placed near the midpoint of the long axis of the bassoon with the bassoon arranged vertically. As the artificial musician was able to sustain prolonged tones, recordings were made as the instrument was rotating. The rotation occurred at a speed of 2° per second. The recordings used a 65.53 kHz sampling rate, and a 16 bit depth.

Three octaves of a B♭ scale were recorded in this manner, using a tuner to provide ±5 cents of accuracy in pitch. Spectral data were produced in 1/3rd octave bands, using a 50% overlap with a one second time block. The results were presented as polar plots at standard 1/3rd octave band center frequencies in both the horizontal and median plane, overlaying data from different played

notes at a given center frequency on the same plot. This provided the ability to examine how directivity changed, depending on the actual note played, while similar frequencies were compared.

A.4.16 Eyring

At BYU, Eyring and his colleagues developed a system using a vertical semicircular arc and repeated captures as a musician was sequentially rotated in an anechoic chamber [34]. The arc was fitted with 37 precision microphones, positioned uniformly from polar 0° to 180°, with a 5° spacing. The microphones were placed at a radius of 1.8 m at a distance of 30.5 cm inward from the arc structure. The arc was made with a curved tubular aluminum beam which had a 2.54 cm × 2.54 cm square cross section. It was not acoustically treated. The microphones were relatively calibrated over frequency using a combination of equal excitation and switching methods. Reference microphones were placed in various stationary locations in the musician reference frame to provide signals for frequency response calculations.

Musical instruments were placed so that their geometric centers coincided with the circular center of the arc when possible. Using a visual target, musicians were asked to play single notes as consistently and with as little motion as possible. Sustained notes were held up to 10 seconds and were monitored for pitch variation during recording. The musicians were also asked to play without vibrato or tremolo. After a successfully recorded note, the musician was rotated 5° azimuthally, using a turntable, and the note was recorded again. Seventy-three such rotations occurred before a subsequent note was recorded.

All notes were recorded with a 48 kHz sampling frequency and a 24 bit depth, using National Instruments data acquisition hardware and a custom LabVIEW code, which also provided all processing algorithms [34]. Using the same basic processing method as Leishman et al. [3], frequency response functions were created at all measurement locations, using the sustained portion of the notes. Spectral resolution was taken in 1 Hz or 10 Hz bin widths, depending on the note. Balloon plots of both directivity and coherence were generated at the fundamental and harmonic frequencies [34].

References

[1] M. Kob, “Impact of Excitation and Acoustic Conditions on the Accuracy of Directivity Measurements,” *Proc. ISMA Le Mans France*, 639-643 (2014).

[2] C. Hughes, “How Accurate is Your Directivity Data?” (2005) [available online at <http://www.excelsior-audio.com/Publications/NWAA_Labs_WhitePaper.pdf> (last viewed December 7, 2015)].

[3] T. W. Leishman, S. Rollins, and H. Smith, “An experimental evaluation of regular polyhedron loudspeakers as omnidirectional sources of sound,” J. Acoust. Soc. Am. **120**, 1411-1422 (2006).

[4] H. Marshall, and J. Meyer, “The directivity and auditory impressions of singers,” Acta Acust. United Acust. **58**, 130-140 (1985).

[5] M. Kob and H. Jers, “Directivity measurement of a singer,” J. Acoust. Soc. Am. **105**, 1003(A) (1999); in *Collected Papers, 137th Meeting of the Acoustical Society of America and the 2nd Convention of the European Acoustics Association* (ISBN 3-9804458-5-4), Paper 2aMU_19 [available at <http://haraldjers.de/html/img/pool/Kob_Jers_1999_Directivity_measurement_of_a_singer.pdf> (last viewed October 16, 2015)].

[6] F. Bozzoli, A. Farina, and M. Viktorovitch, “Balloons of directivity of real and artificial mouth used in determining speech transmission index,” *Audio Engineering Society Convention* **118**, Convention Paper 6492 (2005).

[7] T. Halkosaari, M. Vaalgamaa, and M. Karjalainen, “Directivity of artificial and human speech,” J. Audio Eng. Soc. **53**, 620-631 (2005).

[8] B. Katz, and C. d'Alessandro, “Measurement of 3-D Phoneme-Specific Radiation Patterns in Speech and Singing,” Techincal report, LIMSI, (2007), [available online at <https://rs2007.limsi.fr/PS_Page_14.html> (last viewed December 7, 2015)].

[9] W. T. Chu, and A. C. C. Warnock, “Detailed directivity of sound fields around human talkers,” NRC Publications archive (2002) [available online at <http://doi.org/10.4224/20378930> (last viewed December 7, 2015)].

[10] H. F. Olson, *Music, Physics, and Engineering*, 2nd ed. (Dover Publications, New York, 1967)

[11] J. Meyer, *Acoustics and the Performance of Music: Manual for Acousticians, Audio Engineers, Musicians, Architects and Musical Instrument Makers*, 5th ed. (Springer, Berlin, 2009).

[12] J. Meyer, "Directivity of the bowed stringed instruments and its effect on orchestral sound in concert halls," J. Acoust. Soc. Am. **57**, 1994-2009 (1972).

[13] Z. Otcenasek, and J. Stepanek, "Violin Sound Radiation-Directivity of Violin Timbre," Fortschritte der Akustik **26**, 240-241 (2000).

[14] L. W. Wang, "Radiation Mechanisms from Bowed Violins," Ph. D. dissertation, Pennsylvania State University, State College, PA (1999), available online at < http://search.proquest.com/docview/304486063> (Last viewed December 7, 2015).

[15] H. Vos, O. Warusfel, N. Misdariis, and D. de Vries, "Analysis and reproduction of the frequency spectrum and directivity of a violin," J. Acoust. Soc. Neth. **167**, (2003) [available online through ircam at <http://articles.ircam.fr/textes/Vos03a/index.pdf> (Last viewed on September 7, 2014).

[16] A. Pérez Carrillo, J. Bonada, J. Pätynen, and V. Välimäki, "Method for measuring violin sound radiation based on bowed glissandi and its application to sound synthesis," J. Acoust. Soc. Am. **130**, 1020-1029 (2011).

[17] M. Pollow, G. Behler, and B. Masiero, "Measuring directivities of natural sound sources with a spherical microphone array," *Proc. 1st Ambisonics Symposium*, Graz, 1-6, (2009) [available online at < http://ambisonics.iem.at/symposium2009/proceedings/ambisym09-pollowmasiero-musicalinstrumentdirectivity.pdf/@@download/file/AmbiSym09_PollowMasiero_MusicalInstrumentDirectivity.pdf> (Last viewed December 7, 2015).

[18] M. Pollow, "Measuring directivities of musical instruments for auralization," Fortschritte der Anustin: Tagungsband **35**, 1471-1473 (2009).

[19] M. Pollow, G. Behler, and M. Vorlander, "Post-processing and center adjustment of measured directivity data of musical instruments," Acoustics 2012 Nantes (2012) [available online at <https://hal.archives-ouvertes.fr/hal-00811212/> (Last viewed December 7, 2015)].

[20] M. Pollow, G. K. Behler, and F. Schultz, "Musical instrument recording for building a directivity database," in Fortschritte der Akustik **36**. Deutsche Jahrestagung für Akustik, Berlin, Germany (2010).

[21] T. D. Abhayapala and D. B. Ward. "Theory and design of high order sound field microphones using spherical microphone array," in *Proc. of ICASSP* **2**, 1949-1952 (2002).

[22] D. Fernández Comesaña, S. Morales Cervera, T. Takeuchi, and K. Holland, "Measuring under non stationary conditions with scanning techniques," in *Proc. of Noise and Vibration: Emerging Methods 2*, Sorrento, Italy (2012).

[23] R. Jacques, B. Albrecht, D. de Vries, F. Melchior, and H. P. Schade, "Multichannel source directivity recording in an anechoic chamber and in a studio," Forum Acusticum Budapest (2005) [available online at <http://webistem.com/acoustics2008/acoustics2008/cd1/data/fa2005-budapest/paper/634-0.pdf> last viewed (December 7, 2015)].

[24] F.Gautier, and N. Dauchez, "Acoustic intensity measurement of the sound field radiated by a concert harp," Applied Ac. **65**, 1221-1231 (2004).

[25] J. Le Carrou, Q. Leclere, and F. Gautier, " Some characteristics of the concert harp's acoustic radiation," J. Acoust. Soc. Am. **127**, 3202 -3211 (2010).

[26] J. Pätynen, V. Pulkki, and T. Lokki, "Anechoic recording system for symphony orchestra," Acta Acust. United Acust. **94**, 856-865 (2008).

[27] J. Pätynen, T. Lokki, "Directivities of Symphony Orchestra Instruments," Acta Acust. United Acust. **96**, 138-167 (2010).

[28] J. Pätynen, "Virtual acoustics in practice rooms," M.S. thesis, Helsinki University of Technology, (2007), available online at <http://www.researchgate.net> (Last viewed December 7, 2015).

[29] F. Hohl, and F. Zotter, "Similarity of musical instrument radiation-patterns in pitch and partial," Fortschritte der Akustik, DAGA, Berlin (2010).

[30] C. Nachbar, G. Nistelberger, and F. Zotter, "Listening to the direct sound of musical instruments in freely adjustable surrounding directions," 2nd Ambisonics Symp., Paris (2010).

[31] F. Hohl, "Kugelmikrofonarray zur Abstrahlungsvermessung von Musikinstrumenten" ("Spherical microphone array for radiation survey of musical instruments"), Master's thesis, University of Music and Performing Arts, Graz, Austria (2009) [available at <http://old.iem.at/projekte/acoustics/musik/kugel/hohl.pdf > (last viewed December 7, 2015)].

[32] F. Otondo and J. H. Rindel, "The influence of the directivity of musical instruments in a room," Acta Acust. United Acust. **90**, 1178-1184 (2004).

[33] T. Grothe, and M. Kob. "Investigation of bassoon directivity," in *Proc. of the Stockholm Music Acoustics Conference* (2013).

[34] N. J. Eyring, "Development and Validation of an Automated Directivity Acquisition System Used in the Acquisition, Processing, and Presentation of the Acoustic Far-Field Directivity of Musical Instruments in an Anechoic Space," M.S. thesis, Brigham Young University, Provo, UT (2013), available online through Brigham Young University Electronic Theses & Dissertations at <http://etd.lib.byu.edu> (Last viewed December 7, 2015).

Appendix B

Phantom-to-ICP Converter

Special adapters were needed to utilize prepolarized type 1 microphones with Focusrite RedNet 4 digital audio interfaces. They require a BNC cable connection and a 4 mA constant current ICP power supply. The RedNet units are typically used in professional audio applications and utilize XLR cable inputs and +48V Phantom power.

In order to use both pieces of hardware, an adapter was required to convert both the cable type and power supply to the microphone preamplifier. Off-the-shelf converters typically convert XLR to BNC by grounding the extra pin from an XLR cable and do not account for power conversion. Two companies were found that manufacture such a converter. However, the cost was excessive to purchase 40 units for all array and reference microphones. In addition, the qualities of those tested did not meet the project standards. As a result, a resident electrical engineer, John Ellsworth, aided in the design and fabrication of a circuit that safely converted power from Phantom to ICP power but had the form factor to fit inside the shell of a Neutrik NA2MBNC XLR-to-BNC cable converter.

Several iterations were designed, fabricated, and tested, eventually resulting in the BYU NB8 Phantom-to-ICP power converter (see Figs. B.1 and B.2). Multiple tests were run on the device to ensure it would not detrimentally influence results of the directivity measurements to be taken. Plots for total harmonic distortion and frequency response of the converter are shown as Figs. B.3 and B.4. Total harmonic distortion (THD) was measured using an HP Agiliant 35670A digital signal analyzer. Total harmonic distortion was measured using 20 Hz, 50 Hz, 100 Hz, 200 Hz, 500 Hz, 800 Hz, 1.2 kHz, 2kHz, 7kHz, and 12 kHz as fundamental frequencies. The number of harmonics used in THD calculations included as many as 20. For frequencies above 1.2 kHz there were not 20 harmonics available within the frequency range of 0 Hz to 24 kHz so fewer harmonics were used. A Brüel and Kjær Pulse analyzer was used to collect and calculate frequency response data with a 4 Hz bin width from 0 Hz to 24 kHz.

Table B.1. A complete parts list for the Phantom-to-ICP converter developed for the DMS system at BYU. All references are also shown in Fig. B.1 with the exception of S1 and A1 which represent parts for assembling the casing.

Phantom-to-ICP Converter Parts List

Reference	Value
C1	100μF 16V
C2	100μF 50V
D1	Current limiting diode 4.5mA
D2	Zener diode 28V 500mW
P1	Neutrik NC*MX
P2	BNC
R1	3900 Ω
R2	3900 Ω
S1	Set screw 4-40 x 3/16" pt.
A1	Decorative ring PVC 0.68"ID, 0.75" OD, 0.26 LONG

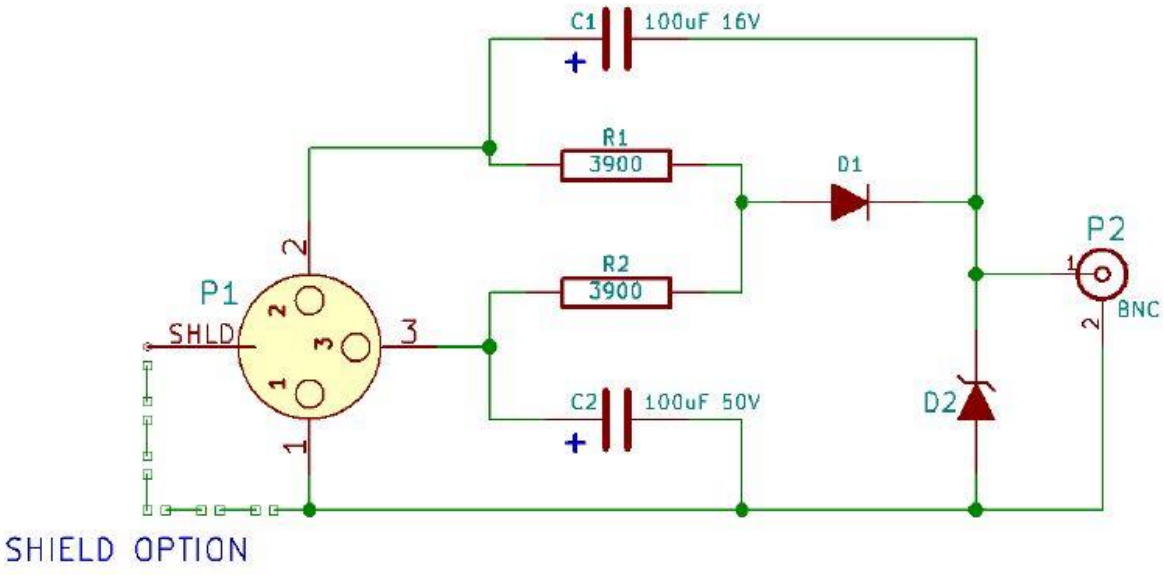

Figure B.1. Circuit diagram of the Phantom-to-ICP converter. A parts list for each element is outlined in Table B.1.

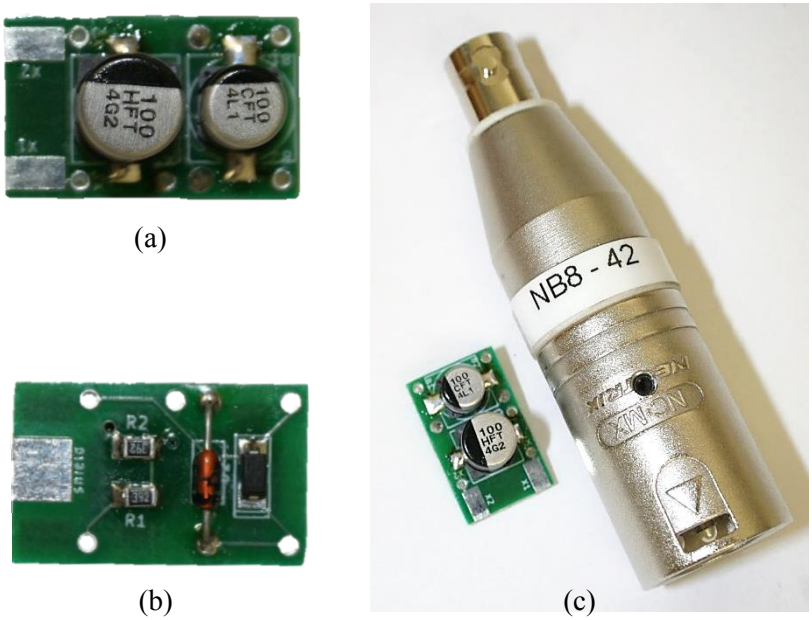

(a) (b) (c)

Figure B.2. (a) Side A of the assembled NB8 circuit. (b) Side B of the assembled NB8 circuit. (c) NB8 Phantom-to-ICP power converter. The interior circuit is shown next to the converter for scale.

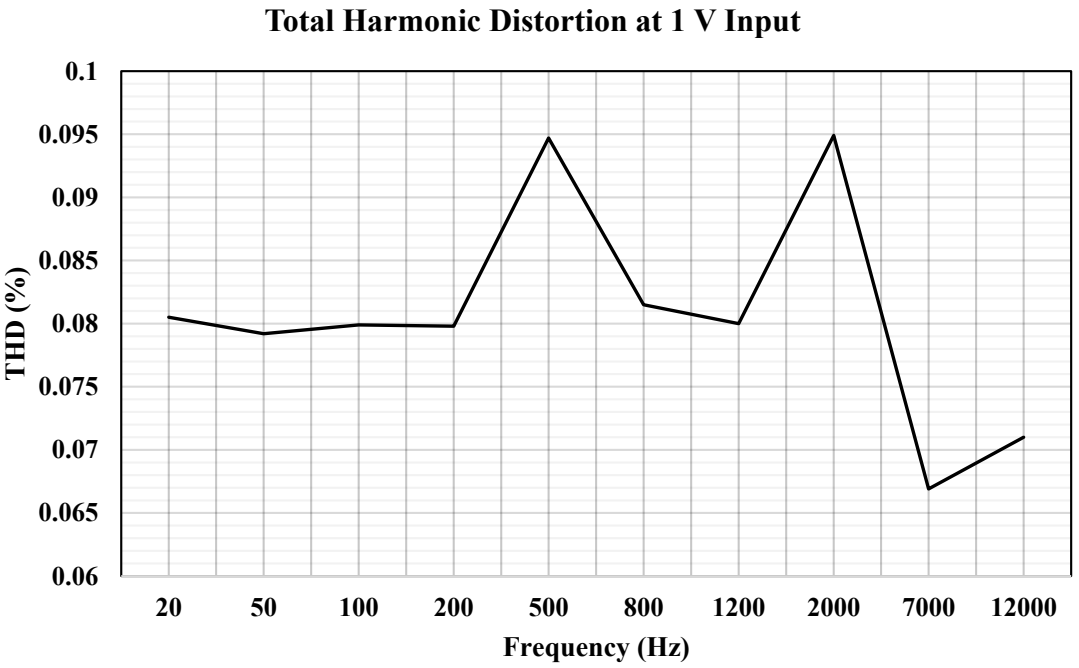

Figure B.3. Total harmonic distortion produced by the NB8 converter over frequency.

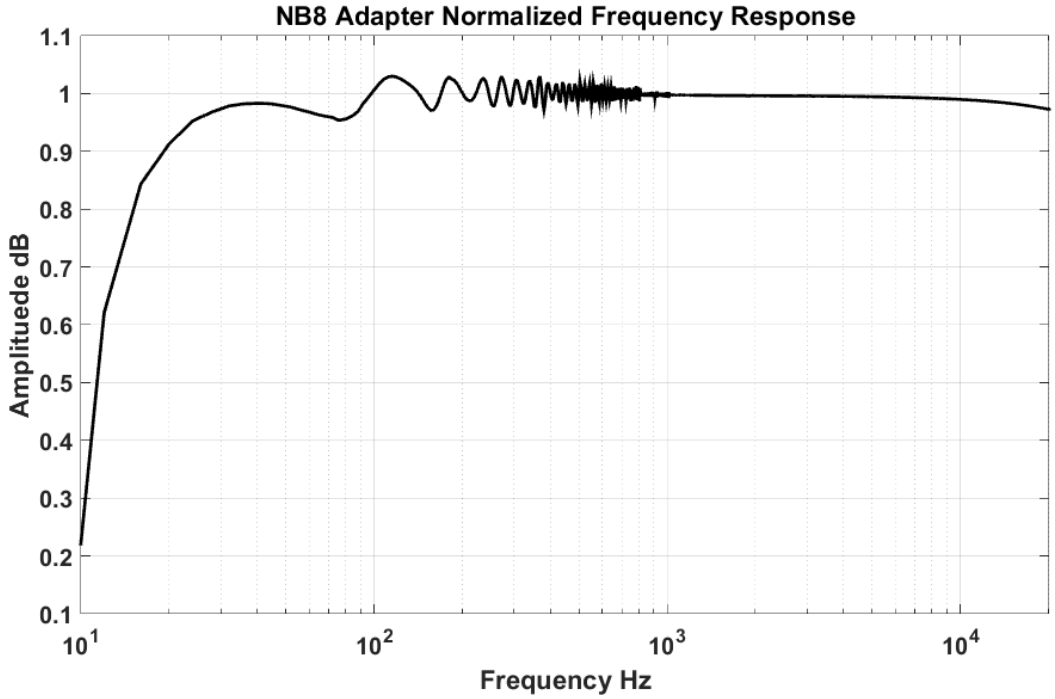

Figure B.4. NB8 converter normalized frequency response placed on a logarithmic scale.